Report
R-17-13
November 2019

Multidisciplinary description of the access area of the planned spent nuclear fuel repository in Forsmark prior to construction

Sven Follin (ed)

SVENSK KÄRNBRÄNSLEHANTERING AB

SWEDISH NUCLEAR FUEL
AND WASTE MANAGEMENT CO

Box 3091, SE-169 03 Solna
Phone +46 8 459 84 00
skb.se

SVENSK KÄRNBRÄNSLEHANTERING

ISSN 1402-3091
SKB R-17-13
ID 1594691
November 2019

Multidisciplinary description of the access area of the planned spent nuclear fuel repository in Forsmark prior to construction

Sven Follin (ed), Golder Associates AB

This report concerns a study which was conducted for Svensk Kärnbränslehantering AB (SKB). The conclusions and viewpoints presented in the report are those of the author. SKB may draw modified conclusions, based on additional literature sources and/or expert opinions.

A pdf version of this document can be downloaded from www.skb.se.

© 2019 Svensk Kärnbränslehantering AB

Preface

The Swedish Nuclear Fuel and Waste Management Company (SKB) has undertaken site characterisation with the objective of siting a deep geological repository for spent nuclear fuel in Forsmark. The understanding concluding the surface-based investigations of a ca 12 km^2 large investigation area was compiled into a site descriptive model named SDM-Site (SKB 2008).

This document is a multidisciplinary description of geoscientific and ecological data of relevance for the access area of the planned repository for spent nuclear fuel in Forsmark prior to construction. The objective is to analyse available data and describe the conceptual understanding of this part of the planned repository for the benefit of a coming update of SDM-Site, which will assess the characteristics of the entire repository prior to construction.

Modelling in the present document is by and large limited to comparisons of old and new data. Specifically, the analyses consider data from the site investigation for SDM-Site (2002–2007), data from preparatory investigations conducted in shallow boreholes drilled inside the access area (2011–2012), and data from the investigation of an approximately 550 m deep borehole drilled in proximity of the planned skip shaft inside the access area (2016). All individuals, investigators and co-authors are gratefully acknowledged for making this document possible.

Topography and regolith geology
Johannes Petrone, SKB

Bedrock geology
Peter Dahlin, SKB, and Jan Hermanson, Golder Associates AB

Bedrock thermal properties and rock mechanics
Diego Mas Ivars, SKB, and Eva Hakami, Geosigma AB

Climate, hydrology and near-surface hydrogeology
Kent Werner, EmpTec, and Jessica Lindmark, Golder Associates AB

Bedrock hydrogeology
Sven Follin and Jessica Lindmark, Golder Associates AB

Hydrogeochemistry
Ann-Chatrin Nilsson, Geosigma AB, and Mats Tröjbom, Mats Tröjbom Konsult AB

Transport properties
Sten Berglund, HydroResearch AB

Ecology and land use
Anders Löfgren, EcoAnalytica

The document has been subjected to internal factual reviews by Johan Andersson and Kristina Skagius.

Stockholm, December 2018

Sven Follin
Editor

Summary

This document is a multidisciplinary description of geoscientific and ecological data of relevance for the access area of the planned repository for spent nuclear fuel in Forsmark prior to construction. The following aspects are addressed:

- Surface system: Topography, regolith geology, climate, hydrology, near-surface hydrogeology and hydrochemistry, transport properties, ecology and land use
- Bedrock system: Bedrock geology, thermal and mechanical properties, hydrogeology, hydrogeochemistry and transport properties.

The spatial scale of the access area comprises the area where the ramp and shafts are planned to be located. The access area also envelopes all parts of the surface access infrastructure, e.g. the rock dump. Hence, the size of the access area at the ground surface is larger than the footprint of the volume of rock in close proximity to the ramp and shafts at depth. In this way a broader spectrum of issues related to important superficial hydrological and ecological processes can be analysed and described more appropriately. For the benefit of some disciplines important data at depth acquired in boreholes drilled outside the immediate access area are also included in the analyses and descriptions of this document.

This document demonstrates that the conditions inside the access area on a whole resemble the conditions already described for the much larger investigation area of SDM-Site. However, it is noted that for some disciplines there are no new data acquired for the access area posterior to the site investigation for SDM-Site. In the cases where this is relevant, the conditions inside the access area have been assessed from SDM-Site data acquired inside the access area.

The access area where the ramp and shafts are planned to be located contains three local deformation zones and three minor deformation zones. The local deformation zones have trace lengths longer than one kilometre and were therefore included in the geological deformation zone model for SDM-Site. Two of the three minor deformation zones described were also identified and modelled in 3D in SDM-Site, but they were not included in the geological deformation zone model for SDM-Site, as their trace lengths were shorter than one kilometre.

The results from the difference flow logging with the Posiva Flow Log (PFL, also PFL DIFF) in the new borehole KFM24, which is drilled in close proximity of the planned skip shaft, reveal 34 flowing fractures. The number and spatial distribution of the flowing fractures observed in borehole KFM24 resemble the number and spatial distribution of flowing fractures observed in boreholes KFM01A, KFM01D, KFM08A and KFM08C, drilled during the site investigation for SDM-Site.

It is noted that many of the flowing fractures in boreholes KFM08A and KFM08C, which are drilled closest to KFM24, were interpreted to coincide with possible deformation zones (PDZ) in the geological single-hole interpretations for SDM-Site. However, the geological single-hole interpretation of borehole KFM24 did not identify any intervals with possible deformation zone type properties. Hence, the flowing fractures in borehole KFM24 are currently associated with the rock between possible deformation zones. As the methodology for geological single-hole interpretation is not taking other data into account than the data observed in the borehole, the interpretation of the PFL results observed in KFM24 are preliminary pending the outcome of the ultimate 3D geological deformation zone model.

The development of the monitored groundwater composition over time in the upper section of borehole KFM08A towards more of glacial contribution and the compositions of the groundwater in the three sampled sections of the new borehole KFM24 show that the glacial component is important for the groundwater evolution in the depth range between −200 to at least −500 m elevation inside the access area. Thus, it is noted that the glacial contribution may be a more frequently occurring component in the groundwater composition than what was outlined in the site investigations for SDM-Site.

Sammanfattning

Detta dokument är en tvärvetenskaplig beskrivning av geovetenskapliga och ekologiska data av relevans för tillfartsområdet för det planerade slutförvaret för använt kärnbränsle i Forsmark innan arbetena med uppförandet av förvaret påbörjas. Följande förhållanden i tillfartsområdet beskrivs:

- Ytsystemet – topografi och klimat, de lösa avlagringarnas geologi och hydrogeologiska egenskaper, hydrologi, hydrokemi, transportegenskaper, samt ekologi och markanvändning.
- Berggrunden – berggrundens geologi, termiska egenskaper, bergmekaniska egenskaper, hydrogeologiska egenskaper, hydrogeokemi och transportegenskaper.

Utsträckningen av tillfartsområdet i berg omfattar området där ramp och schakter planeras vara belägna, men tillfartsområdet inkluderar i vissa avseenden även området där bergupplaget är tänkt att ligga. Därigenom kan ett bredare spektrum av frågor relaterade till viktiga hydrologiska och ekologiska processer analyseras och beskrivas mer ändamålsenligt. För några kunskapsområden ingår dessutom viktiga data i borrhål som borras utanför det omedelbara tillfartsområdet.

Sammantaget visar detta dokument att de geovetenskapliga och ekologiska förhållandena inom tillfartsområdet i mångt och mycket liknar de förhållanden som tidigare beskrivits i SDM-Site. Denna slutsats gäller för alla kunskapsområden, men det ska noteras att det för vissa kunskapsområden inte finns några nya uppgifter (data) som förvärvats efter platsundersökningen för SDM-Site. I de fall där detta är aktuellt har bedömningen av förhållandena inom tillfartsområdet baserats på data från platsundersökningen.

Tillfartsområdet där SKB planerar att bygga ramp och schakter innehåller tre lokala deformationszoner och tre mindre deformationszoner. De lokala deformationszonerna har spårlängder som är längre än en kilometer och inkluderades därför i den geologiska deformationsmodellen för SDM-Site. Två av de tre mindre deformationszonerna som beskrivs i detta dokument identifierades och modellerades också i SDM-Site, men de inkluderades inte i den geologiska deformationsmodellen för SDM-Site, eftersom deras spårlängder var kortare än en kilometer.

Resultaten från differensflödesloggningen med Posiva Flow Log (PFL) i det nya borrhålet KFM24 indikerar 34 flödande sprickor. Antalet flödande sprickor och deras rumsliga fördelning i borrhålet KFM24 liknar antalet och den rumsliga fördelningen av flödande sprickor i borrhålen KFM01A, KFM01D, KFM08A och KFM08C, vilka borrades under platsundersökningen för SDM-Site.

Det noteras att borrhålen KFM08A och KFM08C ligger närmast KFM24 och att många av de flödande sprickorna i dessa två borrhål tolkades sammanfalla med möjliga deformationszoner (PDZ) i de geologiska enhålstolkningarna för SDM-Site. Den geologiska enhålstolkningen av borrhålet KFM24 har inte identifierat några intervall med möjliga deformationszonliknande egenskaper. Följaktligen är de flödande sprickorna i borrhålet KFM24 för närvarande förknippade med berget mellan möjliga deformationszoner. Eftersom geologisk enhålstolkning inte tar hänsyn till andra data än de geologiska data som observerats i borrhålet ifråga, är bedömningen av de flödande sprickornas lägen preliminär tills resultaten från den geologiska 3D-modelleringen föreligger.

Resultat från mätningar av grundvattnets kemi över tid i den övre delen av borrhålet KFM08A visar på en utveckling mot en mer glacial sammansättning. Detta tillsammans med det observerade glaciala inslaget i grundvattnets sammansättning i de tre provtagna sektionerna i det nya borrhålet KFM24 visar att den glaciala komponenten är viktig för grundvattenutvecklingen på djupet inom tillfartsområdet, åtminstone i intervallet −200 m till −500 m. Observationerna indikerar att vatten av glacialt ursprung kan vara en mer vanligt förekommande komponent i grundvattnet än vad som noterades i platsundersökningen för SDM-Site.

Contents

1 Introduction

1.1 Background

The Swedish Nuclear Fuel and Waste Management Company (SKB) has undertaken site characterisation with the objective of siting a deep geological repository for spent nuclear fuel in Forsmark. The understanding concluding the surface-based investigations is compiled in a site descriptive model named **SDM-Site** (SKB 2008). Based on **SDM-Site**, as well as other assessments, SKB in 2009 selected Forsmark as the site for the planned repository for Sweden's spent nuclear fuel. An assessment of the repository's radiological safety after closure, **SR-Site**, was conducted in 2011 (SKB 2011) and the application for a construction license was submitted in March 2011.

SKB has also undertaken site characterisation with the objective of siting an extension of the existing repository for radioactive operational waste (SFR) in Forsmark. The site descriptive model concluding the surface-based investigations undertaken by SKB for the planned extension is referred to as **SDM-PSU** (SKB 2013). Based on **SDM-PSU**, an assessment of the radiological safety of SFR and its extension after closure was conducted, **SR-PSU** (SKB 2015).

1.2 Scope and objective

This document is a multidisciplinary description of geoscientific and ecological data of relevance for the access area facility part of the planned repository for spent nuclear fuel in Forsmark prior to construction (Figure 1-1). The objective is to analyse available data of each discipline and describe the conceptual understanding of this part of the planned facility for the benefit of a coming update of SDM-Site, which will assess the characteristics of the entire repository prior to construction. The spatial scale of the access area facility part is shown in several maps and drawings of this report and denoted by FPS-A in the corresponding legends and/or figure captions. FPS means facility part scale and A means access area, see Section 8.1 of SKB (2018) for a definition of different spatial scales in modelling.

Figure 1-1. *Schematic view of the access area facility part of the planned repository for spent nuclear fuel at Forsmark (Figure 2-2 in SKB 2018).*

Modelling in the present document is by and large limited to comparisons of old and new data. Specifically, the analyses consider data from the site investigation for SDM-Site (2002–2007), data from preparatory investigations conducted in shallow boreholes drilled inside the access area (2011–2012), and data from the investigation of an approximately 550 m deep borehole drilled in proximity of the planned skip shaft inside the access area (2016). The document presents excerpts of the material planned to be included in the ongoing update of the database of the digital elevation model (DEM) and the regolith depth model (RDM) for the Forsmark area, respectively.

1.3 This report and supporting documents

Chapter 2 briefly presents the geoscientific and ecological understanding of the Forsmark site as presented in **SDM-Site** (SKB 2008) and Stephens and Simeonov (2015). This to facilitate the multidisciplinary descriptions presented in Chapters 4 through 10 of both old and more recent data acquired within the access area. The motive for including Stephens and Simeonov (2015) is that the version of the deformation zone model presented in **SDM-Site** refers to modelling stage 2.2. This model was upgraded into model version 2.3 by Stephens and Simeonov (2015), after taking account of the modifications carried out on the geometric position of boreholes in 3D, the new geological and geophysical data that emerged 2006–2007 during modelling stage 2.3 of the Forsmark site investigation and the version 1.0 deterministic model for deformation zones at SFR completed by Curtis et al. (2011) in support of **SDM-PSU** (SKB 2013).

The modelling work by Stephens and Simeonov (2015) followed the established conceptual understanding of deformation zones at the Forsmark site as presented in SKB reports and peer-reviewed publications. The work by Stephens and Simeonov (2015) followed the same methodology, used the same modelling assumptions and is affected by the same uncertainties as those presented in stage 2.2. The changes made in the upgrading to model version 2.3 have no implications for **SDM-Site** or **SR-Site**.

Chapter 3 presents the access area, the volume below, old and recent boreholes and the references to all **SDM-Site** data and more recent data considered in this document. It is noted that the size of the access area is larger than the cross-sectional area of the volume below, which encompasses the rock near the ramp and shafts. In this way a broader spectrum of issues related to important hydrological and ecological processes at the surface can be analysed and described more appropriately. However, for the benefit of some disciplines important data at depth acquired in boreholes drilled outside the immediate access volume are also included in the analyses and descriptions.

In addition to the **SDM-Site** data of geoscientific and ecological relevance to the description of the access area/volume, the following more recent sources of data are recognised and analysed to meet the objective of the present document:

- Preparatory geological and hydrogeological investigations of the regolith and uppermost part of the bedrock within the access area. Eleven short, cored boreholes, KFM13-23, were drilled 2011. These reach a depth less than 200 m and investigations focussed on evaluating the geology and hydrogeology of the shallow bedrock in the area for the planned shaft and access ramp facility constructions (see Chapter 3).
- To validate and gain more information about the current geological model at depth in the area for the planned shaft and access ramp facility constructions, a long borehole, KFM24, was core drilled to a depth of 540 m near the planned skip shaft during 2016 (see Chapter 3). The investigations in KFM24 include single-hole geoscientific interpretation, identification of cross-hole hydraulic responses during difference flow logging with the Posiva Flow Log (PFL) and double-packer pumping tests with the Pipe String System (PSS).
- Long-term monitoring of surface water and groundwater levels, and of hydrochemical and ecological conditions.

The understanding per discipline is presented in Chapters 4 through 10. It is noted that the access area is occasionally referred to as the “FPS-A area”, or the “FPS-A model area” in figure and table legends, which simply means “Facility Part Scale – Accesses”. Chapter 11 concludes this document by collating the key observations of each discipline. The nomenclature used in this document is coherent with the definitions used in **SDM-Site**, see Section 1.6.5 in SKB (2008).

1.4 Coordinate system

The coordinate system used by SKB for data acquisition, visualisation and modelling in all modelling stages including stage 2.3 is the national 2.5 gon V 0:-15, RT 90 system (“RAK”) for X/Y (N/E) and the national RHB 70 levelling system for Z (elevation).

At the time of developing this document, SKB is changing to SWEREF 99 TM 18 00 for X/Y (N/E) and RH 2000 for Z (elevation). SKB’s database Sicada and various computer tools used for 3D visualisation and modelling are not at the same level of implementation of SWEREF 99 1800 and RH 2000 as the tools used for handling geographical information in 2D. Hence, both coordinate systems are used in the presentations in this document.

2 Site descriptive model of the Forsmark site

This chapter is an excerpt of the current understanding of the Forsmark area as presented in **SDM-Site** (SKB 2008), Stephens and Simeonov (2015) and **SDM-PSU** (SKB 2013). It aims to facilitate the understanding of new data presented in the subsequent chapters of this document.

2.1 Investigation area and boreholes

Borehole data in support of the description of the bedrock come from investigations in 25 core-drilled boreholes ranging from ground surface to ca 1 000 m depth and having a total borehole length of ca 17 800 m, and in 38 percussion-drilled boreholes ranging from ground surface to ca 300 m depth and having a total borehole length of ca 6 500 m (Figure 2-1). Borehole data in support of the description of the regolith (mainly Quaternary deposits) come from investigations in more than 100 groundwater monitoring wells (Figure 2-2). The average depth of these wells is approximately four metres.

Twelve drill sites (abbreviated DS in Figure 2-1) were used for core drilling. The target volume of the repository for spent nuclear fuel is inside the surface polygon defined more or less by a polygon passing through DS2-DS6-DS8-DS9-DS10-DS2. The access volume is planned to be located in the north-western part of the target volume between DS7 and DS8. The location of the existing repository for radioactive operational waste, SFR, is also indicated in Figure 2-1. It is located north of the investigation area at shallow depth in the bedrock below the Baltic Sea.

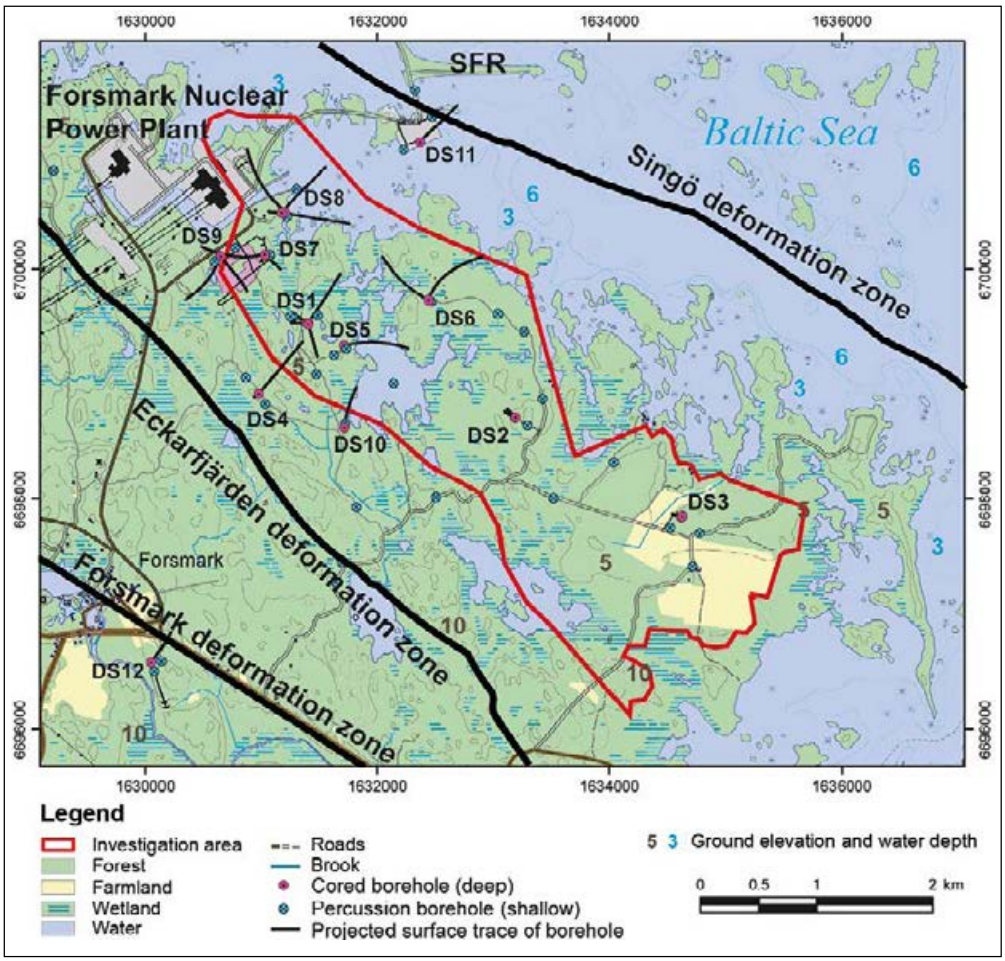

Figure 2-1. *Investigation area, regional deformation zones and bedrock boreholes drilled during the site characterisation for SDM-Site. DS = drill site (Figure 1 in Follin and Hartley 2014).*

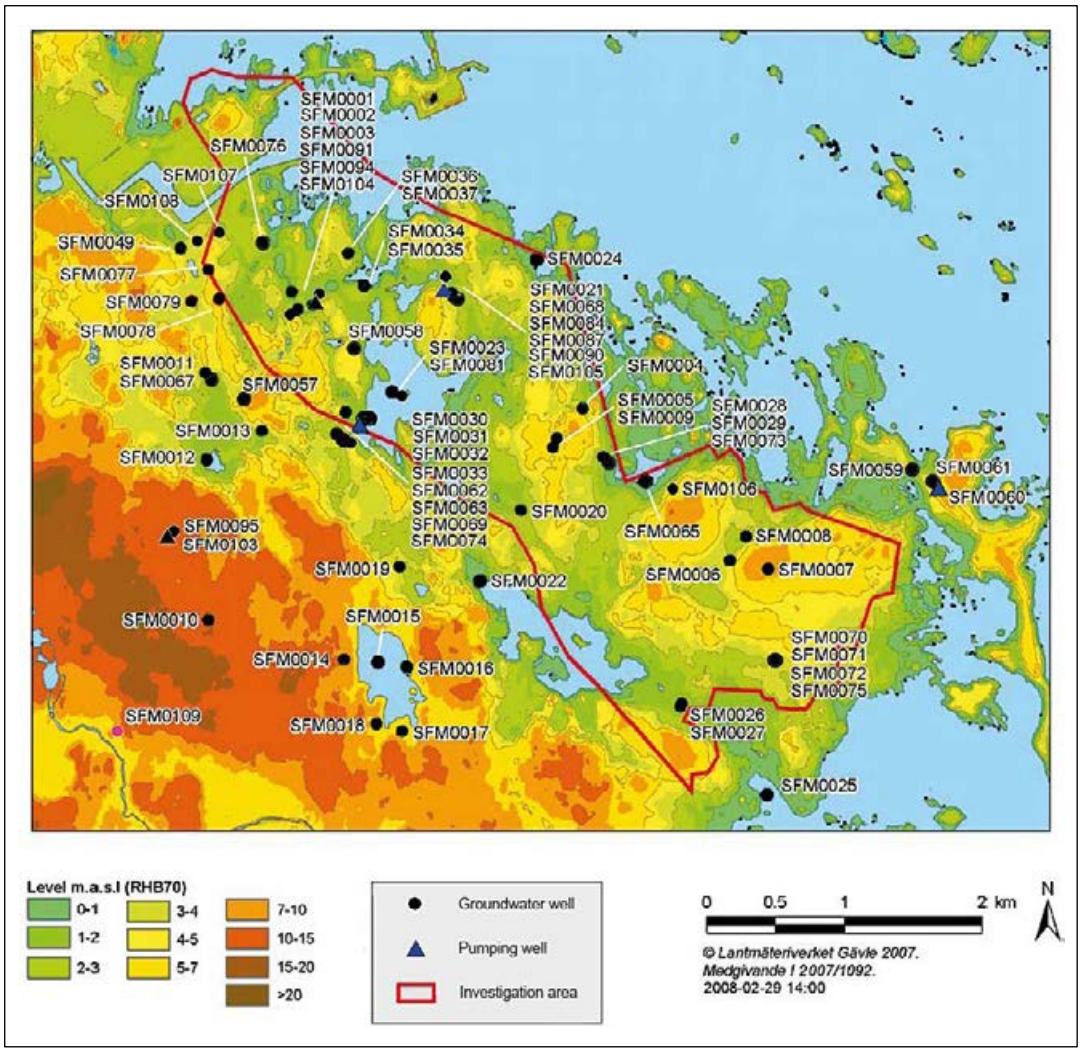

Figure 2-2. *Locations of groundwater monitoring wells in Quaternary deposits. (Modified after Figure 2-31 in Johansson and Öhman 2008.)*

In addition to results from regular borehole measurements in cored and percussion holes, such as borehole logging and core logging, investigations in these boreholes have provided information from, for example, *in-situ* formation factor logging (used as input to modelling of bedrock transport parameters), groundwater flow measurements, cross-hole interference tests and investigations of rock matrix porewater. Overcoring stress measurements, hydraulic fracturing data, hydraulic tests on pre-existing fractures and studies of borehole breakouts and other types of fallout structures from borehole walls have been acquired in several of the boreholes. Furthermore, data from several types of laboratory investigations carried out on samples of rock material from these boreholes are included in the database, including intact rock. The groundwater monitoring wells have provided time-series data on groundwater levels and water chemistry, as well as information on the stratigraphy of the Quaternary deposits in the area. Groundwater level time-series data have been acquired also in cored and percussion boreholes equipped with multi packers.

2.2 Surface system

2.2.1 Topography and regolith geology

The landscape in Forsmark is relatively flat. The most elevated areas (Figure 2-2) are located at ca 25 m above current sea level. Despite the modest topography, the upper surface of the bedrock is found to undulate over small distances implying large variations in the thickness of the Quaternary cover with till as the dominant deposit, especially in the terrestrial part (Figure 2-3). Glacial clay and clay gyttja are predominantly found in the deeper parts of valleys on the sea floor and only minor occurrences have been documented in the terrestrial area. Postglacial gravel and sand frequently superimpose glacial clay. These deposits are interpreted to mainly represent deposition after erosion and transport by currents on the floor of the Baltic Sea that covered the whole Forsmark area 2 000 years ago. The shoreline is currently regressing due to the ongoing isostatic rebound, and new land areas are continuously getting exposed.

The thickness of the Quaternary deposits is generally larger in the marine area (average ca 8 m) than in the terrestrial part (average ca 4 m). Clay gyttja is frequent in the wetlands located at low altitudes, e.g. along the shores of lakes. Wetlands at higher altitudes are covered by peat. Gyttja is formed in lakes and consists mainly of remnants from plants that have grown in the lakes.

2.2.2 Hydrology and near-surface hydrogeology

The **SDM-Site** dataset comprises data gathered up to the Forsmark 2.3 data freeze (March 31, 2007), including hydrogeological properties of regolith and the rock/regolith interface, meteorological monitoring, monitoring of ice freeze/breakup, and ground- and surface-water level monitoring. This dataset is presented, evaluated and utilised for site-descriptive modelling of hydrology and near-surface hydrogeology by Bosson et al. (2008), Johansson (2008) and Johansson and Öhman (2008).

Figure 2-3 shows an overview map of the surface distribution of the regolith in the Forsmark area. Whereas till is the dominant regolith type in the Forsmark area, the regolith in large part of the access area and its environs consists of artificial fill (Figure 2-4), in particular along the cooling-water canal. The artificial fill, the extent of which is larger in the recently produced map, consists of a mixture of blasted rock and regolith excavated from the sea bottom (Sohlenius and Hedenström 2009). A typical top-to-bottom stratigraphy at lake bottoms is nested layers of gyttja, sand and gravel, and glacial and/or postglacial clay above till (Johansson 2008).

SDM-Site data on the hydraulic conductivity of regolith and the rock-regolith interface are obtained from single-hole (slug) tests and empirical relationships based on PSD (particle-size distribution) curves for regolith samples (Johansson 2008, Hedenström and Sohlenius 2008). The generally assigned horizontal hydraulic conductivity for different types of regolith at the **SDM-Site** modelling stage is summarised in Table 2-1. Hydraulic data show that the vertical hydraulic conductivity of the till at Forsmark is significantly lower than the horizontal hydraulic conductivity.

Table 2-1. Horizontal hydraulic conductivity of the regolith and of the rock-regolith interface according to the general parameterisation of the Forsmark area in SDM-Site (Johansson 2008).

Regolith type	Horizontal hydraulic conductivity (m/s)
Till, depth < 0.6 m	
Fine and coarse	1.5×10^{-5}
Till, depth > 0.6 m	
Fine	1.0×10^{-7}
Coarse	1.5×10^{-6}
Rock/tIll interface	1.5×10^{-5}
Glaciofluvial and postglacial sand (and artificial fill)	1.0×10^{-4}
Glacial clay	
Depth < 0.6 m	1.0×10^{-6}
Depth > 0.6 m	1.5×10^{-8}
Postglacial clay-gyttja/gyttja clay	3.0×10^{-7}

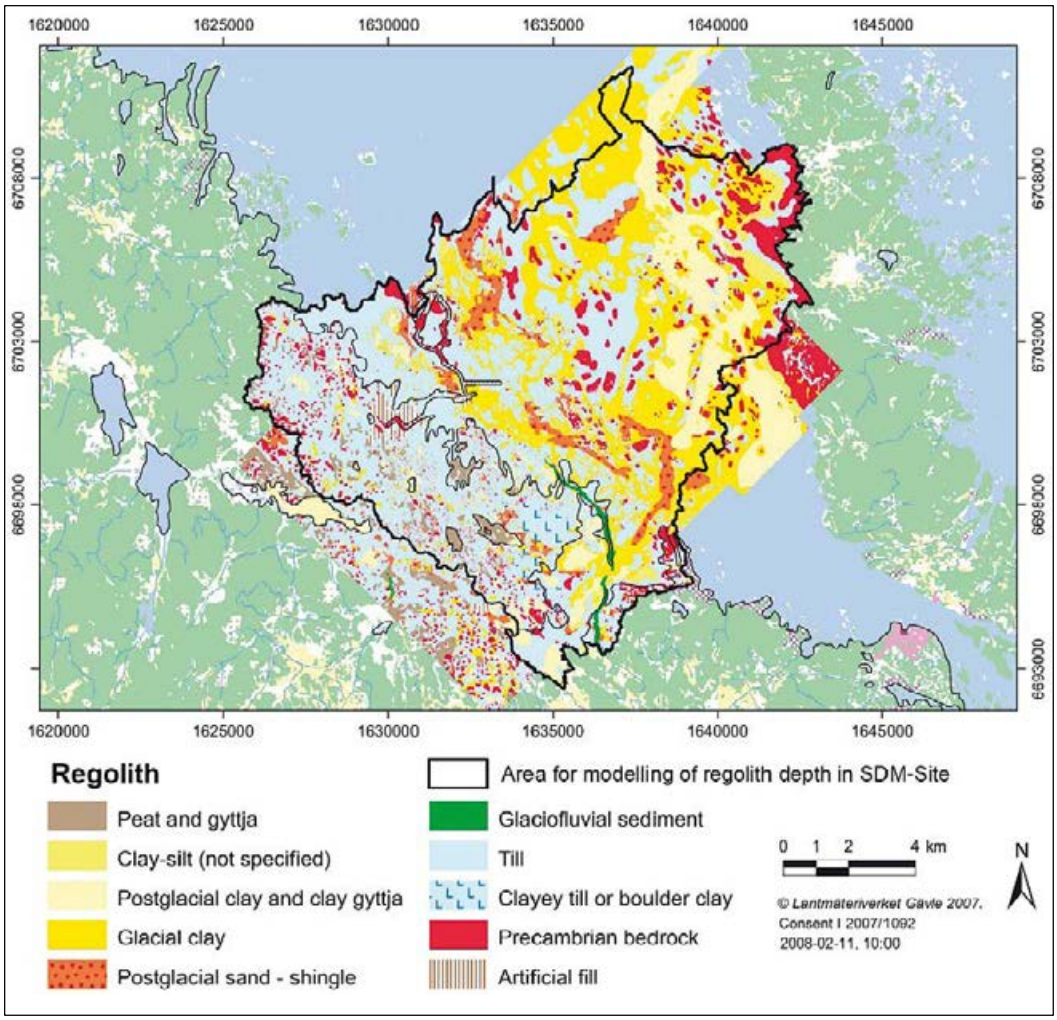

Figure 2-3. *The distribution of regolith in the Forsmark area. The map shows a compilation from several data sources originally presented at various scales. (Modified after Figure 5-10 in Hedenström and Sohlenius 2008.)*

Figure 2-4. *Photograph of artificial-fill profile in a trench (Figure 5-25 in Hedenström and Sohlenius 2008).*

The access area is located in the "Forsmark 1/2 rest catchment area" (Brunberg et al. 2004), which means that the catchment is drained by groundwater discharge and surface runoff directly to the sea. Except for a small lake (Lake Tjärnpussen, see gauge SFM000119 in Figure 3-2) and three small ponds close to the sea shoreline, this catchment does not contain any lakes, streams or other surface waters. As part of **SDM-Site** (Figure 2-5), the components of the long-term, site average annual average water balance were estimated as P (precipitation) = 560 mm/y, E (evapotranspiration) = 400–410 mm/y and R (runoff) = 150–160 mm/y (Johansson 2008). Due to the lack of larger streams, no stream-discharge data are available for the access area.

In general, the groundwater level in regolith closely follows the topography (Figure 2-6), with an observed near-surface groundwater table for most wells and for most of the year (Johansson and Öhman 2008). Two of the wells (SFM0077 and -0107) that demonstrate deviating, large average depths to the groundwater table are located in the vicinity of the access area. Other wells with such deviating, large average depths to the groundwater table include e.g. SFM0059 and -0061, installed in high-conductive glaciofluvial material in the Börstilåsen esker (outside the access area).

An effect of a near-surface groundwater table is rapid responses to precipitation events and evapotranspiration cycles, whereas such responses are notably weaker in wells with larger depths to the groundwater table. The average groundwater table is above sea level (0 m elevation) in all wells, whereas the groundwater table is below sea level in some wells during dry periods (Johansson 2008). Another implication of groundwater levels being close to the ground surface is that water divides for near-surface groundwater flow likely coincide with surface-water divides. The near-surface groundwater flow system is hence a "replica" of the topography, with a general horizontal gradient from inland areas towards the sea.

Based on the data available at time of **SDM-Site**, it was concluded that there are no or small correlations between groundwater levels in regolith and the sea level. It has been observed that sea-water intrusion may occur into low-lying lakes close to the coastline, e.g. during storm events. The lakes at Forsmark are shallow, with maximum depths in the range 0.4 to 2 m. Monitoring of surface-water levels in lakes and groundwater levels in regolith below and in the vicinity of a number of lakes in the Forsmark area show that groundwater-surface water gradients generally are small and temporally variable. Data show that lakes may act as recharge sources to underlying regolith in the riparian zone during dry summer periods, due to water losses by evapotranspiration (Johansson 2008). Elsewhere, lake sediments and underlying till have low vertical hydraulic conductivities, as indicated by level relationships and the presence of relict marine chemical signatures beneath the lakes.

Inside the so-called tectonic lens (see Section 2.3.1), horizontal hydraulic gradients in the upper part of the bedrock are small and groundwater levels are below groundwater levels in regolith, hence indicating groundwater flow from regolith to rock. This suggests that local, small-scale recharge and discharge areas, involving groundwater flow systems in the regolith, overlie larger-scale flow systems associated with groundwater flow in the rock. On the other hand, groundwater levels in regolith are below groundwater levels in the upper part of the bedrock outside the lens.

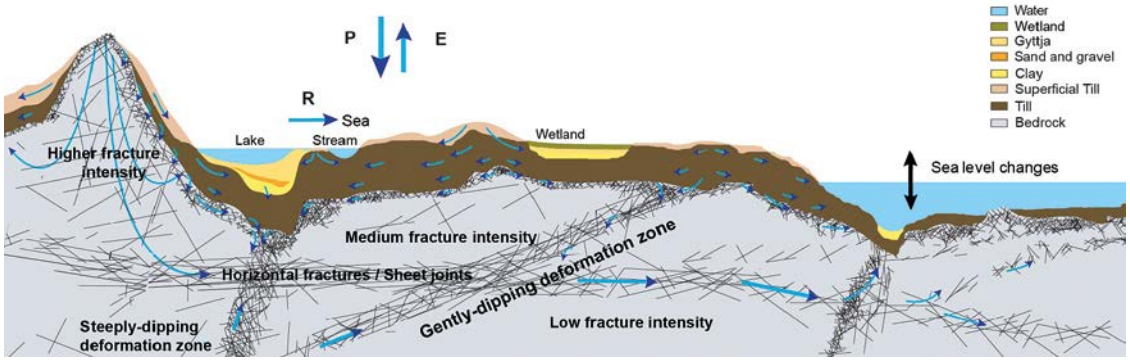

Figure 2-5. *Cross-section cartoon illustrating regolith and the upper ca 150 m of the rock. P = precipitation, E = evapotranspiration, and R = runoff. (Modified after Figure 3-1 in Johansson 2008.)*

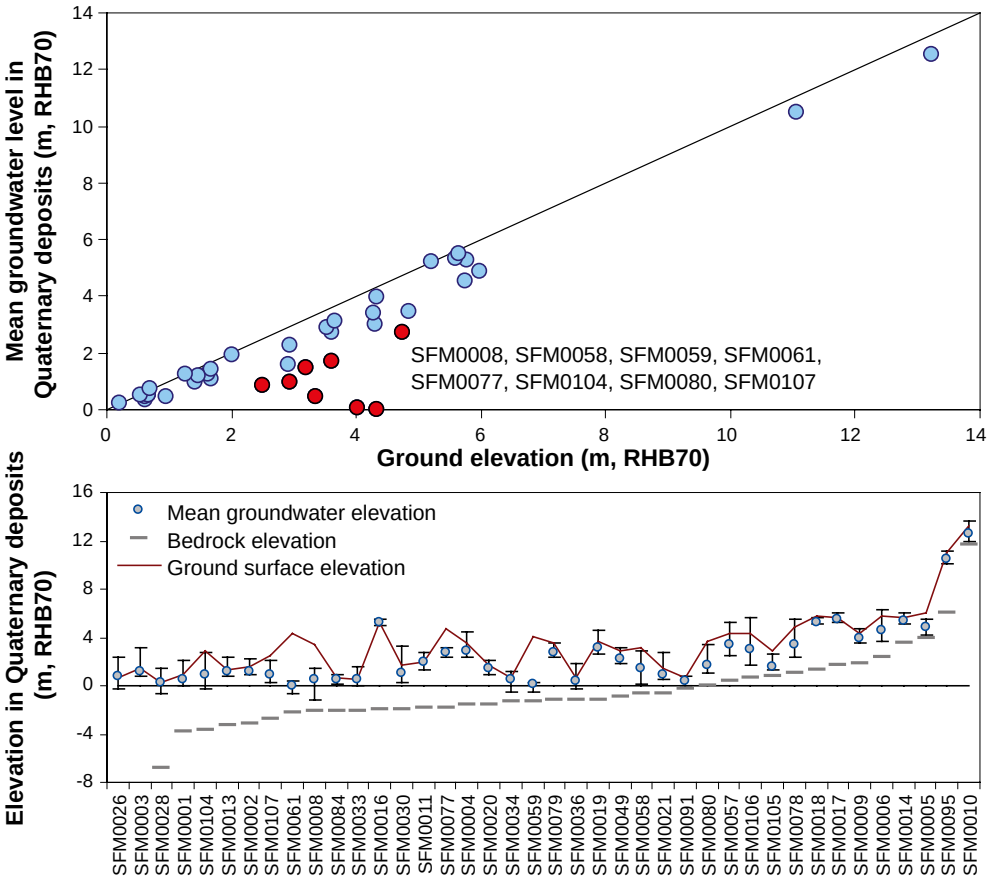

Figure 2-6. *Upper plot: cross plot of average groundwater levels in monitoring wells installed in regolith versus ground-surface elevation. Lower plot: average groundwater levels, local ground-surface elevations and rock-surface elevations, ranked according to rock-surface elevation. (Figure 3-40 and Figure 3-41 in Johansson 2008.)*

In the tectonic lens, well-connected and flowing sub-horizontal, or gently dipping, structures, including sheet joints, in the upper part of the bedrock may be in hydraulic contact with the sea, either directly or, more likely, indirectly via steeply dipping deformation zones that outcrop below the sea (Follin et al. 2007a, Johansson 2008). The sea level may hence act as a "drain" boundary condition resulting in low groundwater levels in the uppermost part of the bedrock with little or no correlation to the local topography (Figure 2-7).

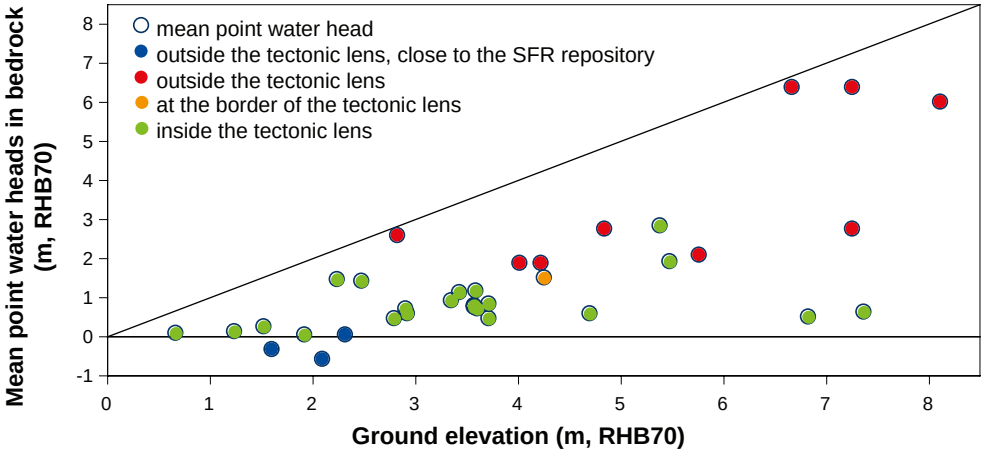

Figure 2-7. *Cross plot of average groundwater levels (interpreted as so-called point-water heads) in the uppermost borehole sections of percussion-drilled boreholes versus ground-surface elevations (Figure 3-47 in Johansson 2008).*

2.2.3 Near-surface hydrochemistry

The till and the glacial clay are rich in calcium carbonate originating from Palaeozoic limestone that outcrops on the sea floor north of the Forsmark area. This, together with the recent emergence of the area above sea level, affects the chemistry of both surface water and shallow groundwater, giving rise to high pH, high alkalinity and high contents of major constituents such as calcium, sodium, chloride and bicarbonate. Furthermore, the surface waters are high in nitrogen and low in phosphorous.

Interpretation of hydrochemical data from surface water and groundwater in Quaternary deposits supports the hydrological evaluation that discharge of deep saline groundwater occurs outside the target area in the lakes that lie along the outcrop lineament of the regional Eckarfjärden deformation zone (Figure 1-1). The discharge of more saline deep groundwater outside the target area is supported by the results of the groundwater flow modelling which predicts discharge of deep saline groundwater at these locations.

2.2.4 Surface system transport properties

Site data from hydrochemical monitoring and chemical characterisation of regolith and biota are processed and delivered as input to calculations of parameters for radionuclide transport modelling in safety assessments. These data constitute the site-specific input to parametrisation processes where site data are combined with literature data to obtain parameters for all radionuclides and environmental conditions to be covered in the safety assessment calculations. Specifically, surface system transport properties are expressed in terms of radionuclide model parameters calculated as element-specific concentration ratios (denoted CR) and solid/liquid distribution coefficients (K_d). These parameters express a variety of equilibrium mass distributions between different combinations of abiotic and biotic components of the surface ecosystems (e.g. Nordén et al. 2010).

The parametrisation activities providing CR- and K_d-values have been carried out entirely within the safety assessments, and no site-descriptive models of surface system transport properties/parameters have been presented in **SDM-Site** or **SDM-PSU**. However, site data and site understanding are important both for the description of present conditions and for the analyses presenting parameters that represent future conditions and radionuclides presently not existing at the site.

As indicated in preceding sections, the geochemical and hydrochemical conditions in the surface and near-surface systems at Forsmark show some special features, which can be expected to have implications also for transport parameters quantified as concentration ratios measured in or otherwise taken to represent these systems. In the evaluations performed to provide input data to the **SR-Site** and **SR-PSU** safety assessments (Tröjbom and Nordén (2010) and Tröjbom et al. (2013), respectively), Forsmark was compared to the Laxemar site, with Laxemar representing more typical Swedish conditions. In the long-term perspective of the safety assessment, the conditions at Forsmark are expected to approach those currently prevailing at Laxemar.

Many elements, materials and environmental conditions must be represented in the dataset to cover the needs of the safety assessment modelling. Therefore, the final safety assessment datasets consist of large numbers of parameters representing all relevant combinations. For example, approximately 2 000 K_d and CR parameter values were derived for the **SR-PSU** assessment. Tröjbom et al. (2013) present these parameters and provide extensive analyses of the site data from Forsmark and how they compare to data from SKB investigations at Laxemar and available literature data. K_d values and their relations to parameters known to affect solid/liquid partitioning were investigated by Sheppard et al. (2009, 2011). The results show relatively large variations among and within data for individual regolith types and emphasise the importance of pH for K_d values.

2.2.5 Ecology and land use

The location close to the sea makes the seashore a prominent feature in the east along with conifer forests, shallow lakes, mires and some agricultural land. The terrestrial vegetation is strongly influenced by the characteristics of the Quaternary deposits and by human land use. Forests cover 73 % of the land area in Forsmark and wetlands occur frequently, whereas agricultural use covers less than 5 % of the land area and is mainly located in the south-eastern part of the investigation area (Figure 1-1). The lakes are all shallow and classified as oligotrophic hardwater lakes, i.e. they contain high calcium

levels, but low levels of nutrients, as phosphorus is precipitated together with the calcium. These characteristics have a strong impact on the limnic ecosystems. The marine ecosystem in the Forsmark area is relatively productive in a region of otherwise fairly low primary production.

2.3 Bedrock system

2.3.1 Tectonic lens

Borehole data support the conceptual model that the investigation area (Figure 2-1) is situated more or less exclusively inside a tectonic lens, which is defined by very strong planar deformation at the rims and linear and planar deformation in its inner part (Figure 2-8). The lens can be traced from the surface to at least ca 1 000 m depth. Folding of an older ductile fabric and a generally lower degree of ductile strain are inferred to be present inside the lens. By contrast, the rocks that surround the lens are inferred to be affected by a generally higher degree of ductile strain and a conspicuous WNW to NW structural grain. This regional-scale anisotropy in the character and degree of ductile strain at Forsmark, which was established at an early stage in the geological evolution in the high-temperature ductile regime, has important implications for an understanding of the spatial distribution of younger deformation zones at the site.

The lithology is divided into four groups; A to D (Figure 2-9). The different rock types are distinguished on the basis of their composition, grain size and relative age. Rhyolitic to dacitic meta-volcanic rocks (Group A) are the oldest (> 1.89 Ga). The meta-intrusive rocks were formed 1.89–1.86 Ga (Group B) and 1.86–1.85 Ga (Groups C and D; Hermanson et al. 2007, 2008, Stephens et al. 2008). The granite to granodiorite that belongs to Group B, which dominate the access area, consists of meta-granitoid rocks, and subordinate ultrabasic, basic and intermediate rocks. The rocks in the subordinate Groups C and D consist solely of granitoids that show a lower degree of metamorphism.

Groups A and B have been subjected to a protracted ductile deformational history, with the development of a penetrative fabric under amphibolite-facies conditions between 1.87 and 1.86 Ga, and folding (Hermanson et al. 2007, 2008, Stephens et al. 2008). Group B and Groups C–D have been distinguished primarily on the basis of their relationships to the penetrative ductile deformation in the area (Stephens et al. 2008). Group B was affected by folding evident in penetrative, ductile foliation and lineation, whereas Groups C and D intruded during the later stages or after the development of the ductile fabric and generally shows a linear or a poorly developed fabric.

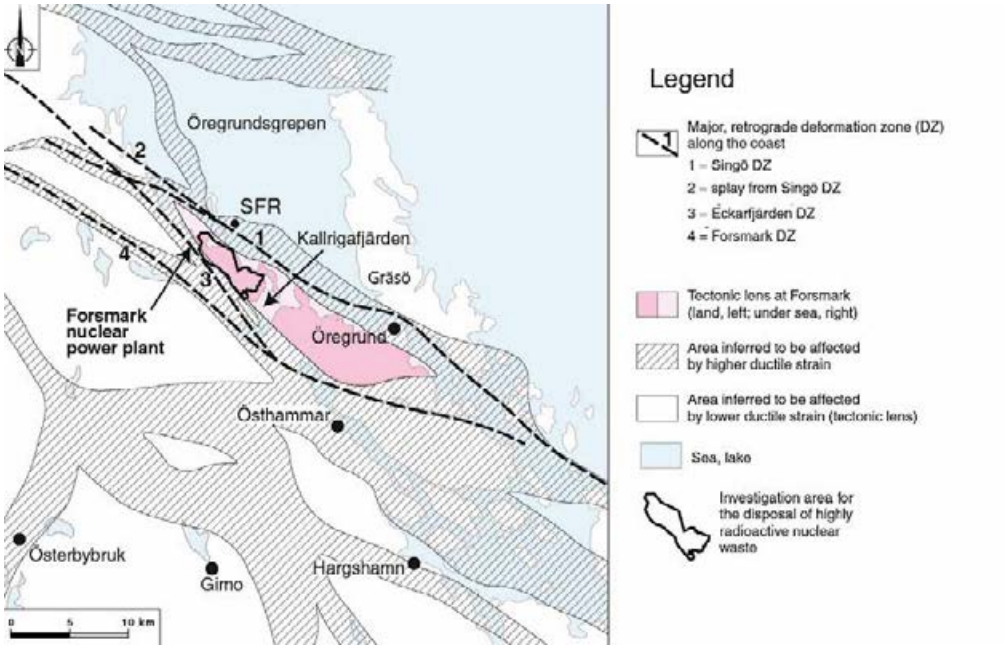

Figure 2-8. *Tectonic lens at Forsmark and areas affected by strong ductile deformation in the area close to Forsmark. Coordinate system: RT90. (Modified after Figure 4-1 in Stephens et al. 2007.)*

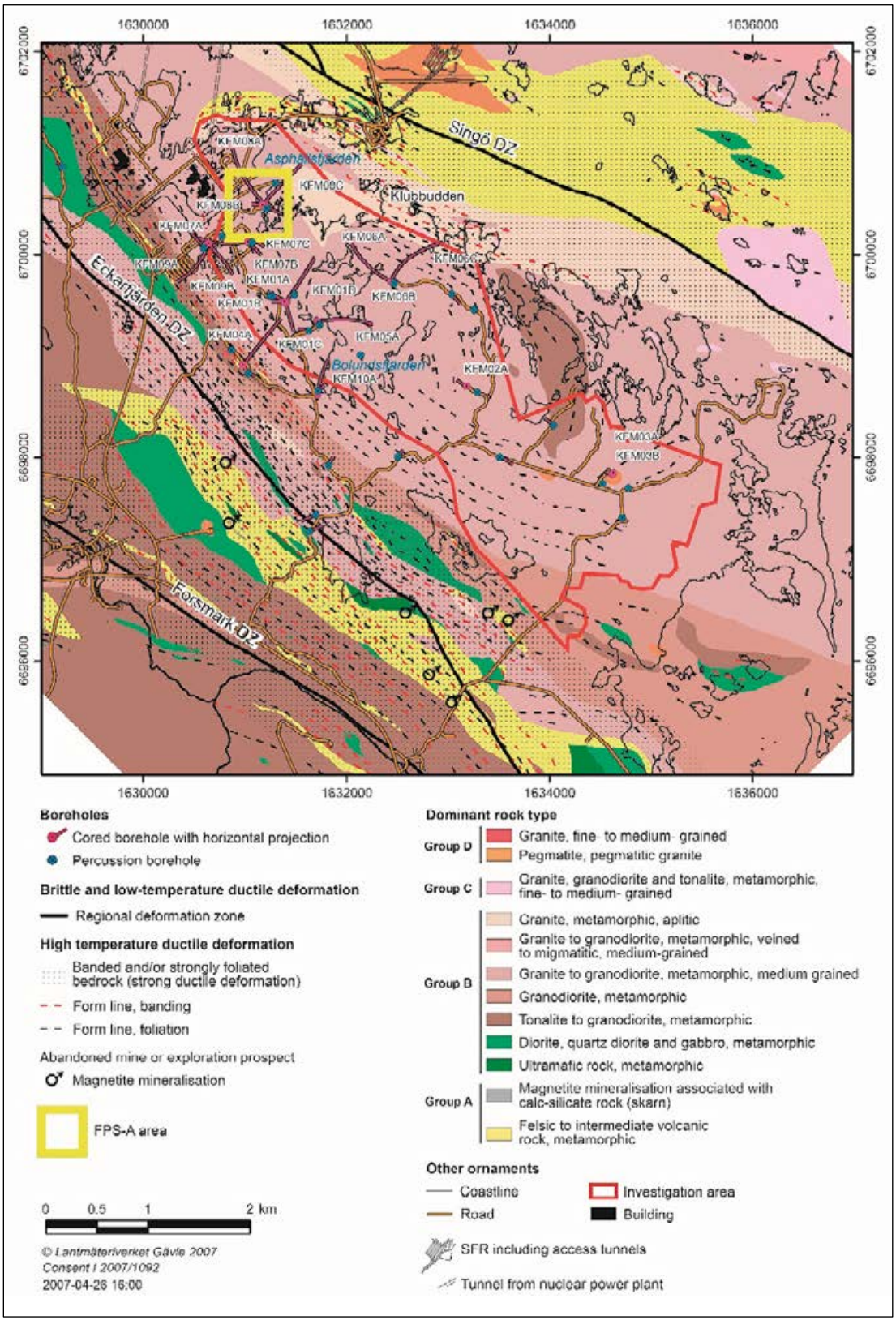

Figure 2-9. *Geological map of the Forsmark area. Major regional deformation zones are shown with solid black lines. The coordinate system is RT90. (Modified after Figure 5-2 in SKB 2008.)*

2.3.2 Rock domains

Due to its internal homogeneity, most of the tectonic lens and, in particular, the north-western part can be described as two rock domains referred to as RFM029 and RFM045 (Figure 2-10). These are also the two domains that define the bedrock in the target volume. On a larger scale the differences between RFM029 and RFM045 are minute. On a regional scale, RFM029 and RFM045 are sometimes referred to as a single rock domain, RFM029R, in **SDM-Site**.

The dominant rock type in rock domain RFM029 is a medium-grained meta-granite. Subordinate rock types are pegmatitic granite or pegmatite, the group C type fine- to medium-grained meta-granitoid, and amphibolite and other minor mafic to intermediate rock types, which occur as minor bodies or lenses and dyke-like sheets (Stephens et al. 2007). With the exception of amphibolite that contains little or no quartz, the dominant and the subordinate rock types have high quartz content. Linear structures, with both folding and stretching that plunge moderately to the SSE and SE, respectively, are apparent in domain RFM029 (Figure 2-11).

Rock domain RFM045 is dominated by group B rocks aplitic meta-granite and the same type of meta-granite as in RFM029. The main difference between RFM029 and RFM045 is that the latter has been subjected to Na-K alteration, so-called albitisation (Stephens et al. 2007). An albitisation process is prevalent in the meta-granites, which increases the quartz content and decreases the K-feldspar content (Stephens et al. 2007). Subordinate rock types include pegmatite and pegmatitic granite, fine- to medium-grained meta-granitoid and amphibolite and other minor mafic to intermediate rocks. Rock domain RFM045 is surrounded by rock domain RFM029 in the target volume and has a constricted rod-like geometry that plunges moderately to steeply to the south-east, close to the mineral stretching lineation in this part of the tectonic lens.

Rock domains outside the tectonic lens and target volume dip steeply towards the south-west, following the trend of the coastal deformation belt. They are dominated by different types of granitoid, predominantly felsic volcanic rocks and quartz-poor or quartz-deficient diorite to gabbro, all of which are affected by amphibolite-facies metamorphism. More inhomogeneous bedrock is conspicuous in rock domains on both sides of the tectonic lens, i.e. towards southwest and northeast, respectively. For instance, the predominantly felsic meta-volcanic rocks found to the northeast of the tectonic lens and the target volume contain abundant pegmatite and pegmatitic granite.

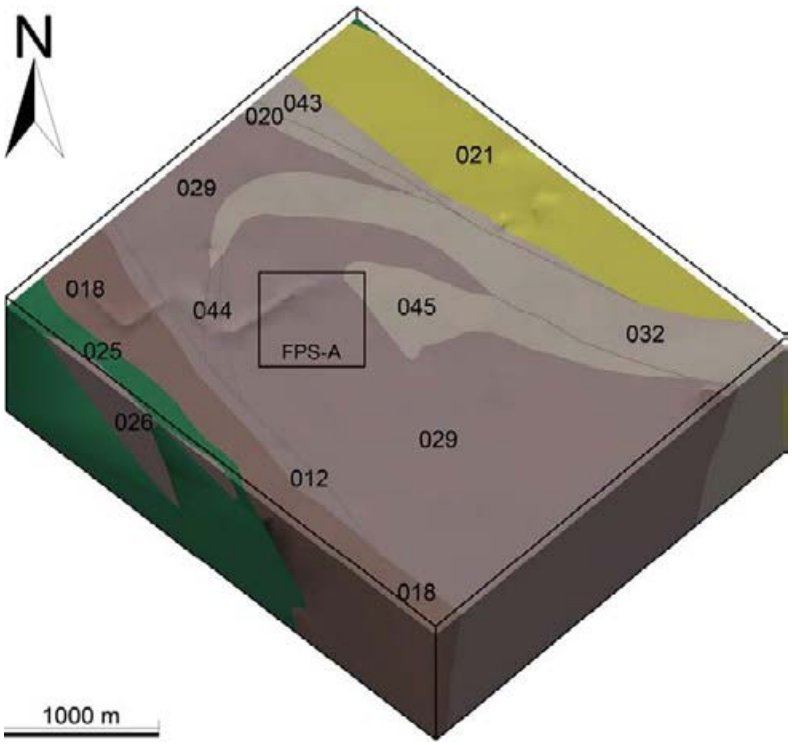

Figure 2-10. *SDM-Site Rock Domain model. The location of the access area presented in Chapter 3 is indicated by the black rectangle.*

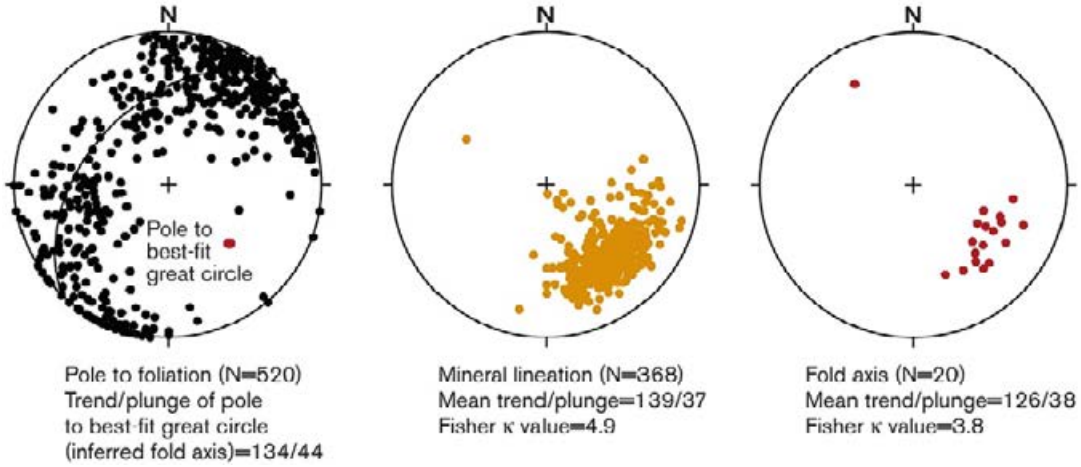

Figure 2-11. *Foliation and lineation measurements displayed in stereonets (lower hemisphere) supporting folding within the Forsmark tectonic lens. (Modified after Figure 5-8 in SKB 2008.)*

2.3.3 Mineral resources

The ore potential in the coastal area in northern Uppland is correlated to the rock types and their characteristics. An assessment of the ore potential came to the conclusion that there is no potential for metallic and industrial mineral deposits within the investigation area (Lindroos et al. 2004).

2.3.4 Thermal properties

Lithology affects the thermal properties of the bedrock i.e. thermal conductivity, heat capacity and thermal expansion, since these properties depend on the mineral composition. The thermal conductivity of the bedrock has been assessed from direct measurements and by calculations based on mineral composition from modal analyses. The heat capacity has been determined from calorimetric measurements and also indirectly from measurements of thermal conductivity and diffusivity. The assessment of thermal expansion is based on results from measurements on samples from five different rock types, including the dominant rock types in RFM029 and RFM045, but not the subordinate rock type amphibolite.

Measurements of thermal conductivity at the cm-scale for the dominant medium-grained meta-granite in rock domain RFM029 show values in the range 3.2 to 4 W/(m·K). The altered granitic rocks that dominate in rock domain RFM045 also have high thermal conductivity, with measured values in the range 3.6 to 4 W/(m·K). However, subordinate rock types in these rock domains yield significantly lower values, e.g. amphibolite in the range 2.2 to 2.5 W/(m·K).

The mean value of the heat capacity assessed from measurements and from calculated thermal conductivity is 2.1 MJ/(m^3·K), both in rock domain RFM029 and RFM045. This value is valid at a temperature of 20 °C. The in-situ temperature constitutes the initial temperature condition for a repository. The current mean temperature at 500 m depth is estimated to be 11.6 °C, based on measurements in eight boreholes (cf Figure 4-9b in Follin 2008).

The mean value of the measured thermal expansion coefficient for the dominant medium-grained meta-granite in RFM029 is $7.7 \cdot 10^{-6}$ m/(m·K), and the corresponding value for the altered meta-granite, which dominates in RFM045, is $7.5 \cdot 10^{-6}$ m/(m·K).

2.3.5 Mechanical properties of intact (nonfractured) rock

The mechanical strength and deformation properties of the bedrock are evaluated from results of measurements on samples from the dominant rock types in RFM029 and RFM045, and also from the subordinate rock type pegmatite. The uniaxial compressive strength (UCS) and Young's Modulus (E) of the intact rock show that the rock types in rock domains RFM029 and RFM045 are strong (UCS > 200 MPa) and stiff (E > 70 GPa). The results for samples taken inside or in the vicinity of deformation zones are in the same range as the results for samples taken in the host rock outside deformation zones.

2.3.6 Deformation zones

Four sets of deformation zones have been identified with high confidence. Vertical and steeply, SW-dipping zones with subsets referred to as WNW and NW show complex, ductile and brittle deformation. Regional zones longer than 10 km that occur outside the investigation area (e.g. the Forsmark, Singö and Eckarfjärden deformation zones shown in Figure 2-1) are restricted to this set. The deformation zones in the remaining three sets only display brittle deformation and can be referred to as fracture zones. Vertical and steeply dipping fracture zones with sub-sets referred to as ENE (NE) and NNE transect the tectonic lens and occur frequently inside the target volume. These zones formed in the brittle regime and are dominated by sealed fractures and sealed fracture networks. Gently dipping fracture zones occur more frequently in the south-eastern part of the investigation area, i.e. outside the target volume. Relative to the other three sets, there is an increased frequency of open fractures, including crush zones, along the gently dipping set. The fourth set consists of vertical and steeply dipping fracture zones referred to as NNW that are dominated again by sealed fractures. On the basis of their low frequency of occurrence, these are judged to be of lower significance relative to the other three sets of zones.

The bedrock in close proximity of the target volume includes sixty-seven deterministically modelled deformation zones. More than 70 % of these zones have been confirmed directly by geological data from borehole or tunnel intersections, or from outcrop observations, and are not identified solely on the basis of indirect geophysical data (e.g. a lineament defined by magnetic minima or a seismic reflector). Only two steeply dipping zones with a surface trace length longer than 3 000 m intersect the target volume (zones ENE0060A and ENE0062A with their attached branches) and a further twenty-nine steeply dipping zones, which either show a trace length at the ground surface between 1 000 and 3 000 m or form minor splays or attached branches to such zones, are present at 400 to 600 m depth inside the potential target volume. Five gently dipping zones, including zones A2 and F1, are also present at 400 to 600 m depth inside or immediately above the target volume.

In general, the zones in the target volume can be characterised as having a transition zone that contains a higher frequency of sealed and open fractures and more hydrothermal alteration than the host rock outside the zone, but also segments that resemble the unaffected host rock. Fault cores, recognised in more than 50 % of all the zones studied in drill cores in the area, are predominantly composed of a sealed fracture network in combination with rock alteration and, locally, cohesive breccia or cataclasite. Fault gouge has not been recognised along the fracture zones.

Inspection of the target volume shows a clear dominance of vertical or steeply dipping, brittle deformation zones with ENE-WSW, NNE-SSW or NE-SW strike, sandwiched between more regionally significant, composite ductile and brittle deformation zones occurring along both the north-eastern and south-western sides of the local model block (Figure 2-12). The more regionally significant zones are vertical or steeply dipping and strike WNW-ESE or NW-SE. Only a few gently dipping, brittle deformation zones are present inside the **SDM-Site** local model volume. Although the gently dipping zones ZFMA2 and ZFMA8 are conspicuous in the south-eastern part of the local model in the near-surface realm (Figure 2-12), gently dipping zones are of little significance at −470 m elevation, corresponding to the depth chosen for the planned repository (Figure 2-13). Indeed, most of the gently dipping brittle deformation zones occur to the south-east of and outside the local model volume. The importance of the vertical or steeply dipping, ENE-WSW, NNE-SSW and NE-SW sub-sets of brittle deformation zones at −470 m elevation inside the selected area for the repository is highly conspicuous (Figure 2-13).

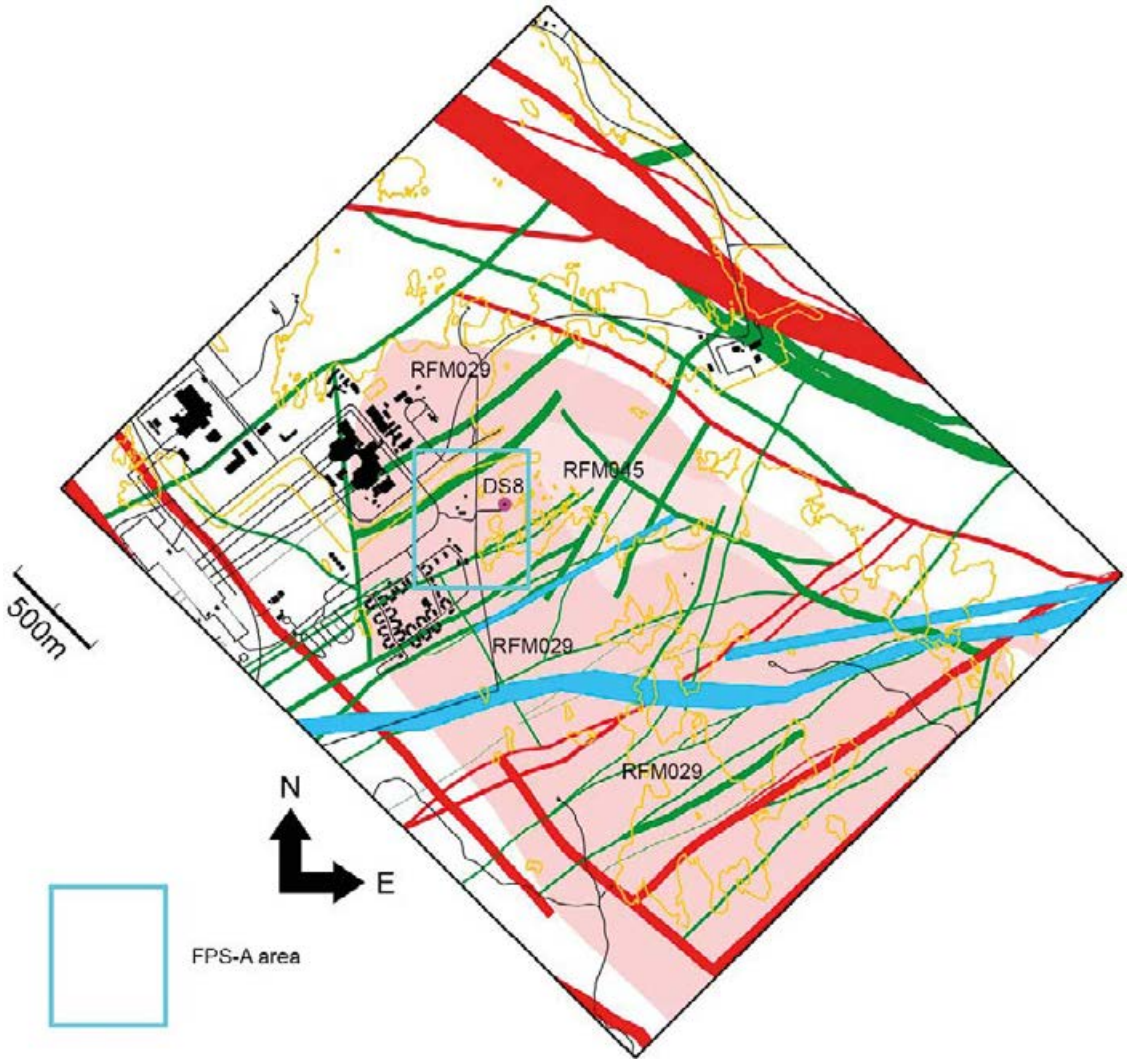

Figure 2-12. *Two-dimensional model at ground surface for deformation zones inside a local block model domain surrounding the target volume. Zones marked in red are vertical or steeply dipping and have a trace length at the surface longer than 3 000 m. Zones marked in green are vertical or steeply dipping and are less than 3 000 m in length. Zones marked in blue are gently dipping to the south and south–east. The locations of drill site 8 (DS8) and rock domains RFM029 and RFM045 are highlighted. (Modified after Figure 5-2 in Stephens and Simeonov 2015.)*

Figure 2-13. *Two-dimensional model at –470 m elevation for deformation zones inside a local block model domain surrounding the target volume. Zones marked in red are vertical or steeply dipping and have a trace length at the surface longer than 3000 m. Zones marked in green are vertical or steeply dipping and are less than 3000 m in length. Zones marked in blue are gently dipping to the south and south–east. The locations of drill site 8 (DS8) and rock domains RFM029 and RFM045 are highlighted. (Modified after Figure 5-3 in Stephens and Simeonov 2015.)*

2.3.7 Fracture domains

Based on a systematic assessment of the variation in the frequency of fractures with depth along each borehole, the bedrock between deterministically modelled deformation zones has been divided into six fracture domains referred to as FFM01–FFM06. Thus, fracture domains and deterministically modelled deformation zones are mutually exclusive volumes, whereas rock domains contain both fracture domains and deterministically modelled deformation zones. Fracture domains FFM01–03 and FFM06 all lie inside the investigation area shown in Figure 2-1, whereas FFM04 and FFM05 lie outside. The target volume lies inside FFM01, FFM02 and FFM06 (Figure 2-14).

Fracture domain FFM01 forms the main component in rock domain RFM029 at depth in the target volume, north-west of and in the footwall of the gently dipping zone ZFMA2 (Figure 2-14) at a depth that varies from ca −40 m elevation close to drill site 8 (large distance from ZFMA2) to greater than ca −200 m elevation close to ZFMA2. Fracture domain FFM01 shows a decreasing frequency of open and partly open fractures with depth.

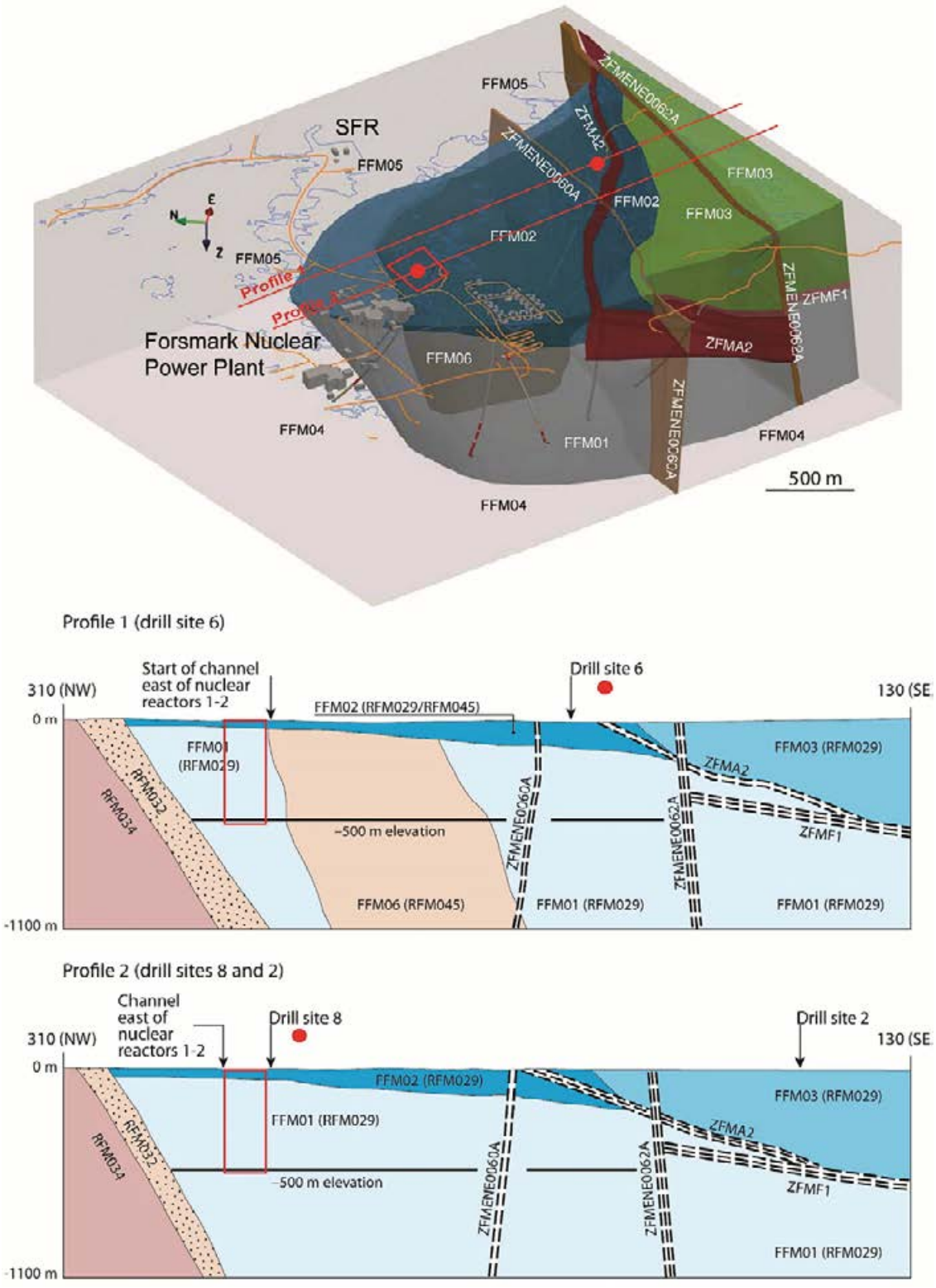

Figure 2-14. *View to the ENE (upper) and vertical profiles in a NW–SE direction (middle and lower) showing the fracture domains and their relation to the gently dipping deformation zones ZFMA2 and ZFMF1 and the steeply dipping zones ZFMENE0060A and ZFMENE0062A that are longer than 3 000 m. The red dots approximately show the locations of drill sites 6 and 8 and the red rectangles indicate the access volume. (Modified after Figures 5-1 and 5-4 in Olofsson et al. 2007.)*

Fracture domain FFM02 comprises the bedrock close to the surface, above fracture domain FFM01, predominantly in the same footwall bedrock segment. Fracture domain FFM02 is located in both rock domains RFM029 and RFM045. Whereas the bedrock in FFM01 shows a low frequency of open and partly open fractures, the bedrock in FFM02 is characterised by a complex network of sub-horizontal or gently dipping, open and partly open fractures, which, locally, merge into minor zones, e.g. at drill site 7 (Figure 2-1). It is apparent that the transition from more fractured bedrock close to the surface (FFM02) to less fractured bedrock at depth (FFM01) takes place deeper down as the distance from zone ZFMA2 decreases (Figure 2-14).

Thus, the character of fracture domain FFM02 is not solely determined by elevation. The occurrence of this domain at greater depths beneath ZFMA2 at drill sites 1, 5 and 6, and even above this zone at or close to drill sites 5 and 6, is related to an inferred higher frequency of older fractures in the vicinity of this zone, to higher rock stresses around zone ZFMA2, or to a combination of these two possibilities. The gently dipping and sub-horizontal fractures are oriented at a large angle to the present-day minimum (vertical) principal stress in the bedrock. This relationship favours the reactivation of older fractures as extensional joints, the development of new sheet joints following the glacial rebound and the development of conspicuous apertures along fractures in the present stress regime. These structural developments all contribute to a general release of the high stress in the bedrock.

Fracture domain FFM06 is defined in the target volume (Figure 2-14). In the same manner as fracture domain FFM01, FFM06 lies beneath FFM02. It forms the main component in rock domain RFM045 (Figure 2-12 and Figure 2-13) and was distinguished from FFM01 simply on the basis of the widespread occurrence of fine-grained, altered (albitised) granitic rock, with slightly higher contents of quartz compared with unaltered granitic rock.

The bedrock south-east of the target volume, in the hanging wall of zone A2, is defined as fracture domain FFM03. It is mainly situated in rock domain RFM029. Open and partly open fractures in this domain are more evenly distributed down to 1 000 m depth and the domain is spatially associated with a high frequency of gently dipping fracture zones containing both open and sealed fractures.

Fractures and minor fracture zones, not covered by the deformation zone model, are handled in a statistical way in **SDM-Site** by means of discrete fracture network (DFN) modelling. The geological DFN model captures all fractures (open, partly open and sealed), since the sealed fractures are also assumed to be potential planes of weakness and could possibly form flow channels in a future stressed regime. However, many of the sealed fractures are mechanically and hydrogeologically indistinguishable from the intact rock.

Geological DFN models are produced for each fracture domain in the target volume, i.e. FFM01, FFM02 and FFM06, and for FFM03. Fracture size and intensity are evaluated from fracture trace length data observed on outcrops, data derived from the interpretation of magnetic lineaments, data derived from the lengths of deterministically modelled deformation zones, and from fracture frequency data observed in boreholes.

In contrast, the hydrogeological DFN models (see Table 2-2) are evaluated from the frequency and properties of open, partly open and flowing fractures measured in cored boreholes solely. Thus, the hydrogeological DFN model avoids fracture traces mapped on outcrops and does not make use of the intensity of large-scale lineaments and deformation zones. Furthermore, the hydrogeological fracture size distribution and intensity vary in space depending on fracture domains and dept. The spatial variation in intensity is inferred by means of connectivity analyses (Follin 2008, Follin et al. 2014). The geological and hydrogeological DFN models derived for **SDM-Site** are both presented as stochastic descriptions of disk-shaped fractures with radii up to 564 m.

2.3.8 Fracture mineralogy

Detailed studies of fracture mineralogy and wall rock alteration have provided information on the character and frequency of fracture minerals at Forsmark. Calcite and chlorite, partly associated with corrensite, are by far the most common minerals. Other common minerals are laumontite, adularia, quartz, albite and hematite, whereas prehnite, pyrite, clay minerals and epidote are less common. Rare occurrences of e.g. asphaltite and goethite are also observed.

The older generations of minerals, including epidote, which formed prior to 1.1 Ga, and adularia, which formed about 1.1 Ga or is older, show no depth dependence. In a similar manner, the wall-rock alteration associated with these mineral generations and referred to as oxidation also shows no depth dependence. These features are consistent with the conclusion that these minerals and the associated alteration formed a long time ago when this part of the bedrock was situated at considerably greater depths. The younger mineral asphaltite, which probably formed between ca 500 and 250 million years ago, occurs almost entirely in the upper part of the bedrock along open fractures. This is also the case for clay minerals and goethite that belong to the youngest generation of minerals, except for some occurrences at larger depths along fractures in zones. Since the current bedrock surface is similar to the sub-Cambrian peneplain, this distribution of fracture minerals with depth suggests that the near-surface bedrock, i.e. including fracture domain FFM02 in the target volume, has been affected by near-surface processes inferred to be related to loading and unloading cycles during the last ca 500 million years.

Fractures without mineral coating or filling have been observed in the near-surface realm in the bedrock but are also present at greater depths. The significance and origin of these fractures are still uncertain. However, errors in the mapping procedure, the possibility that at least some of these fractures formed after the establishment of the sub-Cambrian unconformity and the occurrence of fresh, stress-release sheet joints in the near-surface realm merit consideration in any complementary investigation. Fractures without minerals are predominantly, but not exclusively sub-horizontal or gently dipping. Transmissive variants are present even in fracture domain FFM01.

2.3.9 Mechanical properties of fractures, deformation zones and rock mass

Evaluation of the results from laboratory testing of the mechanical properties of fractures has shown that the deformability and strength properties of open discrete fractures are similar for different fracture sets. Deformation zone mechanical properties have been estimated by means of empirical methods and numerical analysis. The results suggest the properties of open fractures in fracture domain FFM01 and in deformation zones are quite similar. Empirical and numerical analyses of the data show that the deformation modulus and strength properties of the bedrock mass (including fractures) in fracture domains FFM01 and FFM06 are almost equal and representative of a stiff and strong rock.

2.3.10 Rock stress

The assessment of the *in-situ* stress state at the Forsmark site is based on both direct measurements and indirect observations. Data from direct measurements by overcoring, hydraulic fracturing and hydraulic tests on pre-existing fractures are available from a number of boreholes in fracture domains FFM01, FFM02 and FFM03. Indirect observations from boreholes in the same fracture domains include observations of core disking and borehole breakouts in ca 10 km of borehole walls down to depths of 1 000 m. In addition, estimates of the micro-crack porosity in samples from boreholes were used as indirect indicators in the evaluation of stress. Direct measurements as well as indirect observations all indicate a general orientation of the maximum horizontal stress in the range of 120° to 150° (Figure 2-15).

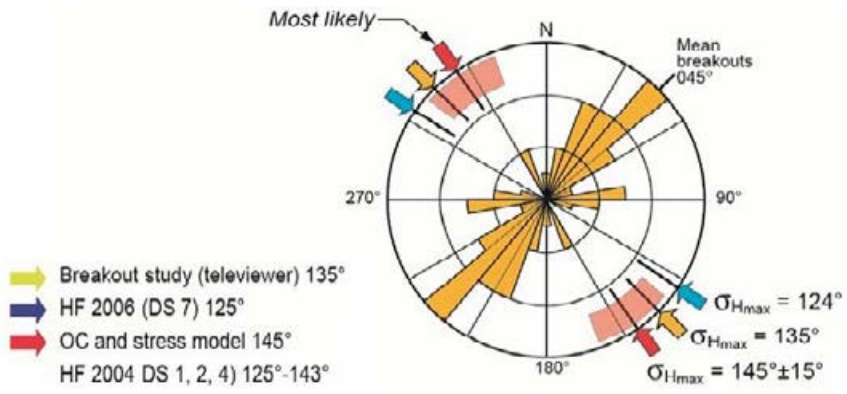

Figure 2-15. *Orientation of maximum horizontal stress from direct measurements by overcoring (OC) and hydraulic fracturing (HF and HTPF), and from indirect observations of borehole breakouts (Figure 11-17 in SKB 2008).*

The stress model for the target volume (Figure 2-16) is developed on the basis of data from over-coring measurements and evaluations of indirect observations, combined with the understanding of the geological conditions at the site and an evaluation of other external influencing factors such as topography, glacial rebound and crustal thickness. As shown by data and supported by findings from regional seismicity studies and the understanding of the deformational history at the site (Stephens et al. 2007), the magnitudes of both the maximum and minimum horizontal stresses are greater than the vertical stress. The stress model implies a most likely value of the maximum horizontal stress of ca 41 MPa (Figure 2-16) and ca 23 MPa for the minimum horizontal stress at 500 m depth in fracture domain FFM01 in the target volume.

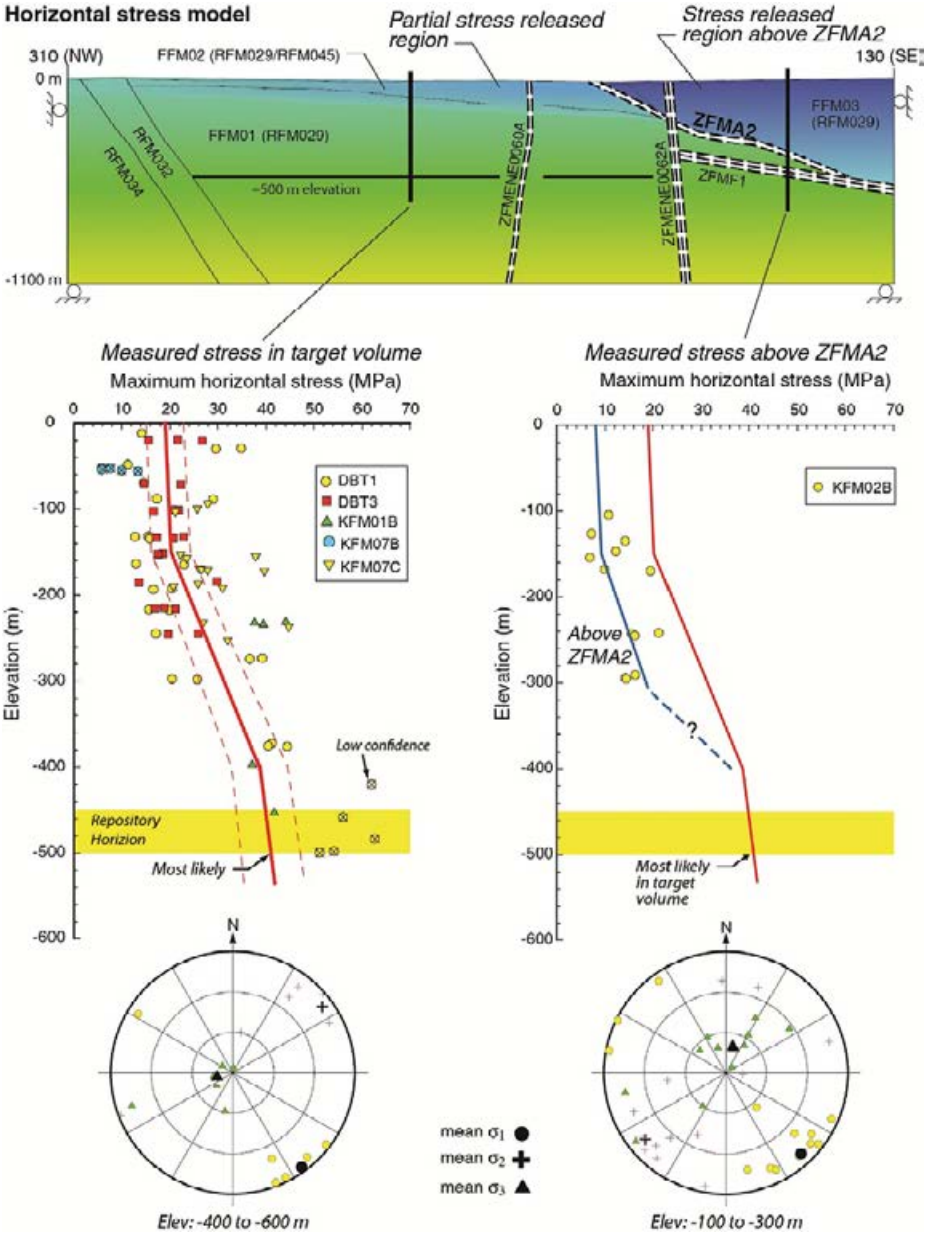

Figure 2-16. *Comparison of the measured maximum horizontal stress magnitudes in the target volume below the gently dipping deformation zone ZFMA2 with those measured above. The change in slope in the target volume at ca 150 m depth corresponds approximately to the boundary between fracture domains FFM02 and FFM01. An illustration of the distribution of maximum horizontal stresses from numerical modelling is also shown (upper insert), with the blue shades representing reduced stress magnitudes caused by stress release above deformation zone ZFMA2 and in fracture domain FFM02 compared with the "normal" stress magnitudes shaded green. The orientations of the measured principal stresses are shown in two lower hemisphere stereonets (lower insert). The principal stresses show generally consistent orientations regardless of depth and spatial location. (Figure 11-18 in SKB 2008.)*

In accordance with the site understanding and site data, the stress model implies that horizontal stress magnitudes are greater than the vertical stress at shallow depths in fracture domain FFM02. Likewise, in FFM01, the horizontal stresses are also greater than the vertical stress. The increase in the horizontal stress magnitudes with depth appears to correlate with the decrease in frequency of open fractures with depth and a corresponding increase in the bedrock stiffness. No stress measurements have been carried out in fracture domain FFM06, but the *in-situ* stress state is expected to be similar to that in FFM01, since it consists of bedrock with similar stiffness properties and is located next to FFM01.

2.3.11 Hydraulic properties of deformation zones and fracture domains

Geological data at the site, including the dating of fracture minerals, indicate that ca 75 % of the fractures mapped in cored boreholes are sealed and that the majority of the fractures are ancient structures, especially in the deeper parts of the bedrock in the target volume, i.e. fracture domains FFM01 and FFM06. The youngest generation of calcite occurs in fractures and deformation zones that are currently hydraulically conductive and may have precipitated during a long period including the present.

The results of high-resolution inflow measurements in 22 core-drilled boreholes and pumping tests in 32 percussion-drilled boreholes provide the basis for the assignment of hydraulic properties of deformation zones and fracture domains at the Forsmark site. These data constrain locations of connected flowing fractures and values of the integrated transmissivity for the connected fractures down to ca 10^{-9} m^2/s. Results from single-hole injection tests and multiple-hole interference tests complement the data base.

Analyses of the hydraulic data have revealed that all deterministically modelled deformation zones, regardless of orientation, are characterised by a substantial decrease in transmissivity with depth, with a contrast of ca 20 000 times over the uppermost 1 000 m of the bedrock (Figure 2-9). The lateral heterogeneity at each depth is also substantial, on the order of 300 times or more, suggesting a channelled flow-field within the deformation zones. Furthermore, the data show that the gently dipping deformation zones, which predominantly occur in the south-eastern part of the investigation area, are the most transmissive at each depth (Figure 2-9). The steeply dipping deformation zones that strike WNW and NW and border the investigation area form structures with a second order of importance as far as transmissivity is concerned. These observations provide support to the hypothesis that involves a pronounced hydraulic anisotropy on a regional scale, where the largest transmissivities observed are associated with deformation zones that are oriented at a high angle to the minimum principal stress or sub-parallel to the maximum horizontal stress, respectively.

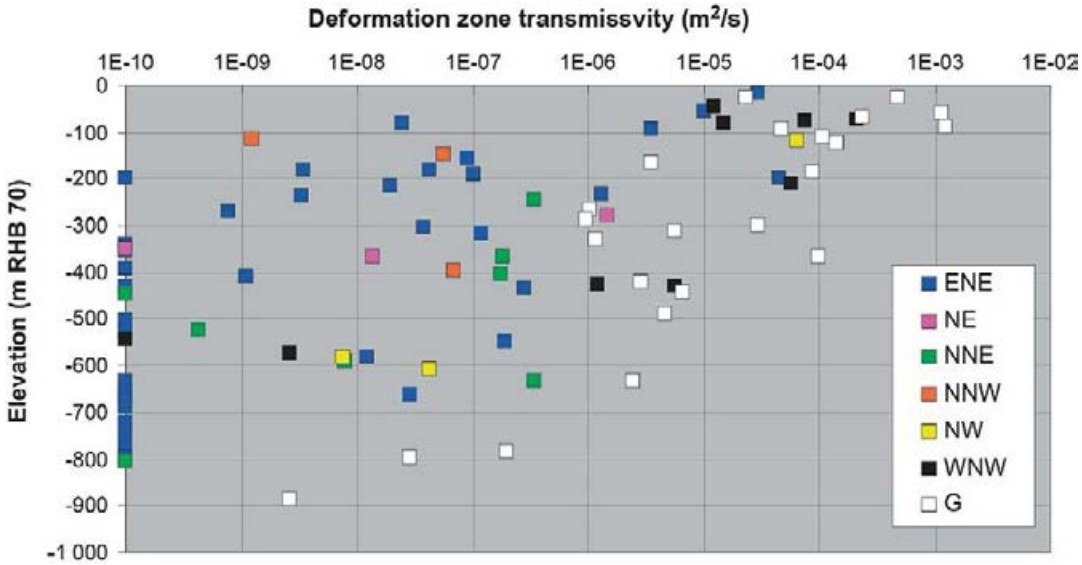

Figure 2-17. *Inferred transmissivities of deformation zones with depth and orientation (Figure 5-1 in Follin 2008).*

In the hydraulic model for the deformation zones, the observed vertical and lateral heterogeneity in transmissivity of the zones are both honoured. An exponential decrease in transmissivity with depth is assigned based on the depth trend in the data. The lateral heterogeneity in transmissivity is represented statistically as a lognormal distribution at each depth based on the variability observed in the data.

The number of open fractures and the number of flowing fractures in the bedrock between deformation zones both decrease significantly with depth. Figure 2-18 shows locations and transmissivities of flowing fractures detected with the Posiva Flow Log (PFL) in borehole situated inside the target volume (FFM01, FFM06 and FFM02) or below deformation zones ZFMA2 and ZFMF1, see Figure 2-14. Figure 2-18 suggests that fracture domain FFM01 could be divided into three elevation intervals. Below −400 m elevation only twelve flowing fractures are observed in total. However, ten of these occur in borehole KFM02A at drill site 2 between ZFMA2 and ZFMF1, see Figure 2-14. Hence, it is highly speculative to define an average separation between flowing fractures inside the target volume below −400 m elevation based on two flowing fractures. Between −200 m and −400 m elevation the number of flowing fractures is larger, but the total is still low. Above −200 m elevation, the number of flowing fractures is considerably larger, not least fractures with high transmissivities.

In the hydraulic model for the bedrock between deformation zones, the geometric and hydraulic properties of fractures in cored boreholes studied with PFL are represented by DFN models, one model for each elevation interval. The DFN models are calibrated against the Terzaghi corrected open fracture frequency, the Terzaghi corrected flowing fracture frequency and the univariate distribution of PFL fracture transmissivity. This calibration is made for fracture domains FFM01, FFM02 and FFM03. Table 2-2 shows data for fracture domains FFM01 and FFM02. Fracture domain FFM06 was inferred to have the same properties as fracture domain FFM01.

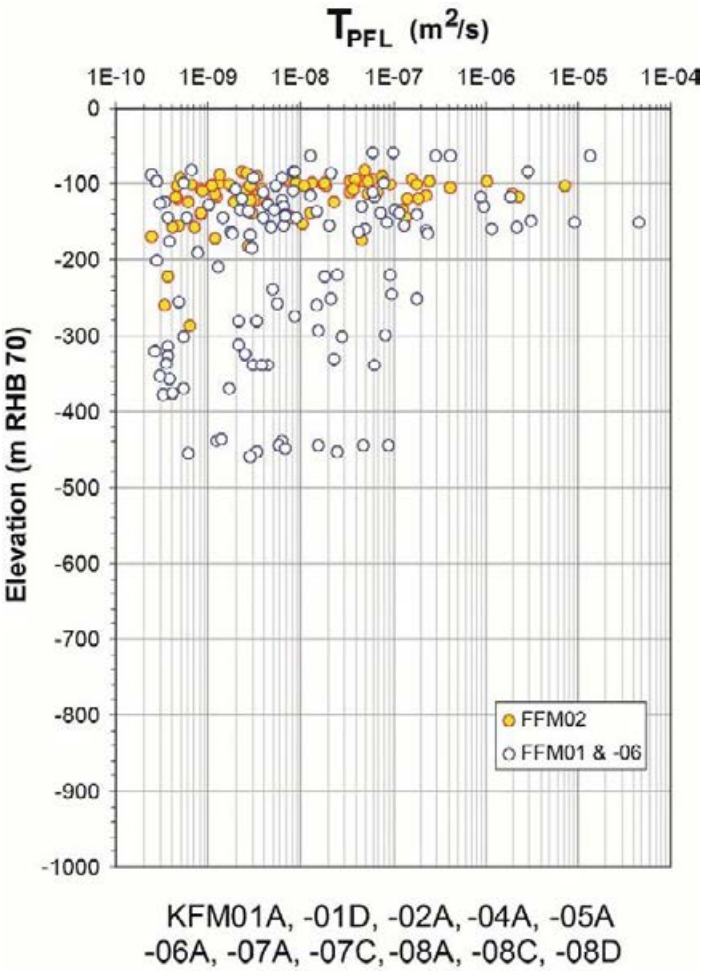

Figure 2-18. *Inferred PFL transmissivities of connected open fractures with depth in FFM02, FFM01 and FFM06. Ten out of twelve data points below –400 m elevation are recorded between deformation zones ZFMA2 and ZFMF1 in borehole KFM02A at drill site 2, see Figure 2-14. (Modified after Figure 11-19 in SKB 2008.)*

Table 2-2. Geometric mean linear fracture intensity of open fractures (<$P_{10,o,corr}$>) and flowing fractures detected with the PFL method (<$P_{10,PFL,corr}$>) for fracture domains FFM01 and FFM02. Maximum and minimum values of PFL fracture transmissivity (T_{PFL}) in each fracture domain and elevation interval are also shown together with the geometric means (<T_{PFL}>). (Modified after Table 3 in Follin et al. 2014.)

Parameter	Fracture domain and elevation interval			
	FFM02 (≥ −200 m)	FFM01 (≥ −200 m)	FFM01 (−200 to −400 m)	FFM01 (< −400 m)
<$P_{10,o,corr}$> (m^{-1})	3.17	1.13	1.02	0.535
<$P_{10,PFL,corr}$> (m^{-1})	0.33	0.153	0.041	0.005
Max T_{PFL} (m^2/s)	7.3×10^{-6}	1.9×10^{-7}	1.8×10^{-7}	8.9×10^{-8}
Min T_{PFL} (m^2/s)	2.4×10^{-10}	2.5×10^{-10}	2.7×10^{-10}	6.2×10^{-10}
<T_{PFL}> (m^2/s)	1.0×10^{-8}	6.9×10^{-9}	2.4×10^{-9}	6.5×10^{-9}

2.3.12 Borehole transmissivities in the uppermost part of the bedrock

Figure 2-19 shows borehole transmissivities in 50 m long intervals for the uppermost part of the bedrock as inferred from impeller flow logging in 38 percussion-drilled boreholes. In some of the boreholes the intersected structures are found to have wide apertures and can be very transmissive, or impervious depending on their infilling.

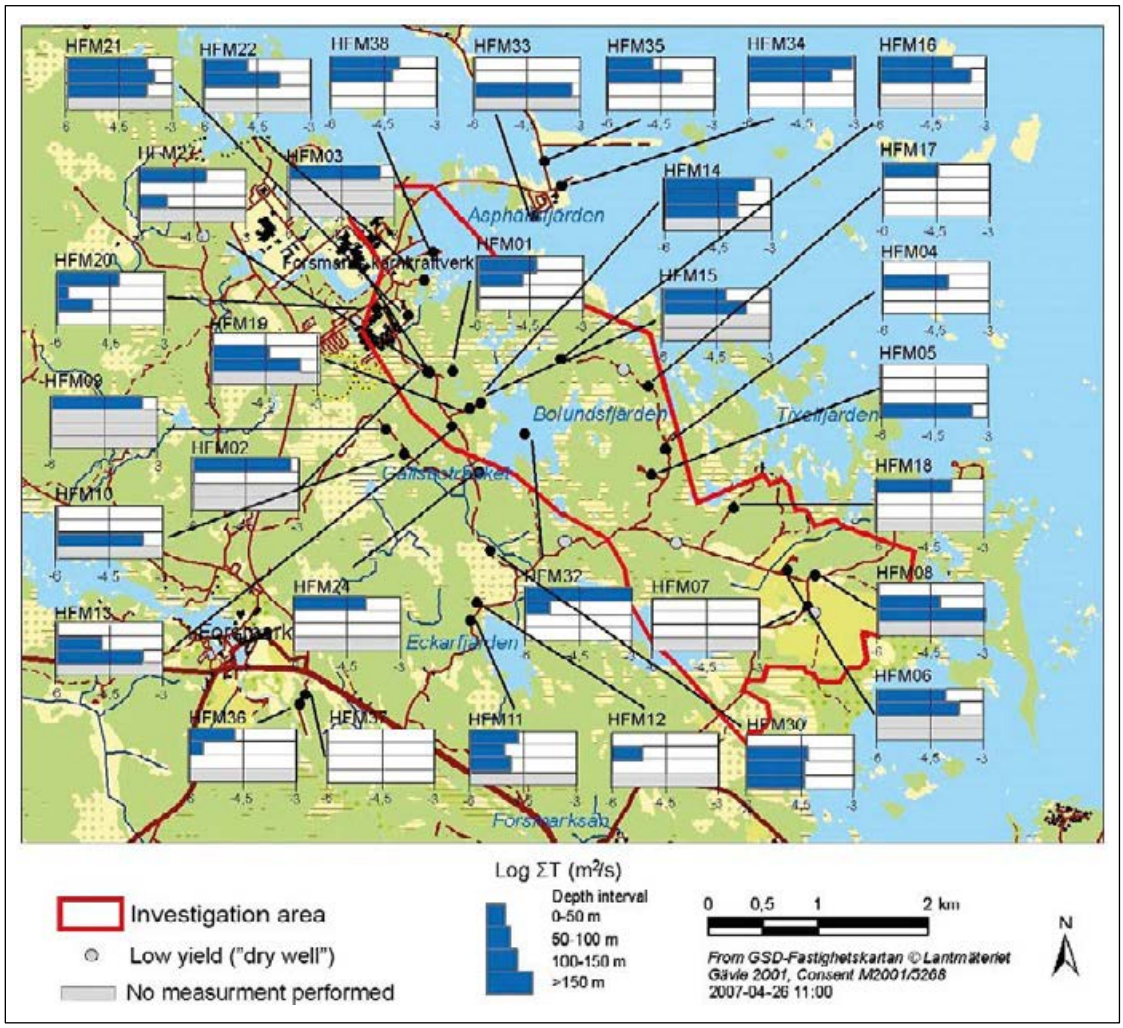

Figure 2-19. *Borehole transmissivities in 50 m long intervals as inferred from impeller flow logging in 38 percussion-drilled boreholes. White intervals indicate no flow or total log-transmissivities less than −6 for that depth interval. (Modified after Figure 3-20 in Follin et al. 2007a.)*

2.3.13 Groundwater composition

The groundwater composition in the bedrock can be associated with past climatic events during the Pleistocene, including inter-glaciations, glaciations, deglaciations, and associated changes in the shore level in connection with transgressions and regressions. Among these, the last glaciation and the post-glacial period (the Holocene) are the most important for the groundwater development in the Fennoscandian Shield, especially in terms of land uplift and shoreline displacement, as well as the development of the Baltic Sea (Figure 2-20).

The groundwater flow in Forsmark is concentrated to the large deformation zones and especially the horizontal and gently dipping ones, whereas the bedrock between the larger zones often has an extremely low frequency of water conductive fractures and generally contain older and more isolated groundwater.

Explorative analyses of groundwater chemistry data from cored boreholes, percussion-drilled boreholes and groundwater monitoring wells, and hydrogeochemical modelling have been used to evaluate the hydrogeochemical conditions at the site in terms of origin of the groundwater and the processes that control the water composition. Although the dataset is quite large, the sampling locations are few, especially at depth, resulting in an uneven data distribution. Nevertheless, the groundwater composition in general supports the occurrence of different hydrogeological regimes within the investigation area (Figure 2-1):

1. Groundwaters in the densely fractured fracture domain FFM02 (cf Figure 2-23) display a wide range of chemical variability, with chloride concentrations in the range 200 to 5 000 mg/L suggesting contributions of both brackish marine water (i.e. recent Baltic or old Littorina Sea relicts) and meteoric waters. The groundwater composition in FFM02 is on a whole governed by flow along highly transmissive, sub-horizontal fractures and sheet joints.
2. The bedrock at depth in fracture domains FFM01 and FFM06 below FFM02 (cf Figure 2-23) is characterised by few deformation zones and a decreasing fracture intensity with increasing depth. The marine signature of the groundwater composition is relatively weak and disappears completely at ca −300 m elevation. Below this elevation, the water composition indicates brackish to saline non-marine groundwater types (i.e. an absence of Littorina Sea influence), reflecting processes that occurred prior to the intrusion of the Littorina Sea waters. These waters further show an increase in calcium/sodium and bromide/chloride ratios with depth, which is indicative of water/rock interactions that occur under increasingly low flow to stagnant groundwater conditions with increasing depth.
3. Below ca −200 m elevation, in the transmissive, gently dipping deformation zones in the south-eastern part of the investigation area and contiguous to fracture domain FFM03 (cf Figure 2-23), the water composition shows a brackish marine signature. The chloride concentrations are in the range 2 000 to 6 000 mg/L with a clear Littorina Sea component, as indicated by the concentrations of magnesium and the ratio of bromide to chloride concentrations. This water type is recognised down to −600 to −700 m elevation. However, the marine component is decreasing, and the brine influence is increasing gradually with depth.

The present groundwaters are a result of mixing and reactions over a long period of geological time and the interfaces between different water types are not sharp but reflect the variability in structural-hydraulic properties. The shallow groundwaters of meteoric and marine origin generally have short residence times in the order of a few hundred years to only a few decades. In contrast the dating, based on ^{36}Cl and ^{4}He, of groundwater in low transmissive bedrock volumes suggests residence times of hundreds of thousands of years.

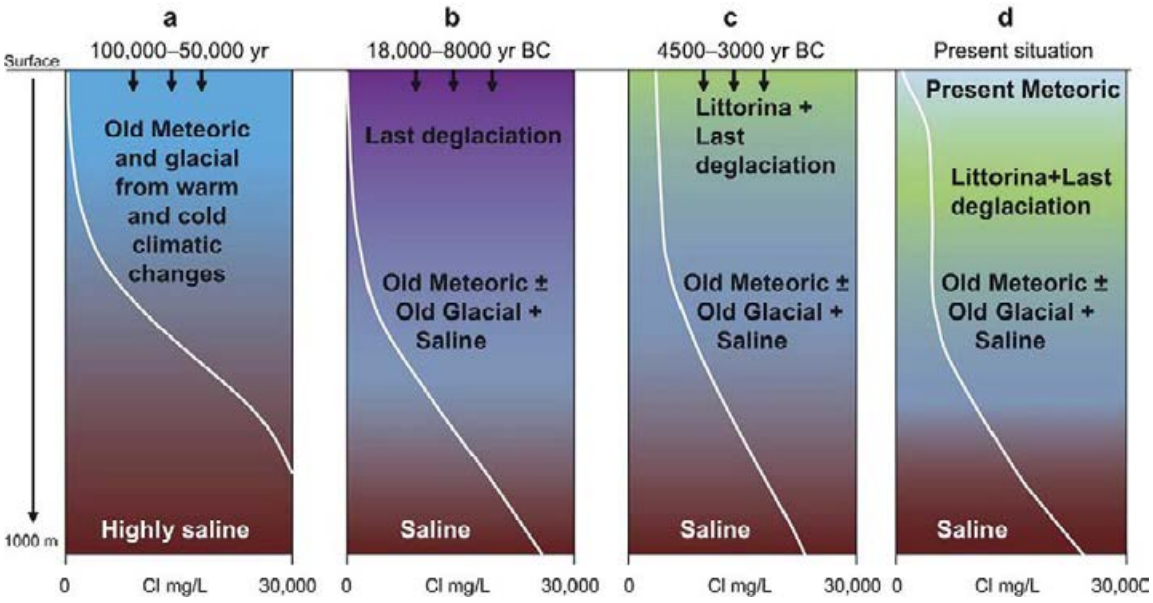

Figure 2-20. *Sketch showing tentative salinities and groundwater-type distributions versus depth for the transmissive zones at the Forsmark site. From left to right: a) situation prior to the last deglaciation, b) last deglaciation and intrusion of meltwater, c) the Littorina Sea water penetration caused by density intrusion, and d) the present situation. Tentative salinity profiles are indicated by the white lines. (Figure 9-4 in SKB 2008.)*

2.3.14 Bedrock transport properties

The site descriptive transport modelling in **SDM-Site** comprised parameters quantifying the diffusion and sorption properties of intact and altered rock materials – referred to as retardation parameters – and parameters characterising the transport by groundwater and the contact between the flowing water and immobile water along the flow paths – flow-related parameters. Crawford (2008) provides a detailed presentation of the **SDM-Site** modelling of these parameter categories, as well as coupled modelling illustrating effects of parameter variations on field scale transport.

In subsequent analyses performed as parts of **SR-Site**, site data were assessed and combined with data from other sources to produce the dataset used in the radionuclide transport and dose calculations in the safety assessment. In particular, sorption parameters are needed for a large number of combinations of geological materials, water compositions and elements (i.e. those with radioactive isotopes of importance for the transport and dose modelling). This means that the sorption database from the site investigations had to be extended by use of modelling and literature data to fulfil the needs of the safety assessment; these analyses of sorption parameters are presented in Crawford (2010).

Site understanding – the retardation model

Site descriptive transport modelling relies to large extent on parameters, models and general understanding provided by other modelling disciplines. In **SDM-Site**, inputs from geological, hydrogeological and hydrogeochemical modelling were used as a basis for the identification of which rock types and type structures, i.e. typical fractures and deformation zones, to include in the transport modelling. The understanding of the site-specific retardation properties of the bedrock at Forsmark that resulted from the joint analysis of transport data and inputs from other disciplines was formulated in terms of a bedrock retardation model (Byegård et al. 2008). This model presented retardation parameter values in the context of qualitative and quantitative descriptions of a set of geological materials and structures identified as typical for the site or otherwise important for site understanding and transport modelling.

Specifically, the site descriptive modelling of transport properties was focused upon the rock domains RFM029 and RFM045, and the retardation model contained data and descriptions of three types of geological materials and structural units: 1) the main rock types within these rock domains, 2) eight basic fracture types, and 3) four structural elements identified as characteristic of deformation zones.

Transport parameters for the main rock types included porosity, diffusion parameters from *in-situ* formation logging (main method) and laboratory measurements, and parameters supporting the analysis of sorption properties (BET surface areas and cation exchange capacities, CEC), see Table 10-3 in SKB (2008) for a summary and Byegård et al. (2008) for details. In the retardation model, representative, "best estimate" transport parameters were presented for rock types where statistically significant datasets existed, i.e. for rock types with SKB codes 101051, 101057, 101058, 101061 and 102017 (see Chapter 5 of the present report for explanations).

The sorption parameters (K_d values) for the main rock types in the retardation model represented rock types 101051 and 101057; the dataset included K_d for three (101051) or seven (101057) elements, and for four different groundwater types (see summary in SKB 2008, Table 10-4 through Table 10-7). In addition, the **SDM-Site** retardation model provided K_d values for rock type 101054 and for "fault rock" intended to be used in the modelling of deformation zones.

The eight fracture types are defined and illustrated in Table 2-3 and Figure 2-21, respectively. The classification of fracture types is based on fracture mineralogy and rock alteration. The information provided for a particular fracture type in the retardation model is exemplified in Table 2-4, which summarises description and transport parameters for fracture type E. It can be seen that a complete fracture description in the retardation gives information on a number of parameters and conditions from both transport and other disciplines.

Table 2-3. Classification of basic fracture types within the retardation model (Crawford 2008, Table 4-2).

Type	Fracture coating	Thickness	Wall rock alteration
A	***Chl+Ca***	≤ 0.5 mm	Fresh
B	***Chl+Clay*** ± *Ep* ± *Pr* ± *Ca*	~1 mm	Altered (~1 cm)
C	***Chl+Hm*** ± *Other*	< 0.5 mm (0.1 mm)	Altered (0.5 cm)
D	***Chl*** ± *other*	< 0.5 mm (0.1 mm)	Fresh
E	***Lau*** ± *Ca* ± *Chl*	0.1–2 mm	Altered (1–5 cm)
F	***Ca*** ± *Qz* ± *Py* ± *other*	0.1–2 mm	Fresh
G	***Clay*** ± *other*	1–5 mm	Altered (≥ 5 cm)
H	***No mineral***		Fresh

Notes: fracture mineral abbreviations are; chlorite (Chl), calcite (Ca), epidote (Ep), hematite (Hm), laumontite (Lau), prehnite (Pr), pyrite (Py), quartz (Qz).

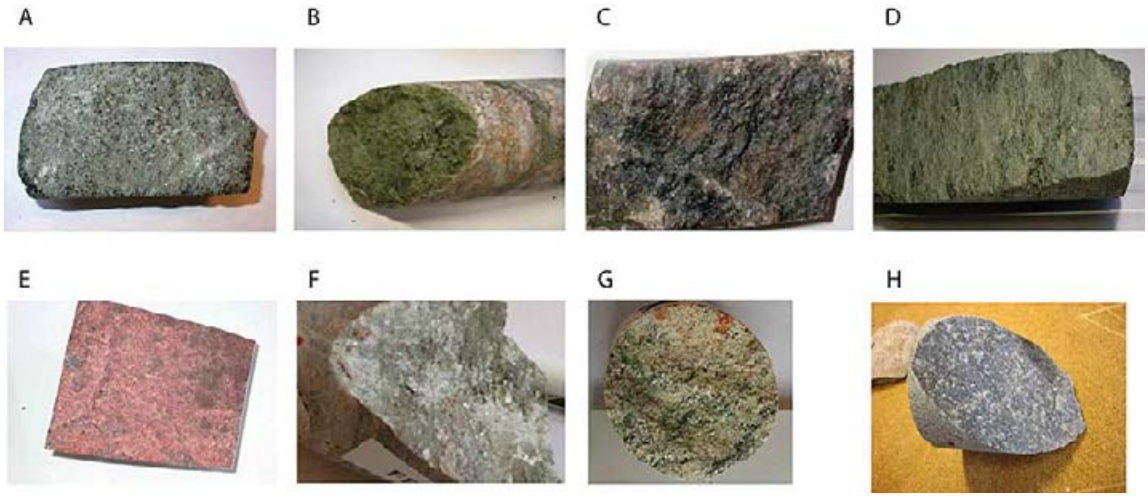

Figure 2-21. *Typical appearances of the surface coating minerals associated with the basic fracture types (Crawford 2008, Figure 4-4).*

Table 2-4. Retardation model for fracture type E, as summarised in the SDM-Site main report (SKB 2008, Table 10-12).

	Fracture coating: *Laumontite ± calcite ± other*			
Thickness	0.1–2 mm			
Porosity (vol%)	n/a			
Formation factor	n/a			
BET surface area (m^2/g)	0.42 ± 0.02			
CEC (cmol/kg)	18 ± 5			
Sorption, K_d (m^3/kg)	Water type (I–IV)			
	fresh	marine	saline	brine
Cs(I)	$(2.9 \pm 1.4) \times 10^{-1}$	$(1.6 \pm 0.24) \times 10^{-2}$	$(1.6 \pm 0.3) \times 10^{-2}$	$(4.1 \pm 0.4) \times 10^{-3}$
Sr(II)	$(5.1 \pm 2.1) \times 10^{-2}$	$(1.3 \pm 3.8) \times 10^{-4}$	$(0.35 \pm 3.32) \times 10^{-4}$	$(0.31 \pm 5.1) \times 10^{-4}$
Ln-Ac(III)	1.0 ± 0.4	1.3 ± 2.1	1.2 ± 0.14	2.1 ± 0.4
Percentage of all open fractures	14 %			
Percentage of transmissive fractures	1 %			
Transmissivity interval (m^2/s)	$> 10^{-10}$ (no evidence for preferential transmissivity interval)			
Preferred orientation	ENE-NW, steeply dipping			
Altered rock surrounding the fracture	yes, 1–5 cm			

Notes: entries given as “n/a” in the table signify data “not available”.

A potentially important consideration for the transport modelling is whether retardation parameters show differences between different rock types that would motivate the use of different parameter values in radionuclide transport models. In the **SDM-Site** work (Crawford 2008, SKB 2008), it was found that there were generally no significant differences in the retardation properties between the main rock types present in the rock domains RFM029 and RFM045. However, it was also emphasised that this observation was based on limited data.

Another factor of potential significance is that rock samples used in laboratory investigations are subject to stress release, which introduces uncertainties in parameter values due to differences between laboratory data and the *in-situ* conditions they are intended to represent. Based on the analyses in **SDM-Site**, where diffusion parameters were obtained from both laboratory and *in-situ* measurements, it was found that the porosity and effective diffusivity parameters of the rock matrix were well constrained.

The uncertainty in sorption parameters was considered only semi-quantitatively established in **SDM-Site** and was large for many species and water compositions. Regarding sorption and K_d values, it should be noted that the measured site data presented in the retardation model covered only a few of the elements for which the safety assessment needed input data. This was in line with the strategy established before the site investigations (Widestrand et al. 2003), which stated that the laboratory programme should be focused on a limited set of elements representing different groups in terms of dominant sorption processes and other relevant characteristics.

Site understanding – flow-related parameters

In the **SDM-Site** analyses of flow-related parameters and long-range solute transport presented in Crawford (2008), site understanding was expressed in terms of a conceptualisation where transport occurs along advective flow paths in a multi-compartment system (Figure 2-22). Specifically, this conceptualisation considered a transport model consisting of three compartments: 1) the non-engineered near field (NNF) comprising the network of poorly transmissive flow channels linking canister deposition holes with typical flowpaths featuring relatively high flow rates, 2) the immediate far field (IFF) comprising relatively transmissive flowpaths that can persist for several hundred metres distance until encountering deformation zones, and 3) the distant far field (DFF) comprising very transmissive flowpaths hosted in deterministically modelled deformation zones that provide fast conduits for flow to the near surface.

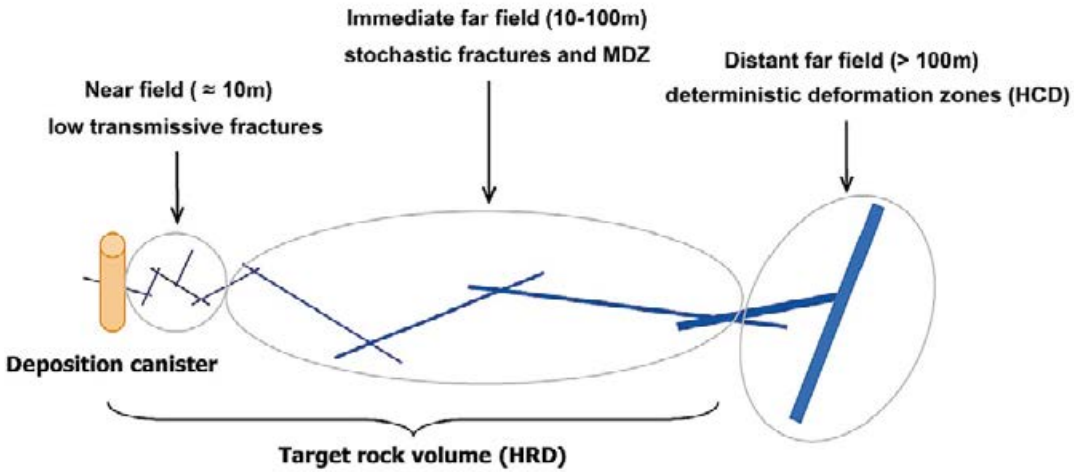

Figure 2-22. *Illustration of a potential flow path from a canister in the planned repository for spent nuclear fuel to the near-surface domain. Transport is conceptualised to occur along a sequence of flow path segments featuring increasing transmissivity (Crawford 2008, Figure 3-1).*

This description of flow paths in the fractured rock was used as a basis for analysing flow-related transport parameters, i.e. the advective residence time and the parameter referred to as the "F-factor" or the "hydrodynamic transport resistance" (see Crawford 2008 for details). The parameter analysis was complemented and further developed into an investigation of transport phenomena (primarily flow channelling) and modelling exercises focusing on the potential implications of parameter and model uncertainties for radionuclide transport. This modelling of coupled advection and retardation constituted an intermediate step between **SDM-Site** and **SR-Site** that set the parameters into a relevant site context and provided useful information on sensitivities and effects of uncertainties.

Essentially, flow-related transport parameters are calculated by use of groundwater flow models with some additional assumptions and/or data to support the description of the flow paths. More developed and detailed flow models were available for the subsequent **SR-Site** modelling than at the **SDM-Site** stage, especially for the repository volume and its immediate vicinity, and an extensive analysis of flow-related parameters was performed as part of the safety assessment based on these updated models (e.g. Joyce et al. 2010). This implies that the quantitative **SDM-Site** results and the understanding directly derived from them probably are of limited interest to elaborate on here. Conversely, the **SDM-Site** conceptualisation and the methodology for coupled advection-retardation modelling could provide useful starting points for similar analyses in forthcoming site descriptive modelling.

2.4 Integrated fracture domain, rock stress, hydrogeological DFN and groundwater composition models

An important prerequisite for confidence in the understanding of the Forsmark site involves consistency between the conceptual models derived in an independent manner from different sets of data in different disciplines. For purposes of comparison, four models are visualised in Figure 2-23 which shows a NW-SE profile inside the north-western part of the investigation area (Figure 2-1):

- A geological model for the spatial distribution of fracture domains FFM01, FFM02, FFM03 and FFM06 that focused on the spatial variation in the frequency of particularly open fractures in the bedrock.
- A rock mechanics model for the spatial variability in the magnitude of the maximum horizontal stress.
- Hydrogeological DFN models for the fracture domains that focused on the spatial variation in the size and intensity of connected open fractures, i.e. the fractures that are important from a hydrogeological viewpoint.
- A paleo-climatic model for the evolution of groundwater composition during the last ca 10 000 years, i.e. during the Holocene.

The bedrock below the gently dipping zones ZFMA2 and ZFMF1 (Figure 2-23) is inhomogeneous with respect to the spatial distribution of open fractures. This attribute, together with some consideration for increased alteration (albitisation) in fracture domain FFM06, formed the basis for the recognition of three different fracture domains in this volume (FFM02, FFM01 and FFM06).

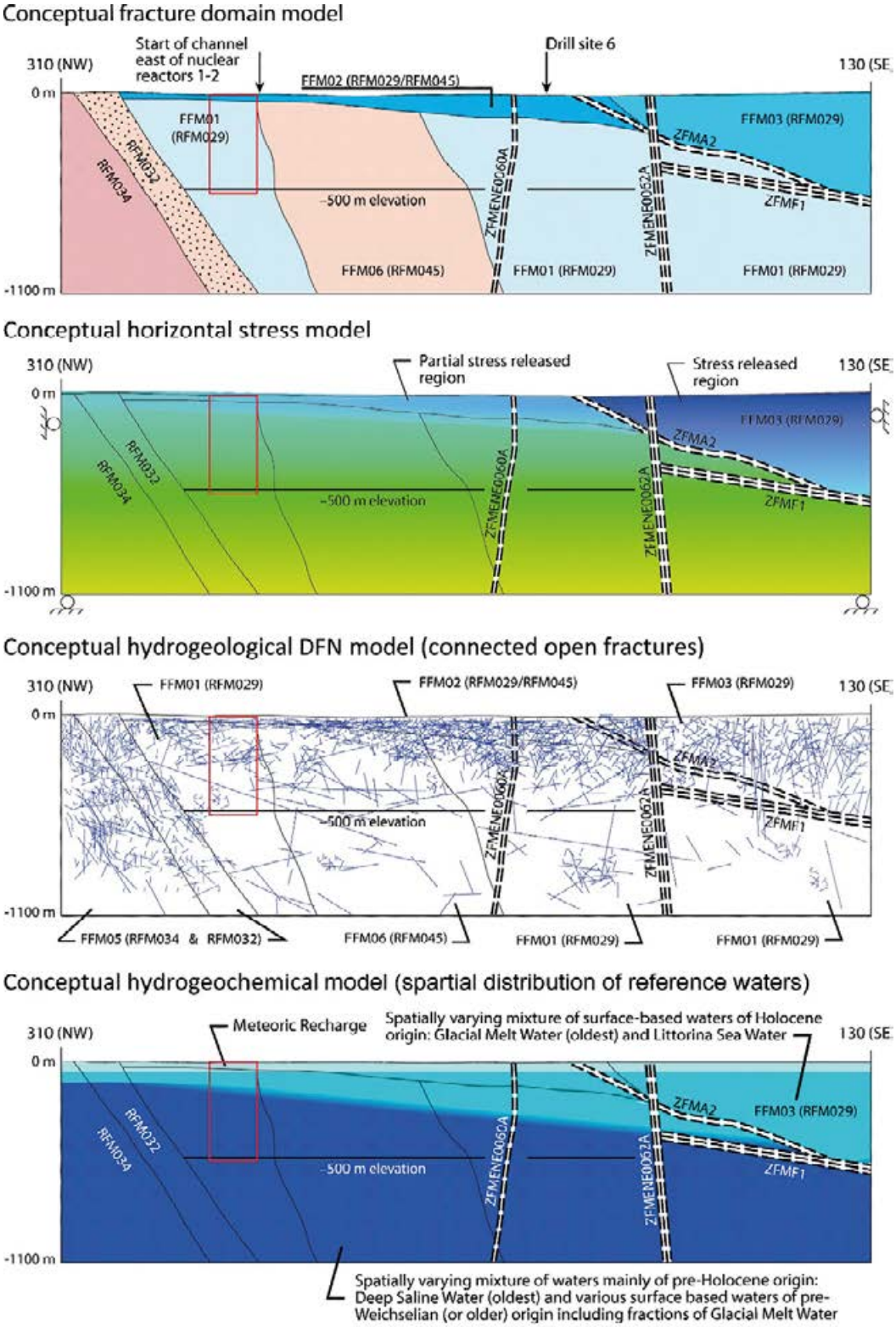

Figure 2-23. *A cross section through the north-western part of the investigation area at Forsmark showing the integrated understanding of the site at the completion of site investigation. The red rectangles indicate the access volume. (Modified after Figure 5 in Follin and Hartley 2014.)*

An increased intensity of connected open fractures and reduced maximum horizontal stress characterise the upper part of the bedrock in the footwall to zone ZFMA2, and this volume corresponds more or less to fracture domain FFM02 (Figure 2-23). A striking consistency between the different models concerns how the intensity of connected open fractures and the stress-released volume conform with the increased thickness of domain FFM02 as the gently dipping zone ZFMA2 is approached (Figure 2-23). It is suggested that this change with respect to zone ZFMA2 is related to the increased frequency of sub-horizontal and gently dipping fractures in the vicinity of this zone. Since these structures are oriented at a high angle to the vertical stress, which corresponds to the minimum principal (vertical) stress, there is a more favourable environment for the modification of the aperture of ancient fractures and even formation of new stress-release joints and, consequently, the more pronounced release of stress closer to the ZFMA2 zone.

In contrast, the major part of fracture domains FFM01 and FFM06 inside the target volume, including especially the potential repository volume around 500 m depth, is characterised by relatively few open fractures, a compartmentalised fracture network (with properties close to the percolation threshold for the connected open fractures), and higher maximum horizontal stress (Follin 2008). It is inferred that the low intensity of open fractures favoured a more significant build-up of horizontal stresses. The character of the connected open fractures in this volume implies restricted groundwater circulation with a spatially varying mixture of waters of mainly pre-Holocene origin. In summary, a bedrock volume where there is a limited number of open fractures and, by corollary, a low permeability is consistent with higher rock stresses. However, at Forsmark, inside the tectonic lens, the properties of such a bedrock are affected by the stress-released conditions in the near-surface realm and close to gently dipping ancient structures.

2.5 Geological data assembled posterior to SDM-Site

During the preparatory investigations conducted between 2011 and 2012 eleven core drilled boreholes, three percussion drilled boreholes and three cleared outcrops were completed in the planned shaft and access ramp facility area (Table 2-5). Each of these boreholes reached a depth less than 200 m and focussed on evaluating the geological and hydrogeological conditions of the shallow bedrock, see Chapter 5 and Chapter 8, respectively.

To validate and gain more information about the current geological and hydrogeological models near the planned skip shaft a long borehole, KFM24, was core drilled during spring 2016 to a depth of 540 m, i.e. ca 40 m below the bottom of the access volume (Nilsson 2017). The geological and hydrogeological data from KFM24 are presented in Chapter 5 and Chapter 8, respectively.

Table 2-5. Activities performed during the preparatory investigations 2011–2012.

Task	Investigation	SKBdoc id	Reference	Data source[1]
Percussion boreholes, HFM39–41	Drilling	1338601	Nilsson (2013)	Sicada_11_135
	Geological mapping	1327873	Winell (2012)	Sicada_11_123
Cored boreholes, KFM13–23	Drilling	1338601	Nilsson (2013)	Sicada_11_135
	Geological mapping	1327873	Winell (2012)	Sicada_11_123
Outcrop, AFM001392–1394	Geological mapping	1338506	Petersson et al. (2010)	
	Detailed fracture mapping	1338599	Curtis et al. (2012)	

[1] Sicada_xx_xxx is the internal identification of a data delivery from SKB's Sicada database.

3 Access area, boreholes and data

3.1 Access area

Figure 3-1 shows a plane view of the footprint of the volume considered in the geoscientific descriptions of the bedrock conditions in this document. The coordinates of the volume are shown in Table 3-1. The area considered in the geoscientific and ecological descriptions of the surface conditions is larger, see Figure 3-2, in order to allow for an elaborated account of the surface environment.

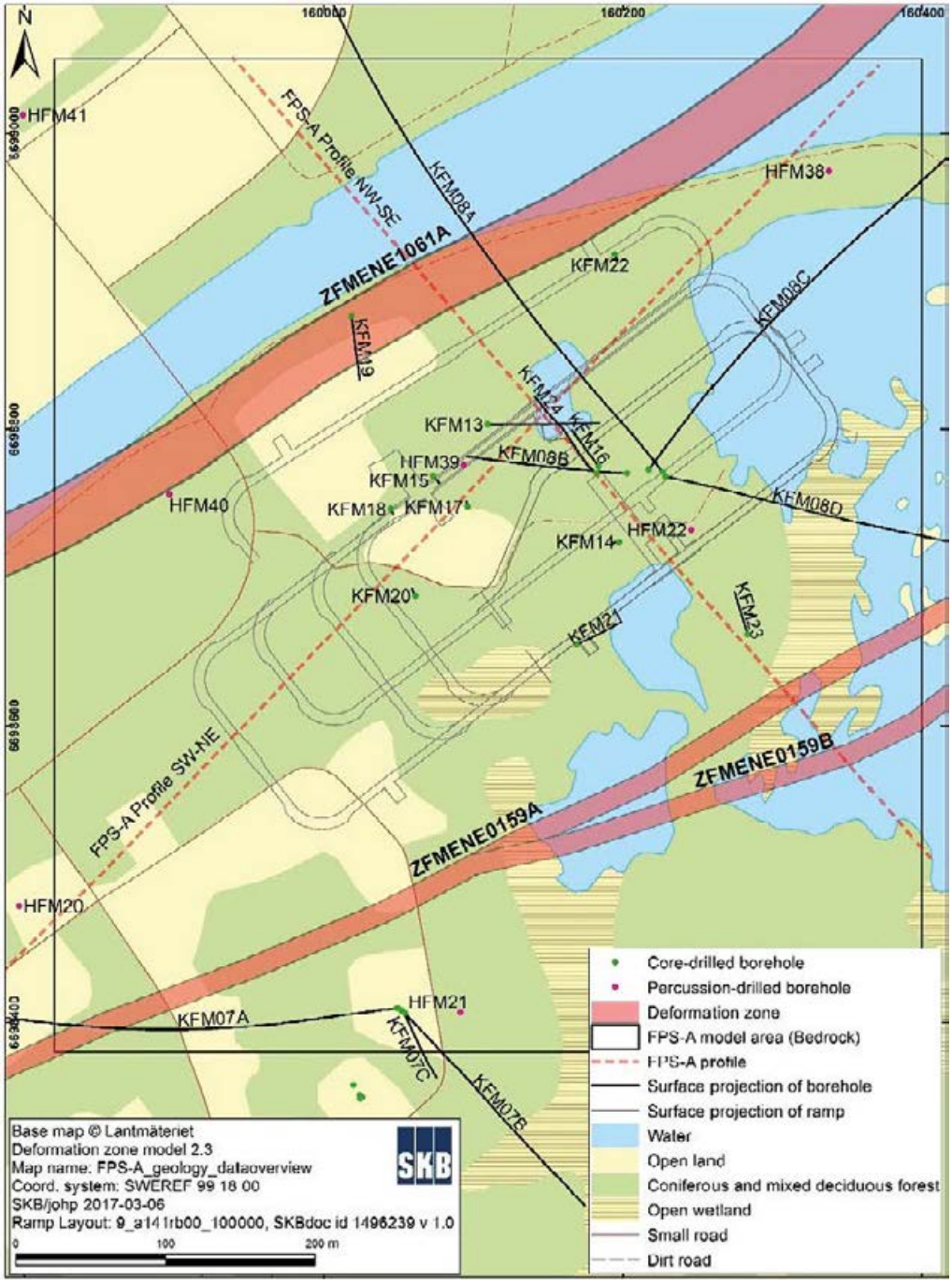

Figure 3-1. *Map showing steeply dipping deformation zones and bedrock boreholes considered in the geoscientific descriptions of the bedrock in proximity of the ramp and shafts of the planned repository for spent nuclear fuel (solid black line). (See Appendix A for a larger view.)*

Table 3-1. Coordinates and elevations of the volume considered in this document for the geoscientific descriptions of the bedrock conditions near the ramp and shafts.

Corner coordinates (RT90 2.5 gon V)		Corner coordinates (SWEREF 99 18 00)		Vertical extent (RHB 70*)	Vertical extent (RH 2000*)
Easting	Northing	Easting	Northing	Elevation (m)	Elevation (m)
1631383.405	6700109.269	160400.000	6698380.000	100, −500	100, −500
1630803.602	6700089.957	159820.000	6698380.000	100, −500	100, −500
1630781.293	6700759.729	159820.000	6699050.000	100, −500	100, −500
1631361.096	6700779.042	160400.000	6699050.000	100, −500	100, −500

* The difference in elevation between RHB 70 and RH 2000 is approximately 0.185 m.

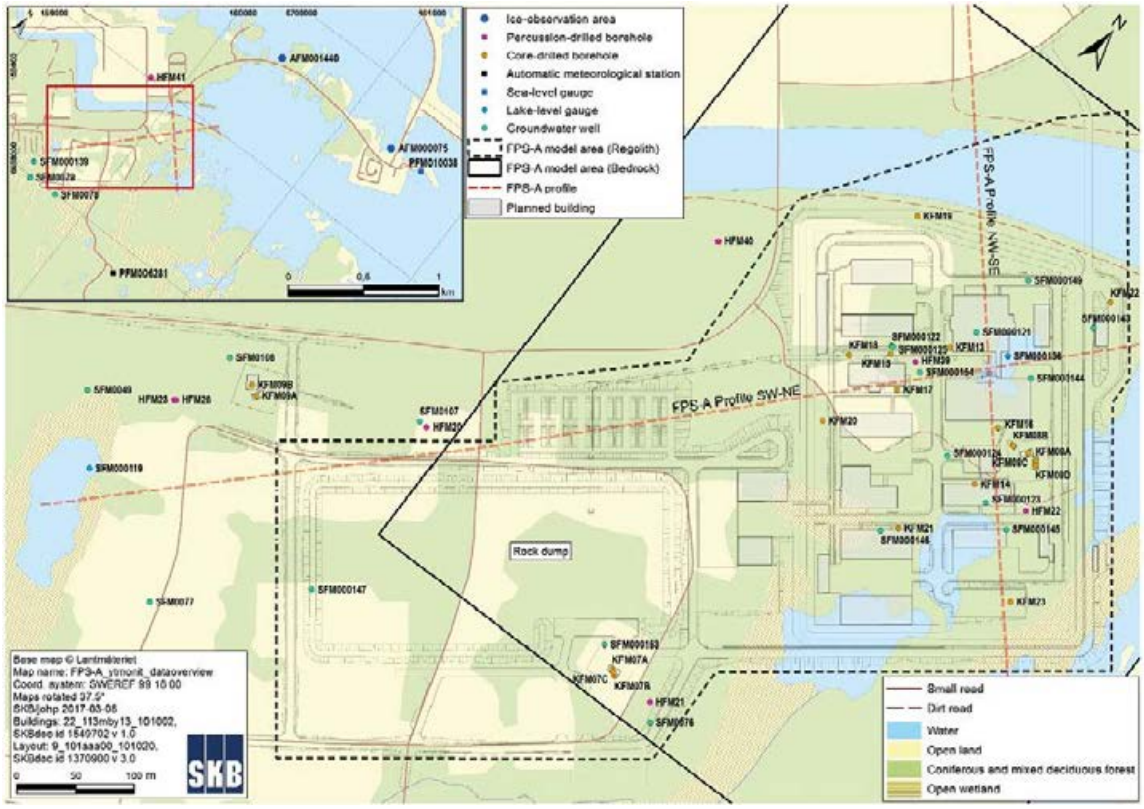

Figure 3-2. *Map showing planned buildings and rock dump together with the present-day land use and boreholes used for monitoring of groundwater levels. The solid and dashed black lines represent the model areas considered in the geoscientific descriptions of the bedrock and the regolith, respectively. (See Appendix A for a larger view.)*

3.2 Boreholes and groundwater wells

There are in total 30 bedrock boreholes and 20 groundwater wells in the regolith within or in close proximity to the access area. These have been drilled and investigated at different stages and for various purposes. The types of data acquired from each borehole with regard to the investigation stage are shown for the bedrock in Table 3-2 and for the regolith in Table 3-3. Technical information of relevance for the monitoring of groundwater levels and groundwater composition is also provided in these tables.

Table 3-2. Compilation of data for the 21 core-drilled and 9 percussion-drilled boreholes considered. R = regolith geology, G = bedrock geology, M = rock mechanics, S = near-surface hydrogeology, H = bedrock hydrogeology, C = hydrogeochemistry, T = transport properties.

Borehole A: SDM-Site B: Post SDM-Site	Borehole length (m TOC)	End of borehole (m RHB 70)	Data by discipline R, G, M, S, H, C, T	Number of monitoring sections[$]	Parameter P = pressure C = chemistry
KFM07A (A)	1002.10	−820.94	R, G, H, C, T	6	P, C
KFM07B (A)	298.93	−237.91	R, G, M, H	3	P
KFM07C (A)	500.34	−494.35	R, G, M, H	4	P
KFM08A (A)	1001.19	−759.40	R, G, H, C, T	9	P, C
KFM08B (A)	200.54	−166.86	R, G, H	3	P
KFM08C (A)	951.08	−780.81	R, G, H, C, T	5	P, C
KFM08D (A)	942.30	−748.28	R, G, H, C	7	P, C
KFM09A (A)	799.67	−621.21	R, G, M, H, C, T	3	P
KFM09B (A)	616.45	−472.00	R, G, M, H, C	3	P
KFM13 (B)	150.21	−127.63	R, G, S, H	1 (open)	–
KFM14 (B)	60.18	−58.03	R, G, S, H	1 (open)	–
KFM15 (B)	62.30	−58.48	R, G, S, H	1 (open)	–
KFM16 (B)	60.35	−50.50	R, G, S, H	1 (open)	P
KFM17 (B)	60.45	−56.66	R, G, S, H	1 (open)	P
KFM18 (B)	60.46	−56.89	R, G, S, H	1 (open)	P
KFM19 (B)	102.37	−90.13	R, G, S, H	1 (open)	P
KFM20 (B)	60.50	−57.49	R, G, S, H	1 (open)	P
KFM21 (B)	101.06	−92.58	R, G, S, H	1 (open)	P
KFM22 (B)	60.26	−57.36	R, G, S, H, C*	1 (open)	P
KFM23 (B)	100.64	−93.93	R, G, S, H, C*	1 (open)	P
KFM24 (B)	550.17	−545.09	R, G, H, C	1 (open)	–
HFM20 (A)	301.00	−297.58	R, G, S, H, C	4	P
HFM21 (A)	202.00	−153.37	R, G, S, H, C	4	P, C
HFM22 (A)	222.00	−155.59	R, G, S, H, C	1 (open)	P
HFM23 (A)	211.50	−72.78	R, G, S, H, C	1 (open)	P
HFM28 (A)	151.20	−143.77	R, G, S, H, C	1 (open)	P
HFM38 (A)	200.75	−140.68	R, G, S, H, C	3	P
HFM39 (B)	151.20	−144.85	R, G, S, H	1 (open)	P
HFM40 (B)	101.70	−98.34	R, G, S, H	1 (open)	P
HFM41 (B)	101.50	−97.22	R, G, S, H	1 (open)	P

[$] The number of sections refers to pressure measurement sections. Water samples for chemical analyses are usually restricted to one section per borehole.
* Only porewater in the rock matrix.

Table 3-3. Compilation of data for the 20 groundwater monitoring wells considered. R = regolith geology, S = near-surface hydrogeology, C = hydrogeochemistry.

Borehole A: SDM-Site B: Post SDM-Site	Borehole length (m TOC)	End of borehole (m RHB 70)	Data by discipline R, S, C	Number of monitoring sections	Parameter P = pressure C = chemistry
SFM0049 (A)	6.00	−1.97	R, S, C	1 (open)	P, C
SFM0076 (A)	3.16	0.66	R, S	1 (open)	P
SFM0077 (A)	8.00	−2.98	R, S, C	1 (open)	P, C
SFM0078 (A)	5.60	−0.36	R, S, C	1 (open)	P, C
SFM0079 (A)	6.70	−2.50	R, S, C	1 (open)	P, C
SFM0107 (A)	7.05	−3.90	R, S	1 (open)	P
SFM000121 (B)	6.50	−3.82	R, S	1 (open)	P
SFM000122 (B)	7.50	−4.65	R, S	1 (open)	P
SFM000123 (B)	3.50	−2.01	R, S	1 (open)	P
SFM000124 (B)	3.50	−1.32	R, S	1 (open)	P
SFM000125 (B)	4.50	−0.96	R, S	1 (open)	P
SFM000139 (B)	3.00	0.68	R, S	1 (open)	P
SFM000143 (B)	3.00	−0.73	R, S	1 (open)	P
SFM000144 (B)	2.50	−0.04	R, S	1 (open)	P
SFM000145 (B)	2.00	−0.54	R, S	1 (open)	P
SFM000146 (B)	3.10	0.00	R, S	1 (open)	P
SFM000147 (B)	2.40	0.38	R, S	1 (open)	P
SFM000149 (B)	2.25	−0.96	R, S	1 (open)	P
SFM000153 (B)	3.20	0.97	R, S	1 (open)	P
SFM000154 (B)	2.40	1.63	R, S	1 (open)	P

It is noted that chemical data from three additional boreholes drilled in bedrock, but away from the access area, are referenced in Chapter 9. The boreholes are KFM01D, HF02 and HFM27, see Figure 9-1 for their locations relative to the access area.

Figure 3-3 shows a plane view of the access area considered in the geoscientific description of the bedrock (cf Figure 3-1) together with locations and projections of all short bedrock boreholes listed in Table 3-2, i.e. HFM20-23, -28, -38–41 and KFM13–23. Figure 3-3 also shows the planned location of the skip shaft and the location and projection of the long bedrock borehole KFM24 (cf Table 3-2). The information shown in Figure 3-3 is also included in Figure 3-4, which shows a vertical projection running from West to East.

Likewise to Figure 3-3, Figure 3-5 shows a plane view of the access area but with locations and projections of all long boreholes listed in Table 3-2, i.e. KFM07A–C, KFM08A–D and KFM09A–B. Figure 3-6 shows a vertical projection running from West to East and includes the information shown in Figure 3-5.

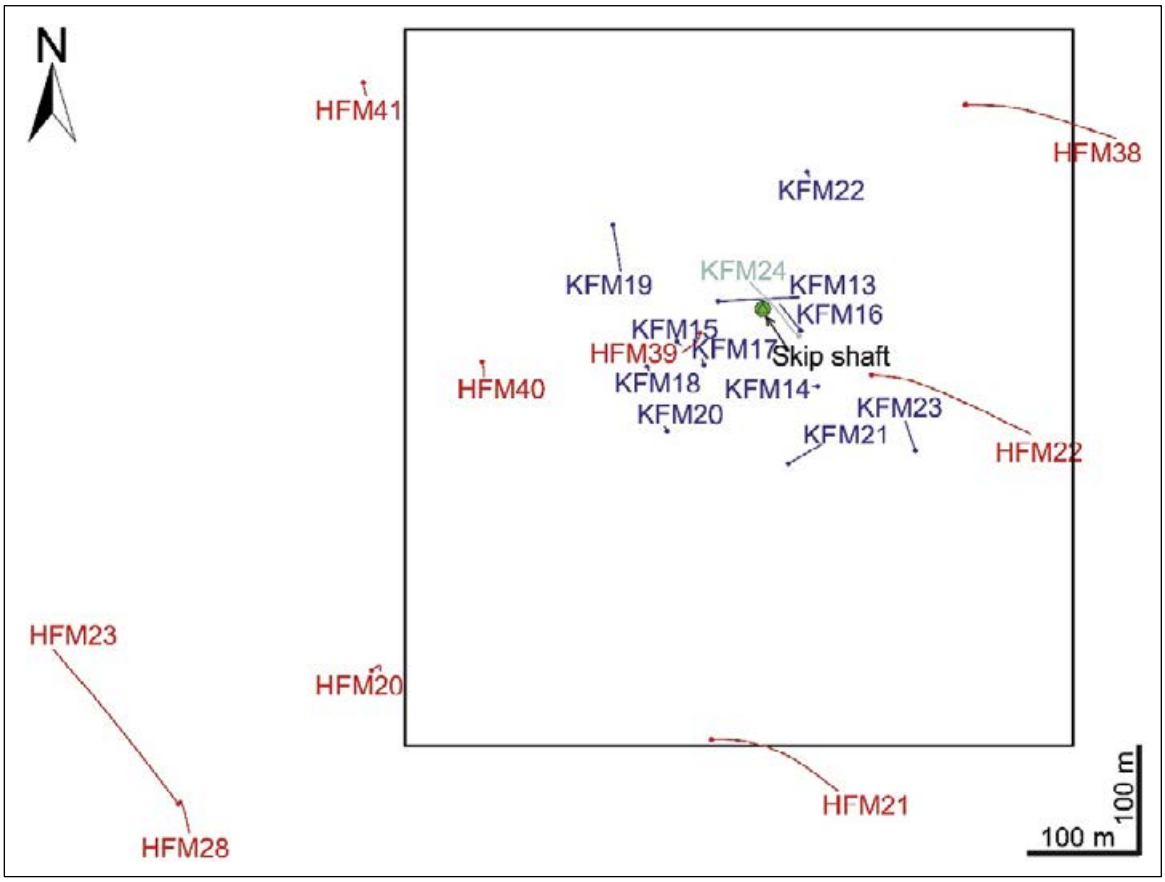

Figure 3-3. *Plane view of the top of the access volume considered in the geoscientific description of the bedrock together with locations and projections of all shallow bedrock boreholes drilled in proximity of this volume. The planned location of the skip shaft and the location and projection of the deep borehole KFM24 are also shown.*

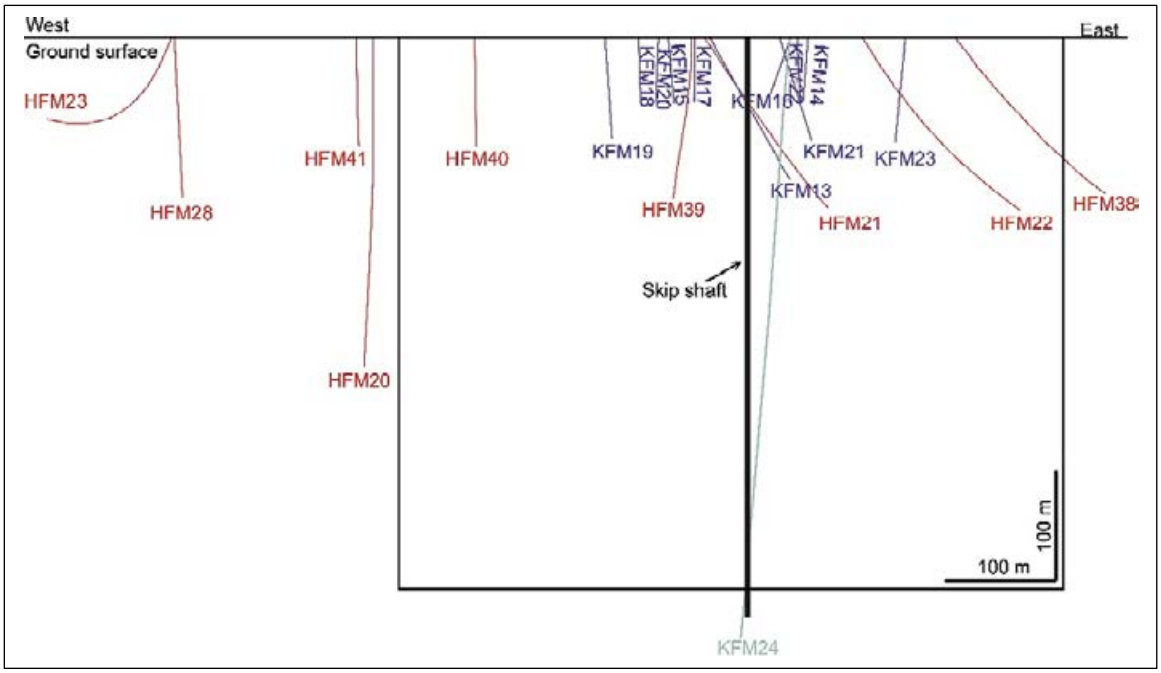

Figure 3-4. *Vertical projection running from West to East showing the same information as shown in Figure 3-3.*

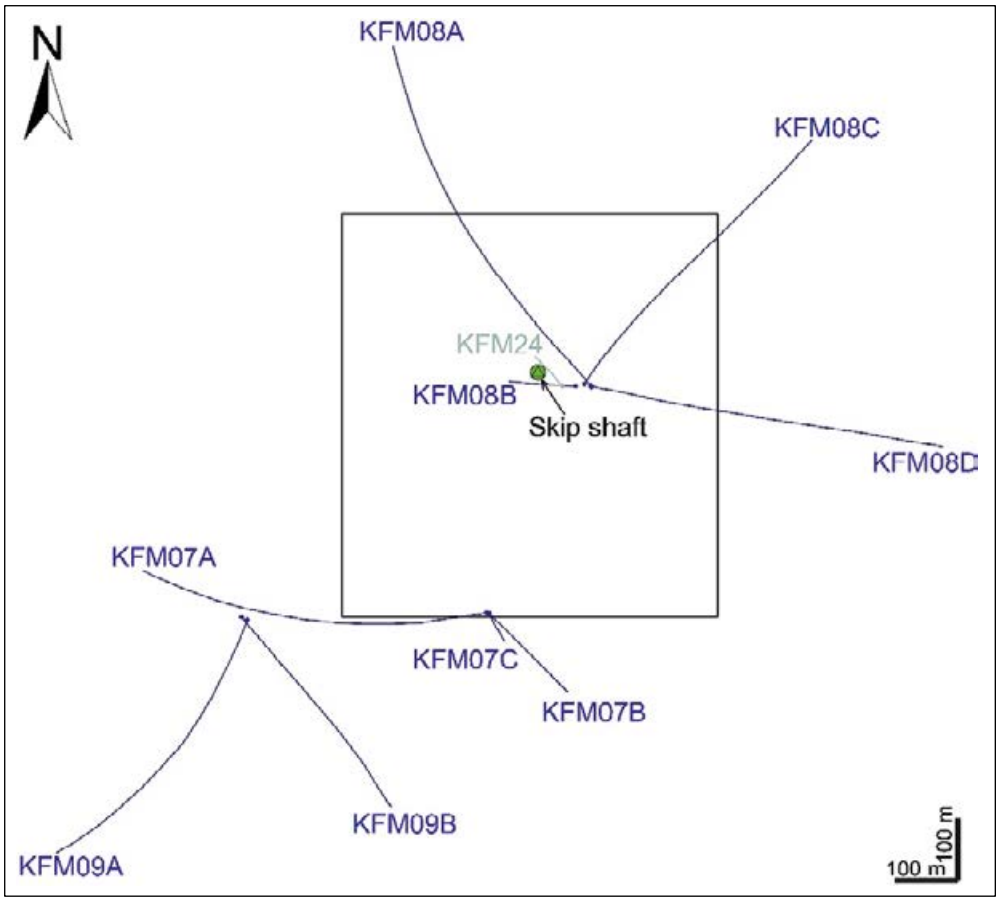

Figure 3-5. *Plane view of the top of the access volume considered in the geoscientific description of the bedrock together with locations and projections of all deep bedrock boreholes drilled in proximity of this volume. The planned location of the skip shaft and the location and projection of the deep borehole KFM24 are also shown.*

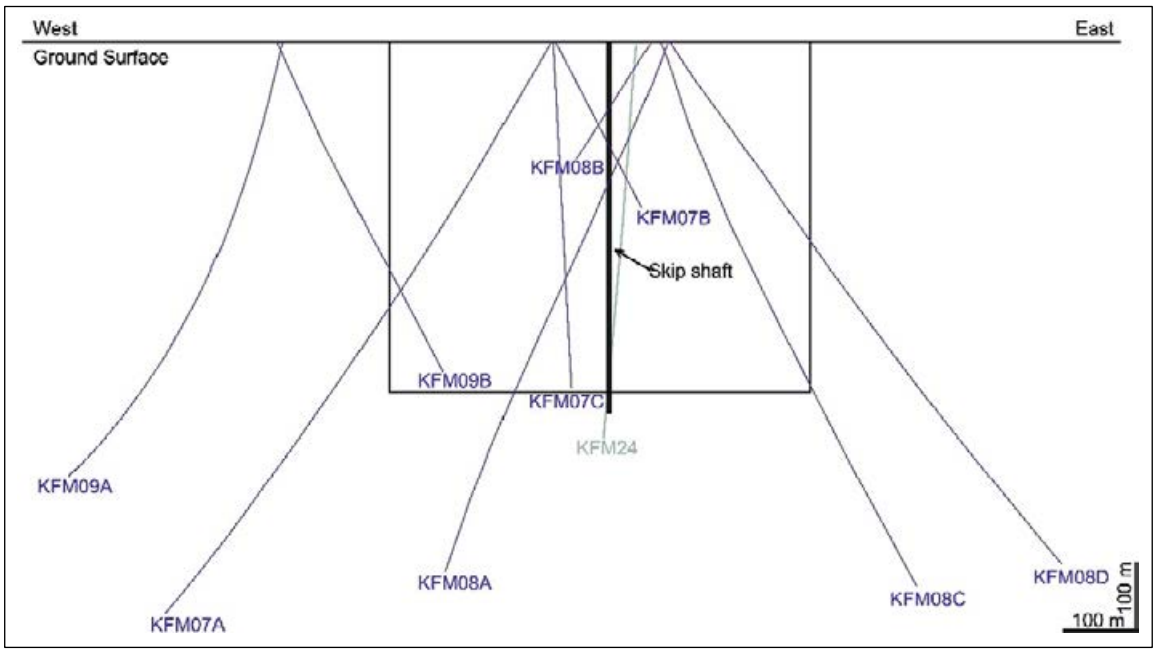

Figure 3-6. *Vertical projection running from west to east showing the same information as shown in Figure 3-5.*

3.3 Assessment of characterisation data from bedrock boreholes

The assessment of borehole data is made in two steps. First, data acquired from the characterisation of 15 boreholes drilled and investigated during the site investigation for **SDM-Site** are revisited, and an assessment is made to conclude whether these have any particular geoscientific characteristics with regard to the bedrock inside the considered access volume. Second, data acquired from the characterisation of 15 boreholes drilled and investigated posterior to **SDM-Site** are assessed for the same reason. The following activities/datasets are recognised in the second step.

- Drilling and investigation of 14 shallow boreholes KFM13–23 and HFM39–41 located inside, or near the access volume, see Figure 3-3 and Figure 3-4.
- Drilling and investigation of the deep borehole KFM24, see Figure 3-5 and Figure 3-6.

Appendix B and Appendix C present WellCad plots for the bedrock boreholes drilled and investigated during the site investigation for **SDM-Site**, i.e. KFM07A-7C, KFM08A-8D, KFM09A-9B, HFM20–23, HFM28 and HFM38, and posterior to **SDM-Site**, i.e. KFM13–KFM24 and HFM39–41, respectively. The documents used to construct the WellCad plots shown in Appendix B and Appendix C are listed in Table 3-4 and Table 3-5, respectively. It is noted that no hydrogeochemical or rock mechanics data in these reports are shown in the WellCad plots.

Table 3-4. Compilation of reports[1] with data from bedrock boreholes KFM07A-7C, KFM08A-8D, KFM09A-9B, HFM20–23, HFM28 and HFM38. WellCad plots with data are shown in Appendix B. The references to the listed report numbers are found in SDM-Site (SKB 2008, see Table 9 in Appendix 3 for a list that links P report numbers to full references).

Activity	References
Drilling and drill core mapping	P-04-245, P-05-102, P-05-103, P-05-142, P-05-172, P-05-203, P-05-278, P-06-80, P-06-130, P-06-131, P-06-166, P-06-169, P-06-170, P-06-171, P-06-203, P-06-205, P-06-206, P-07-103
Borehole geophysics and BIPS	P-05-01, P-05-17, P-05-52, P-05-58, P-05-64, P-05-158, P-05-159, P-06-22, P-06-44, P-06-64, P-06-120, P-06-123, P-06-177, P-06-178, P-07-04, P-07-05, P-07-60, P-07-96, P-07-194
Geophysical interpretation	P-05-51, P-05-119, P-05-157, P-05-202, P-06-126, P-06-152, P-06-258, P-07-125
Geological single-hole interpretation	P-05-157, P-05-262, P-06-126, P-06-134, P-06-135, P-06-207, P-06-258, P-07-108
Hydraulic characterisation	P-05-14, P-05-43, P-05-63, P-05-133, P-05-235, P-06-52, P-06-56, P-06-86, P-06-122, P-06-189, P-06-191, P-06-194, P-06-247, P-07-06, P-07-22, P-07-84, P-07-127, P-07-128
Hydrogeochemical investigations	P-05-170, P-06-63, P-06-217, P-07-190
Rock mechanics characterisation	P-04-311, P-05-239, P-07-07, P-07-76, P-07-115, P-07-166
Transport properties characterisation	P-06-60, P-06-187, P-07-137, P-07-138, P-07-139

[1] The listed reports are published by SKB and available for downloading from www.skb.se/publications. They are not included in the references of the present document.

Table 3-5. Compilation of reports with data from bedrock boreholes KFM13–24[1] and HFM39–41. WellCad plots with data are shown in Appendix C.

Activity	References
Drilling and drill core mapping	Nilsson (2013), Winell (2012), Nilsson (2017), Dahlin and Maskenskaya (2017)
Hydraulic characterisation	Jönsson (2011), Walger et al. (2012), Odén and Follin (2016), Harrström et al. (2017), Hurmerinta (2017)
OPTV logging of borehole KFM24	Lundgren (2017)
Geological single-hole interpretation of borehole KFM24	Dahlin et al. (2017)
Porewater characterisation	Waber and Smellie (2012)

[1] A report describing the hydrochemical characterisation of borehole KFM24 is under production and will be published as SKB P-17-33.

3.4 Assessment of data on climate, hydrology and groundwater levels

The assessment of climate data, hydrological data and data from groundwater monitoring wells is also made in two steps. First, data acquired from two meteorological stations, one ice station, one surface-water level station and six groundwater monitoring wells established in or near the access area during the site investigation for **SDM-Site** are revisited and an assessment is made to conclude whether these have any particular characteristics with regard to the access area. Second, data acquired from one additional meteorological station, one ice station, two surface-water level gauges and 12 groundwater monitoring wells established posterior to **SDM-Site** are assessed for the same reason. The key data in these assessments come from the on-going long-term monitoring. The locations for long-term monitoring of surface and groundwater levels in gauges and wells within or in the vicinity of the access area are shown in Figure 3-2. No corresponding points exist for monitoring of surface water and shallow groundwater hydrochemistry.

Table 3-6 and Figure 3-7 give overviews of available data related to meteorology, hydrology and groundwater levels in the regolith. Figure 3-7 also includes groundwater levels from the upper sections of boreholes or open boreholes drilled into the shallow bedrock. The analyses of these data are described in Werner (2018) and the current understanding of the near-surface hydrological system is presented in Chapter 7. The analyses by Werner (2018) comprise the following.

- Hydrogeological properties of regolith and the rock/regolith interface: data from single-hole (slug) tests in groundwater monitoring wells installed subsequent to **SDM-Site** (SFM000121–125, -139, -143–147, -149, and -153–154.
- Meteorological monitoring: meteorological data (e.g. precipitation, air temperature and potential evapotranspiration) gathered at the Högmasten and Storskäret meteorological stations (PFM010700, -010701) from the Forsmark 2.3 data freeze (March 31, 2007) up to June 2007 and June 2015, respectively, and from the Labbomasten meteorological station (PFM006281) from June 2015 and onwards (Wern and Jones 2007, 2008, Andersson and Jones 2009, 2010, 2011, 2012, 2014, Andersson 2013, Jones and Kindell 2015, 2016).
- Monitoring of ice freeze/breakup: observations of ice freeze/breakup in the nearby sea bay (Nyberg and Wass 2008a, 2009a, 2010a, Wass 2011, 2012, 2013a, 2014a, 2015a, 2016a) from the 2007/2008 winter season to the 2015/2016 winter season. Specifically, there was one ice-observation area up to the 2014/2015 winter season (AFM000075) and two observation areas (also including AFM001449) from the 2015/2016 winter season.
- Monitoring of groundwater and surface water levels: additional datasets from pre-existing groundwater monitoring wells (SFM0049, SFM0077–79 and SFM0107) and the sea-level gauge PFM010038 (Nyberg and Wass 2008b, 2009b, 2010b, Wass 2013b, 2014b, 2015b, 2015c, 2016b, 2018). Moreover, the dataset includes monitoring data from wells (SFM000121–125, -139, -143, -145, -146–147, -149 and -153) and lake-level gauges (SFM000119 and -156) installed subsequent to **SDM-Site**.

In connection to the above, it is noted that parts of the data acquired posterior to **SDM-Site** were indeed presented, evaluated and utilised for site-descriptive modelling of hydrology and near-surface hydrogeology within the framework of **SR-PSU** (the safety assessment for the SFR extension project). Specifically, the **SR-PSU** dataset includes data available up to the end of 2010 (Werner et al. 2013, 2014).

Table 3-6. Compilation of start and stop dates of meteorological data, ice data, surface-water levels and groundwater levels in the regolith available for the assessments reported in this document. Dates are given as YYYY-MM-DD.

Data type and id	Start	Stop (this report)
Meteorological data		
PFM010700 (Högmasten)	2003-05-12	2015-06-10 (station decommissioned)
PFM010701 (Storskäret)	2003-05-12	2007-06-30 (station decommissioned)
PFM006281 (Labbomasten)	2013-04-14	2016-06-30
Ice freeze and breakup in sea bay (winter seasons)		
AFM000075	2002/2003	2015/2016
AFM001449	2015/2016	2015/2016
Surface-water levels		
PFM010038 (sea level)	2003-05-22	2016-09-30
SFM000119 (Lake Tjärnpussen)	2009-05-07	2016-09-30
SFM000156 (nameless pond)	2016-03-15	2016-09-30
Groundwater levels in regolith		
SFM0049	2003-05-13	2016-06-20
SFM0076	2005-01-10	2005-02-02
SFM0077	2005-10-18	2016-09-30
SFM0078	2005-10-18	2016-09-30
SFM0079	2005-10-18	2016-09-30
SFM0107	2006-06-20	2016-09-30
SFM000121	2011-05-12	2016-09-30
SFM000122	2011-05-12	2016-09-30
SFM000123	2011-05-12	2016-09-30
SFM000124	2011-05-12	2016-09-30
SFM000125	2011-05-12	2016-09-30
SFM000139	2014-07-03	2016-09-30
SFM000143	2016-07-05	2016-09-30
SFM000144	No data	
SFM000145	2016-08-24	2016-09-30
SFM000146	2016-07-05	2016-09-30
SFM000147	2016-07-05	2016-09-30
SFM000149	2016-07-05	2016-09-30
SFM000153	2016-07-05	2016-09-14
SFM000154	The well is dry	

3.5 Assessment of groundwater levels and hydrochemical monitoring data in the bedrock boreholes at depth

Figure 3-7 also gives an overview of the long-term monitoring of groundwater levels at depth in the bedrock boreholes located in proximity of the access area. Groundwater levels at depth are affected by the spatial variations in total pressure and groundwater density (Berglund and Lindborg 2017). Specific events of the recorded point-water heads from cross-hole (interference) tests are analysed in Chapter 8. Likewise, available long-term hydrochemical monitoring data in basically the same boreholes are analysed in Chapter 9.

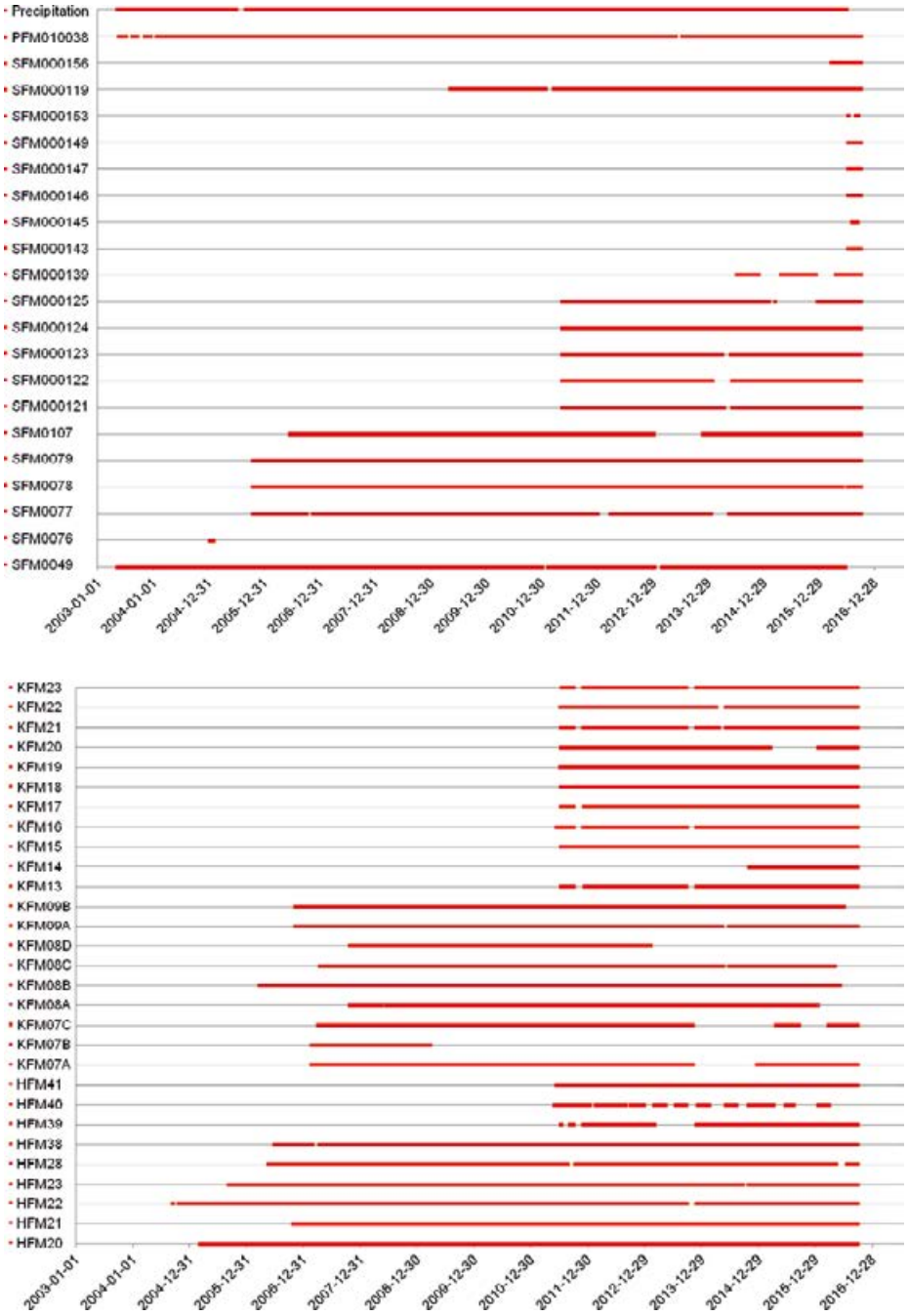

Figure 3-7. *Plots of periods of monitoring data available for analysis. Upper plot: meteorology (here represented by precipitation measured at the Storskäret, Högmasten and Labbomasten stations), sea level (PFM010038), surface-water levels (SFM000119 and -156), and groundwater levels in wells installed in regolith. Lower plot: groundwater levels in core-drilled (KFM) and percussion-drilled boreholes (HFM).*

4 Topography and regolith geology

4.1 Status of site understanding and models

Geometric modelling related to topography and bathymetry aims to describe the terrain and variation in topography and bathymetry, including terrestrial areas (land), lakes (lake bottoms) and marine areas (ocean bottom). The product of the geometric modelling is a digital elevation model (DEM). This is based on interpolated point measurements of elevation, and the resolution and accuracy of the DEM is a function of point density and type of measurement. The resolution of the DEM used for **SDM-Site** was fit for purpose, but for the purpose of guiding the groundwork of the geotechnical constructions in the access area a higher resolution is needed, see below.

Regolith refers to all unconsolidated deposits which overlay the bedrock. In the Forsmark area, all regolith was deposited during the Quaternary period and is therefore often referred to as Quaternary deposits (QD). The term regolith also includes man-made deposits, in the Forsmark area mainly artificial fill. In the terrestrial areas, the upper part of the regolith that has been affected by climate and vegetation is referred to as soil. Modelling regolith thickness results in a regolith depth model (RDM).

Since the start of the site investigations for the spent fuel repository (PLU) in Forsmark, a series of models have been produced, refined and updated. Model reports related to geometrical modelling and regolith geology are shown in Figure 4-1. A comprehensive site description of the regolith was produced during **SDM-Site** (Hedenström and Sohlenius 2008), whereas the DEM, the RDM and the marine geological map were updated for **SR-PSU** and were reported in Strömgren and Brydsten (2013), Sohlenius et al. (2013) and Nyberg et al. (2011), respectively. The geologic evolution of the area is presented in Söderbäck (2008). The **SDM-Site** description and the **SR-PSU** models are the basis for this chapter and are further described below. Data acquired since, and models produced after, these reports are described in Section 4.2.

The DEM presented in Strömgren and Brydsten (2013) is in raster format (GRID) and has a 20 by 20 m^2 horizontal resolution. The model covers approximately 30 by 30 km^2 (Figure 4-2). The DEM describes the topography on land and the bathymetry (bottom topography) of lakes and the near-coastal sea areas. Hence, the DEM has no water levels. The highest elevation within the DEM is 50 m above sea level, whereas the lowest elevation is 55.4 m below sea level (height system RHB 70). The extremely flat topography in Forsmark is evident in this model. Larger elevation differences can mainly be found in and around the Gräsö trough running between the mainland area and the Island of Gräsö. The largest elevation uncertainties in the DEM are in the deeper marine parts of the model, where elevation has been mapped by echo sounding along transects up to 1 km apart (Strömgren and Brydsten 2013), which has been reduced to approximately 500 m in the recently acquired data.

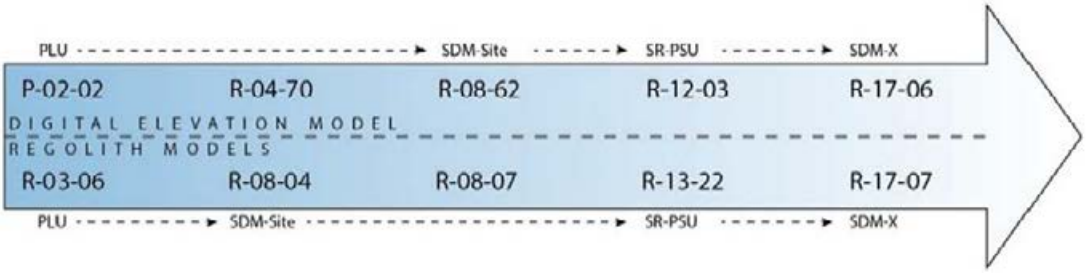

Figure 4-1. *Model development related to geometrical modelling and regolith geology in the Forsmark area. Reports R-17-06 and R-17-07 will present the basis for the access area models referred to herein; these reports are under production and will be completed after the publication of the present report. The SDM-Site DEM and RDM reports are R-08-62 (Strömgren and Brydsten 2008) and R-08-07 (Hedenström et al. 2008), respectively, whereas R-12-03 (Strömgren and Brydsten 2013) and R-13-22 (Sohlenius et al. 2013) are the corresponding SR-PSU reports.*

The latest published regolith depth model (RDM, Figure 4-2) has a horizontal resolution of 20 m (Sohlenius et al. 2013). The regolith thickness ranges from zero at bedrock outcrops to a maximum of 47 m in deep parts of Öregrundsgrepen, and the mean regolith thickness is 6.7 m (Figure 4-2). Generally, the regolith thickness is larger on the sea floor (mean thickness 8.3 m) compared to land (mean thickness 4.0 m). Regolith covers approximately 90 % of the ground surface within the **SR-PSU** model domain (Sohlenius et al. 2013). Figure 4-3 shows the **SR-PSU** regolith map and an excerpt covering the access area. This means that also the access area map in Figure 4-3 is based on **SR-PSU** data only.

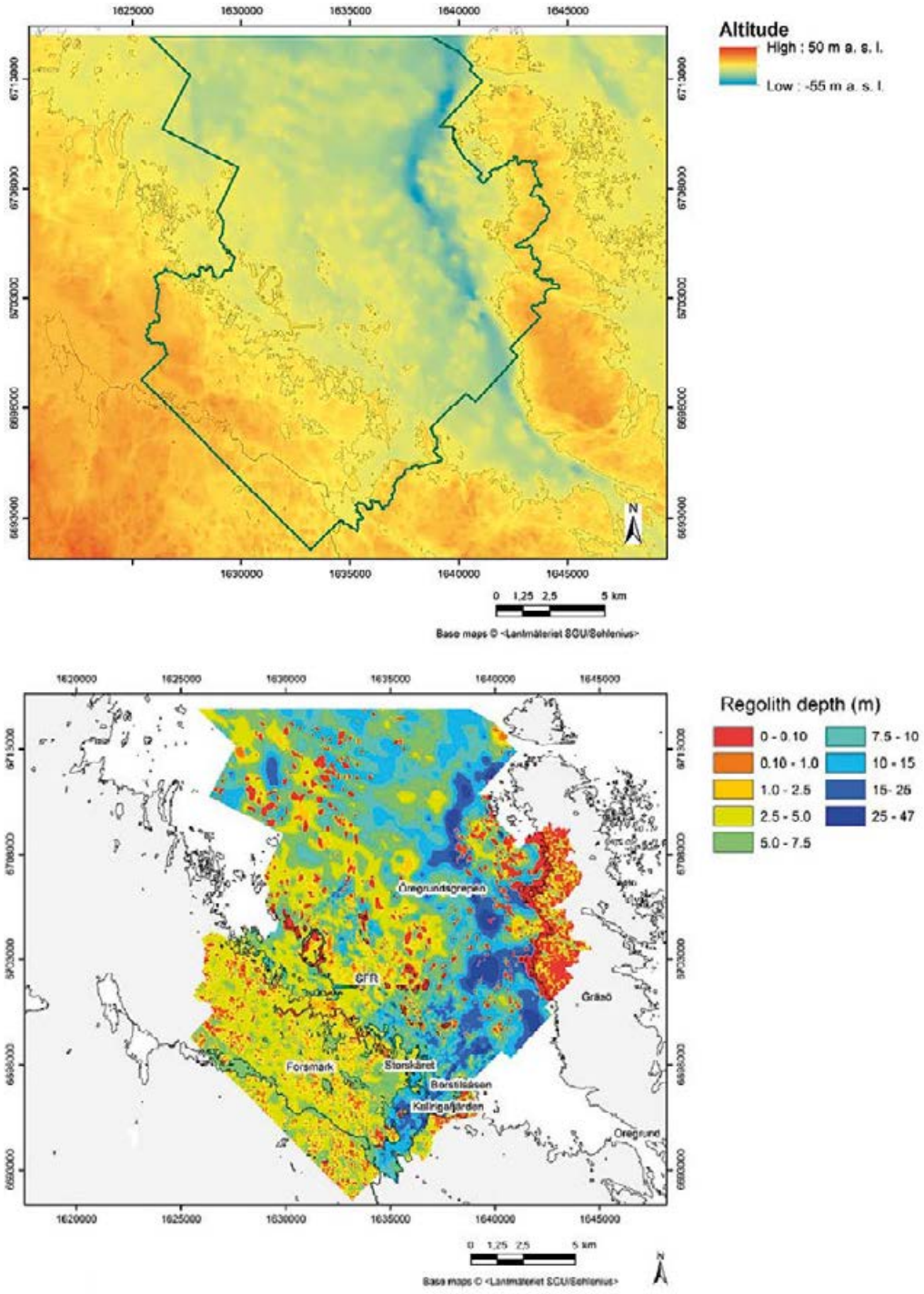

Figure 4-2. *Geometry and regolith geology models from SR-PSU: digital elevation model (DEM) from Strömgren and Brydsten (2013) (top; Figure 2-1 in Sohlenius et al. 2013), regolith depth model (RDM) from Sohlenius et al. (2013) (bottom; Figure 5-1 in Sohlenius et al. 2013).*

On the relatively large scale of the **SR-PSU** model area, the bedrock surface topography is well correlated with the ground surface topography. Exceptions to this are the eskers found within the area, with the largest esker Börstilsåsen visible as the green elongated outline in the south-central part of Figure 4-3, and where the surface topography has been altered by man-made deposits (artificial fill). Furthermore, detailed investigations on much smaller scales of excavations within the access area have shown examples of much larger variations in bedrock topography than indicated by the ground surface topography (cf below).

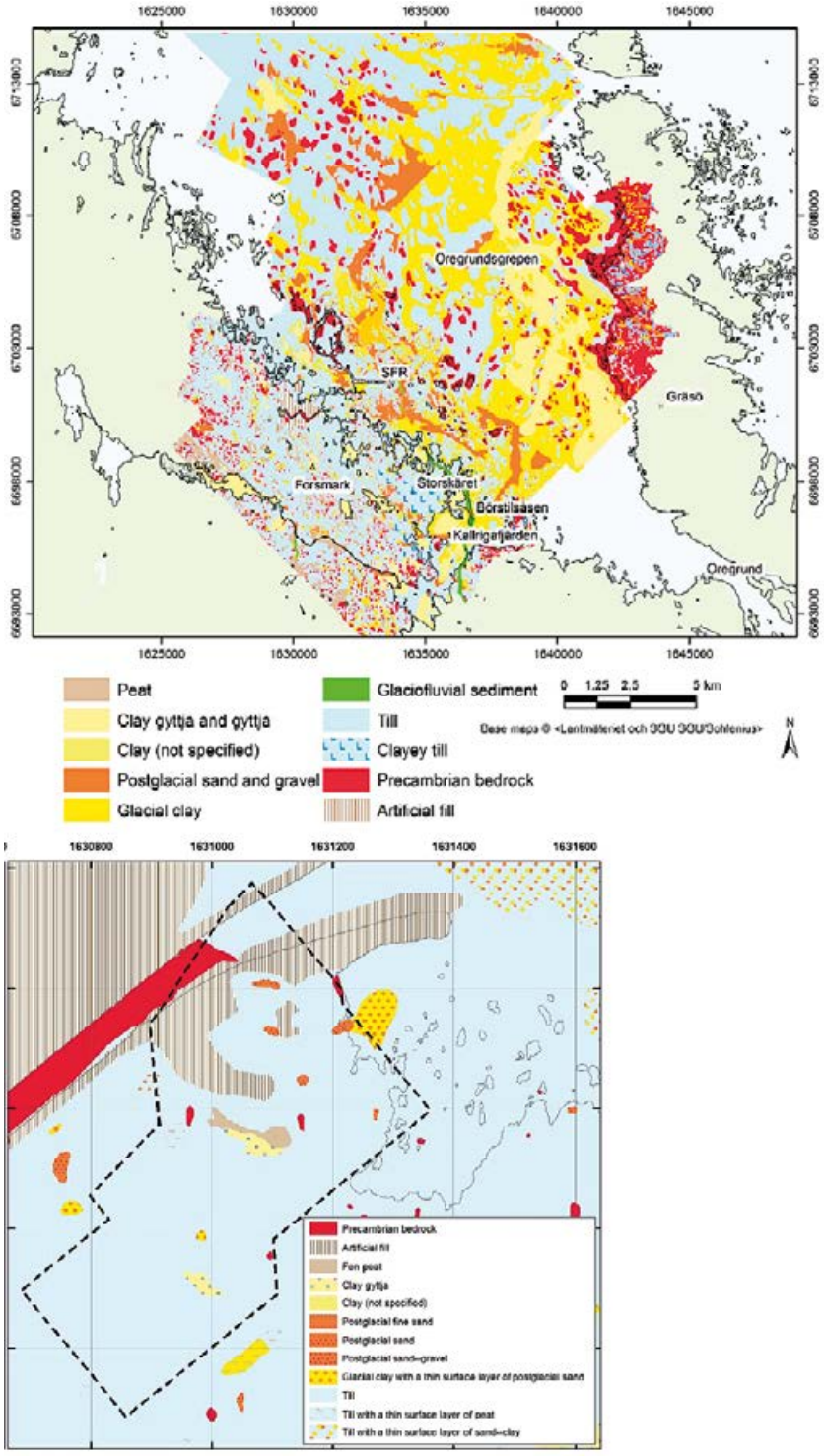

Figure 4-3. *Surface distributions of regolith based on data presented in Sohlenius et al. (2013): SR-PSU model area (top; Figure 3-1 in Sohlenius et al. 2013), excerpt covering the access area (indicated by the broken line) and its vicinity (bottom). The centre of the access area is at approximately (1631000, 6700300); more detailed identification and description of this area is provided below.*

For detailed descriptions of **SDM-Site** and **SR-PSU** investigations and modelling related to topography, bathymetry and regolith geology and geometry, the reader is referred to Hedenström and Sohlenius (2008), Sohlenius et al. (2013) and Strömgren and Brydsten (2013). Generally, the access area is relatively flat with little relief and elevations between 0 and ca 6 m on land. The nuclear power plant cooling-water inlet canal, which was constructed by excavation and blasting during the construction of the power plant in the 1970s, is the deepest part of the area with a maximum depth of about 9 m below sea level in the access area part.

The access area covers approximately 0.26 km^2 and constitutes only a small part of the model areas used for the DEM (c 900 km^2) and RDM (300 km^2) in **SR-PSU**. It does not include high-elevation areas or deep parts of the sea. The average regolith thickness is smaller in the access area than in the **SR-PSU** model area. Since no thick clay deposits are present within the access area, the maximum regolith thickness is also much smaller (approximately 10 m), compared to the regional **SR-PSU** area (nearly 50 m).

The access area and the **SR-PSU** model area also show differences in the distributions of different types of deposits. One major difference is the high abundance of artificial fill on the surface within the access area compared to the **SR-PSU** area (Figure 4-3). This is because the access area has been affected by the major construction works for the nuclear power plant and associated facilities carried out from the 1970s and onwards. Figure 4-3 also shows that till is the dominating regolith type within the access area. There is no occurrence of glaciofluvial material (e.g. eskers) in the access area.

The conceptual model of the stratigraphy in Forsmark (see Figure 4-4) is based on geological data and interpretations, especially regarding genetic stratification, where the oldest regolith unit is located at the bottom of the layer sequence and any overlaying unit is younger. Age here refers to depositional age. The conceptual model is based on knowledge from the site obtained from studies conducted for the repository for spent nuclear fuel (Hedenström and Sohlenius 2008).

The regolith can be grouped into two main categories: glacial deposits and postglacial deposits. Glacial deposits were deposited directly by the ice sheet or from meltwater from the ice sheet and are highly inorganic. Postglacial deposits pertain from the period after the ice sheet had retreated from the area and often contain organic material. This conceptual understanding of the regolith stratigraphy at Forsmark is the foundation of the RDM and assists in the assessment of the distribution of layers based on the surface distribution of regolith. Each layer seen in Figure 4-4 is further explained in Table 4-1 and in Hedenström and Sohlenius (2008).

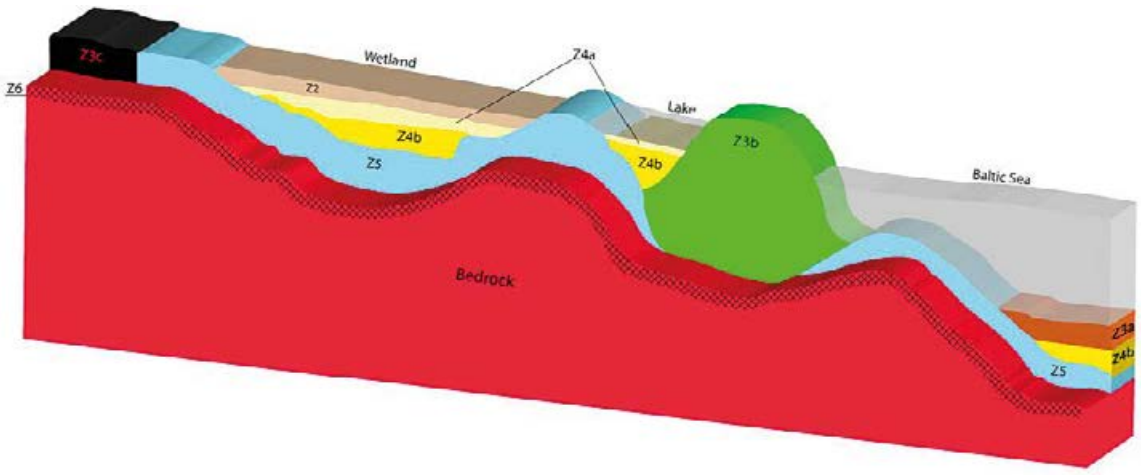

Figure 4-4. *General distribution of regolith layers (Z-layers) of the RDM (Sohlenius et al. 2013). The uppermost layer, Z1, which represents the uppermost regolith layer and bedrock outcrops, is not shown in the figure. See Table 4-1 for additional information.*

Table 4-1. The regolith types represented by Z-layers, which are included in the description of regolith stratigraphy in the RDM.

Layer	Regolith type (English term)	Jordart (Swedish term)	Comment
Z1	Surface layer		The upper regolith that has been affected by soil processes and/or other surface processes
Z2_l	Peat	Torv	–
Z3c	Artificial fill	Fyllning	Corresponds to material deposited by humans
Z4c	Gyttja	Gyttja	Sediments deposited in lakes and characterised by a high organic content
Z4a	Clay gyttja	Lergyttja	Represents also postglacial clay with lower organic content than clay gyttja
Z3a	Postglacial sand/gravel	Postglacial sand/grus	Sand and gravel deposited by water after the ice-sheet retreat
Z4b	Glacial clay	Glaciallera	Clay deposited directly from the retreating ice sheet
Z3b	Glaciofluvial sediment	Isälvssediment	Material (mainly sand and gravel) deposited by meltwater from the ice
Z5	Till	Morän	Deposits of varying size fractions
Z6	Bedrock	Berggrund	Upper bedrock

A large part of the area was submerged beneath the sea as recently as the 18th century (Figure 4-5). During the construction of the power plant and inlet canal, much of the natural landscape seen to the right in Figure 4-5 was altered. Many areas, including the cape in the north, have artificial fill overlaying natural deposits. At some locations, the artificial fill overlays glacial clay and postglacial sand. The majority of the natural deposits consist of till deposited during the latest glacial cycle. The continuous land uplift has sealed off a couple of water bodies. Three ponds are present (12, 13a and 13b in Figure 4-6). The till layer in these ponds is overlain by glacial clay, postglacial sand, and clay gyttja. A thin layer of peat has accumulated in some of the wetlands surrounding these ponds.

The most reliable and complete information regarding the deposits and stratigraphy comes from a handful of excavations done in the area in addition to the numerous drillings and regolith sampling. Several trenches have been excavated to uncover the bedrock in order to enable investigations of the bedrock surface and its properties as well as the stratigraphy of the pit walls.

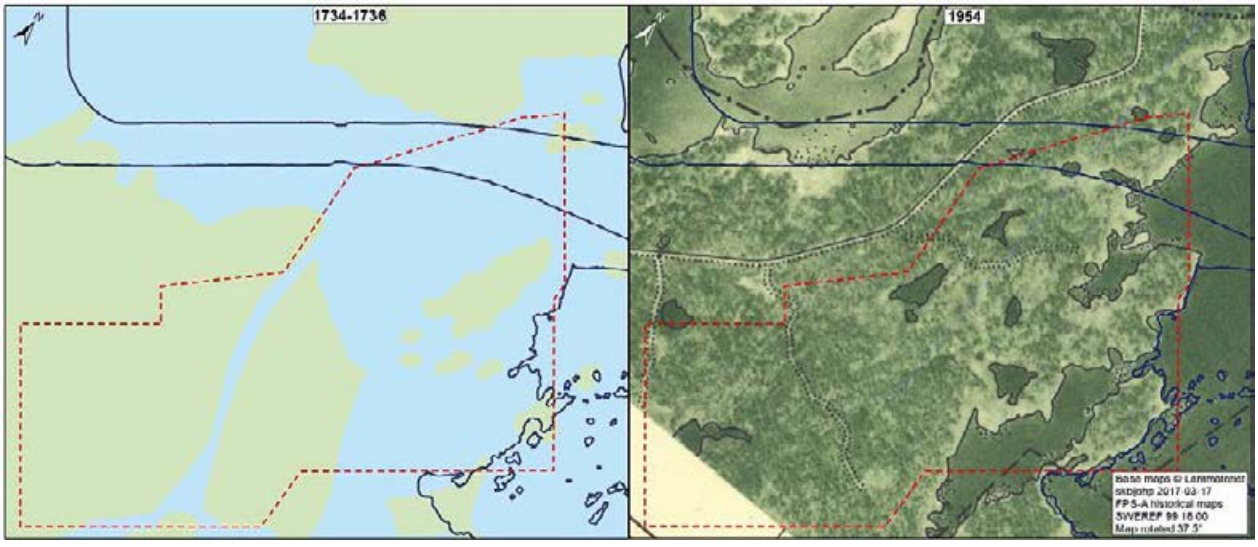

Figure 4-5. *Historical maps of the access area: 1734–1736 to the left (blue indicates sea) and 1954 to the right. The present-day shoreline (including the intake channel) is marked as blue lines and the red broken line shows the access area.*

Forssberg et al. (2007) investigated bedrock outcrops at AFM001264 close to Drill site 7 (Figure 4-6). The excavations showed a varied bedrock surface elevation with both sediment-filled sub-horizontal fractures with an aperture of approximately 20 cm as well as narrower vertical fractures. The fracture-filling material mainly consists of silt, fine sand and diamicton. The sedimentary lamination of the fracture-filling material shows that the sediments are mostly undisturbed. Some graben structures close to vertical fractures might indicate percolating water through the fractures, indicated by collapsed structures seen in the laminated layers. The fracturing of the uppermost bedrock is interpreted to be the result of glacial tectonics. The regolith mapped along the walls of the excavation shows a ca 1 m thick layer of artificial fill overlaying sandy and/or silty till. At one location towards the north in the excavation a hard till was found, interpreted to be an older lodgement till.

A little bit further north, another outcrop, AFM001265, was excavated (Petersson et al. 2007), see Figure 4-6. No large sub-horizontal fractures are present at this location. However, similar to the excavation to the south, large blocks were separated from the bedrock surface by approximately 20 cm with filling (laminated sand, silt and till) between the bedrock and the blocks. Another similarity between AFM001264 and AFM001265 is the presence of a harder lodgement till at deeper locations along the trench.

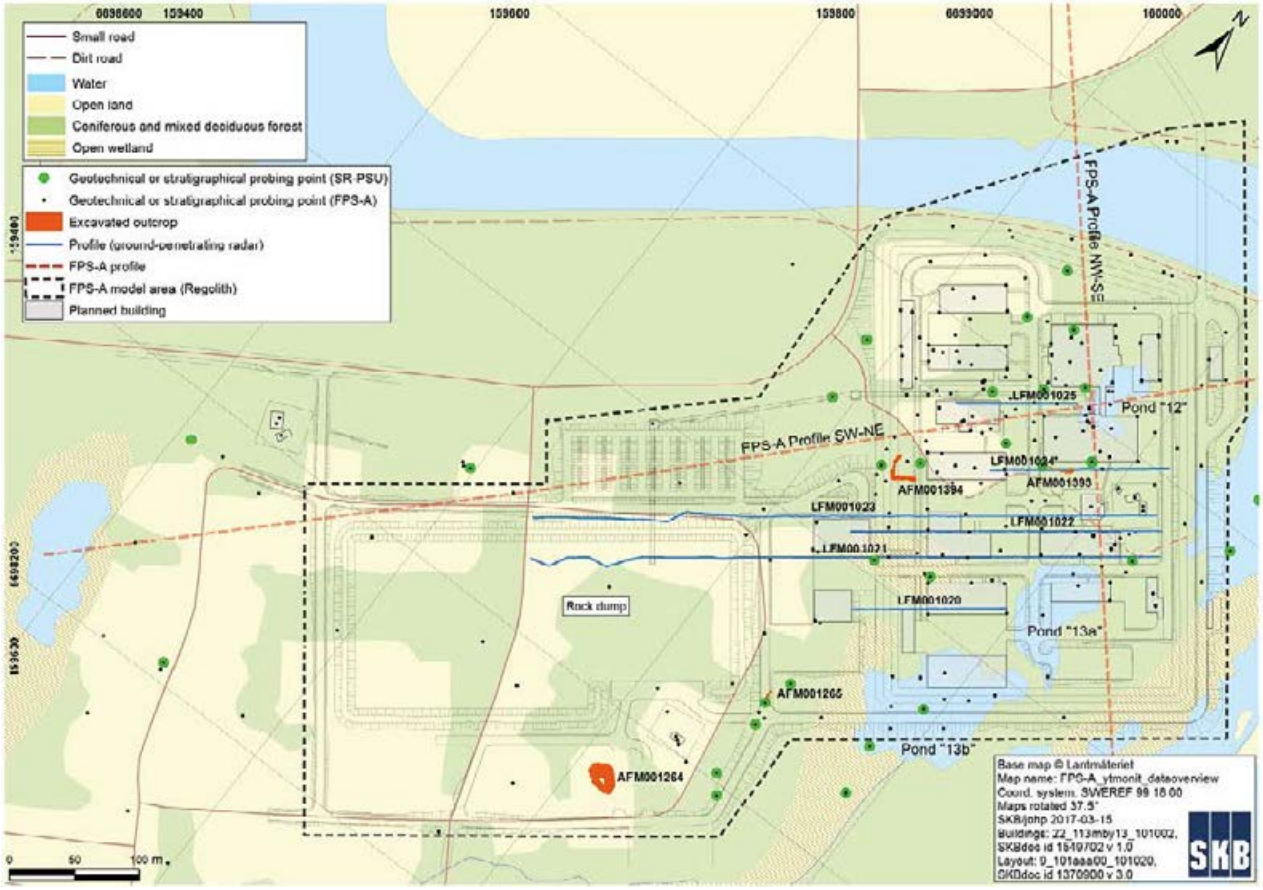

Figure 4-6. *Geotechnical, geophysical and stratigraphical investigations used in the modelling and evaluation of the regolith depth model (RDM) for the access area.*

4.2 Presentation and evaluation of input data

When evaluating the **SR-PSU** RDM, some improvement needs were identified (Sohlenius et al. 2013). For example, unrealistic changes in regolith depth were noted at the transition from terrestrial to marine areas. Furthermore, the RDM did not include all regolith layers that could be important for transport modelling, e.g. sand layers in areas covered by postglacial clays. A new RDM has therefore been produced and is now available in the SKB model database. The production of this model is described in Section 4.3 and the resulting model in Section 4.4, whereas the present section provides an overview of the input data used to produce the updated RDM.

Table 4-2 lists new data and models with relevance for the access area that have been acquired after **SDM-Site** and **SR-PSU**. Most of the data were collected in activities performed within a specific programme focusing on preparations for design of the surface and subsurface parts of the planned repository. The results are briefly presented below, and in more detail in the reports listed in the table.

A new Forsmark DEM has been produced (report soon to be available, cf Figure 4-1), based on LiDAR data from the Swedish national land survey and additional data from the marine areas. Table 4-2 gives the SKBmod id for this DEM, i.e. the SKB model database reference for the model. The new input data made it possible to produce a DEM with higher resolution and accuracy, especially in the terrestrial areas where the model has a resolution of 1×1 m^2. The DEM reference concerns a specific model variant (high resolution, no bathymetry). It should be noted that other model variants, e.g. other (lower) resolutions are available. A refined regolith map for the access area has also been produced, see model database reference in Table 4-2.

Table 4-2. New topographical, stratigraphical and geotechnical data acquired after SDM-Site and SR-PSU. SKBmod id refer to SKB's model database.

Data	SKBmod id or SKB report reference	Comment
DEM, based on LiDAR and echo-sounding data	SKBmod 1859072	Model variant without bathymetry Resolution: 1×1 m^2
Updated and refined regolith map of the access area	SKBmod 1859082	
Geotechnical drillings (2010)	Hellgren (2010, 2011)	
Geotechnical drillings (2016)	Henriksson (2016)	
Excavated bedrock outcrop (AFM001393)	Curtis et al. (2012)	
Excavated bedrock outcrop (AFM001394)	Curtis et al. (2012)	
GPR measurements (2011)	Mattsson (2011)	
Excavated pits (2016)	Petrone (2017)	

Figure 4-7 shows a high-resolution (1 x 1 m^2) topographic map of the access area and Figure 4-8 shows the updated map of the regolith. Artificial fill now constitutes a larger portion of the regolith compared to the corresponding map in Figure 4-3. However, it should be noted that Figure 4-8 shows the distribution of the uppermost regolith, whereas the map in Figure 4-4 shows the distribution of regolith at a depth of 0.5 m below the ground surface. Irrespective of this difference, it is clear that the updated descriptions of ground surface elevation and surface distribution of regolith provide much more detailed representations of the access area than pre-existing models. Thereby, the updated DEM and regolith map constitute a significantly improved basis for surface facility design and development of a detalied RDM (cf below).

Two outcrops of the bedrock were excavated in 2010 (pits/trenches AFM001393 and AFM001394, Curtis et al. 2012). The outcrops are shown in Figure 4-9 and their locations are indicated on the map in Figure 4-6. The bedrock topography was measured to acquire data on the bedrock elevation and its variation. Four samples of till (PFM007690–93) were collected in AFM001393 and one sample of till (PFM007694) was collected in AFM001394. The samples were analysed for a number of physical and chemical parameters. The analyses and the results are presented in Sheppard et al. (2011). The excavations revealed a highly varied bedrock surface elevation. In pit/trench AFM001393, the bedrock surface exhibits a step-like formation and vertical drops of several metres (Figure 4-9A). In the second excavation, AFM001394, a large vertical drop of more than 4 m is visible in Figure 4-9B.

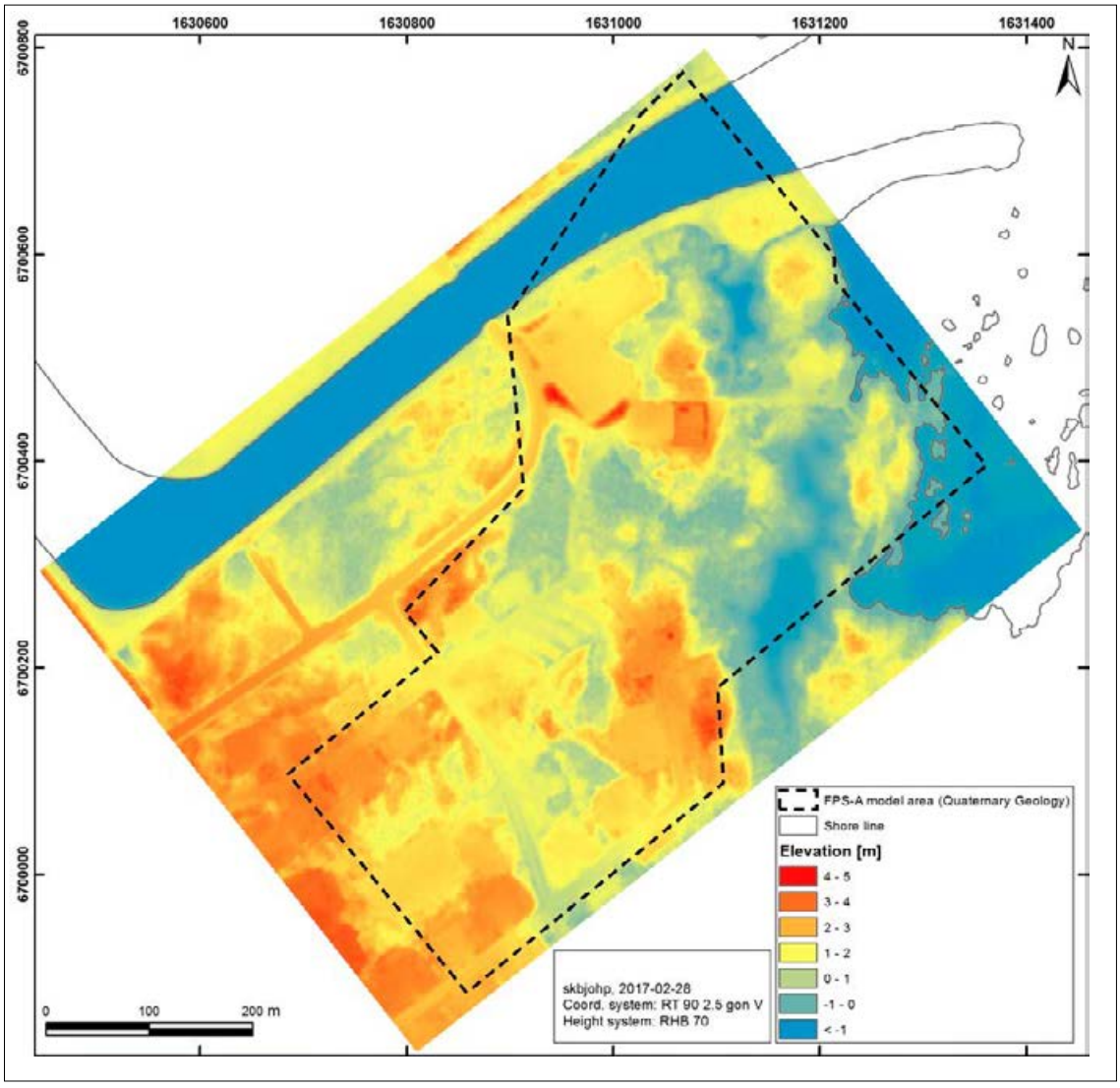

Figure 4-7. *High-resolution topographic map of the access area.*

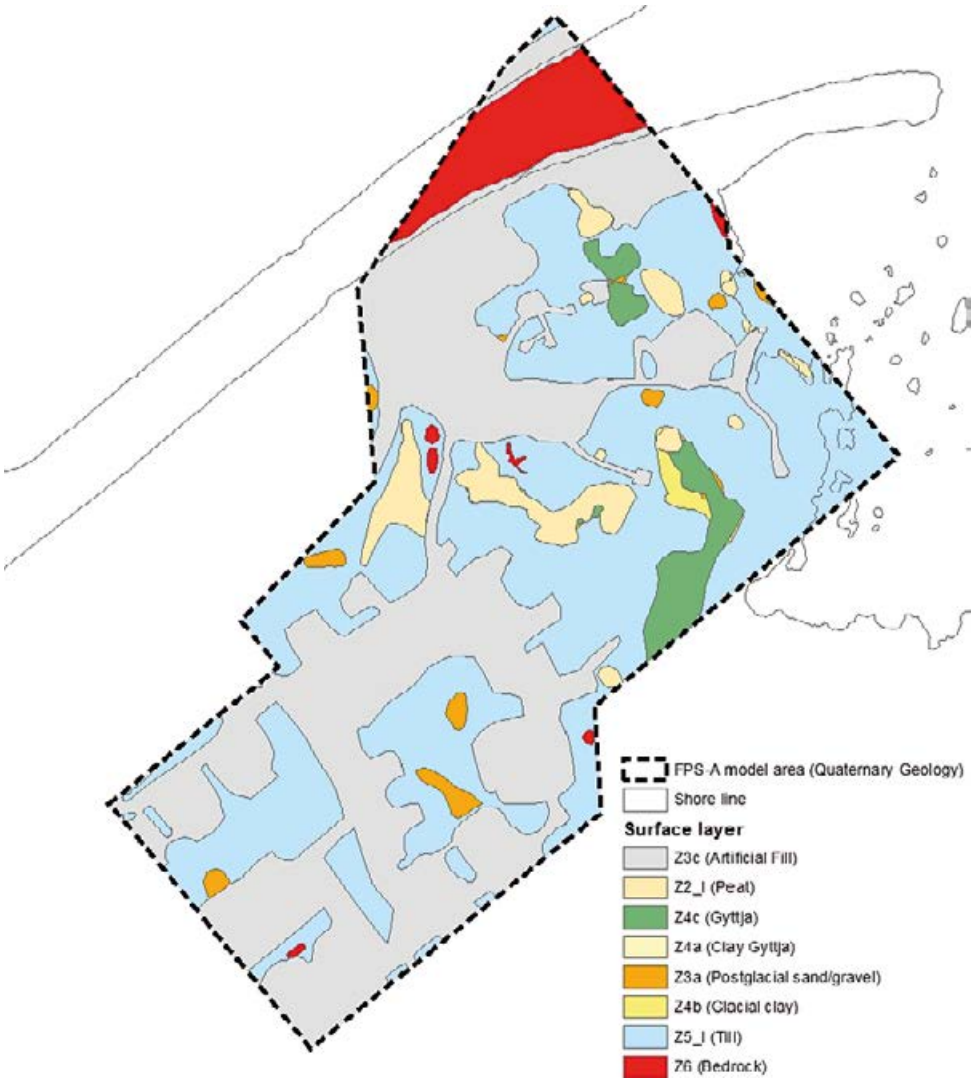

Figure 4-8. *Refined and updated surface regolith map of the access area (cf Figures 4-6 and 4-7).*

Figure 4-9. *Highly varied bedrock surface in A) AFM001393 and B) AFM001394. (Photo: Lars Bergkvist, Golder Associates.)*

In 2016, 11 pits were excavated to study and sample till at different locations within the access area (Petrone 2017). Figure 4-10 shows the resulting logs of the stratigraphy. The high abundance of artificial fill is evident in the logs as well as underlying clay at one location (PFM007791). No pits were deep enough to encounter the bedrock. It can sometimes be difficult to differentiate between artificial fill and till due to the fact that much of the material used as fill within the access area is previously excavated till. In three pits (PFM007784, PFM007786 and PFM007791), buried fine sediments were encountered below the artificial fill. It is possible that these layers are remnants of wetlands that were present before in the area. Before the construction works in the area, it contained more wetlands and depressions; these have either been buried or removed (see Figure 4-5).

For the modelling of the access area regolith, there were in total 159 boreholes with information regarding the depth to the bedrock within or in close proximity to the access area (Figure 4-11). Regolith depths range from 0 m (at bedrock outcrops) to approximately 9.5 m at these 159 borehole locations, and the mean regolith depth is 4.22 m.

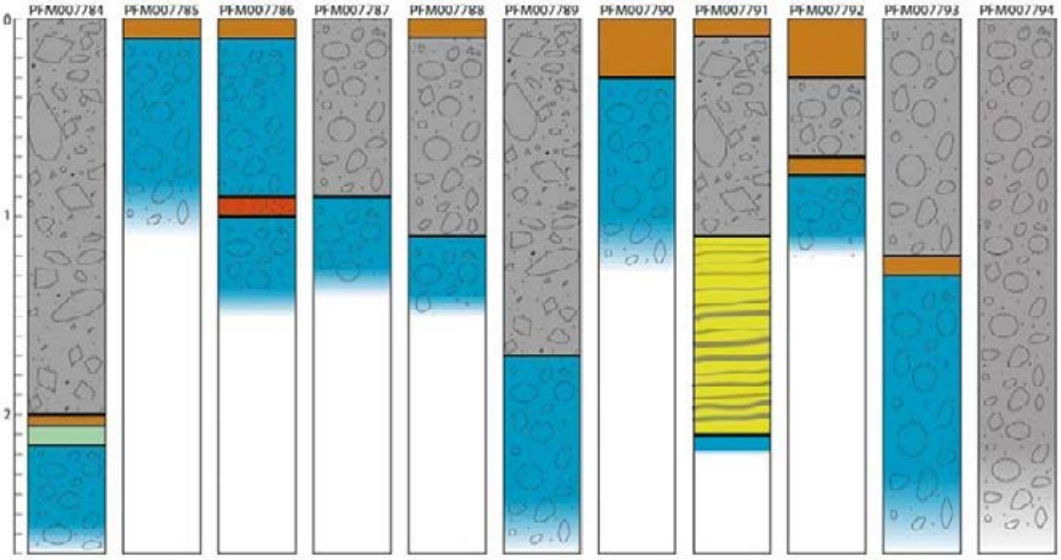

Figure 4-10. *Mapped stratigraphy in the pits excavated during 2016 (PFM007784–PFM007794, shown from left to right). Grey = artificial fill, brown = humus (decomposed organic matter), light green = clay gyttja, blue = till, orange = sand/gravel, striped yellow = glacial clay.*

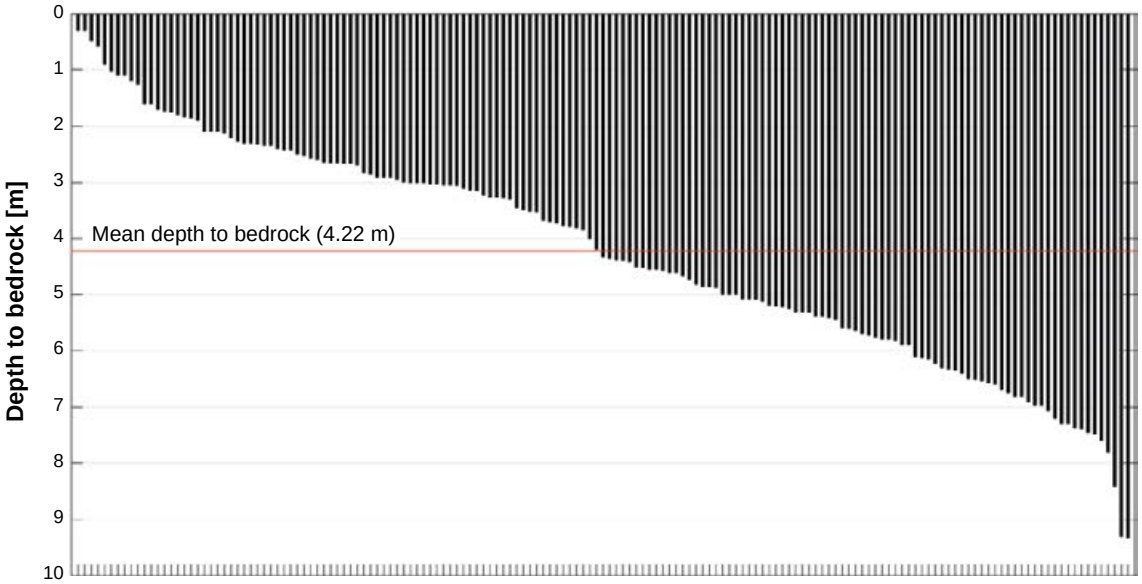

Figure 4-11. *Distribution of depth to bedrock for boreholes included in the modelling; plot of all boreholes within or near the access area with information regarding the depth to the bedrock surface.*

4.3 Description of modelling

The SubsurfaceViewer MX software version 6.0.33 (INSIGHT 2014) was used to interpret and model the thickness of different regolith layers. The software makes it possible to use conceptual knowledge of the stratigraphical distribution of regolith layers (Figure 4-4 and Table 4-3) to construct a model based on available data (topography, boreholes, excavations, maps of surface distribution of regolith). The method for modelling regolith layers with SubsurfaceViewer is illustrated in Figure 4-12 and thoroughly described in the forthcoming RDM report (cf Figure 4-1).

Table 4-3. Stratigraphical distribution of regolith in relation to the map of surface distribution of regolith (Figure 4-4). The information was used for the regolith depth model (RDM) and shows for each type of surface regolith (first column) the stratigraphy from surface to bedrock (from left to right in second column). Note that in some areas with e.g. peat there is evidence from observations showing that one or more regolith layers are missing.

Regolith class on the regolith surface map	Stratigraphy in model (surface → bedrock)	Comment
Bedrock (Z6)	Z6	
Till (Z5_I)	Z5_I/Z6	Till is always situated directly on top of the bedrock (Z6)
Glacial clay/Glacial silt/Clay (Z4b)	Z4b/Z5_I/Z6	Glacial clay is always situated above till (Z5_I)
Postglacial sand and/or gravel (Z3a)	Z3a/(Z4b)/Z5_I/Z6	Postglacial sand is sometimes situated on top of glacial clay (Z4b) but always above the till (Z5_I)
Clay gyttja/Gyttja (Z4a)	Z4a/Z3a/Z4b/Z5_I/Z6	
Gyttja (Z4c)	Z4c/Z4a/Z3a/Z4b/Z5_I/Z6	
Artificial fill (Z3c)	Z3c/Z2_I/Z3a/Z5_I/Z6	Most artificial fill lays directly upon till but occasionally overlays peat (Z2_I) and/or sand (Z3a) in the access area
Peat (Z2_I)	Z2_I/Z4a/Z3a/Z4b/Z5_I/Z6	

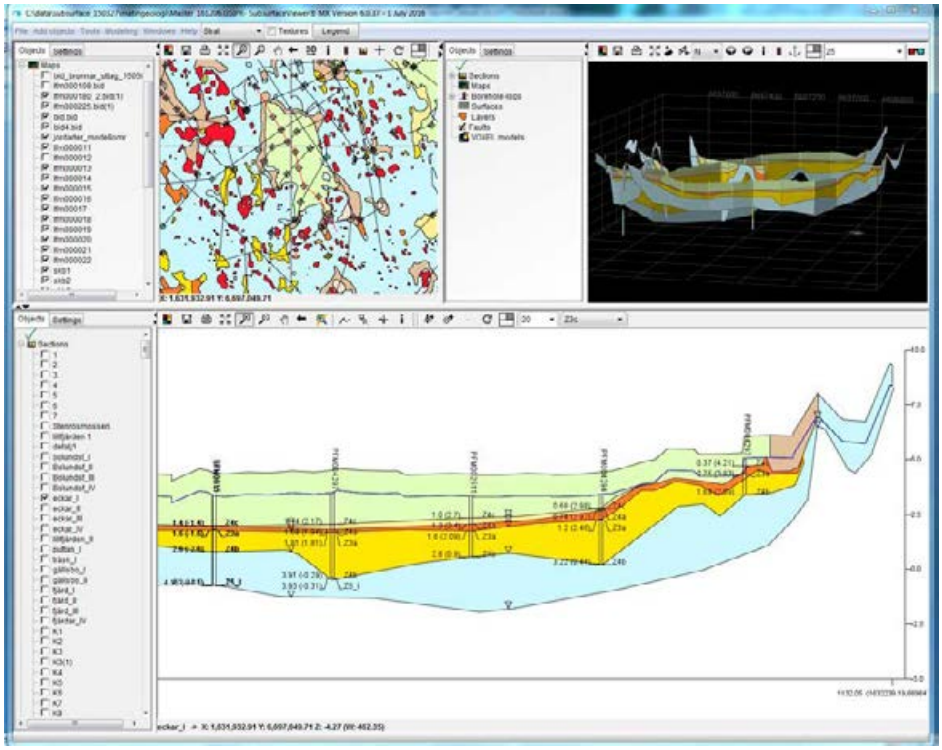

Figure 4-12. *Illustration of modelling methodology and the SubsurfaceViewer tool. The map of regolith and location of stratigraphical observations are shown in the upper left window, which also displays the positions of the sections. The distributions of regolith layers along the sections were interpreted in the lower window, by using the map of regolith together with the stratigraphical observations. The regolith map is shown in the upper part of the sections and the stratigraphical observations are displayed as staples. The triangles show where sections cross. The regolith is displayed with the same colours in the sections and on the regolith map. All sections can be displayed and studied from different directions in the upper right window.*

There are several reports presenting results of stratigraphical studies of regolith in the Forsmark area (e.g. Ising 2005, Hedenström 2004, Sohlenius and Hedenström 2009). A general model of regolith stratigraphy was constructed based on this knowledge (Table 4-1 and Table 4-3). This information was used together with stratigraphical data and the regolith map for interpretations needed to produce the RDM. The regolith map was then used to interpret the probable vertical stratigraphy of regolith in areas where stratigraphical data are missing. At some locations, some of the regolith layers shown in Table 4-1 are missing. This was considered when making the interpretations in SubsurfaceViewer.

All data, including DEM, regolith map and stratigraphical information, was imported to SubsurfaceViewer. Thereafter, 60 stratigraphical sections/profiles were interpreted using the software. Data from boreholes was first imported and sections constructed, connecting nearby boreholes. These sections were then manually interpreted using data from the borehole observations in combination with the topography and map of the surface distribution of regolith.

The general stratigraphy shown in Figure 4-4 was used when drawing the profiles. The map of regolith was used to delineate occurrences of different regolith types. Since till is the oldest regolith type, no other deposits than till (Z5_I) are allowed in areas where the surface regolith map indicates till (Table 4-3). Figure 4-12 shows an example of a section. Interpolation is done by linear triangulation between interpreted sections for the regolith map as well as the topography. The model is then post-processed to remove any incorrect clipping of layers. The settings used for the modelling in SubsurfaceViewer are shown in Table 4-4.

Table 4-4. Parameter values used for the calculation of layers in SubsurfaceViewer (INSIGHT 2014).

Parameter name	Value
Use same settings for all layers	Checked
Calculate top of layers	Checked
Smooth TINs	Unchecked
Refine TINs	Checked
High	Checked
Clean top-base	Checked
Clip top-base	Unchecked
Minimal thickness (m)	0.2

4.4 Resulting regolith model

The resulting model describes the top and bottom of layers listed in Table 4-1 and can be seen in Figure 4-13. The SKB model database id of the access area RDM is SKBmod 1719983. The majority of regolith within the access area is till, making up 91.6 % of the total regolith volume. Artificial fill constitutes 7.3 % of the regolith, whereas the other materials make up the remaining 1 % (Table 4-5). The layers were exported in ASCII format with a cell size of 5 m and converted to ESRI ARC grids in ArcGIS.

Table 4-5. Areal extent and volume of layers in the regolith model for the access area.

Layer	Areal extent (m^2)	Volume (m^3)	Mean thickness (m)
Z3c (Artificial fill)	112 168	72 666	0.65
Z2_I (Peat)	10 811	2 303	0.21
Z4c (Gyttja)	8 438	2 508	0.30
Z4a (Clay gyttja)	52	9	0.17
Z3a (Postglacial sand)	7 024	1 279	0.18
Z4b (Glacial clay)	11 506	4 432	0.39
Z5_I (Till)	248 067	911 280	3.67
Z6 (Bedrock)	259 326	-	-

The variation in bedrock topography is evident with larger variation in modelled elevation where there is a higher concentration of probing points (northern area). An elongated structure can be seen in the bedrock running in a northwest-southeast direction, marked by a dashed line in Figure 4-14 and Figure 4-15. This is the same feature that was excavated in AFM001394 (Figure 4-9B). It is possible

that this structure continues further south, but this has not been verified in the model due to the low concentration of probing points to the south. Further studies of the bedrock elevation to the south may reveal an extension of the feature.

By subtracting the bedrock elevation from the DEM it is possible to calculate regolith thickness (Figure 4-15). The mean and maximum regolith thicknesses inside the access are ca 4 m and ca 10 m, respectively. The largest thickness of the regolith can be found in the above-mentioned bedrock depression where the regolith exceeds 8 m in thickness. In general, the thickness of the regolith is higher where the bedrock is at a lower elevation, since the ground surface is relatively flat in the area. If the ground surface topography was correlated to the bedrock surface topography one would expect less variation in regolith thickness, which is not the case (Figure 4-15). The cross-sections shown in Figure 4-16 and Figure 4-17 refer to the two profiles shown in Figure 4-6. These illustrations clearly demonstrate that till is the dominant regolith type in the access area.

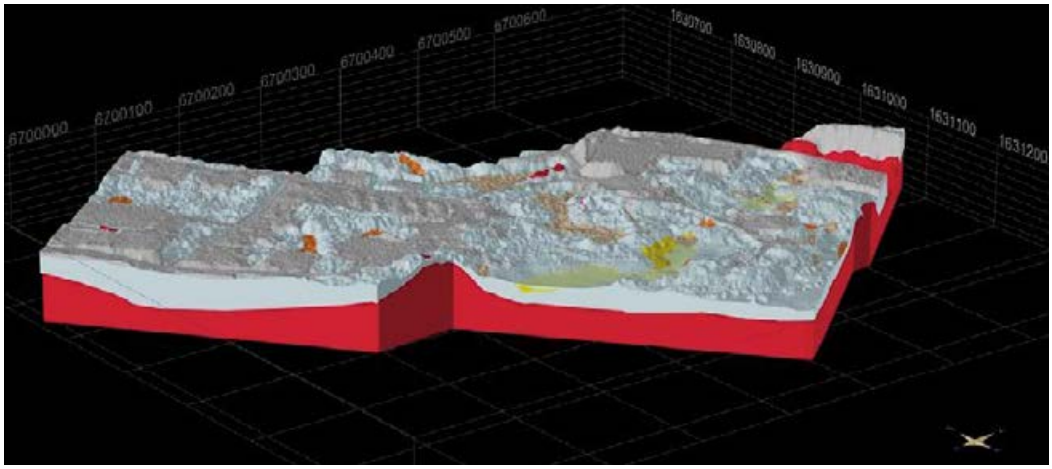

Figure 4-13. *Final interpolated RDM (SKBmod 1719983) viewed in SubsurfaceViewer with a vertical exaggeration of 5. Bedrock is represented by red colour, till with light blue, artificial fill with grey and the fine-grained sediments by different shades of yellow. Coordinate system: RT 90 2.5 gon V.*

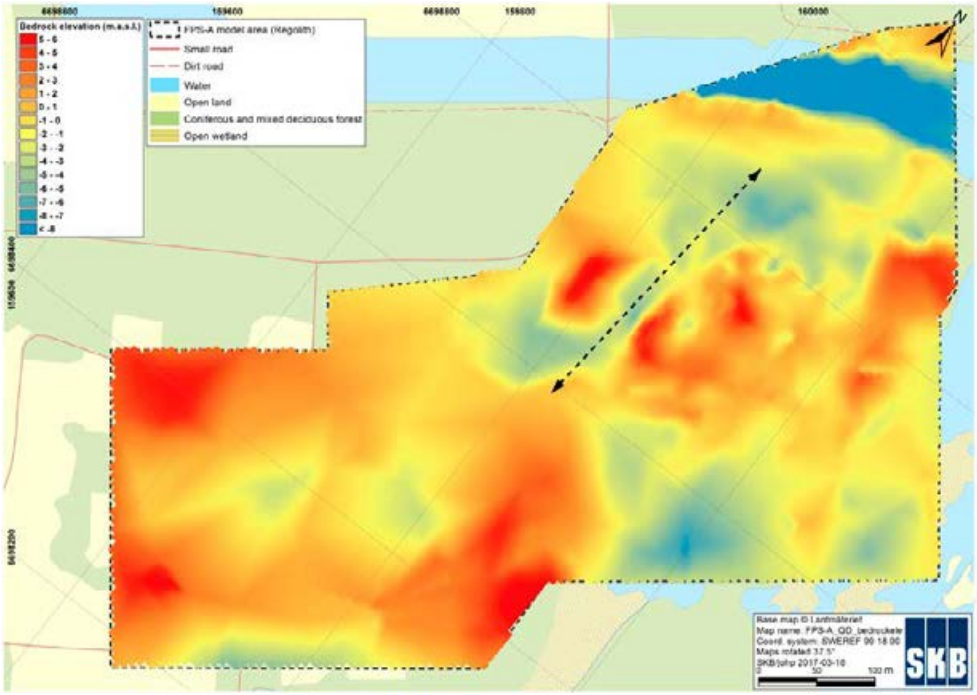

Figure 4-14. *Interpolated bedrock surface in the access area. A northwest–southeast feature in the bedrock can be seen, indicated by the dashed line.*

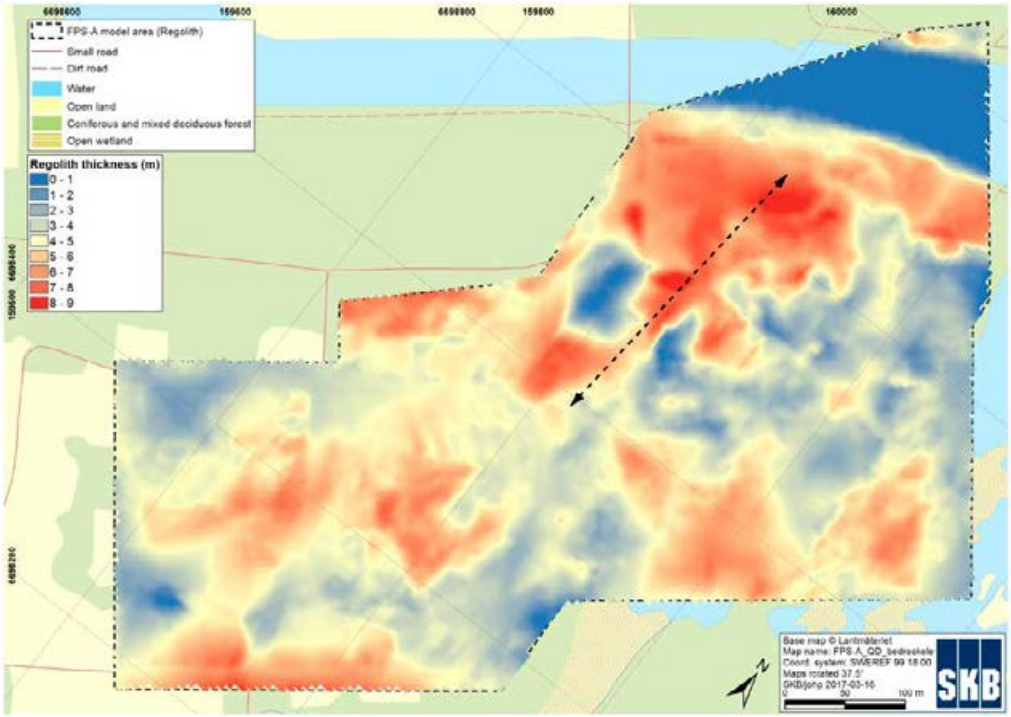

Figure 4-15. *Regolith thickness in the access area. Red indicates thicker regolith. The thickest regolith can be found in the bedrock depression marked by the dashed line.*

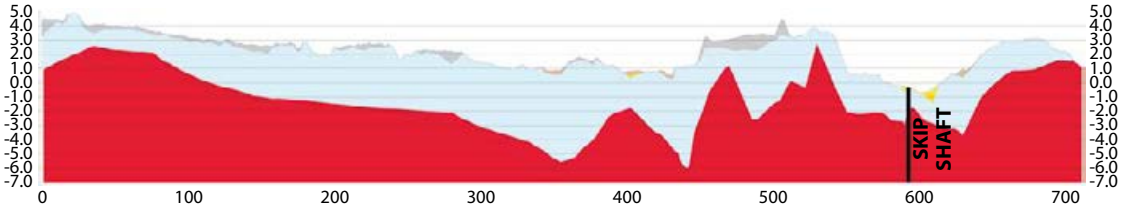

Figure 4-16. *Profile SW-NE with a vertical exaggeration of 5. The location of the profile outline is indicated in Figure 4-6 and the colours of the regolith layers are explained in Figure 4-4. Bedrock is represented by a red colour, till by light blue and artificial fill by grey.*

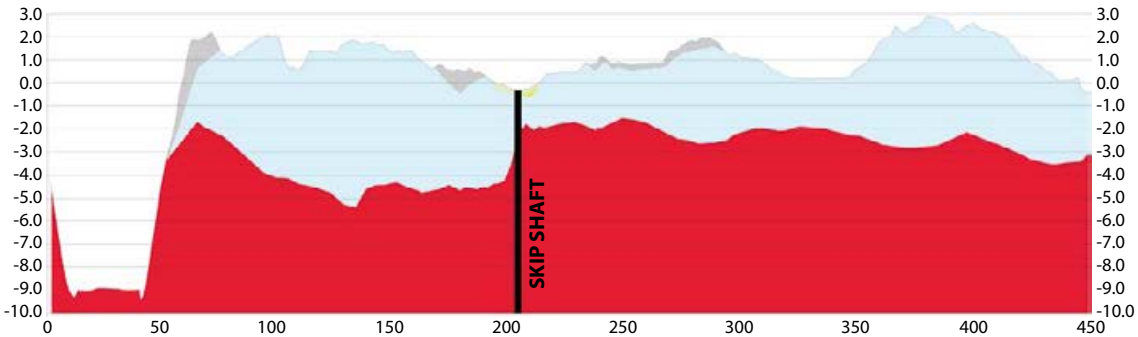

Figure 4-17. *Profile NW-SE with a vertical exaggeration of 5. The location of the profile is shown in Figure 4-6 and the colours of the regolith layers are explained in Figure 4-4. Bedrock is represented by a red colour, till by light blue, artificial fill by grey and clay by yellow. The inlet canal is clearly visible in the left part of the profile.*

4.5 Evaluation of uncertainties

The distance between data points has a large impact on the uncertainties of the final model. As discussed above, the bedrock surface has large vertical variations of several metres within small distances, and with data points sometimes spaced 50–100 m apart from each other it is impossible to capture these features. Thus, the seemingly smooth bedrock surface in areas with low data density is most likely much more rugged in reality. Figure 4-18 shows the Euclidian distance to the nearest stratigraphical data point. Green areas have stratigraphical information within 5 m and the stratigraphy and bedrock depth is more certain here than in areas where the distance is longer to data points (orange and red areas). The green areas also include exposed bedrock.

Another issue that influences model uncertainties is the interpreted depth to bedrock from borehole data. The high occurrence of large boulders near the real bedrock surface can sometimes lead to underestimation of the depth to the bedrock. Conversely, the existence of large, sediment-filled fractures can lead to overestimation of the depth to the bedrock, since they can be interpreted as regolith below blocks instead of fractures in bedrock.

A large portion of the surface deposits are also artificial fill, with varying origin. In some places, the fill is jagged blast rocks from the construction of the nearby power plant, in other places the fill is made up of redeposited till from the area and in yet other places the fill is a mixture of both. Determining the border between the fill and the till is therefore sometimes difficult.

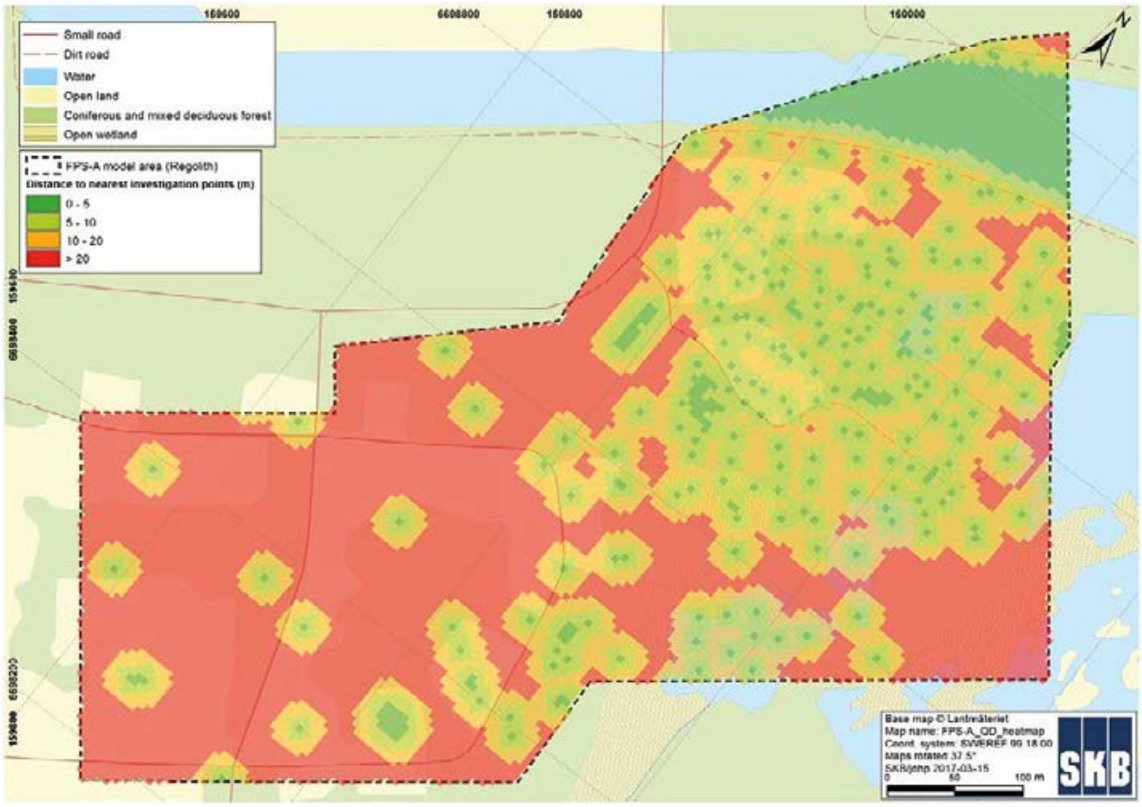

Figure 4-18. *Heat map showing the distance to stratigraphical data points used in the access area. Green indicates areas with short distance to a stratigraphical observation and red indicates areas with relatively long distance to an observation. Consequently, the RDM has a higher confidence in the green areas compared to the red areas.*

5 Bedrock geology

5.1 Scope of work

The geological models of rock domains, deformation zones and fracture domains in **SDM-Site** were finished in 2007 (Stephens et al. 2007, SKB 2008) and included information from the following cored boreholes: KFM01A–KFM08C and KFM09A–KFM10A. The deformation zone model was updated in 2014 (Stephens and Simeonov 2015) and included information from three additional cored boreholes: KFM08D, KFM11A and KFM12A. Stephens and Simeonov (2015) did not include data from the cored boreholes drilled during preparatory investigations in the access volume, i.e. the short boreholes KFM13–23 and the long borehole KFM24, see Section 2.5 and Figure 3-3 through Figure 3-6. In this chapter data inside the access volume are evaluated regarding the existing site-descriptive model for rock domains, deformation zones and fracture domains in Forsmark. Focus is put on the analysis of properties of the fracture domains FFM01 and FFM02, i.e. whether the properties of these domains inside the access volume in general are consistent with the data of these domains outside the access volume. This is done by the following:

1. Comparison of geological data inside versus outside the access volume acquired during **SDM-Site.**
2. Comparison of geological data inside the access volume acquired during the preparatory investigations with geological data outside the access volume acquired during **SDM-Site.**

The size of the access volume is defined in Table 3-1 and illustrated in Figure 3-3 through Figure 3-6. Figure 5-1a and b show the location of the access volume in relation to the location of the cored boreholes listed above, which are analysed in this chapter. Most of the long, cored boreholes are completely located outside the footprint of the access volume (Figure 5-1a). A few long boreholes, namely KFM07A, KFM07C, KFM08A, KFM08C, KFM08D and KFM24, are drilled partly inside and partly outside the access volume (Figure 5-1b). In the analyses data from a borehole which is partly inside and partly outside are split at the borders of the access volume to meet the definition of what is meant by “inside” and “outside” the access volume. It is noted that the short, cored boreholes drilled during the preparatory investigations, KFM13-23, are all situated inside the access volume.

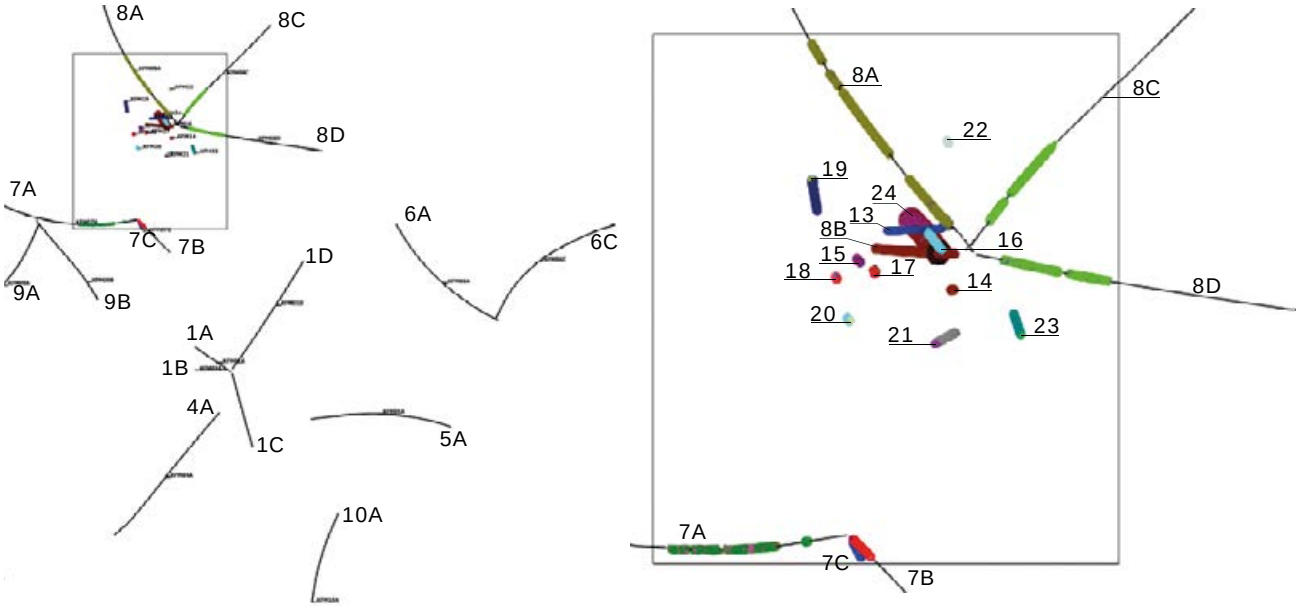

Figure 5-1. *Plane views illustrating that a) most boreholes are drilled completely outside the footprint of the access volume, and b) a few boreholes, namely KFM07A, -7C, -08A, -08C, -08D and KFM24, are drilled partly inside and partly outside the access volume.*

5.2 Current understanding

For the Forsmark area a local model and a regional model were produced for the rock domains and deformation zones at the completion of **SDM-Site** (Table 5-1). All rock outside the deformation zones are by definition called fracture domains (Olofsson et al. 2007).

Table 5-1. Models and documents stored in SKB's model database (SKBmod). RVS = Rock Visualisation System, i.e. SKB's tool for geological modelling and visualisation.

SKBmod id	Model name (in Swedish)	Comment	File name (Application)
1492438	DZ modell lokal PLU v. 2.3.	Deformation zones > 1000 m	PFM_DZ_LOC_v.2.3. (RVS)
1492517	DZ modell regional PLU v. 2.3	Deformation zones > 3000 m	PFM_DZ_REG_v.2.3. (RVS)
1492496	DZ modell regional PLU v. 2.3	Description of the model	PFM_DZ_v.2.3. Description (Word doc.)
1492607	RD modell lokal PLU v. 2.3	Rock domains	PFM_RD_LOC_v.2.3. (RVS)
1492880	RD modell regional PLU v. 2.3	Rock domains	PFM_RD_REG_v.2.3. (RVS)

5.2.1 Rock domain model

The geological information assembled for the bedrock inside the access volume does not change any conclusions regarding this volume from **SDM-Site**. In short, the access volume consists of two rock domains (RFM): RFM029 and RFM045 (Figure 5-2). The dominating rock type in RFM029 is a medium-grained and clearly deformed meta-granite. Subordinate rock types include pegmatite to pegmatitic granite, fine- to medium-grained meta-granitoid and amphibolite. The subordinate RFM045 (Figure 5-2) consists of an albitised (Na-K altered) medium-grained meta-granite together with aplitic meta-granite and smaller amounts of pegmatitic granite and amphibolite. Fresh rock types are common, thus the albitisation is not pervasive in this domain.

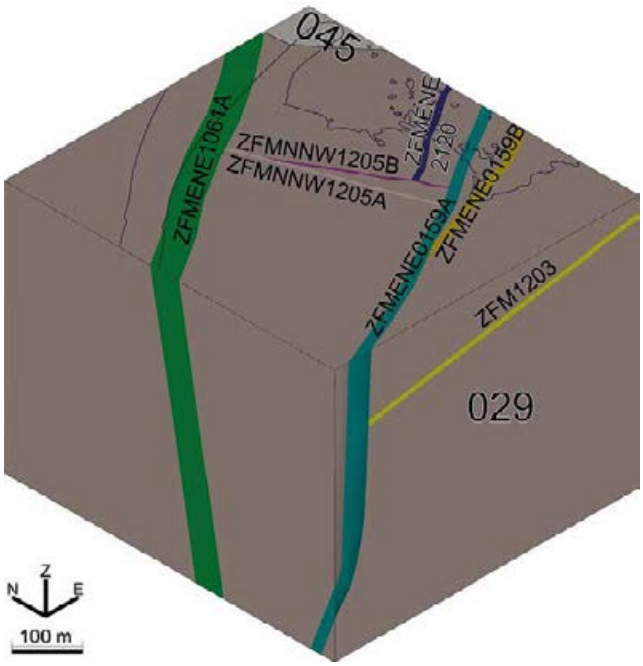

Figure 5-2. *View looking at the model volume towards north-east, displaying the rock domains RFM029 (brown) and RFM045 (beige) and seven deformation zones (cf Figure 5-3).*

5.2.2 Deformation zone model

Most of the deformation zones modelled deterministically in 3D for **SDM-Site** by Stephens et al. (2007) and Stephens and Simeonov (2015) have surface trace lengths greater or equal to 1 000 m. Deformation zones with shorter trace lengths were regarded as minor deformation zones and denoted by MDZ. Table 5-2 lists all deformation zones that transect the access volume and Figure 5-3 shows a transparent view of their spatial arrangement within the access volume. Three of these zones are MDZ, i.e. ZFMENE2120, ZFMNNW1205A and ZFMNNW1205B. The latter zone, ZFMENE1205B, was not modelled in **SDM-Site** but inferred in the data assessment for this document. Figure 5-4 shows that the orientation pattern of the deformation zones inside the access volume is coherent with the orientation pattern of all deformation zones modelled in **SDM-Site** and in Stephens and Simeonov (2015).

Table 5-2. Deformation zones inside the access volume.

Deformation zone	Trace length (m)	Thickness (m)	Orientation	Reference
ZFMENE1061A	1 192	48	056/81	SKB 2008
ZFMENE0159A	1 833	18	239/80	SKB 2008
ZFMENE0159B	672	14	238/80	SKB 2008
ZFMENE2120*	240	10	236/82	Stephens et al. 2007
ZFMNNW1205A*	367	5	159/78	Stephens et al. 2007
ZFMNNW1205B*	284	4	153/79	This document
ZFM1203	1 142	10	240/19	SKB 2008

* Minor deformation zone (MDZ).

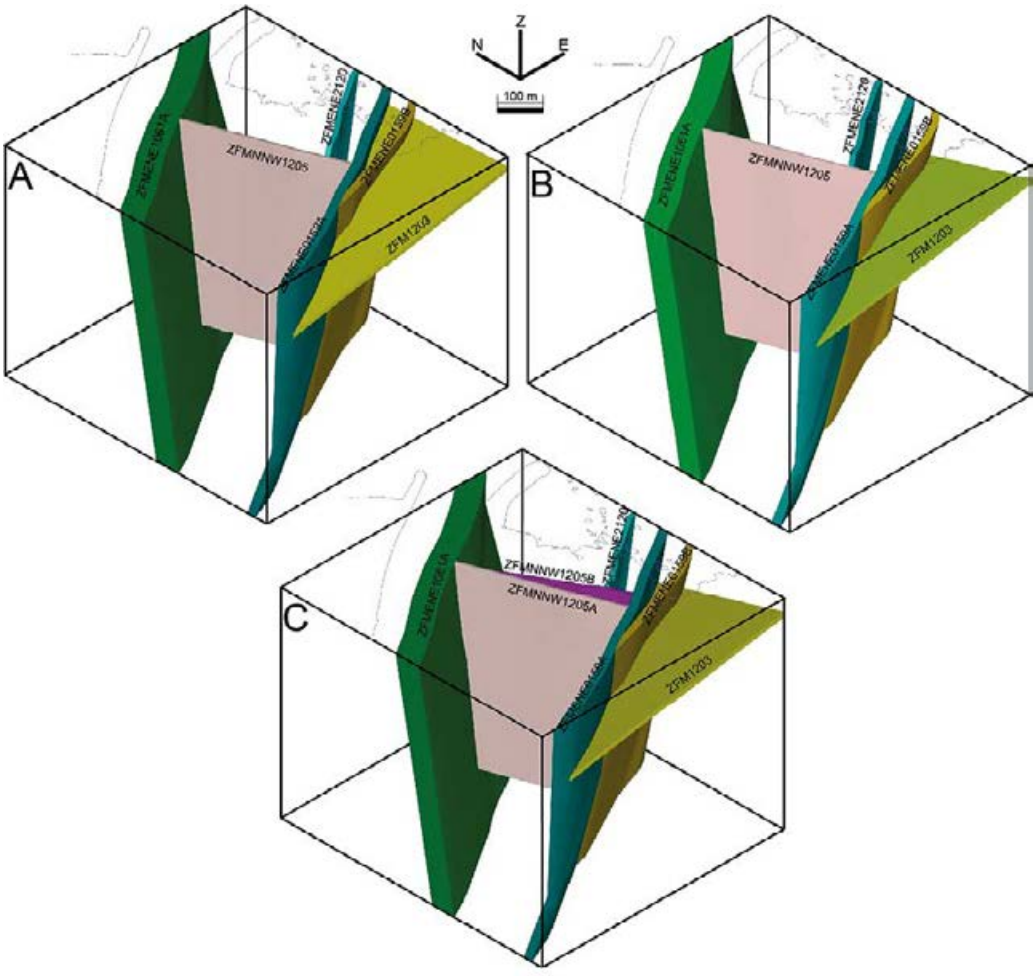

Figure 5-3. *View looking at the model volume towards north-east. A) Deformation zones in model version 2.2, B) deformation zones in model version 2.3, and C) deformation zones based on the information acquired from the boreholes drilled in the access volume during the preparatory investigations of the access volume, i.e. KFM13–24.*

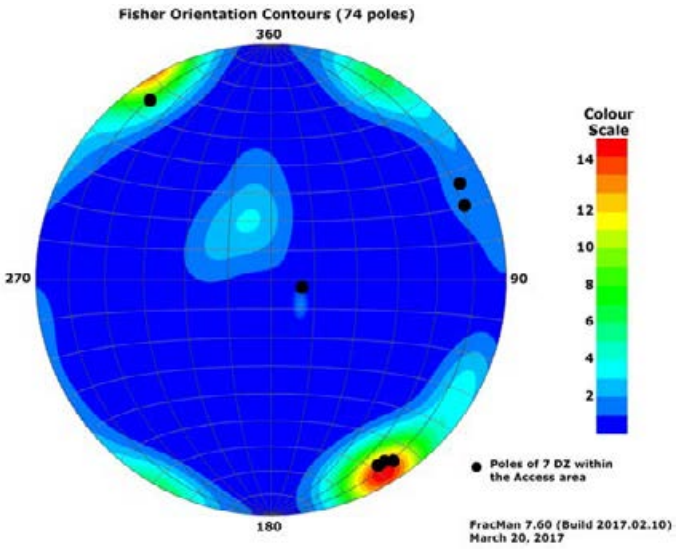

Figure 5-4. *Concentration contours showing orientation poles of the deformation zones (n = 67) reported by Stephens and Simeonov (2015). Black markers show orientation poles of the deformation zones (n = 7) inside the access volume.*

The individual characteristics of the deformation zones, their extents and possible kinematics are as follows:

ZFMENE0159A has a brittle character and is established by the presence of a magnetic lineament (MFM0159G), an outcrop (AFM001265) and four borehole intercepts. **ZFMENE0159A** is truncated in the west against ZFMNW0017 (outside the access volume) and is open ended in the east. The zone is characterised by elevated frequency of mainly sealed fractures but also a network of sealed fractures, whereas increased frequencies of open fractures occur sporadically. The wall rock of the zone is commonly oxidised. The sense of displacement is inconclusive, i.e. both sinistral and dextral strike-slip have been identified.

ZFMENE0159B is interpreted as a splay from **ZFMENE0159A** and corresponds to the magnetic lineament MFM2326G0. It is defined by predominantly sealed fractures.

ZFMENE1061A is a mainly brittle deformation zone and is identified from a short magnetic lineament and intercepts of four boreholes. The zone is truncated in the west by ZFMNNW100 (outside the access volume) and open ended in the east. It is interpreted to terminate at −1 150 m elevation. ZFMENE1061A is characterised by an elevated frequency of open and mainly sealed fractures, and commonly oxidised wall rock. The sense of displacement is dominantly sinistral strike-slip. It is noted that according to the deformation zone model for **SDM-Site** the ending of the trajectory of borehole KFM24 intersects **ZFMENE1061**. This notion assumes that the thickness of this zone is uniform. However, no deformation zone type properties were observed in the geological single-hole interpretation of borehole KFM24 (Dahlin et al. 2017).

Inside the access volume, the gently dipping **ZFM1203** terminates against ZFMENE0159A. Outside the access volume, ZFM1203 terminates against ZFMNNW0404, ZFMNNE2309, ZFMWNW2225, ZFMNNE2280 and the ground surface in the south-east (outcrops). Kinematic analysis rendered inconclusive results on movements. The orientation of ZFM1203 was reassessed in modelling stage 2.3 (Stephens and Simeonov 2015), resulting in a slightly different orientation (cf Figure 5-3A and B).

Deformation zone **ZFMNNW1205**, which was interpreted as a 15 m wide zone has here been divided into **ZFMNNW1205A** and **ZFMNNW1205B**. These two zones are brittle in their character. They are interpreted from magnetic lineaments, intercepts of three boreholes and the outcrop AFM001393 (**ZFMNNW1205B**). Kinematic analysis of **ZFMNNW1205** rendered sinistral strike-slip movements.

The interpretation of the brittle **ZFMENE2120** is based on a magnetic lineament (MFM2120G) and three borehole intercepts. It is truncated in the south-west by ZFMNNW1205B and has an open end in the north-east. ZFMENE2120 is mainly characterised by elevated frequency of both open and sealed fractures. The wall rock is sporadically oxidised.

5.2.3 Fracture domain model

Three fracture domains occupy the access volume, FFM01, FFM02 and FFM06, where FFM02 overlies both FFM01 and FFM06 (Figure 2-14 and Figure 5-5). FFM06 is only present in rock domain RFM045 and obscured by FFM02 in Figure 5-5. The upper metres of FFM02 are characterised by long and persistent undulating subhorizontal fractures, with locally large apertures (up to a couple of decimetres). These are often filled with silty to clayey sediment, in places layered (Carlsson 1979). The current understanding is that these slabs of bedrock were formed due to stress relief during rapid retreat of the thawing ice sheet. The topography of the bedrock surface within the access volume is uneven on a small scale (< 10 m) but has a more moderate to low relief on larger spatial scales.

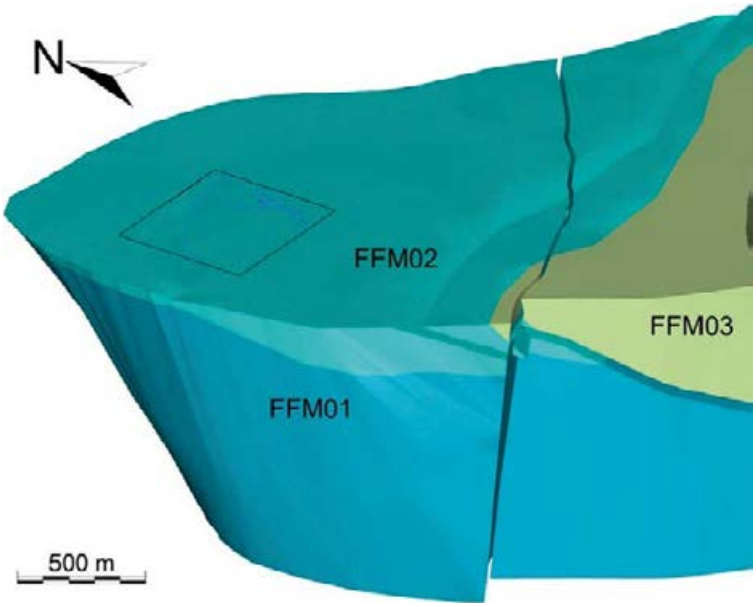

Figure 5-5. *Distribution of the three fracture domains FFM01, FFM02 and FFM03. The black square shows the location of the footprint of the access volume. The maximum thickness of FFM02 inside the access volume is ca 50 m. FFM06 is not visible in the picture.*

5.3 Comparison of geological data inside and outside the access volume acquired during SDM-Site

The data evaluated in this section were acquired during **SDM-Site** in KFM01A–KFM08D and KFM09A–KFM10A. The data comparison intends to evaluate if there are any significant geological differences between the rock between deformation zones inside the access volume and the rock between deformation zones outside of the access volume, and to discuss what potential impacts the observed differences might have in terms of the geological conditions inside the access volume.

5.3.1 Rock types

As shown in Figure 5-6, the rock both inside and outside the access volume is dominated by granite to granodiorite (101057). This distribution does not differ significantly from what has been observed in the **SDM-Site** local model volume. This implies that the rock composition is generally in line with the conditions explained in more detail in SKB (2008).

Observations of minor rock occurrences (less than one metre of occurrence in cored boreholes) show that amphibolites are less common and the pegmatites are more common inside the access volume compared to data outside the access volume, cf Figure 5-7. Other minor rock occurrences show similar distributions as stated in the **SDM-Site** report (SKB 2008). The less frequent occurrence of amphibolites is not considered to have implications for the construction of the shaft and access ramp. However, at repository depth, occurrences of amphibolites may influence the thermal behaviour of the rock.

5.3.2 Fracture orientations

Fracture data between deformation zones were divided into fracture domains in the **SDM-Site** model (SKB 2008). This division allows for a comparison of fracture orientations between the fracture domains FFM01–02 inside and outside the access volume. However, it is noted that the data coverage is larger for FFM01 than FFM02 due to two reasons: 1) FFM02 only covers the upper ca 50 m of the bedrock inside the access volume, whereas it is approximately 150–200 m thick outside the access volume, and 2) several of the cored boreholes both inside and outside the access volume have casings installed in their upper parts down to about 100 m depth.

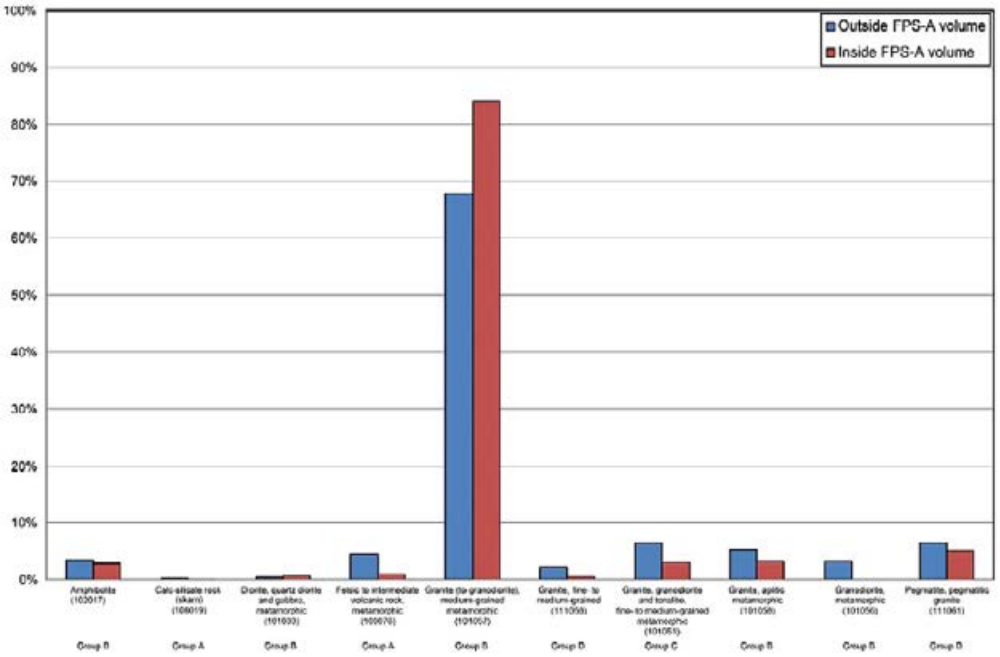

Figure 5-6. *Comparison of rock types identified in boreholes inside and outside the access volume (SDM-Site data).*

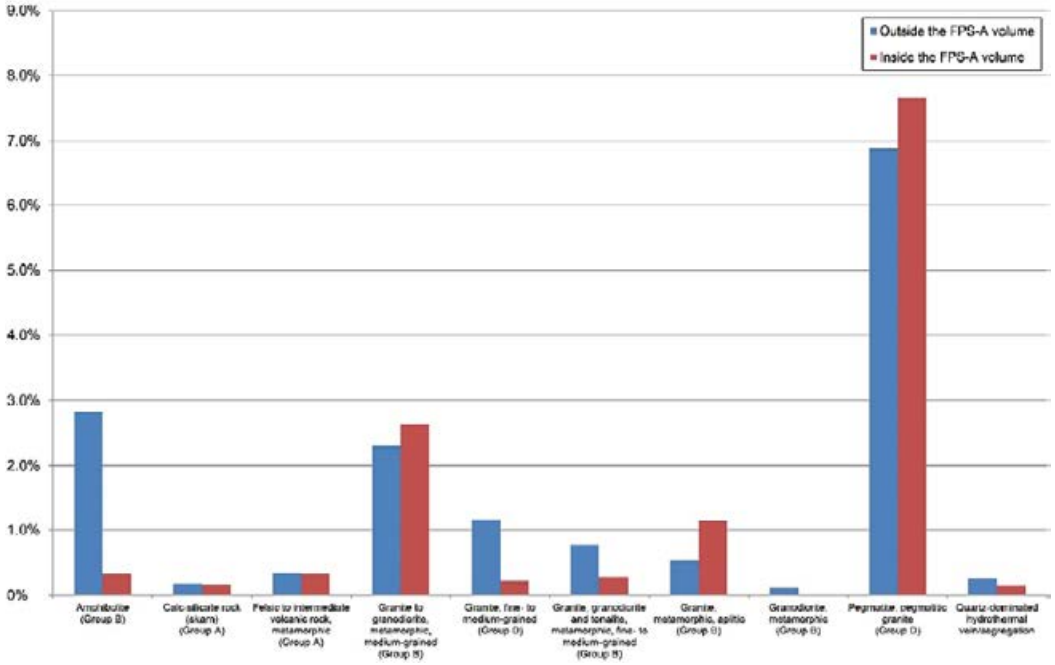

Figure 5-7. *Illustration of minor rock occurrences inside and outside the access volume (SDM-Site data). It is worth to highlight that amphibolites are less common inside than outside the access volume.*

Figure 5-8 illustrates open fracture orientations in FFM01 (excluding fractures in identified deformation zones). Outside the access volume, the fracture pattern is dominated by north-easterly striking and sub-horizontal fractures, which is also evident inside the access volume. It is noteworthy that there is a population of open fractures striking north-east that is perpendicular to the main horizontal stress (SKB 2008). In relation to FFM01, open fracture orientations in FFM02 display stronger influence of sub-horizontal fractures both inside and outside of the access volume, cf Figure 5-9.

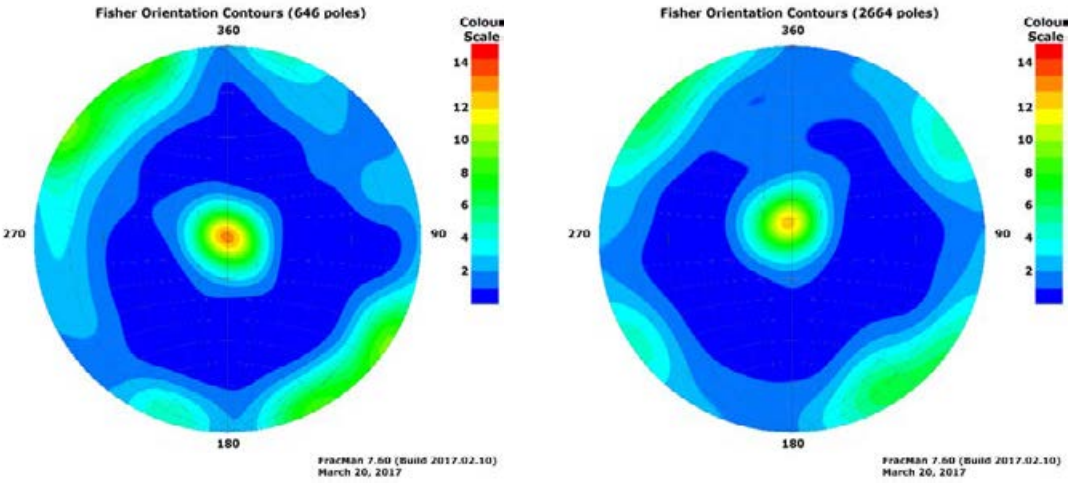

Figure 5-8. *Open fracture orientations in FFM01 inside the access volume (left) and outside the access volume (right) (SDM-Site data). Terzaghi corrected (max = 7.00) poles to open fractures, Fisher contoured (K = 50) on a lower hemisphere Schmidt equal area stereonet.*

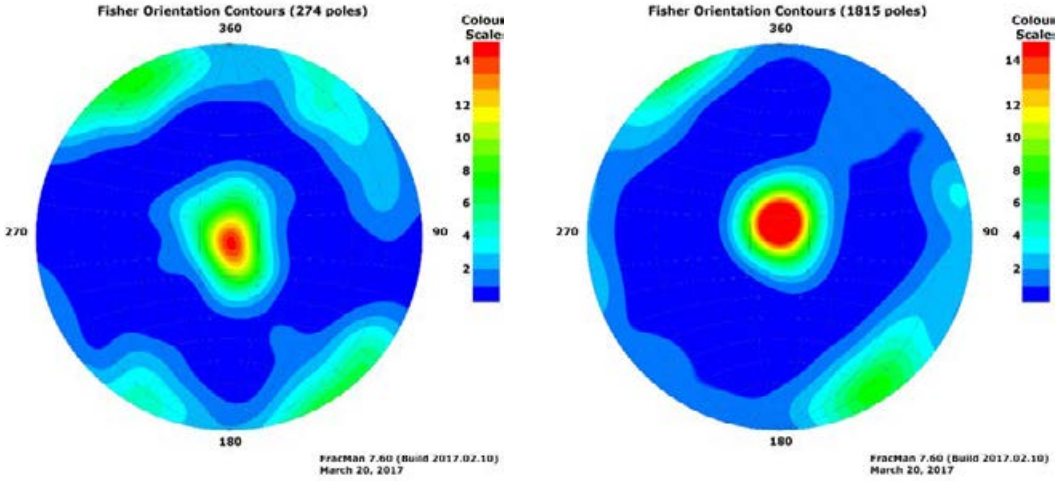

Figure 5-9. *Open fracture orientations in FFM02 inside the access volume (left) and outside the access volume (right) (SDM-Site data). Terzaghi corrected (max = 7.00) poles to open fractures, Fisher contoured (K = 50) on a lower hemisphere Schmidt equal area stereonet.*

The sealed fracture orientations in FFM01 are dominated by a steep north-easterly striking set, whereas there is only a minor component of sub-horizontal fractures, cf Figure 5-10. The pattern of sealed fractures inside the access volume is similar to the pattern outside the access volume.

The orientations of sealed fractures in FFM02 clearly show two steep fracture sets, a north-eastern set and a north-western set, together with a well-developed sub-horizontal set, cf Figure 5-11. The north-western set is more evident in the sealed fractures than in the open fractures in FFM02, cf Figure 5-9. The pattern inside the access volume is similar to the pattern outside the access volume.

5.3.3 Fracture frequency (intensity)

Figure 5-12 shows average Terzaghi corrected fracture frequencies (intensities, $P_{10,corr}$) over 10 m long elevation intervals inside and outside the access volume of open and sealed fractures in both FFM01 and FFM02, respectively. The data shown exclude borehole sections identified as deformation zones, sealed networks and crush.

The lack of deep boreholes below −500 m elevation inside the access volume is evident as is the effect of having sparse or no core information the uppermost 100 m. Neither open nor sealed fractures in FFM01 and FFM02 suggest there are any clear differences of $P_{10,corr}$ inside and outside the access volume.

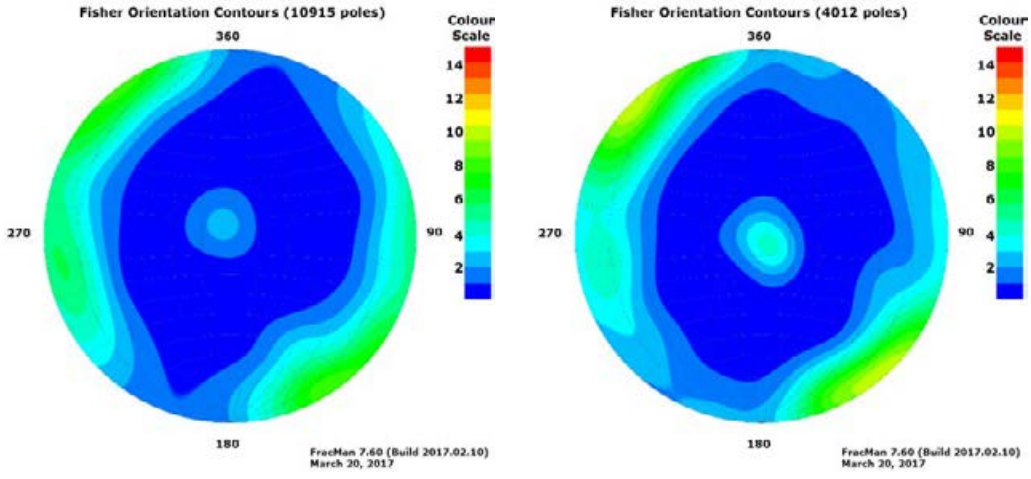

Figure 5-10. *Orientations of sealed fractures in FFM01 inside the access volume (left) and outside the access volume (right) (SDM-Site data). Terzaghi corrected (max = 7.00) poles to sealed fractures, Fisher contoured (K = 50) on a lower hemisphere Schmidt equal area stereonet.*

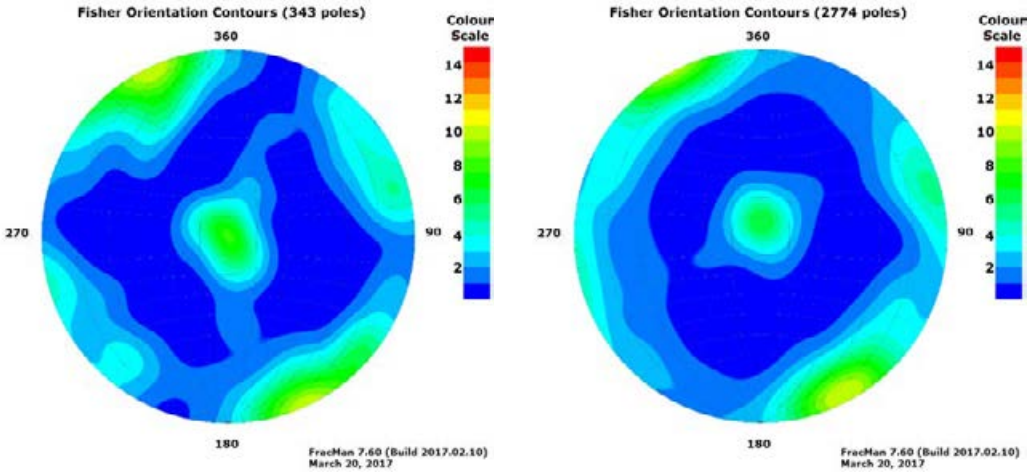

Figure 5-11. *Sealed fracture orientations in FFM02 inside the access volume (left) and outside the access volume (right) (SDM-Site data). Terzaghi corrected (max = 7.00) poles to sealed fractures, Fisher contoured (K = 50) on a lower hemisphere Schmidt equal area stereonet.*

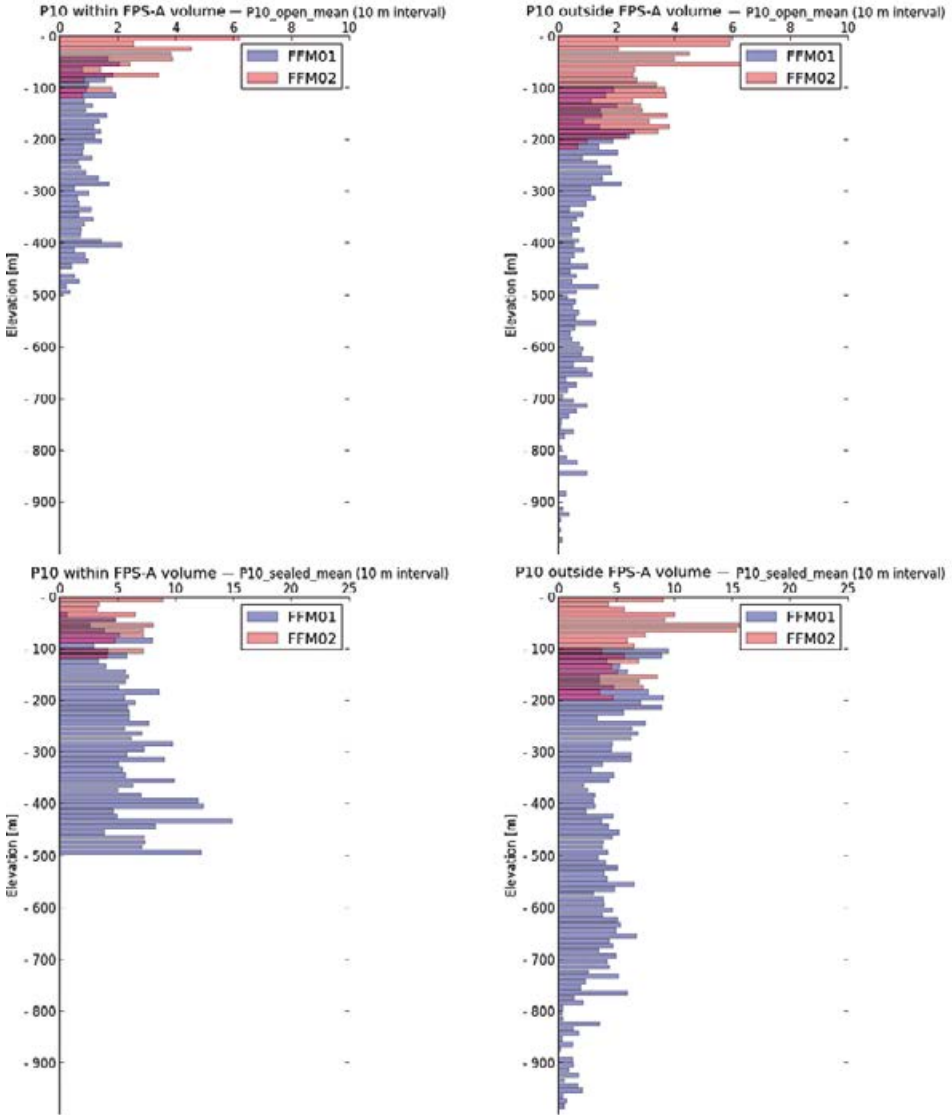

Figure 5-12. *Terzaghi corrected (max = 7.00) fracture frequency ($P_{10,corr}$) inside (left) and outside (right) the access volume expressed as average values over 10 m elevation intervals derived from all available borehole intersections in each fracture domain. Purple illustrates overlapping data as the fracture domains occur in boreholes at different elevations.*

5.3.4 Alteration

In SKB (2008) alteration is used as an important indicator of secondary processes that may influence thermal properties and mechanical behaviour of the bedrock. It is particularly identified as being of importance in the north-eastern part of the target volume, where the Group B granitic rocks are affected by alteration that has been mapped and referred to as albitisation. On a mesoscopic scale, this alteration is recognised by a whitening of the feldspar in the granitic rocks.

Analysing data within the access volume, albitisation is the most common alteration type. Albitisation is Na-K redistribution in granitic rocks and result in a fine-grained, K-feldspar deficient granodiorite to tonalite. Albitisation has at least affected group A and B rocks prior to regional deformation and metamorphism and is absent in Group C rocks. On a small scale, this alteration is conspicuous with whitish contacts to amphibolites, whereas the more pervasive albitisation in the rock mass is suggested to be related to the heat provided by later and larger intrusions (Stephens et al. 2007). Albitisation is more common inside the access volume than outside – rock domain RFM 045 is characterised by this alteration – whereas both oxidation and quartz dissolution are more common outside the access volume (Figure 5-13).

Oxidation (hematite dissemination) is in general related to fractures and deformation zones. It occurs in the vicinity to fractures and results in complete saussuritisation of plagioclase, chloritisation of biotite and fine dissemination of hematite inside plagioclase and along grain boundaries (Sandström and Tullborg 2006).

Quartz dissolution intervals found in KFM08A and KFM08C are less common within the access volume than in the rest of the investigation area for **SDM-Site** (Table 5-3). The quartz dissolution resulted in a vuggy rock (Figure 5-14a). The total lengths of quartz dissolution occurrences outside the access volume are shown in Table 5-4. The vuggy rock, also known as epi-syenite, contains cavities from selectively removed quartz. The cavities have later been partly filled with new quartz and albite, evident in the euhedral small crystals (Figure 5-14b).

Almost all occurrences of vuggy rock are in the vicinity of deformation zones (Stephens et al. 2007). This correlation between deformation zones and vuggy rock implies that the latter acted as channels for hydrothermal fluids that affected the quartz content in the rock mass (Stephens et al. 2007).

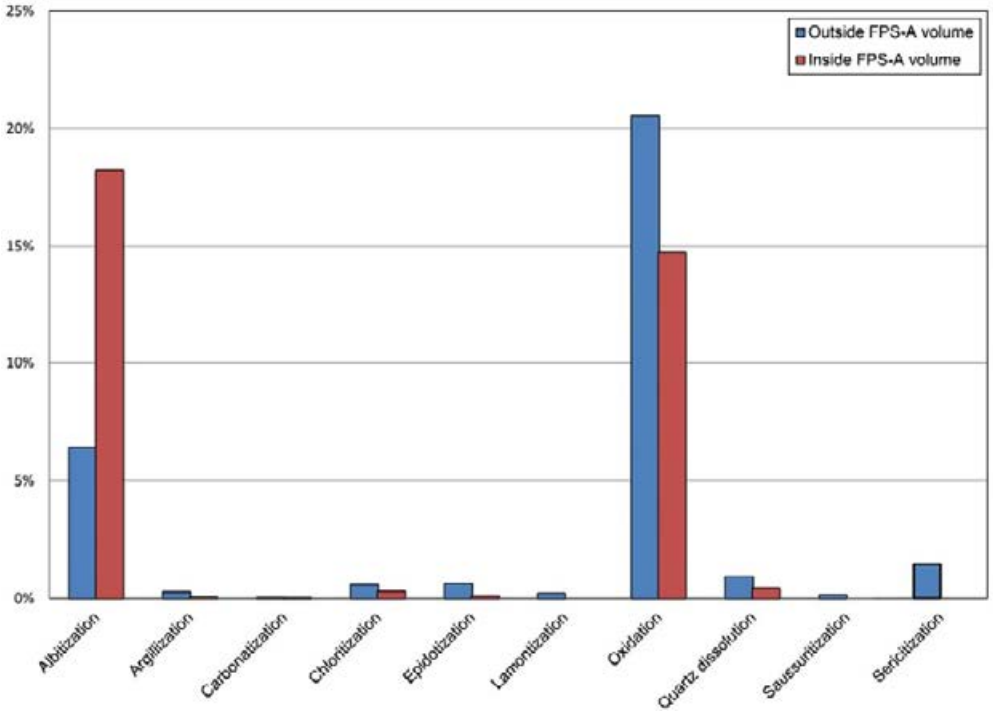

Figure 5-13. *Rock alteration within and outside the access volume. Note that albitisation is more common inside the access volume than outside.*

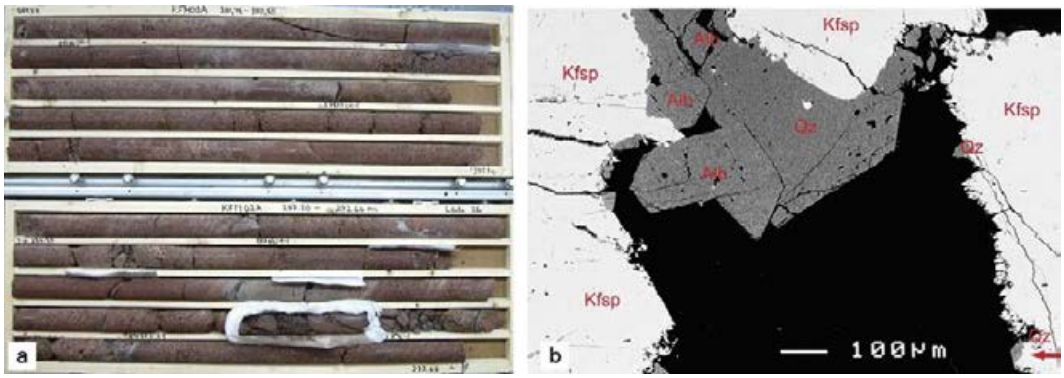

Figure 5-14. *a) Drill core box of KFM02A, interval 281.72 m to 292.66 m that displays a vuggy rock. b) Back-scatter electron image, where black fields are cavities and grey fields are euhedral quartz (Qz) and Na-plagioclase i.e. albite (Alb) (figure adopted from SKB 2005).*

Table 5-3. Occurrences of quartz dissolution in boreholes KFM08A and KFM08C inside the access volume. Adjusted Secup and Seclow refer to upper and lower section limits used in the SKB Sicada database (DZ = deformation zone).

Borehole	Adjusted Secup (m)	Adjusted Seclow (m)	Total length (m)	Relationship to DZ
KFM08A	409.854	412.04	2.186	No relationship
KFM08C	454.964	458.287	9.317	ZFMNNE2312

Table 5-4. Occurrences of quartz dissolution outside the access volume. Adjusted Secup and Seclow refer to upper and lower section limits used in the SKB Sicada database (DZ = deformation zone).

Borehole	Adjusted Secup (m)	Adjusted Seclow (m)	Total length (m)	Relationship to DZ
KFM02A	171.402	180.053	2.324	ZFMA3
KFM02A	247.860	301.707	48.572	ZFM1189
KFM02B	166.795	168.902	2.105	ZFMA3
KFM06A	332.496	332.746	0.250	ZFMENE0060A and ZFMB7
KFM06A	610.642	611.086	0.444	No relationship
KFM06A	770.841	770.886	0.045	ZFMNNE0725
KFM06B	66.564	66.911	1.851	ZFMA8
KFM06C	451.458	452.226	0.768	No relationship
KFM08D	932.623	932.683	0.060	ZFMNNE2300 (outside the access volume)
KFM09A	511.750	513.934	8.281	Transition between FFM05 and FFM01
KFM09B	382.312	382.325	4.537	ZFMENE2320
KFM09B	568.925	569.398	4.524	ZFMENE2325B
KFM10A	86.859	88.730	15.495	ZFMWNW0123
KFM10A	483.552	487.775	4.223	ZFMA2

5.4 Comparison of geological data inside the access volume acquired during the preparatory investigations with geological data outside the access volume acquired during SDM-Site

In this section, data from the new boreholes drilled inside the access volume, i.e. KFM13–23 and KFM24, are compared with data from old boreholes drilled outside the access volume during **SDM-Site**, i.e. KFM01A–KFM08D and KFM09A–KFM10A.

5.4.1 Rock types

Compared to Figure 5-6, the new borehole data inside the access volume shown in Figure 5-15 emphasise the dominance of granite to granodiorite (101057). Furthermore, a comparison of Figure 5-7 and the new borehole data inside the access volume shown in Figure 5-16 reveals that the occurrence of rock types less than one metre borehole length shows fewer minor rock bodies compared to the bedrock outside the access volume.

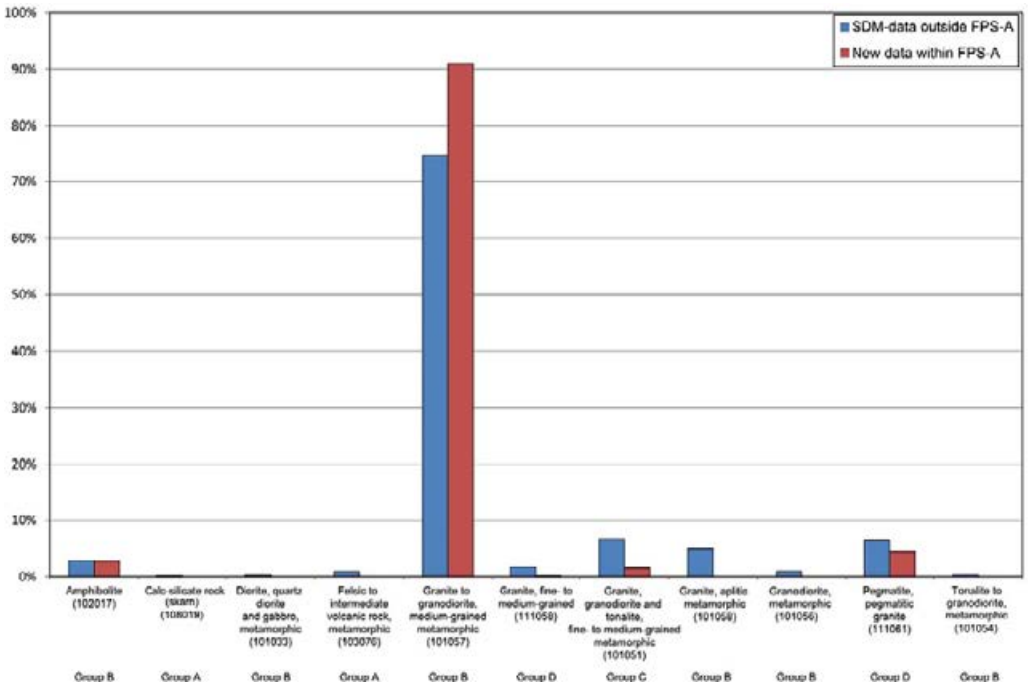

Figure 5-15. *Comparison of rock types identified in boreholes inside and outside the access volume.*

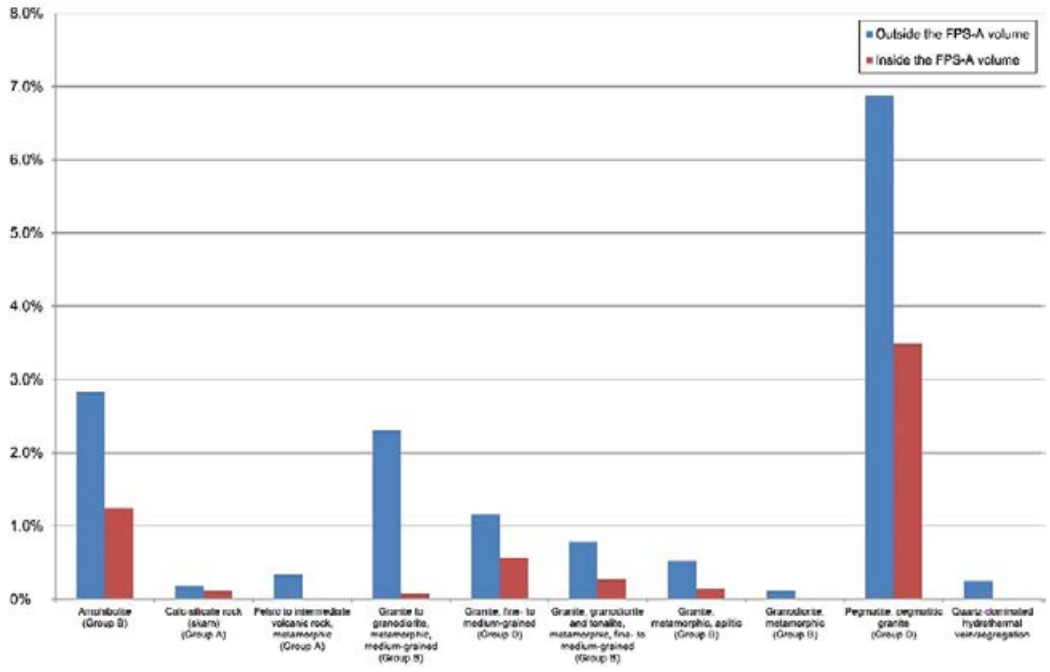

Figure 5-16. *Illustration of occurrences of minor rock types inside and outside the access volume.*

5.4.2 Fracture orientations

The shallow boreholes KFM13–23 provide valuable fracture information on the uppermost part of the rock inside the access volume, particularly on the properties of the thin fracture domain FFM02. KFM24 has a casing installed down to about −35 m elevation, and thus provides more detailed information of the deeper parts of the access volume, predominantly in FFM01.

The orientations of open fractures in FFM01 inside the access volume are similar to the orientations outside the access volume, which exhibit a strong steep north-eastern and sub-horizontal preference (Figure 5-17). However, the steep north-western set is less dominant, which suggests that the uppermost part of FFM01 is influenced by the pattern in FFM02. The open fractures in FFM02 are dominated by the north-eastern and sub-horizontal sets (Figure 5-17), with a subordinated steep north-western population. It is noteworthy that open north-eastern striking fractures are dominating, despite the fact that the largest principal stress component is oriented north-west and south-west in the Forsmark area (SKB 2008).

With increasing data coverage within the access volume, it is evident that the sealed fractures in FFM01 (Figure 5-18) are similar to what has been observed in the **SDM-Site** modelling. Inside the access volume, the orientations of sealed fractures in FFM02 (Figure 5-18) show a similar pattern as the data from FFM01, which suggests a gradual change between the fracture domains and not as distinct as described in **SDM-Site**.

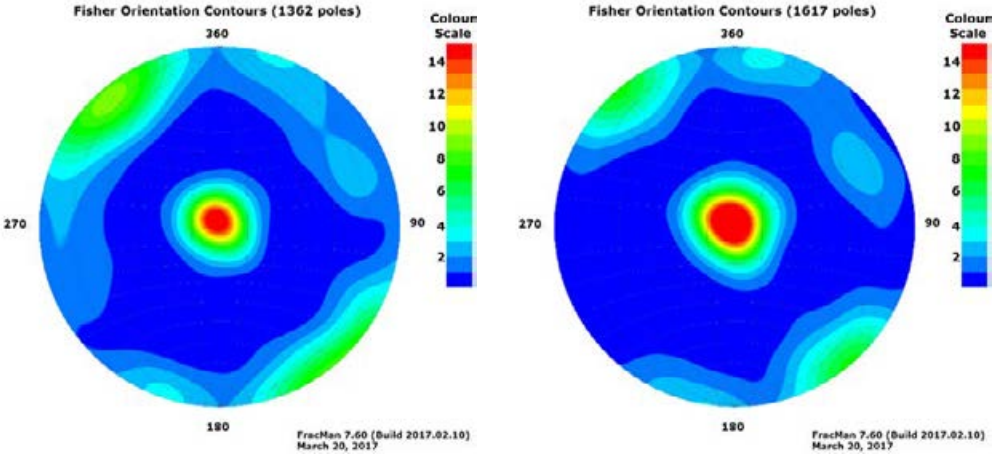

Figure 5-17. *Orientations of open fractures in FFM01 (left) and FFM02 (right) inside the access volume. Terzaghi corrected (max = 7.00) poles to open fractures, Fisher contoured (K = 50) on a lower hemisphere Schmidt equal area stereonet.*

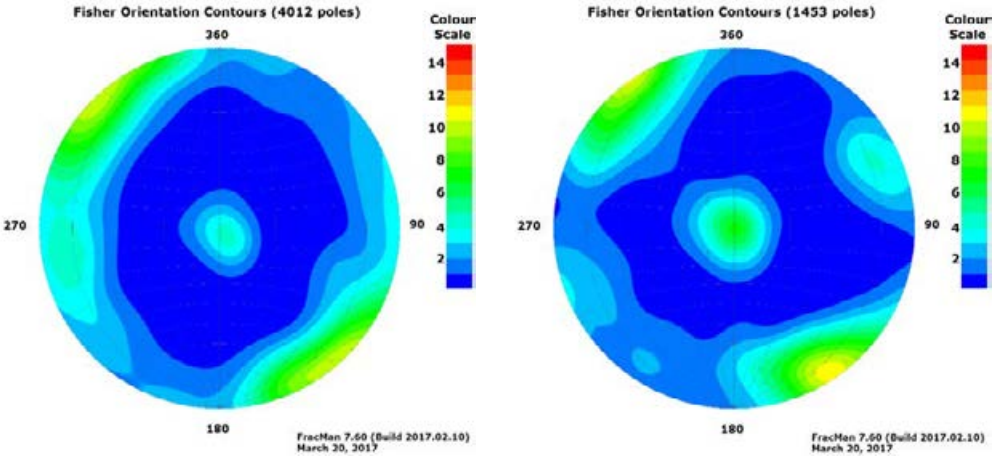

Figure 5-18. *Orientations of sealed fractures in FFM01 (left) and FFM02 (right) inside the access volume. Terzaghi corrected (max = 7.00) poles to sealed fractures, Fisher contoured (K = 50) on a lower hemisphere Schmidt equal area stereonet.*

5.4.3 Fracture frequency (intensity)

Figure 5-19 shows that the Terzaghi corrected frequencies (intensities, $P_{10,corr}$) of open and sealed fractures decrease with depth both inside and outside the access volume, regardless of fracture domain. Whereas the information from KFM13–23 suggests that the fracture intensity of both open and sealed fractures in FFM02 inside the access volume are similar to those outside, the information from KFM24 suggests that the fracture intensities of both open and sealed fractures in FFM01 appear to increase more with depth inside than outside the access volume.

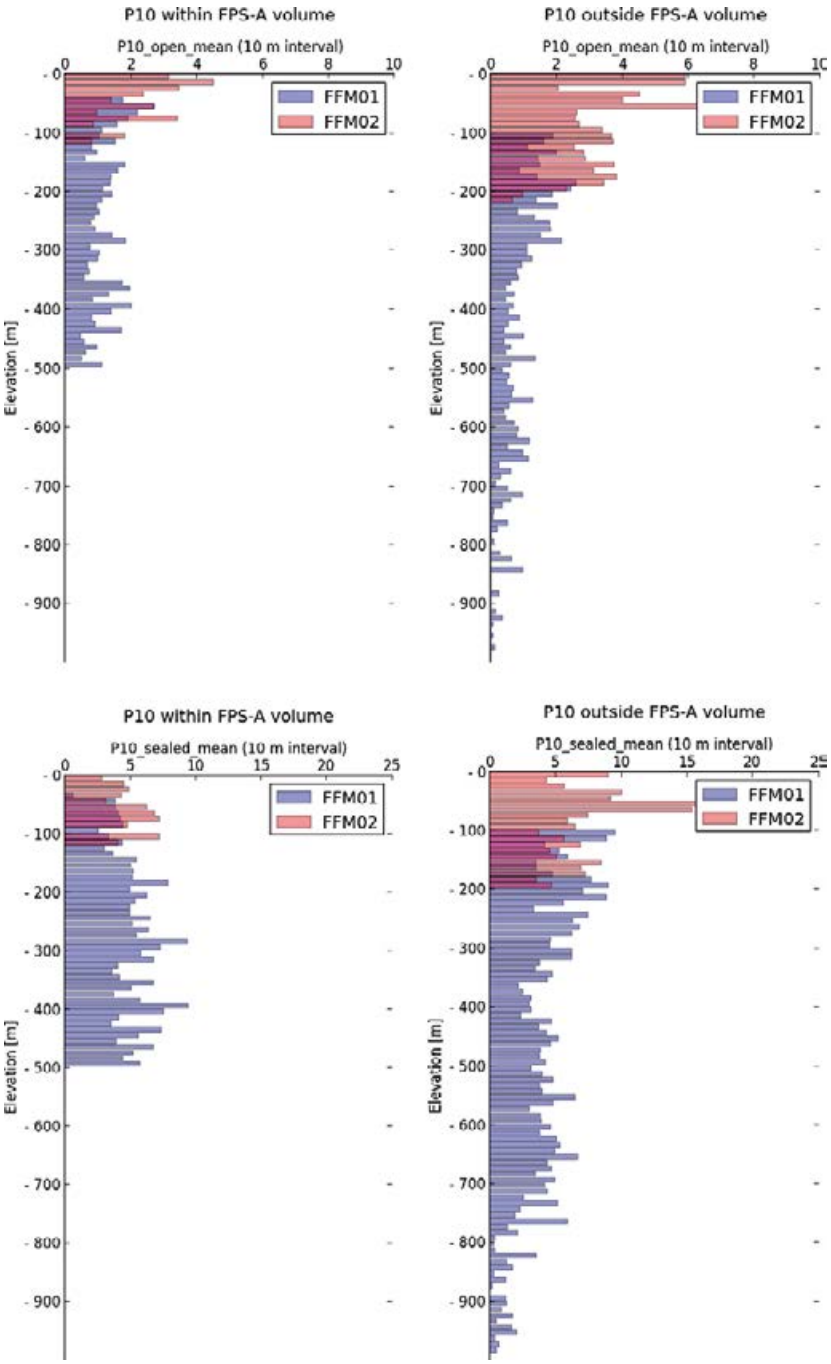

Figure 5-19. *Terzaghi corrected (max = 7.00) fracture frequency ($P_{10,corr}$) inside (left) and outside (right) the access volume, expressed as average values over 10 m elevation intervals derived from all available borehole intersections in each fracture domain. Purple illustrates overlapping data as the fracture domains occur in boreholes at different elevations.*

6 Bedrock thermal properties and rock mechanics

6.1 Status of site understanding and models

Chapter 2 presents a summary of the current version of the site descriptive model for bedrock thermal properties and rock mechanics at Forsmark. Table 6-1 presents the data and modelling reports on which the current version of the site descriptive model is based.

Table 6-1. List of reports covering sub-models or specific modelling topics in rock mechanics and thermal properties for SDM-Site and SDM-PSU.

Report	Title	Comment
SKB TR-08-05	Site description of Forsmark at completion of the site investigation phase. **SDM-Site** Forsmark (SKB 2008)	The main report, all disciplines (Level I)
SKB R-07-06	Mechanical modelling of the Singö deformation zone. Site descriptive modelling Forsmark stage 2.1 (Glamheden et al. 2007b)	Specific topics (Level III)
SKB R-07-15	Site descriptive modeling. Forsmark, stage 2.2. A fracture domain concept as a basis for the statistical modelling of fractures and minor deformation zones, and interdisciplinary coordination (Olofsson et al. 2007)	Specific topics (Level III)
SKB R-07-26	Quantifying in situ stress magnitudes and orientations for Forsmark. Forsmark stage 2.2 (Martin 2007)	Specific topics (Level III)
SKB R-07-31	Rock mechanics Forsmark. Site descriptive modelling Forsmark stage 2.2 (Glamheden et al. 2007a)	The discipline-specific main report for rock mechanics stage 2.2 (Level II)
SKB R-07-47	Thermal properties. Site descriptive modelling Forsmark – stage 2.2 (Back et al. 2007)	The discipline-specific main report for thermal properties stage 2.2 (Level II)
SKB R-08-65	Thermal properties Forsmark. Modelling stage 2.3. Complementary analysis and verification of the thermal bedrock model, stage 2.2 (Sundberg et al. 2008)	The discipline-specific main report for thermal properties stage 2.3 (Level II)
SKB R-08-66	Rock mechanics Forsmark. Modelling stage 2.3. Complementary analysis and verification of the rock mechanics model (Glamheden et al. 2008)	The discipline-specific main report for rock mechanics stage 2.3 (Level II)
SKB R-09-30	Statistical analysis of results from the quantitative mapping of fracture minerals in Forsmark. Site descriptive modelling – complementary studies (Löfgren and Sidborn 2010).	Specific topics (Level III)
SKB TR-11-04	Site description of the SFR area at Forsmark at completion of the site investigation phase. **SDM-PSU** Forsmark (SKB 2013).	The main report, all disciplines (Level I)
SKB R-14-28	Description of deformation zone model version 2.3, Forsmark (Stephens and Simeonov 2015).	Specific topics (Level III)

6.2 Presentation and evaluation of new data

The core-drilled borehole KFM24 is logged with acoustic televiewer[1]. This enables the study of borehole breakouts in the borehole wall, which can be used to interpret the orientation of the *in-situ* stress, see e.g. Ringsgaard (2007a, b) for description of instrument and methodology. A similar analysis was used also within **SDM-Site** based on the available acoustic logger data at that time, see Glamheden et al. (2008). Two small "classical" breakouts are found in KFM24, at 127 m and at 399 m borehole length, respectively (Figure 6-1). A few points with so called "Micro-Fallout" are also identified, showing the same main orientation as the breakouts.

[1] Borehole KFM24 is not a fully vertical borehole. As the dip is 84° it was judged that the borehole could still be useful for breakout analysis. The televiewer data used in this analysis was obtained from the Sicada_17_026 data delivery (Sicada_xx_xxx is the internal identification of a delivery from the Sicada database).

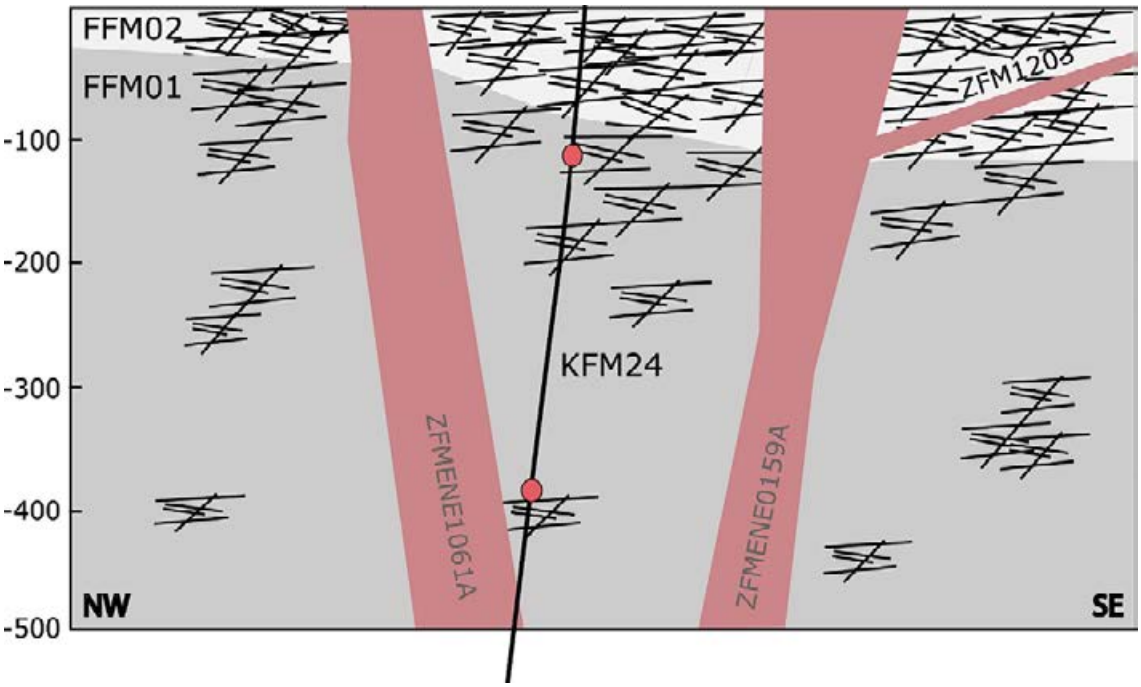

Figure 6-1. *Generalised cross section corresponding to "FPS-A profile NW-SE" in Figure 3-1. The circles show where two small "classical" breakouts were identified, at 127 m borehole length (Figure 6-3) and at 399 m borehole length (Figure 6-2), respectively.*

Figure 6-2 shows the result from the acoustic log at 399 m borehole length where the most certain breakout is visible. The two dark areas in the unfolded borehole wall correspond to the two areas where the borehole diameter is larger. The length along the borehole where these breakouts are noticed is about 10 cm. The fact that the two areas are exactly opposite each other and that they have this typical shape make the anomaly to be defined as a classical "borehole breakout" (BB).

When the rock stress situation is anisotropic, as it is in Forsmark, the direction of borehole breakouts is expected to be perpendicular to the main horizontal stress. In this case, the left border of the images corresponds to the bearing direction of the borehole, which is 311°. This means that the azimuth of the centre point of the breakout is 41° (and 221°). A tentative azimuth of 131° (and 311°) of the major horizontal stress indicated by Figure 6-2 compares well with previous stress orientation data from the overcoring measurements performed during the site investigation for **SDM-Site**, where the azimuth of the main horizontal stress was determined to 145° ± 15° (and 325° ± 15°) (Figure 2-15 and Figure 2-16).

Figure 6-3 similarly shows the breakout found at 127 m borehole length in KFM24. However, in this case the breakouts are oriented about 1° (and 181°), which, if correct, suggests that a tentative azimuth of the main horizontal stress of 91° (and 271°) at shallow depth in Forsmark, i.e. roughly in east-west direction.

From the OPTV log in Figure 6-3b (Lundgren 2017) it can be noted that the breakout found at 127 m borehole length is situated in a small pegmatite vein, and the breakouts also terminate against two fractures. The presence of these fractures makes it very difficult to conclude with certainty whether there is a potential stress domain change in the upper part. Such a rotation was not noted in **SDM-Site** (SKB 2008).

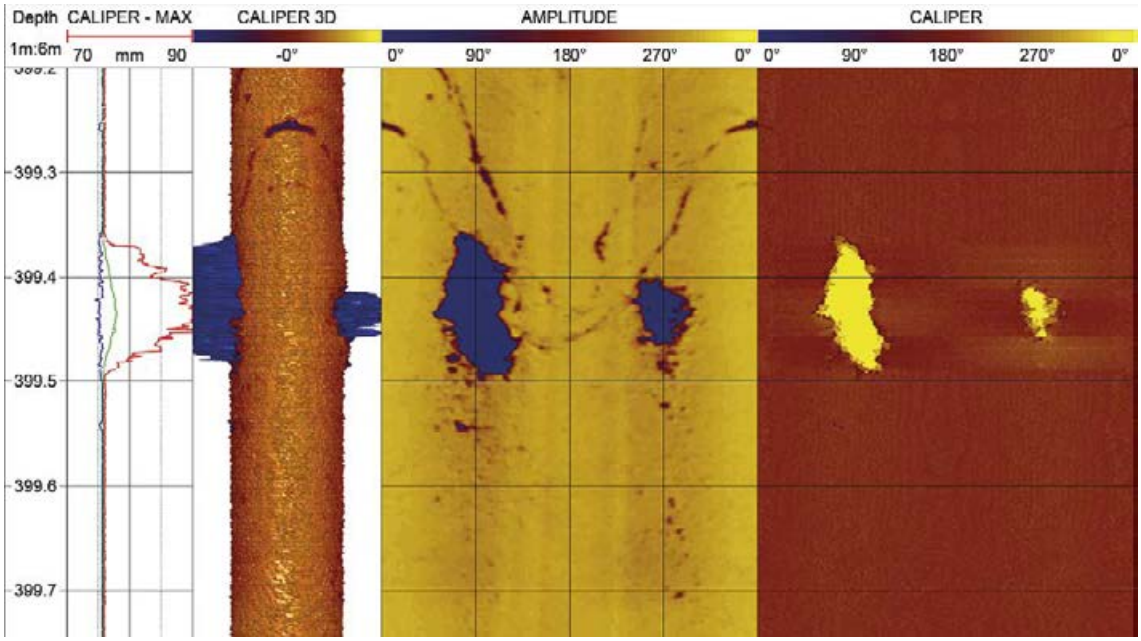

a

b

Figure 6-2. *a) Excerpt from the log result of the acoustic televiewer. The small breakout at 399.4–399.5 m depth is clearly seen in both the "Amplitude" and "Caliper" columns. The left border of the images corresponds to the bearing of the borehole. The central points of the breaks are located opposite each other in a direction, at 90 and 270 degrees from the bearing direction. Below the breakout in the same direction some darker dots in the "Amplitude" log can also be noted, indicating small starting "Micro fallout". b) The same location of KFM24 in the optical log (OPTV). The OPTV log (Lundgren 2017) gives the colours of the rock of the borehole wall. It can be noted that the rock seems reddish in the area of the breakout. This example also illustrates why acoustic televiewer is needed to clearly identify breakouts, and other small geometrical variations, in the borehole wall.*

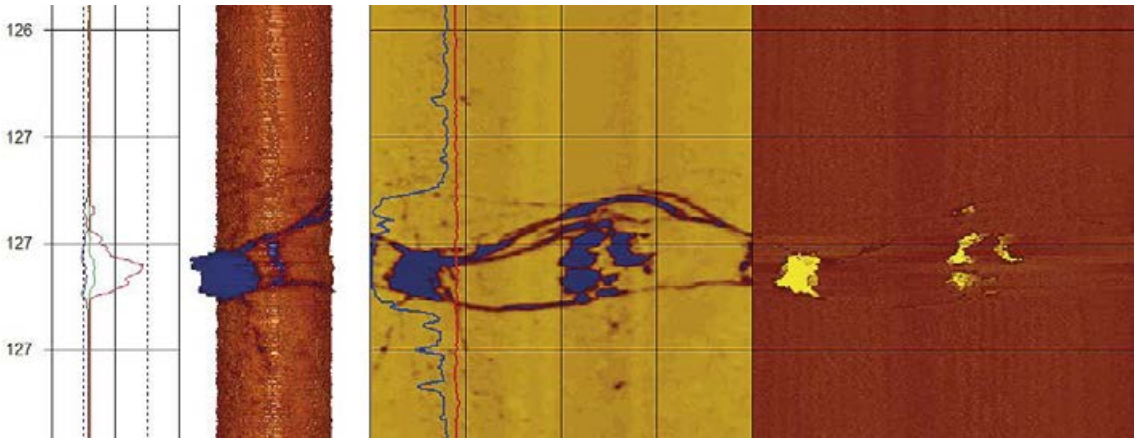

a

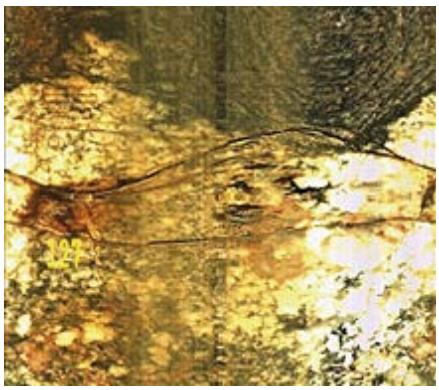

b

Figure 6-3. *a) Excerpt from the log result of the acoustic televiewer. A ca 5 cm long breakout at about 127.1 m borehole length is seen in both the "Amplitude" and "Caliper" columns. The left border of the images corresponds to the bearing of the borehole. The breakouts are located opposite each other at about 50° (and 230°) from the bearing of the borehole. b) OPTV Image (Lundgren 2017) of the same position in KFM24 as a). The breakouts are situated between two fractures. The rock seems more oxidised in the breakout area.*

6.3 Description of modelling approach and analysis of data

6.3.1 Intact rock properties and single fracture properties

No new laboratory data are available for a description of the mechanical properties of intact rock inside the access volume. This is also true for single open fractures. The approach here therefore consists of a comparison between the old data sampled within the area coinciding with the access volume and the total dataset. The comparison is meant to potentially indicate any differences coupled to spatial variation at Forsmark. If no such evidence is present, the **SDM-Site** model for mechanical properties of intact rock will be considered the most relevant model also for the access volume. It is noted that no laboratory tests have so far been performed on sealed fractures in the Forsmark area.

6.3.2 Rock mass properties

The approach to model the mechanical properties of the rock mass inside the access volume is, in absence of new data for intact rock and fractures, again to stay with the **SDM-Site** model. The main factor controlling the result from both the theoretical and empirical determination of rock mass properties is the fracture intensity, see Chapter 5.

6.3.3 Rock stress

Available direct stress measurement data using the overcoring method are shown in Figure 6-4. There are 14 single overcoring points acquired between −100 m to −270 m elevation in borehole KFM07C, which is the only borehole with stress data that is situated inside the access volume (Figure 3-1). The spread in magnitude of the overcoring stress data acquired in KFM07C is significant, which makes it difficult to make meaningful comparisons with data from other boreholes and provide conclusions about differences and similarities.

6.3.4 Thermal properties

No particular studies of thermal properties or temperatures have been carried out for the FPS-A modelling, and the approach taken here to describe the thermal properties has therefore been to use the results from the **SDM-Site** modelling work. Thermal properties are generally governed by the rock type distribution, and thus the applicability of **SDM-Site** models to the access area depends on the similarity of this rock volume compared to the whole Forsmark site, which is discussed in Chapter 5.

Thermal conductivity will have a spatial variability following the spatial variability of the rock types. The way to describe the thermal conductivity parameter is to present a distribution for the conductivity at a certain scale, 5 m, based on simulations, see further Sundberg et al. (2008) regarding the modelling approach used in **SDM-Site**.

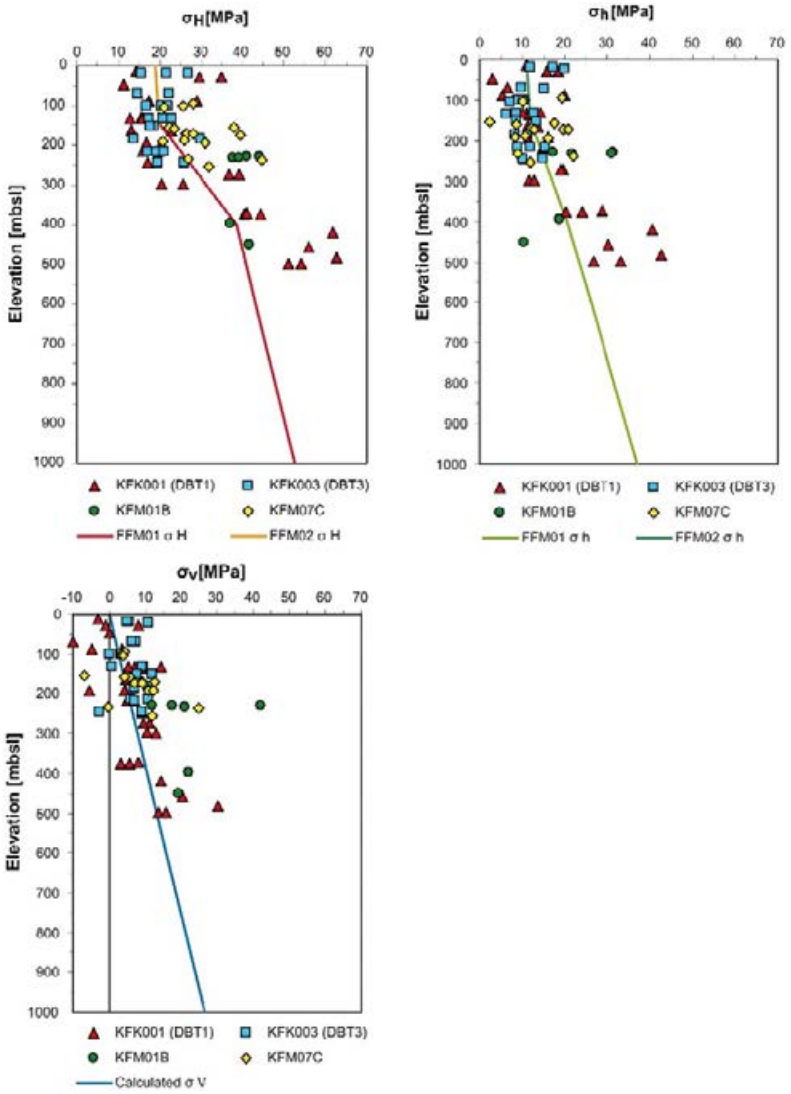

Figure 6-4. *Results from overcoring measurements in boreholes at the Forsmark site. The borehole KFM07C is situated inside the access volume. Solid lines indicate the stress model derived for SDM-Site (Figure 6-16 in Glamheden et al. 2007a).*

6.4 Resulting description

This section presents the resulting description of bedrock thermal properties and rock mechanics of the bedrock volume inside the access volume.

6.4.1 Intact rock

The resulting mechanical properties of the intact rock inside the access volume are the same as those derived for **SDM-Site**, see Table 6-2.

Table 6-2. Deformation and strength properties for intact rock in fracture domains FFM01 and FFM06 and for deformation zones mainly composed of sealed fractures (modified after Table 7-3 in SKB 2008).

Parameter	FFM01		FFM06	
	101057 **Mean/std dev** **Min–Max** **Uncertainty**	**101061** **Mean/std dev** **Min–Max** **Uncertainty**	**101057** **Mean/std dev** **Min–Max** **Uncertainty**	**101058** **Mean/std dev** **Min–Max** **Uncertainty**
Number of tests	47	13	10	5
Young's modulus (GPa)	76/3 69–83 *±1 %*	74/4 69–80 *±3 %*	80/1 78–82 *±1 %*	83/3 80–86 *±3 %*
Poisson's ratio	0.23/0.04 0.14–0.30 ±4 %	0.30/0.03 0.26–0.35 ±5 %	0.29/0.02 0.26–0.31 ±4 %	0.27/0.03 0.25–0.31 ±8 %
Uniaxial compressive strength (MPa)	226/29 157–289 ±4 %	214/32.8 158–266 ±8 %	373/20 338–391 ±3 %	310/58 229–371 ±16 %
Crack initiation stress (MPa)	116/23 60–187 ±7 %	114/18 85–140 ±15 %	196/20 180–250 ±6 %	169/29 125–200 ±15 %
Cohesion M-C (MPa)	28	33	–	–
Friction angle M-C (MPa)	60	56	–	–
Constant m_i H-B	28	18	–	–
Number of tests	82	12	10	–
Indirect tensile strength (MPa)	13/2 10–18 ±2 %	12/3 8–16 ±9 %	15/1 13–17 ±5 %	–

101057 – Granite to granodiorite, metamorphic, medium grained (albitised in FFM06).
101058 – Granite, metamorphic, aplitic (albitised).
101061 – Pegmatite, pegmatitic granite.

6.4.2 Single fractures

The resulting mechanical properties of open single fractures inside the access volume are the same as those derived for **SDM-Site**, see Table 6-3.

Table 6-3 Results from direct shear tests on open single fractures in fracture domain FFM01 and deformation zones intersecting the target volume (modified after Table 7-4 in SKB 2008).

Parameter	FFM01	
	Mean/std dev Uncertainty	Min–Max
Normal stiffness (MPa/mm)	656/396 ±22 %	159–1 833
Shear stiffness, KS20, (MPa/mm)	34/10 ±11 %	18–52
Peak friction angle (°)	37/3 ±3 %	29–42
Peak cohesion (MPa)	0.8/0.3 ±14 %	0.2–1.3
Residual friction angle (°)	34.9/3.4 ±4 %	28–42
Residual cohesion (MPa)	0.3/0.2 ±24 %	0.1–0.8

Note: shear stiffness at 20 MPa normal stress. The uncertainty of the mean is quantified for a 95 % confidence interval. Minimum and maximum truncation values are based on the observed min' and max' for the tested population.

6.4.3 Rock mass

The resulting mechanical properties of the rock mass between deformation zones are the same as those derived for **SDM-Site**, see "Harmonised values" in Table 6-4.

Table 6-4 Suggested rock mechanics properties of the rock mass between deformation zones in FFM01 and FFM06 after harmonisation between theoretical and empirical approaches (Table 7-6 in SKB 2008).

Parameter	Empirical approach		Theoretical approach		Harmonised values	
	Mean/std. dev. Min–max Uncertainty of mean		Mean/std. dev. Min–max Uncertainty of mean		Mean/std. dev. Min–max Uncertainty of mean	
	FFM01	FFM06	FFM01	FFM06	FFM01	FFM06
Deformation modulus (GPa)	72/8 39–76 ±1 %	70/12 40–81 ±3 %	69/4 59–79 ±2 %	68/5 56–81 ±3 %	70/8 39–79 ±2 %	69/12 40–81 ±3 %
Poisson's ratio	0.23/0.03 0.12–0.30 ±1 %	0.23/0.04 0.12–0.33 ±3 %	0.24/0.03 0.19–0.33 ±5 %	0.3/0.03 0.23–0.37 ±4 %	0.24/0.03 0.12–0.33 ±5 %	0.27/0.04 0.12–0.37 ±4 %
Uniaxial compressive strength Hoek–Brown (MPa)	92/27 23–153 ±3 %	95/32 30–149 ±7 %	No values	No values	92/27 23–153 ±3 %	95/32 30–149 ±7 %
Friction angle, Mohr–Coulomb (°)	50/2 32–52 ±0 %	50/2 43–53 ±1 %	53/2 50–56 ±2 %	52/2 47–57 ±2 %	51/2 32–56 ±2 %	51/2 43–57 ±2 %
Cohesion Mohr–Coulomb (MPa)	27/4 12–35 ±1 %	27/4 18–34 ±3 %	21/6 5–42 ±13 %	18/6 1–40 ±15 %	24/5 6–42 ±13 %	23/5 1–40 ±15 %
Tensile strength (MPa)	2.4/1.0 0.6–5.0 ±3 %	2.3/1.0 0.6–4.0 ±8 %	No values	No values	2.4/1.0 0.6–5.0 ±3 %	2.3/1.0 0.6–4.0 ±8 %

Note: the uncertainty of the mean is quantified for a 95 % confidence interval. Minimum and maximum truncation values are based on the observed minimum and maximum for the tested population.

6.4.4 Rock stress

The resulting stress magnitudes for the bedrock inside the access volume are the same as those derived for **SDM-Site**, see Table 6-5. The stress magnitudes are based on previous modelling work (Martin 2007).

Table 6-5. Stress model for the bedrock inside the access volume (modified after Table 6-7 and Table 6-8 in Glamheden et al. 2007a).

Parameter	Most likely value[1)] < 400 m depth	Most likely value[1)] > 400 m depth
Major horizontal stress, σ_H	9.1 + 0.074z MPa	29.5 + 0.023z MPa
Minor horizontal stress, σ_h	6.8 + 0.034z MPa	9.2 + 0.028z MPa
Vertical stress, σ_v	0.0265z MPa	0.0265z MPa
Major horizontal stress trend, σ_H	145°	145°

[1)] The symbol z corresponds to the depth from the ground surface in metres.

6.4.5 Thermal properties

The resulting thermal conductivity description selected for the bedrock inside the access volume is the same as those derived for **SDM-Site** (SKB 2008), presented in Table 6-6. The values in Table 6-6 are valid at 20 °C.

The clear difference in heterogeneity of thermal conductivity between the two rock domains RFM029 and RFM045 is essentially caused by the difference in amphibolite content of the domains. The access volume is almost completely located within the RFM029 domain from **SDM-Site** (Figure 5-2). Evaluation of thermal anisotropy due to the occurrence of subordinate rock bodies, primarily amphibolite, indicates a slightly lower thermal conductivity on a 5 m scale in a direction perpendicular to the plane of maximum flattening of the amphibolite bodies, i.e. in the vertical direction.

Similarly, the heat capacity model for the access volume is the same as the one for **SDM-Site**, see Table 6-6. The mean coefficient of thermal expansion for the different rock domains is $7–8 \times 10^{-6}$ m/(m·K) (SKB 2008). The mean *in-situ* temperature, based on measurements in eight boreholes at 400 m, 500 m and 600 m depth is estimated at 10.5 °C, 11.6 °C, and 12.8 °C respectively.

Table 6-6. Thermal conductivity and heat capacity for domains RFM029 and RFM045. The access volume is expected to be located mainly in RFM029 (modified after Table 6-16 and 6-17 in SKB 2008).

Statistic	Thermal conductivity RFM029 5 m scale W/(m·K)	Thermal conductivity RFM045 5 m scale W/(m·K)	Heat capacity RFM029 1 m scale MJ/(m³·K)	Heat capacity RFM045 1 m scale MJ/(m³·K)
Mean	3.57	3.56	2.06	2.12
Standard deviation	0.13	0.28	0.10	0.15
0.1-percentile	2.87	2.36		
1-percentile	3.12	2.56		
2.5-percentile	3.23	2.73		

6.5 Uncertainties in the models for bedrock thermal properties and rock mechanics

6.5.1 Mechanical properties of intact rock

The certainty in the model for intact rock in **SDM-Site** is generally high (SKB 2008), but the number of tests performed in aplitic granite (101058) and albitised granodiorite (101057) are few which means a more uncertain description for these rock types. Amphibolite (102017) and other mafic rocks have not been sampled and tested for rock mechanics properties, and no modelling has been made. The amount

of amphibolite is estimated to about 5 % of the bedrock volume inside the access volume. Also for the rock types that have a higher degree of oxidation, there are no particular test series performed and no particular modelling made. Oxidised rock types are expected to constitute about 15 % of the bedrock volume inside the access volume, see Figure 5-13.

6.5.2 Mechanical properties of single fractures

The mechanical properties of open single fractures have been studied by laboratory tests on small samples. There is an uncertainty related to the potential scale effect as there is no general methodology to go from small scale test results to the large-scale fracture properties (Helgstedt 1997). The site investigation for **SDM-Site** did not include laboratory tests on sealed fractures and hence the description in **SDM-Site** does not contain any model for the mechanical properties of sealed fractures. This could introduce an uncertainty in the determination of the rock mass properties in areas with mainly sealed fractures (see Section 6.5.3).

6.5.3 Mechanical properties of rock mass

The uncertainties in elastic parameters are fairly low, but the strength parameters are more uncertain due to the uncertain influence of fractures, both open and sealed (Helgstedt 1997).

In the upper parts of the ramp the stress conditions are expected to be significantly lower than the stresses used to describe the rock mass characteristics at repository depth. Therefore, the model presented for the rock mass at depth may not be representative for the rock mass in the uppermost part of the access volume.

In the lower part of the bedrock inside the access volume, sealed fractures seem to be more frequent than open fractures, with a frequency in the order of 5–10 m^{-1}. This means that the rock mass strength at depth will be influenced by the sealed fracture properties, a condition not yet included in the description (see Section 6.5.2).

6.5.4 Rock stress

The uncertainty in stress orientation is considered fairly low because different, fully independent, types of measurements and indicators have given the same orientation results. However, the orientation is more certain towards depth and, as one would expect, more uncertain at shallow depths.

The reason for borehole breakouts to occur at a few points in borehole KFM24, and not along the entire borehole length, is most probably the variation in strength of the rock in the borehole wall (Hakami 2011), possibly in combination with local increase of the *in-situ* stress and with local variation of the load from drilling and heat expansion during drilling. This issue is an area for further study.

The uncertainty in the stress magnitude is relatively high because measurements have shown large spread within the same method, and this could possibly be due to methodology problems. Also significant differences in results between different types of measurements have been observed ant the reasons are not fully resolved. The total number of performed stress measurements behind the stress model for **SDM-Site** is not large. Inside the access volume. only 14 overcoring measurements have been performed between −100 m and −270 m elevation, which means that measurements in the uppermost and the deepest parts of the bedrock volume inside the access volume are lacking.

6.5.5 Thermal properties

Small uncertainties in the lower tail of the thermal conductivity distributions will have a significant impact on canister spacing in the repository design and therefore the description of uncertainties is focused on the lower tail of the thermal conductivity distribution. Confidence in the lower tails of the thermal conductivity distributions is higher for rock domain RFM029 than for rock domain RFM045 because uncertainty is related to the spatial and size distributions of amphibolite (SKB 2008). The access volume is located almost entirely in RFM029 (Figure 5-2).

7 Climate, hydrology and near-surface hydrogeology

7.1 Meteorological and ice freeze/breakup monitoring

Werner (2018) presents annual data measured at the Storskäret, Högmasten and Labbomasten meteorological stations. At the Högmasten station, which has the longest data record, the annual accumulated precipitation (P) and the annual calculated potential evapotranspiration (PET) during the full-year period 2004–2014 vary between 428–812 and 402–538 mm, respectively. During the same period of time the annual average temperature (T) varies between ca 5–7 °C. These time series are too short to identify any potential trends with certainty. However, it is noted that subsequent to **SDM-Site** the annual accumulated P has been above the estimated long-term average of 560 mm most of the years (2007 and 2013 are the only exceptions).

The length of the ice-covered period demonstrates large inter-annual variations, both for the period up to (60–133 days) and subsequent to **SDM-Site** (9–146 days). In particular, the ice-covered period during the 2007/2008 winter season was exceptionally short (only ca one week in total), and very long (almost 5 months) during the 2012/2013 winter season. It is also noted that there was equal length of the ice-covered period during the 2015/2016 winter season at the two observation areas AFM000075 and AFM001449 (cf Figure 3-2).

7.2 Hydraulic properties of regolith and the rock-regolith interface

Table 2-1 shows hydraulic conductivity data of the regolith and the rock-regolith interface according to the general parameterisation of the Forsmark area in **SDM-Site**. Additional data are available from slug tests conducted in a number of wells installed subsequent to **SDM-Site** (SFM000121–125, -139, -143–147, -149, and -153–154). These slug tests are evaluated by Werner (2018).

7.3 Groundwater levels and depths in regolith

Werner (2018) presents a delineation of topography-controlled boundaries of sub-catchment areas within the “Forsmark 1/2 rest catchment area” (see Brunberg et al. 2004 for explanation), using the high-resolved DEM presented in Chapter 4. According to this analysis, groundwater discharge and surface runoff pass through surface waters (Lake Tjärnpussen and the three small ponds close to the sea shoreline) prior to drainage to the sea. Subsequent to **SDM-Site**, 14 additional wells have been installed in and in the vicinity of the access area (Table 3-3). Some of these wells were installed recently, which means that available monitoring periods yet are short. Werner (2018) presents statistics (average, standard deviation, minimum and maximum) of groundwater levels and -depths below ground surface available for modelling, for the whole data period, for individual years and for three-month seasons. According to Werner (2018), hydraulic disturbances are not considered to have any major influence on the presented statistics.

Average groundwater-table depths are ca 1 m below ground surface in many wells. Figure 7-1 shows a cross plot of average groundwater levels in wells installed in regolith versus local ground-surface elevations. Moreover, Figure 7-1 illustrates averages and intervals of groundwater levels in wells installed in regolith, local ground-surface elevations, and rock-surface elevations (cf Figure 2-6). The groundwater level in regolith has a general trend from inland areas towards the coastline (Figure 7-2), due to the close relation between groundwater level and topography and the general topographic trend (for corresponding maps for wet and dry periods, see Werner 2018). The average groundwater table is located at larger depths at some well locations, possibly due to relatively coarse-grained artificial fill.

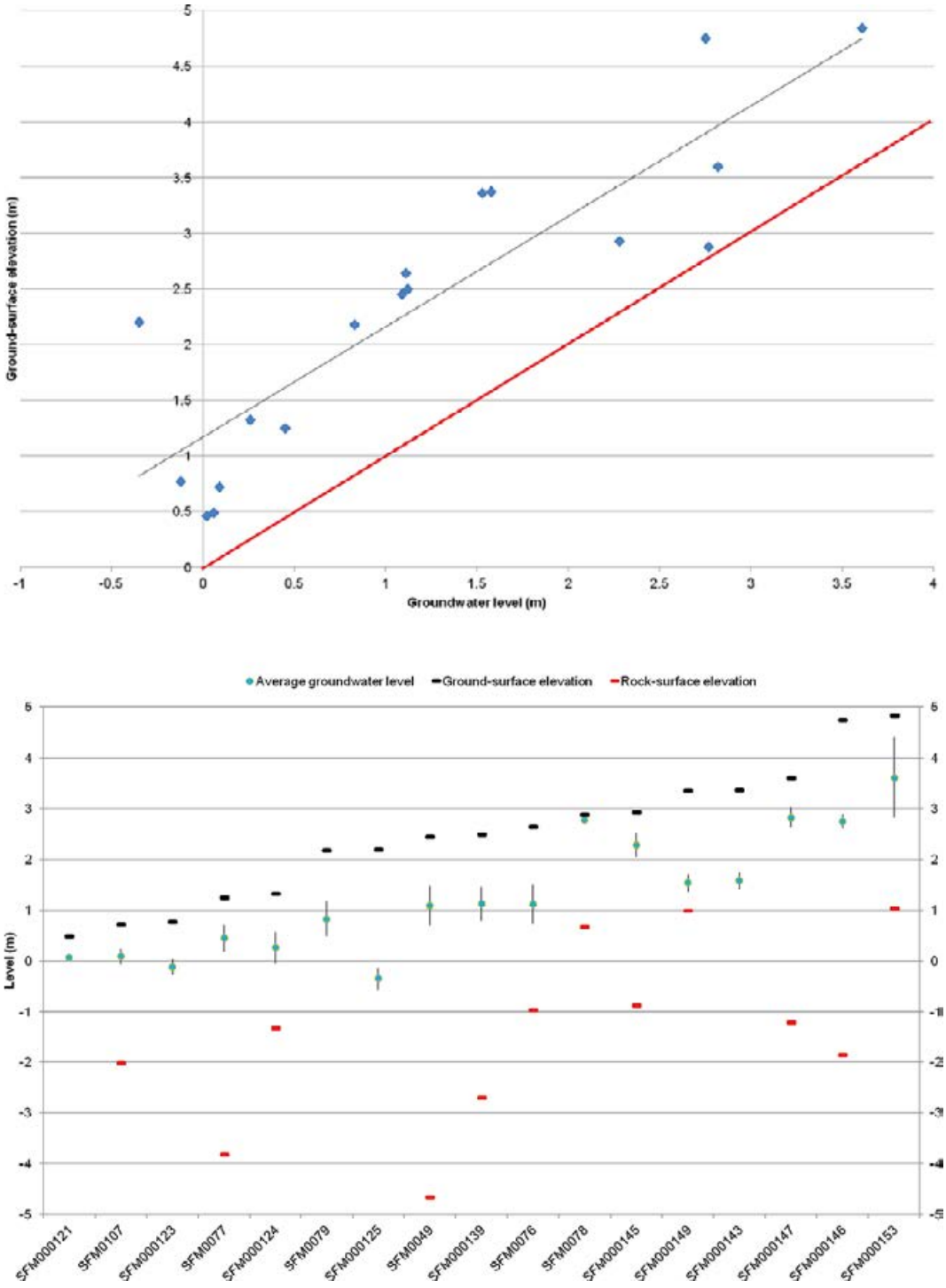

Figure 7-1. *Upper plot: cross plot of average groundwater levels in wells installed in regolith versus local ground-surface elevations. The black line is a linear match against data, whereas the red line represents a perfect linear groundwater-level/ground-surface elevation relationship. Bottom plot: averages and intervals (average ± 1 std dev) of groundwater levels in wells installed in regolith, local ground-surface elevations (black lines) and rock-surface elevations (red lines), ranked according to ground-surface elevations. Note that SFM000143, -145–147, -149 and -153 are sorted according to ground-surface elevation in the lower plot, as rock-surface elevation data are missing for these wells.*

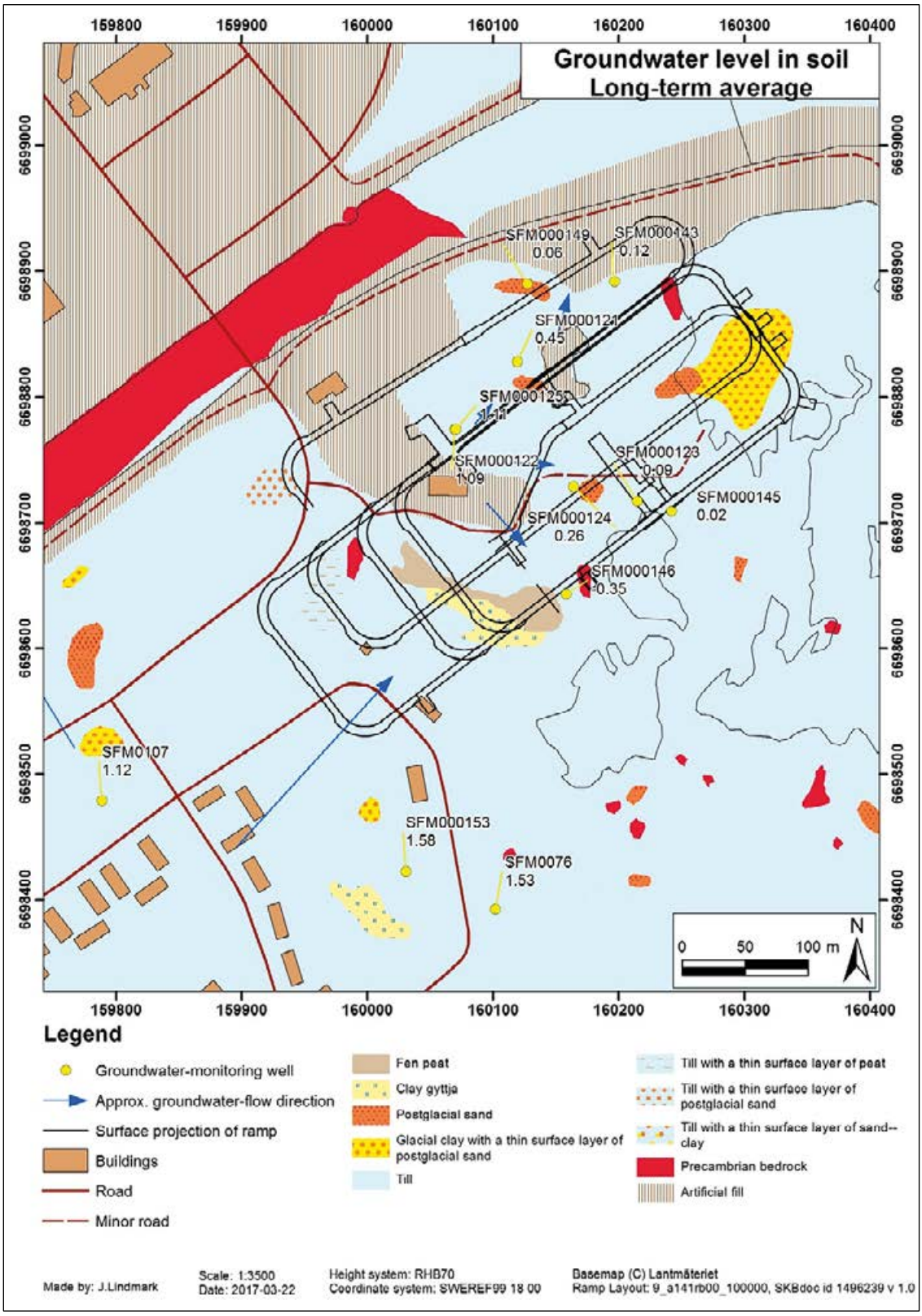

Figure 7-2. *Interpreted horizontal groundwater-flow directions (arrows), based on average groundwater levels in monitoring wells installed in regolith. The average sea level is ca −0.06 m in RHB 70 (ca +0.12 in RH 2000).*

7.4 Relations between groundwater levels and surface-water levels

Werner (2018) presents surface-water level data available for modelling, including basic statistics (average, standard deviation) of surface-water levels and -depths. A surface-water level gauge (SFM000156) was recently installed in a pond in the access area. The correlation between groundwater levels in wells installed in regolith and the sea level (PFM010038) is low for most wells, but relatively high for some of the wells installed close to the coastline. Groundwater levels in regolith are also influenced by rainfall/snow-melt induced groundwater recharge and demonstrate some degree of time lag (on the order of one or a few days) in relation to sea-level changes.

There is some degree of correlation between surface-water levels of Lake Tjärnpussen and the nameless pond and the groundwater level in neighbouring wells. Surface-water levels are always above the groundwater level, except for well SFM000121 in which the groundwater level dropped below the surface-water level of the pond, and also below sea level, during the summer of 2016. The surface-water level of the nameless pond (short time series) shows no correlation to the sea level.

7.5 Groundwater levels in the upper part of the rock

Subsequent to **SDM-Site**, monitoring has been initiated in 15 additional percussion-drilled and core-drilled boreholes in and in the vicinity of the access area (Table 3-2). Werner (2018) presents statistics (average, standard deviation, minimum and maximum) of groundwater levels and -depths below ground surface available for the access area, for the whole data period, for individual years and for three-month seasons.

According to Figure 7-3, there is little correlation between the groundwater level in the upper part of the rock and the local topography (cf Figure 2-6 and Figure 2-7). This is likely due to hydraulic contacts with the sea, which lowers the groundwater levels in deformation zones and subhorizontal fractures inside the tectonic lens (cf Section 2.2.2). The average groundwater level in some boreholes is close to or even below sea level. For example, the average groundwater level in percussion-drilled borehole HFM41, located north of the cooling-water canal, is ca 0.5 m below sea level possibly due to pumping below the reactor buildings of the Forsmark nuclear power plant.

According to Figure 7-4, the groundwater level in the upper part of the rock has a general trend from inland areas towards the coastline (for corresponding maps for wet and dry periods, see Werner 2018). The cross sections shown in Figure 7-5 use the RDM (cf Chapter 4) as background cartoon to illustrate interpreted two-dimensional groundwater flow in the planes of the SW-NE and NW-SE cross sections (cf Figure 3-2). As shown in these cross sections, groundwater flow is directed both from inland areas towards the coastline, but also from regolith to rock.

The correlation between groundwater levels in the upper part of the rock and sea level (PFM010038) is rather high or very high for some of the boreholes (Werner 2018). Time lags are short compared to groundwater-level responses in regolith (see Section 7.4), as pressure changes are transmitted relatively fast in the fracture network of the rock, characterised by high hydraulic diffusivity.

Groundwater-level correlations are quite high for many combinations of upper borehole sections (or open boreholes) and neighbouring wells installed in regolith (Werner 2018). The groundwater level in the upper part of the rock is below the groundwater level in the regolith for most such combinations. However, the groundwater level in some boreholes is above the groundwater level in the regolith, possibly due to occurrences of relatively coarse-grained, easily-drained artificial fill, i.e. a mixture of blasted rock and excavated regolith, at some well locations. In addition to potential effects of coarse-grained regolith, the small-scale undulating topography may influence interpretation of vertical hydraulic gradients between regolith and rock (Werner 2018).

Werner (2018) also analyses interactions between groundwater in regolith and rock as interpreted from known hydraulic disturbances in the rock (flow logging, interference tests and air-lift pumping). The results of the analysis indicate that the hydraulic contact between regolith and rock likely varies across the access area, which is consistent with the interpretation of the uppermost rock as strongly affected by subhorizontal fractures of various sizes (cf Chapter 2).

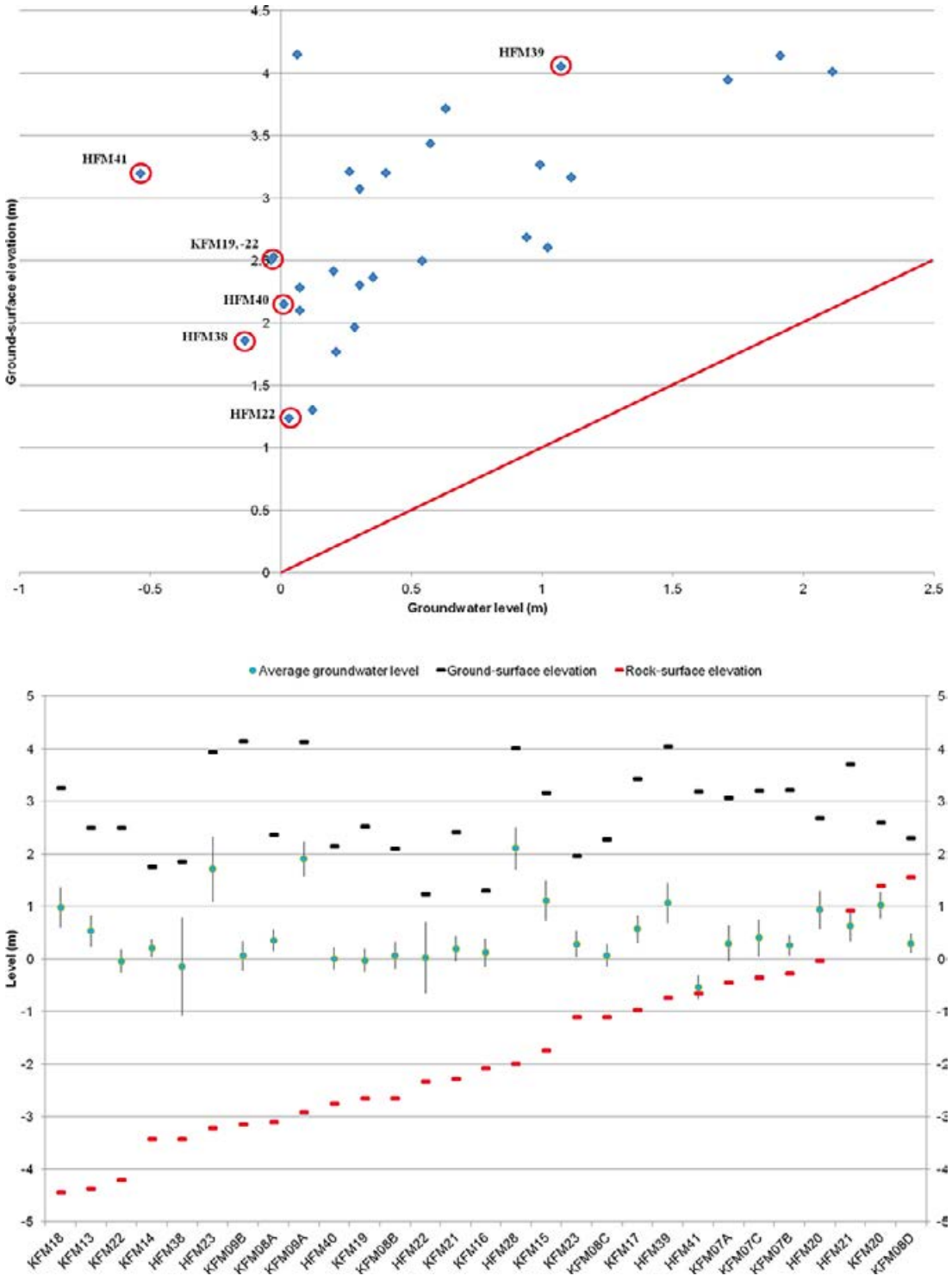

Figure 7-3. *Upper plot: cross plot of average groundwater levels in percussion- and core-drilled boreholes (upper borehole sections in sectioned boreholes) versus local ground-surface elevations. The red line represents a perfect linear groundwater-level/ground-surface elevation relationship. Lower plot: averages and intervals (average ± 1 std dev) of groundwater levels, local ground-surface elevations (black lines) and rock-surface elevations (red lines), ranked according to rock-surface elevation.*

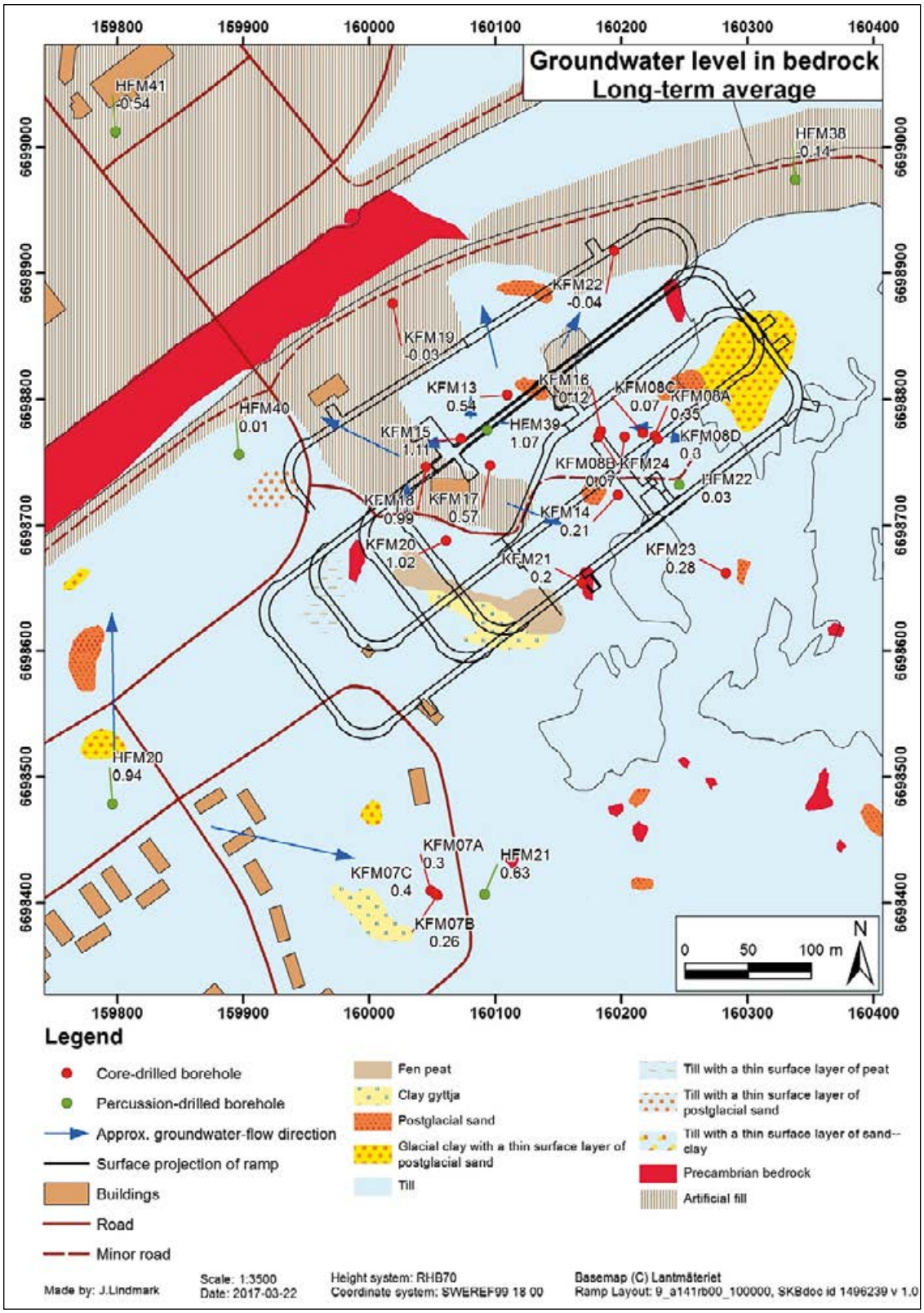

Figure 7-4. *Interpreted horizontal groundwater-flow directions (arrows), based on average groundwater levels in upper borehole sections or open boreholes in rock.*

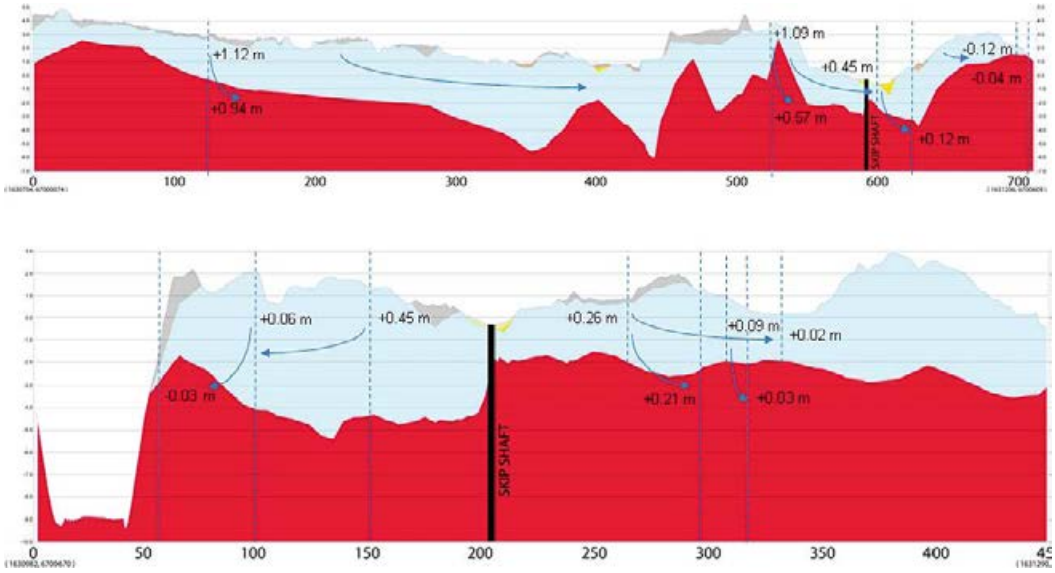

Figure 7-5. *Interpreted two-dimensional groundwater flow directions (arrows) in and between regolith and rock in the planes of the SW-NE (upper figure) and NW-SE (bottom figure) cross sections (cf Figure 3-2, Figure 4-16 and Figure 4-17). Interpreted flow directions in the upper figure are based on average groundwater levels (from SW to NE) in SFM0107, HFM20, KFM17, SFM000122, SFM000121, KFM16, SFM000143, and KFM22 (Werner 2018). The bottom figure is based on average groundwater levels (from NW to SE) in KFM19, SFM000149, SFM000121, SFM000124, KFM14, SFM000123, HFM22, and SFM000145.*

The cartoon in Figure 7-6 illustrates overall, relative relations between ground- and rock-surface elevations, and groundwater levels in monitoring wells installed in regolith, and in percussion- and core-drilled boreholes with different casing depths. Specifically, monitoring wells (in some cases installed across the regolith/rock interface) are equipped with an impermeable casing to some depth into the regolith, whereas percussion-drilled boreholes and short (on the order of 100 m) core-drilled boreholes have a casing across the regolith and a few metres into the upper parts of the rock. For stability reasons, deep core-drilled boreholes typically have a casing that extends some 100 m into the rock.

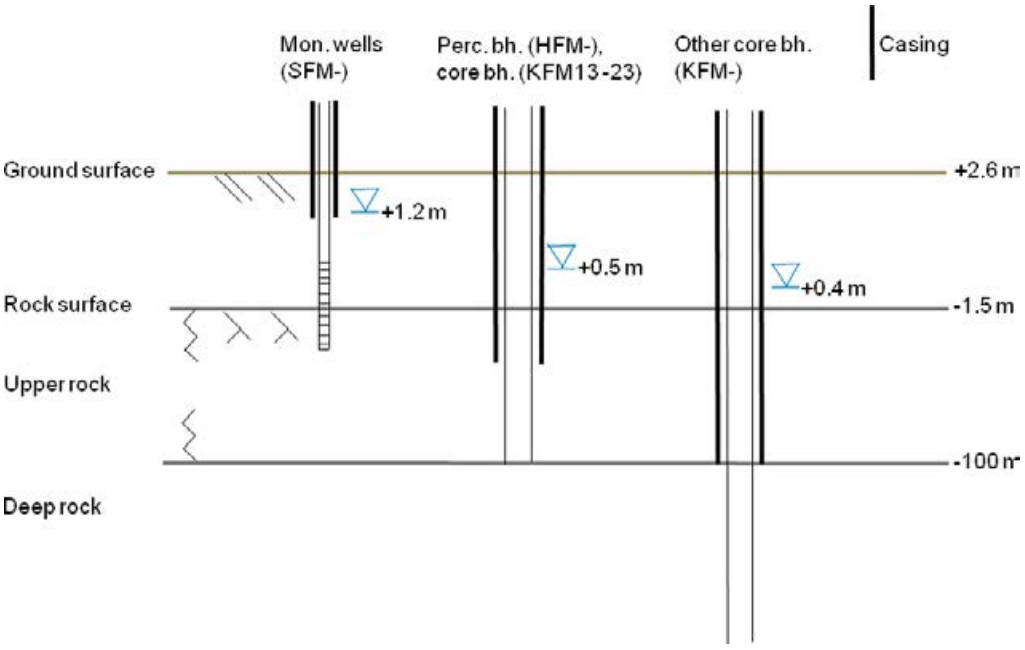

Figure 7-6. *Cartoon illustrating overall relative relations between ground- and rock-surface elevations, and groundwater levels in monitoring wells installed in regolith, percussion- and core-drilled boreholes with different casing depths. Note that neither well/borehole dimensions nor depths are to scale.*

7.6 Summary, uncertainties and remaining issues

The findings from the evaluation of monitoring data gathered subsequent to **SDM-Site**, in and around the access area, do not contradict overall **SDM-Site** findings related to the hydrology and near-surface hydrogeology of the Forsmark area. A potentially important characteristic of the access area and its environs is the occurrence of coarse-grained, easily-drained artificial fill, the extent of which is larger in a recently produced map of the surface distribution of the regolith in Forsmark compared to what was conceived in **SDM-Site** (Figure 4-8). This may cause local deviations from overall Forsmark characteristics, for instance in terms of relations between groundwater levels, topography and surface-water levels.

Data evaluations indicate that groundwater flow is directed both from inland areas towards the coastline, but also from regolith to bedrock. There is little or no correlation between the groundwater level in the upper part of the bedrock and the local topography, due to transmissive, near-surface, subhorizontal fractures, which are in hydraulic contact with the sea. The subhorizontal fractures lowers the groundwater levels in the bedrock within the tectonic lens. This observation agrees with the conclusion drawn in **SDM-Site**. It is noted that the average groundwater level in one of the percussion-drilled boreholes (HFM41), located north of the cooling-water canal, is ca 0.5 m below sea level, possibly due to pumping below the reactor buildings of the Forsmark nuclear power plant.

At present, the description of hydrology and near-surface hydrogeology within and near the access area is associated with two major uncertainties:

- Evaluation of presently available groundwater-level time series shows that the average groundwater table is located at relatively large depths in some wells. The reason for this might be the occurrence of coarse-grained, easily-drained artificial fill and/or the occurrence of transmissive, subhorizontal fractures in the shallow bedrock, the size and location of which were not modelled by the geologists in **SDM-Site**.
- There is a low density of regolith-investigation points and monitoring wells primarily in the area of the planned temporary rock dump, which cause uncertainties regarding hydrological and near-surface hydrogeological properties and processes in this area.

Subsequent to **SDM-Site**, monitoring has been initiated in a number of additional groundwater-monitoring wells, surface-water level gauges, and percussion-drilled and core-drilled boreholes in rock, in and in the vicinity of the access area. However, some of these installations, e.g. most of the monitoring wells, were installed quite recently (during 2016), and presently available time series are yet short. Short time series cause uncertainties related to the evaluation of many aspects addressed in this chapter, including relations between groundwater levels, topography and surface-water levels. Hence, continued monitoring and data evaluations are required to further address such issues.

8 Bedrock hydrogeology

8.1 Status of site understanding and models

The bedrock inside the investigation area of **SDM-Site** (Figure 2-1) was investigated with both single-hole and cross-hole (interference) tests. Constant-head injection tests between packers and difference flow logging pumping tests were used to characterise the fracture properties close to the deep core-drilled boreholes, and impeller flow logging was used to characterise the inflow locations in the shallow percussion-drilled boreholes. Long term pumping tests in open percussion-drilled boreholes were used for cross-hole characterisation. The overall experience from these investigations is that the spatial variability in the structural geology significantly affects the bedrock hydrogeology, and associated hydraulic properties. There is a considerable depth trend in deformation zone transmissivity and the uppermost part of the bedrock between the deformation zones is found to be significantly more fractured than the deeper parts, see Figure 2-17, Figure 2-18, Figure 2-19 and Table 2-2.

Below, data from hydraulic investigations of the bedrock inside the access volume are presented. Some of the data were acquired during the site investigation for **SDM-Site**, and some of the data were acquired posterior to **SDM-Site**.

8.2 Hydraulic investigations of the uppermost part of the bedrock

Eleven core-drilled boreholes and nine percussion-drilled boreholes have been investigated with single-hole impeller flow logging (Jönsson et al. 2005, Jönsson and Ludvigson 2006, Walger et al. 2007, Jönsson 2011). Six cross-hole (interference) tests have also been conducted (Walger et al. 2012, Odén and Follin 2016).

8.2.1 Single-hole hydraulic tests

Figure 8-1 shows the depth below ground surface of the 20 boreholes investigated with impeller flow logging. The average borehole depth and regolith thickness in HFM20–23, -28 and -38 are 164 m and 3.3 m, respectively, and 84 m and 4.6 m in KFM13–23 and HFM39–41, respectively.

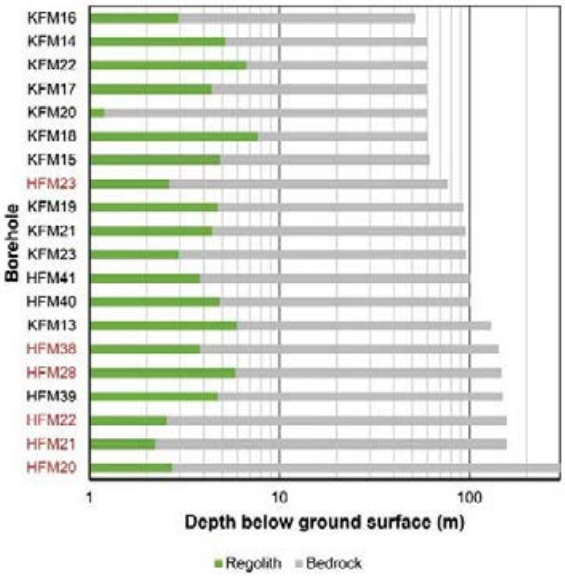

Figure 8-1. *Regolith thickness and borehole depth of the 20 boreholes investigated with impeller flow logging. Borehole names shown in red were drilled as part of SDM-Site and those with names in black were drilled in post SDM-Site investigations.*

Figure 8-2 shows the total borehole transmissivity below the regolith depth as inferred from the impeller flow logging. The geometric mean of the total borehole transmissivity in HFM20–23, -28 and -38 is 5.8×10^{-5} m^2/s, and 2.5×10^{-5} m^2/s in KFM13–23 and HFM39–41.

Figure 8-3 shows a scatter plot of the data shown in Figure 8-1 and Figure 8-2. There is no apparent correlation between the total borehole transmissivity and the borehole depth below ground surface. Further, the borehole transmissivity in the uppermost part of the bedrock varies about three orders of magnitude, with the majority of data centred on 1×10^{-4} m^2/s.

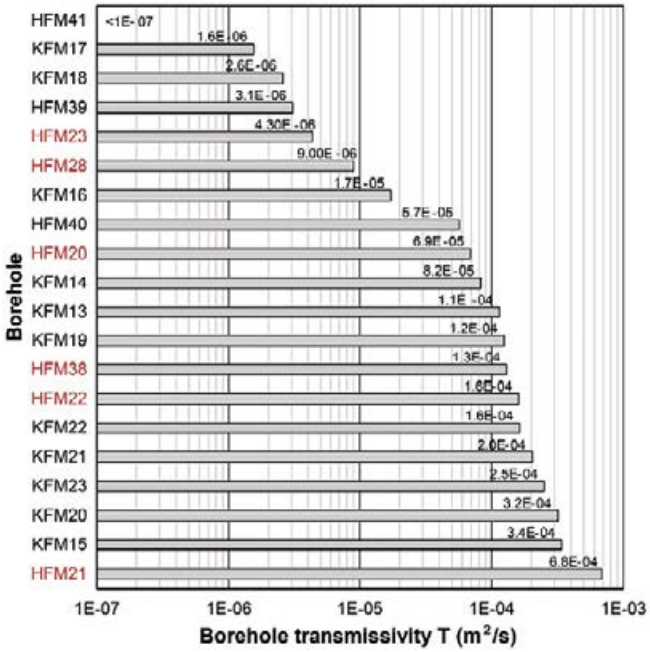

Figure 8-2. *Total borehole transmissivity below the regolith as inferred from the impeller flow logging. Borehole names shown in red were drilled as part of SDM-Site.*

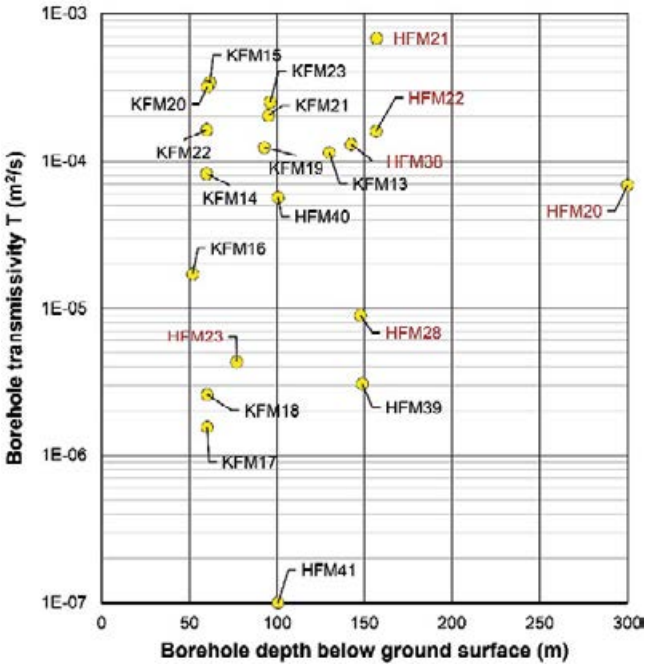

Figure 8-3. *Scatter plot of the total borehole transmissivity below the regolith versus the borehole depth below ground surface. Borehole names shown in red were drilled as part of SDM-Site.*

Figure 8-4 shows the distribution of inflows in each of the 20 boreholes investigated with impeller flow logging. The inflow locations are irregularly distributed within each borehole as well as from one borehole to the next. The majority of the open fractures are associated with subhorizontal to gently dipping structures (Appendices B and C).

The depth to the bottom of the superficial fracture domain FFM02 varies within the investigation area (Figure 2-14) as well as in the access volume (Figure 8-4). In borehole KFM19, which is located towards north-west inside the access volume, the bottom of FFM02 is found at −20.5 m elevation and the Terzaghi corrected fracture frequency of open fractures is ca 9 m^{-1}. In borehole KFM21, which is located towards south-east inside the access volume, the bottom of FFM02 is found at −59.6 m elevation and the Terzaghi corrected fracture frequency of open fractures is ca 3.7 m^{-1}. The average depth to the bottom of FFM02 in the core-drilled boreholes KFM13–23 is −43.6 m elevation and the average value of the Terzaghi corrected fracture frequency of open fractures is 4.85 m^{-1}.

The distribution of borehole inflows shown in Figure 8-4 is lumped into 20 m intervals for each of the 20 boreholes investigated with impeller flow logging and a transmissivity plot similar to the one shown in Figure 2-19 is compiled, see Figure 8-5.

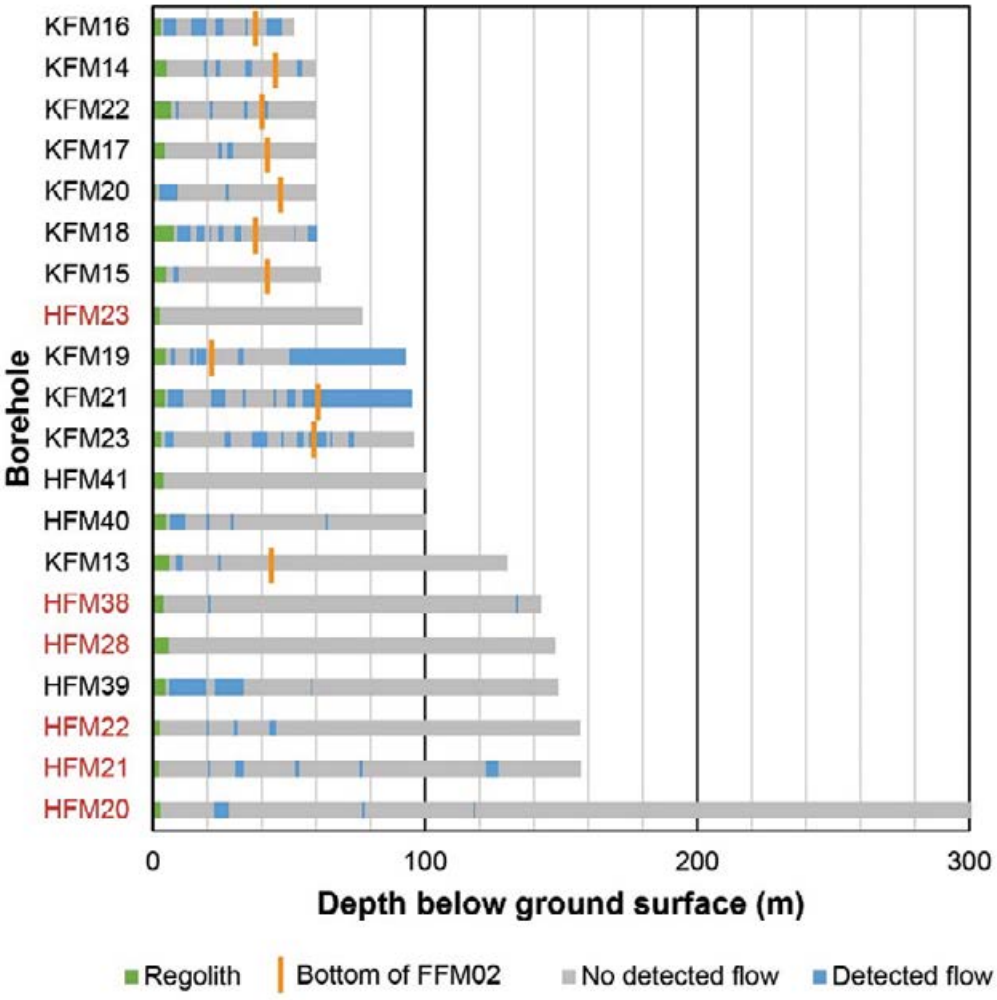

Figure 8-4. *Distribution of inflow in the 20 boreholes investigated with impeller flow logging. The depth to the bottom of fracture domain FFM02 has been evaluated for the core-drilled boreholes KFM13–23.*

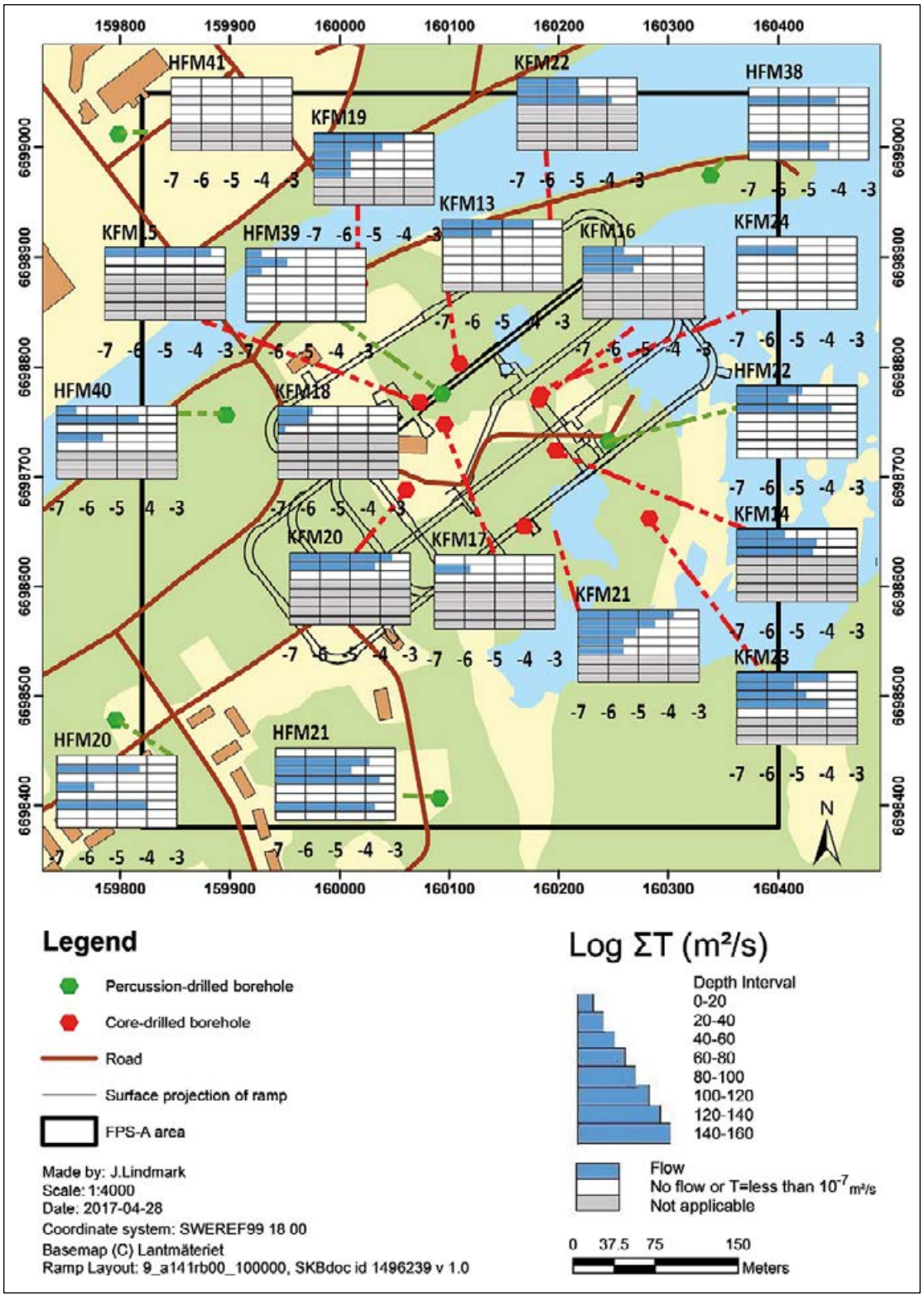

Figure 8-5. *Borehole transmissivities in 20 m long intervals inferred from impeller flow logging in the boreholes shown in Figure 8-4. Data from the uppermost 160 m of borehole KFM24 are also shown in this figure. KFM24 has a steel casing to about 35 m depth below ground surface and there are no flowing fractures with transmissivities greater than 1×10^{-7} m^2/s between –40 and –160 m elevation (cf Figure 8-7). Before the steel casing was installed in KFM24, an inflow of about 15 L/min was observed at about 24.5 m depth (Nilsson 2017), which suggests a bedrock transmissivity of approximately 1×10^{-5} m^2/s in the interval 20–40 m.*

8.2.2 Cross-hole hydraulic tests

Two kinds of cross-hole (interference) tests have been carried out in the uppermost part of the bedrock inside the access volume; pumping using a single packer in KFM16 and KFM23, and pumping during the completion of the percussion-drilled part of borehole KFM24.

Pumping using a packer in KFM16 and KFM23

Hydraulic interference tests were carried out from November to December, 2011 with the core-drilled boreholes KFM16 and KFM23 as pumping boreholes (Walger et al. 2012). The interference tests comprise five pumping tests with two different sections in borehole KFM16 and three different sections in borehole KFM23 (Table 8-1) while measuring the hydraulic head interferences due to pumping in selected surrounding boreholes (Figure 3-3 through Figure 3-6). The interference tests were designed according to the results of the previous impeller flow logging (IFL) in the boreholes (Jönsson 2011) together with supporting geological information (Appendices B and C).

The hydraulic head responses in the observation borehole sections were similar during the two interference tests in KFM16 (sections 0–31.0 m and 0–60.4 m, respectively) (Table 8-2). The most distinct and fastest responses occurred in borehole sections KFM08B:2, KFM08B:3 and KFM14:2.

During the three interference tests in KFM23, different responses were obtained (Table 8-3). In the test in KFM23: 0–10.0 m, a rather high-transmissive fracture was pumped, but no hydraulic head interferences were observed in available surrounding boreholes during this test. During the tests in KFM23: 0–58.5 m and 0–100.6 m, almost identical responses were observed. The most distinct and fastest responses occurred in sections HFM22:1, HFM22:2, KFM08D:4, KFM08D:7, KFM08C:5 and KFM14:1. In the test in 0–58.5 m also sections KFM08B:3 and KFM16:2 responded significantly.

Table 8-1. Overview of the pumping tests together with transmissivities from previously performed impeller flow logging (IFL), T_{IFL} (Walger et al. 2012).

Borehole: Interval (borehole length, m)	Pumping time (days)	Flow rate (m^3/s)	Drawdown (m)	Specific capacity (m^2/s)	T_{IFL} [1] (m^2/s)
KFM16: 0–31.0	0.33	3.34×10^{-4}	16.1	2.1×10^{-5}	1.2×10^{-5}
KFM16: 0–60.4	0.33	3.36×10^{-4}	11.8	2.8×10^{-5}	1.7×10^{-5}
KFM23: 0–10.0	0.35	2.00×10^{-4}	2.9	6.9×10^{-4}	1.1×10^{-4}
KFM23: 0–58.5	0.33	9.64×10^{-4}	10.6	9.1×10^{-5}	1.4×10^{-4}
KFM23: 0–100.6	0.33	1.00×10^{-3}	2.2	4.5×10^{-4}	2.5×10^{-4}

[1] Jönsson (2011).

Table 8-2. Overview of responses in nearby boles while pumping in KFM16 (Walger et al. 2012).

Borehole: Interval (borehole length, m)	Response borehole and section	Interval (borehole length, m)
KFM16: 0–31.0	KFM08B:2, KFM08B:3, KFM14:2	71–112, 0–70, 0–26
KFM16: 0 –60.4	KFM08B:2, KFM08B:3, KFM14:2	71–112, 0–70, 0–26

Table 8-3. Overview of responses in nearby boles while pumping in KFM23 (Walger et al. 2012).

Borehole: Interval (borehole length, m)	Response borehole and section	Interval (borehole length, m)
KFM23: 0–10.0	None	–
KFM23: 0–58.5	HFM22:1, HFM22:2, KFM08D:4, KFM08D:7, KFM08C:5, KFM14:1, KFM08B:3, KFM16:2	53.5–222, 37–52.5, 660–680, 0–160, 0–145, 27–60.2, 0–70, 13.5–30.5
KFM23: 0–100.6	HFM22:1, HFM22:2, KFM08D:4, KFM08D:7, KFM08C:5, KFM14:1	53.5–222, 37–52.5, 660–680, 0–160, 0–145, 27–60.2

Pumping during the completion of the percussion-drilled part of borehole KFM24

The percussion-drilled part of borehole KFM24 was completed between March 31 and April 1 2017 (Nilsson 2017). The length of the percussion-drilling was 35.7 m (35.5 m vertical depth). A flowing fracture was observed at 24.5 m borehole length. The fracture yielded ca 900 L/h implying a specific capacity of ca 1×10^{-5} m^2/s. During the completion the borehole was pumped in conjunction with reaming and cleaning activities. Hydraulic interferences were observed in boreholes KFM08A, KFM08B, KFM13, KFM14, KFM16, KFM17, KFM21, KFM22, KFM23 and HFM22 (Table 8-4). The responses were generally distinct (Figure 8-6).

Table 8-4. Overview of responses in nearby boles while during reaming and cleaning of the percussion-drilled part of borehole KFM24 (Odén and Follin 2016).

Response borehole and section	Interval (borehole length, m)
KFM08A:9	0–161
KFM08B:2, KFM08:3	71–112, 0–70
KFM13 (open borehole)	0–150.2
KFM14 (open borehole)	0–60.4
KFM16 (open borehole)	0–60.4
KFM17 (open borehole)	0–60.5
KFM21 (open borehole)	0–101.1
KFM22 (open borehole)	0–60.3
KFM23 (open borehole)	0–100.6
HFM22 (open borehole)	0–222

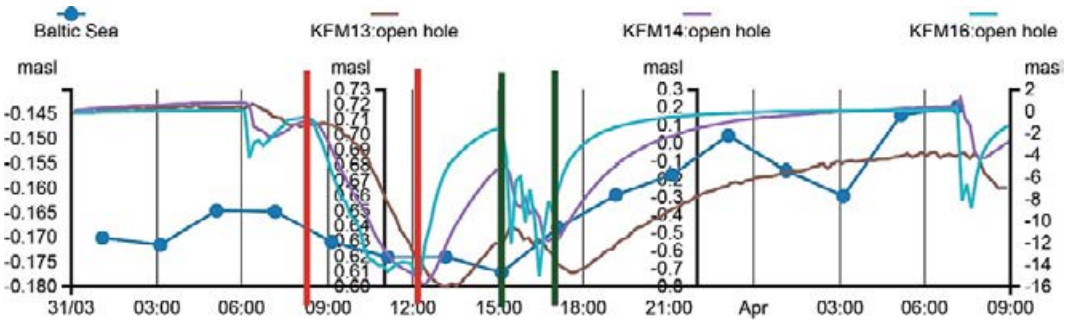

Figure 8-6. *Example of responses in boreholes KFM13, KFM14 and KFM16 during the completion of the percussion-drilled part of borehole KFM24. Red lines show start and stop times of the reaming and green lines show the start and stop times of the cleaning. Changes in sea level are shown as a reference. (Modified after Figure 3-1 in Odén and Follin 2016.)*

8.3 Hydraulic investigations of the bedrock at depth

The approximately 550 m long cored borehole KFM24 was drilled in proximity of the planned skip shaft inside the access volume (Figure 3-3 through Figure 3-6). The drilling and difference flow logging of KFM24 is described in Nilsson (2017) and Hurmerinta (2017), respectively. The geoscientific single-hole interpretation is described in Dahlin et al. (2017). Six cross-hole tests have also been conducted in borehole KFM24 (Odén and Follin 2016, Harrström et al. 2017).

8.3.1 Single-hole hydraulic tests

The result from the difference flow logging with the Posiva Flow Log (PFL) in borehole KFM24 is shown in Figure 8-7. Thirty-four flowing fractures were identified. All these fractures are to be associated with the bedrock between deformation zones according to the geoscientific single-hole interpretation, which did not identify any intervals with deformation zone type properties. A preliminary analysis of the flowing fractures in borehole KFM24 suggests two dominant flowing fracture sets; one subhorizontal set and one NE striking steeply dipping set. Further, all flowing fractures are situated in fracture domain FFM01 and the greatest PFL fracture transmissivities in borehole KFM24 are observed at about −190 m elevation where the fractures are gently dipping.

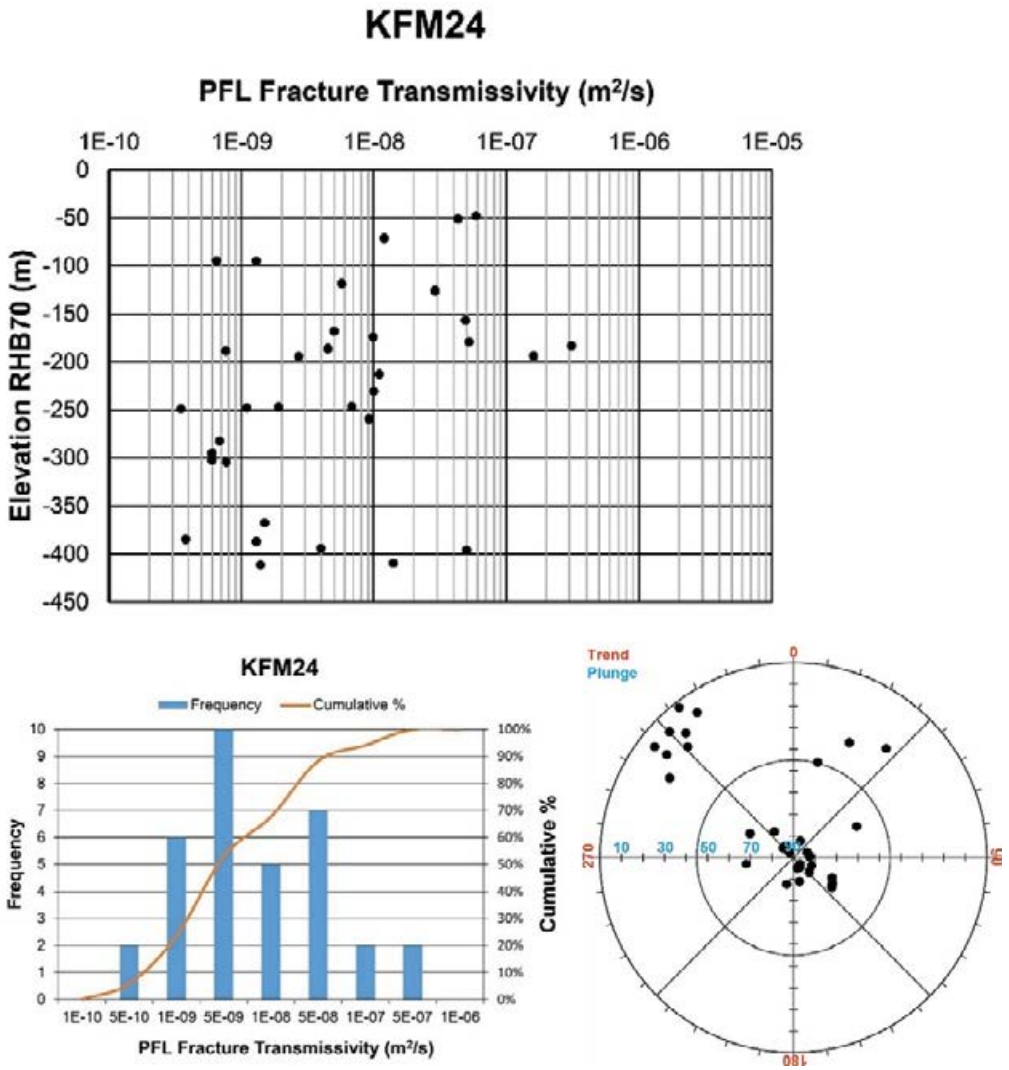

Figure 8-7. *Thirty-four flowing fractures were identified during the difference flow logging with the Posiva Flow Log (PFL). All flowing fractures are associated with fracture domain FFM01. The interval –184 to –194 m elevation contains five flowing fractures and is the most conductive interval of KFM24.*

The results from the difference flow logging of borehole KFM24 are compared with the results from corresponding measurements in nearby core-drilled boreholes, see Table 8-5 and Figure 8-8. The number and spatial distribution of flowing fractures observed in borehole KFM24 resemble the number and spatial distribution of flowing fractures observed in boreholes KFM01A, KFM01D, KFM08A and KFM08C. However, many of the flowing fractures in the latter two boreholes were interpreted to coincide with possible deformation zones (PDZ) in the single-hole interpretations of these boreholes for **SDM-Site**.

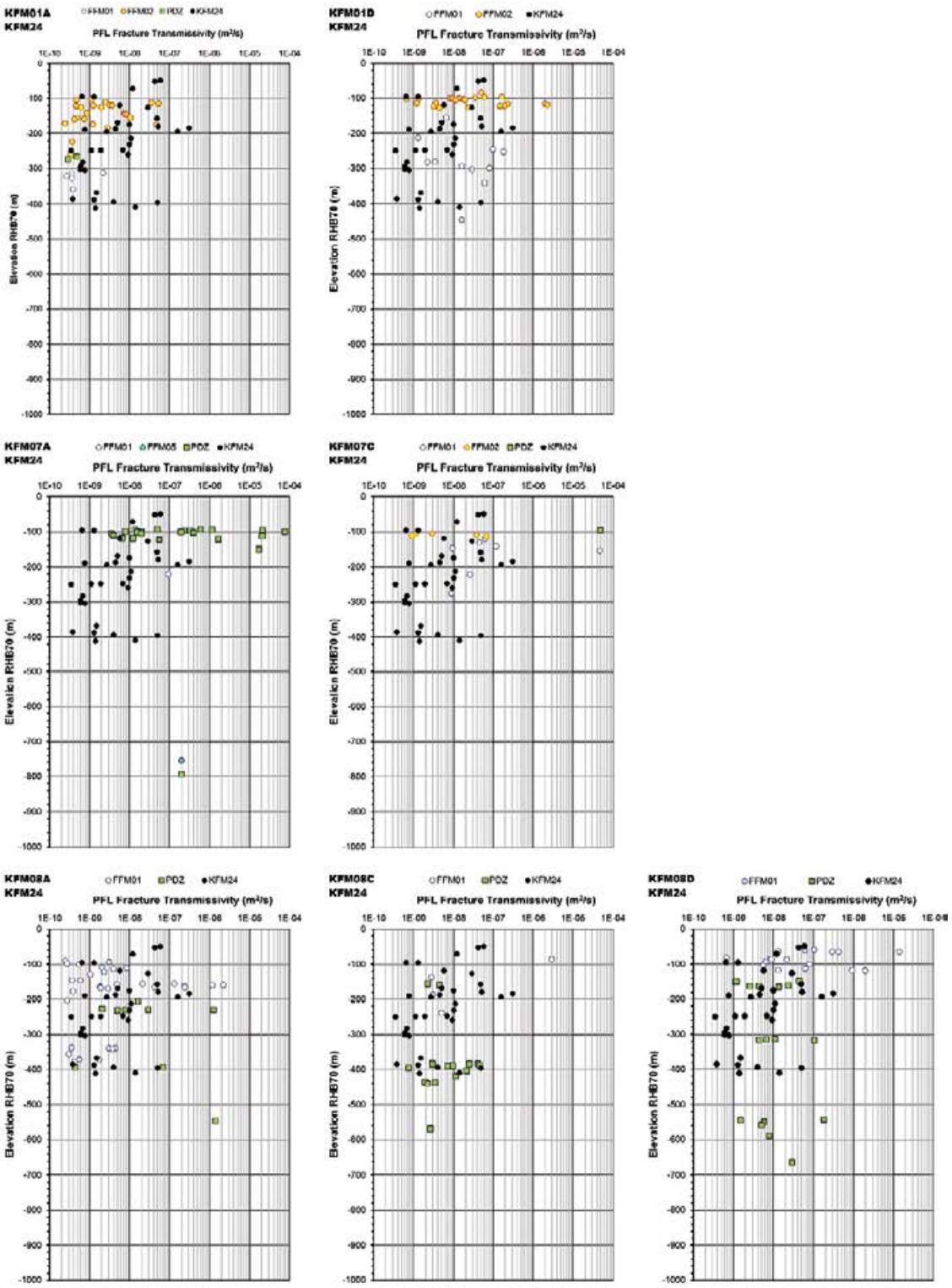

Figure 8-8. *Comparison of difference flow logging measurements in KFM24 versus KFM01A, KFM01D, KFM07A, KFM07C, KFM08A, KFM08C and KFM08D, respectively. PDZ = possible deformation zone as inferred in the single-hole interpretation.*

Table 8-5. Flowing fractures identified during difference flow logging.

Feature	KFM24	KFM01A	KFM01D	KFM08A	KFM08C	KFM08D	KFM07A	KFM07C
FFM02*	0	26	23	0	0	0	0	5
FFM01	34	6	11	32	5	17	1	8
FFM05	NA	NA	NA	NA	NA	NA	2	NA
FFM06	NA	NA	NA	NA	NA	0	NA	NA
PDZ	0	2	0	9	16	17	23	1
Total	**34**	**34**	**34**	**41**	**21**	**34**	**26**	**14**

* Data acquisition is biased by steel casing.
NA = not applicable.
PDZ = possible deformation zone.

8.3.2 Cross-hole hydraulic tests

Two kinds of cross-hole tests have been conducted at depth in KFM24: responses during difference flow logging and pumping between packers.

Difference flow logging

Odén and Follin (2016) evaluated hydraulic interferences in surrounding boreholes observed during the six-day PFL difference flow logging in borehole KFM24 in the beginning of August 2016 (Hurmerinta 2017). Responses were observed in boreholes KFM08A–C (Table 8-6). The responses were distinct (Figure 8-9).

Table 8-6. Overview of responses in nearby boreholes during difference flow logging in borehole KFM24 (Odén and Follin 2016).

Response borehole and section	Interval (borehole length, m)
KFM08A:6–9	265–280, 216–264, 162–215, 0–161
KFM08B:1	113–200
KFM08C:4	146–310

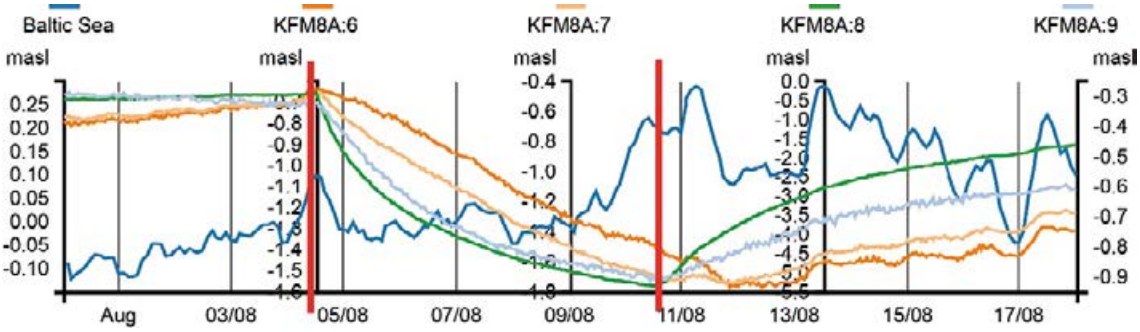

Figure 8-9. *Example of responses in borehole KFM08A, sections 6–9, during difference flow logging in KFM024 (red lines show start and stop times of the flow logging). Changes in sea level are shown as a reference. (Modified after Figure 3-7 in Odén and Follin 2016.)*

Pumping between packers

Hydraulic interference tests were carried out in borehole KFM24 from September to October 2016 (Harrström et al. 2017). The interference tests comprise pumping in five sections of borehole KFM24 (Table 8-7) while monitoring head responses in selected surrounding boreholes (Figure 3-3 through Figure 3-6). The interference tests were designed according to the results of the previous difference flow logging in the boreholes together with supporting geological information (Hurmerinta 2017, Odén and Follin 2016, Dahlin et al. 2017).

During the five interference tests in KFM24, only a few responses were obtained in the surrounding boreholes (Table 8-8). The responses were mainly distinct but slow. No responses were observed during the tests in KFM24: 45–65.0 m and 396–416.0 m. In the test in KFM24: 121–141.0 m, a strong but very slow response was observed in section KFM08A:9 and during the test in KFM24: 145–165.0 m, KFM08A:8 responded slowly but strongly. No other responses were observed during these tests.

The interference test in KFM24:177–197.0 m was the most active test, both in terms of obtained flow and responses. The responding sections were KFM08A:6–9, KFM08B:1 and KFM08C:4. The strongest responses occurred in sections KFM08A:8 and KFM08B:1 and the most rapid response occurred in section KFM08A:8.

Table 8-7. Overview of pumping test data and results from previous flow logging[1)] in borehole KFM24 (Harrström et al. 2017).

Section (borehole length, m)	Pumping time (days)	Flow rate (m^3/s)	Drawdown (m)	Specific capacity (m^2/s)	T_{PFL}[1)] (m^2/s)
45–65	3.9	1.53×10^{-6}	31.3	4.8×10^{-8}	4.8×10^{-8}
121–141	3.9	3.50×10^{-7}	34.1	1.0×10^{-8}	7.8×10^{-8}
145–165	4.0	1.15×10^{-6}	47.0	2.4×10^{-8}	4.9×10^{-8}
177–197	3.0	1.95×10^{-5}	39.9	4.9×10^{-7}	5.3×10^{-7}
396–416	3.0	3.17×10^{-6}	44.2	7.2×10^{-8}	6.4×10^{-8}

[1)] Odén and Follin (2016).

Table 8-8. Overview of responses in nearby boles while pumping in borehole KFM24 (Harrström et al. 2017).

Section in KFM24 (borehole length, m)	Response borehole and section	Interval (borehole length, m)
45–65	None	–
121–141	KFM08A:9	0–161
145–165	KFM08A:8	162–215
177–197	KFM08A:6–9	265–280, 216–264, 162–215, 0–161
	KFM08B:1	113–200
	KFM08C:4	146–310
396–416	None	–

8.4 Transmissivity of deformation zones

Table 8-9 collates transmissivity data of the deformation zone model inferred for the access volume, based on the results reported from the single-hole hydraulic tests conducted during the site investigations for **SDM-Site** (Follin et al. 2007a) and the preparatory investigations in the access volume (Jönsson 2011).

Table 8-9. Compilation of transmissivity data on the deformation zones modelled for the access volume, see Table 5-2 and Figure 5-3C (RVS = Rock Visualisation System).

Deformation zone	Transmissivity (m^2/s)	Borehole	Borehole intercept (m borehole length)	Modelled borehole elevation in RVS (m RHB 70)	Note
ZFM1203*	1.1×10^{-4}	KFM07A	From 110 to 123	From −95 to −100	2
	Below LML**	KFM07B	From 93 to 102	From −74 to −78	1
	4.8×10^{-5}	KFM07C	From 92 to 103	From −91 to −96	2
	3.0×10^{-4}	HFM21	From 94 to 102	From −74 to −80	1
ZFMENE0159A	Below LML**	KFM07A	From 417 to 422	From −355 to −506	1
	1.1×10^{-7}	KFM08D	From 318 to 324	From −298 to −332	3
	1.2×10^{-7}	KFM09A	From 217 to 280	From −165 to −213	1
	3.6×10^{-6}	KFM09B	From 106 to 132	From −83 to −104	1
ZFMENE1061A	1.3×10^{-6}	KFM08A	From 244 to 315	From −205 to −262	1
	Below LML**	KFM08C	From 829 to 832	From −604 to −780	2
	Below LML**	KFM08C	From 946 to 949	From −604 to −780	2
	1.4×10^{-4}	KFM19	From 7 to 103	From −4 to −90	4
ZFMNNW2120	Below LML***	HFM22	From 110 to 129	From −86 to −99	1
	9.0×10^{-8}	KFM08D	From 184 to 210	From −150 to −165	3
	8.2×10^{-6}	KFM23	From22 to 35	From −11 to −69	4
ZFMNNW1205A	5.6×10^{-8}	KFM08B	From 167 to 185	From −139 to −154	1
	Below LML***	KFM13	From 37 to 49	From −28 to −34	4
	1.2×10^{-5}	KFM21	From 18 to 28	From −15 to −23	4
ZFMNNW1205B	1.2×10^{-9}	KFM08B	From 133 to 140	From −111 to −117	1
	Below LML***	KFM13	From 37 to 49	From −36 to −42	4
	9.6×10^{-6}	KFM21	From 86 to 95	From −79 to −86	4

* The intercepts with boreholes are based on the deformation zone model version 2.3 (Stephens and Simeonov 2015).

** Lower measurement limit = 8.4×10^{-10} m^2/s.

*** Lower measurement limit = 1.0×10^{-6} m^2/s.

1. Follin et al. 2007b, SKB R-07-48.

2. Follin et al. 2007b, SKB R-07-48; Reassessed in this document.

3. Follin et al. 2008, SKB R-08-23.

4. Jönsson 2011, SKBdoc 1321424.

8.5 Summary

The thickness of the uppermost fracture domain, FFM02, varies between 20 m and 60 m inside the access volume. The thinnest parts are found in the north-western part and the thickest towards south-east. The average Terzaghi corrected fracture frequency of open fractures in FFM02 is estimated to 4.85 m^{-1} based on data from KFM13–23.This information is coherent with the understanding resulting from the site investigation for **SDM-Site**.

The average total depth of short boreholes within the access volume is 164 m for the six boreholes drilled and investigated during the site investigation for **SDM-Site** and 84 m for the 14 boreholes drilled and investigated during the preparatory investigations 2011–2012. There is no correlation between the total borehole transmissivity and the total borehole depth below ground surface for these boreholes. The total borehole transmissivity in the uppermost 100–150 m of rock varies about three orders of magnitude, with most data centred on 1×10^{-4} m^2/s. The geometric mean of the total borehole transmissivity is approximately 5×10^{-5} m^2/s.

A preliminary analysis of the flowing fractures in borehole KFM24 suggests two dominant flowing fracture sets; one subhorizontal set and one NE striking steeply dipping set. This is coherent with the understanding of data acquired for **SDM-Site**. All flowing fractures identified with the PFL method in borehole KFM24 are situated in fracture domain FFM01 because the borehole has a steel casing down to ca −35 m elevation that made observations in FFM02 impossible.

The results from the difference flow logging with the Posiva Flow Log (PFL) in the 550 m long (ca 450 m deep) borehole KFM24 reveal 34 flowing fractures. The results from the difference flow logging of borehole KFM24 are compared with the results from corresponding measurements in nearby core-drilled boreholes investigated with the PFL method. As expected, the number and spatial distribution of flowing fractures observed in borehole KFM24 resemble the number and spatial distribution of flowing fractures observed in boreholes KFM01A, KFM01D, KFM08A and KFM08C. However, many of the flowing fractures in the latter two boreholes were interpreted to coincide with possible deformation zones (PDZ) in the single-hole interpretations of boreholes for **SDM-Site**. Apart from this observation the differences between borehole KFM24 and boreholes KFM01A, KFM01D, KFM08A and KFM08C appear minute. Noteworthy, the interval −184 to −194 m elevation contains five flowing fractures and is the most conductive interval of KFM24. The largest value (3.1×10^{-7} m^2/s) occurs at −184 m elevation and the second largest (1.6×10^{-7} m^2/s) occurs at −194 m elevation. The five fractures are gently dipping.

During the completion of the percussion-drilled part of borehole KFM24 the borehole was pumped in conjunction with reaming and cleaning activities. Hydraulic cross-hole interferences were observed in the uppermost ca 100 m of bedrock in the nearby boreholes KFM08A, KFM08B, KFM13, KFM14, KFM16, KFM17, KFM21, KFM22, KFM23 and HFM22 (cf Figure 3-3 and Figure 3-4). Likewise, hydraulic cross-hole interferences were observed in the nearby boreholes KFM08A–C during the difference flow logging of borehole KFM24 (the pumped borehole acted as a line sink). The maximum depths of responding monitoring intervals in KFM08A–C reach approximately −240 m elevation (cf Figure 3-5 and Figure 3-6). The results from the cross-hole observations during the difference flow logging are corroborated by conventional pumping tests between packers. Interpreted cross-hole transmissivities are low och moderate in magnitude, 5×10^{-8} to 5×10^{-7} m^2/s.

9 Hydrogeochemistry

9.1 Status of site understanding and models

Sections 2.2.3 and 2.3.13 describe the basic ideas and the conceptual understanding of the near-surface and bedrock hydrochemistry, respectively, as concluded at the completion of the site investigations for **SDM-Site** and **SDM-PSU**. Below, a somewhat more detailed outline of the groundwater hydrochemistry in the bedrock is presented. The data presented come from boreholes within or adjacent to the access volume, see Figure 9-1. There are no hydrochemical data representing surface water or groundwater in the regolith in this area.

A system to display the chemical characteristics of the groundwaters in a simplified way was introduced in Laaksoharju et al. (2008) and further developed in Nilsson et al. (2011).The samples were divided into water types based on the main origin of the water according to the paleo-climatic evolution of the site, see Section 2.3.13. The groundwater types that were defined for **SDM-Site** and **SDM-PSU** as well as the parameters used for the subdivision are summarised in Table 9-1. The brackish glacial groundwater type (important for the access volume) was not defined for the Forsmark site during the site investigation since only a few sampling locations showed this groundwater character and they appeared late in time during the investigations. However, a significant glacial component was frequently observed later in the SFR samples and therefore a special water type (Brackish-Glacial) was defined in **SDM-PSU** (Nilsson et al. 2011).

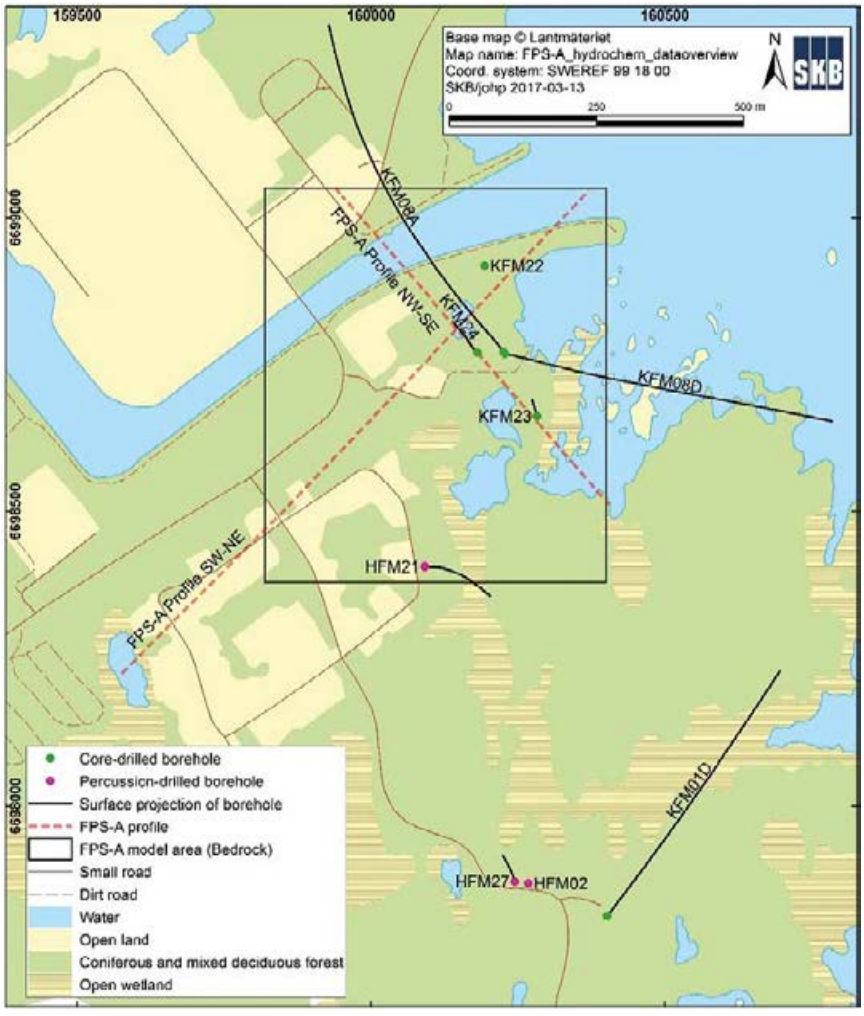

Figure 9-1. *Map showing the footprint of the access volume defined in Figure 3-1 together with investigated percussion-drilled and core-drilled boreholes within or adjacent to this volume. The NW-SE profile marked on the map is discussed in Figure 9-11.*

Taking all the available information together, it is obvious that intrusion of glacial meltwater has been very important for the groundwater evolution at Forsmark: 1) Glacial meltwater from the latest or earlier glaciations has intruded to great depth in the deformation zones (e.g. recognised in the KFM03A borehole at almost 1 000 m depth). Glacial meltwater has also intruded single fractures in the upper 500 m that are now less transmissive and have therefore preserved more of the glacial component compared with fractures of higher transmissivity at corresponding depth. 2) The fact that glacial water filled up the conductive fracture system facilitated the later intrusion of the Littorina Sea which characterises the transmissive larger deformation zones of the Forsmark and SFR areas down to 400 to 500 m depth.

This knowledge is crucial for the understanding of the groundwater hydrogeochemistry within the access volume. To describe these processes a somewhat modified water type configuration compared with **SDM-Site** is used in this chapter. The modified water type configuration is moderate and does not prohibit comparisons with the conclusions drawn in **SDM-Site**.

Table 9-1. Defined water types from the site investigations in Forsmark (PLU) and SFR (PSU) as well as a modified set of groundwater types used in this report. The colours and abbreviations presented in this table are used in the figures throughout this chapter, when applicable.

Groundwater types	Forsmark (SDM-Site)	SFR (SDM-PSU)	Preliminary modified set of types used in this report
Meteoric type (fresh) (Meteoric)	Cl ≤ 200 mg/L $\delta^{18}O$ = −12.3 to −11.2 ‰ V-SMOW	-	Cl ≤ 200 mg/L $\delta^{18}O$ = −12.3 to −11.2 ‰ V-SMOW
Local Baltic type	See brackish marine below	Cl = 2 500 to 3 500 mg/L $\delta^{18}O$ at −9 to −7.5 ‰ V-SMOW	Not used in this report
Littorina type	See brackish marine below	Cl = 3 500 to 6 000 mg/L $\delta^{18}O$ at −9.5 to −7.5 ‰ V-SMOW	Not used in this report
Mixed Brackish type (MxBrack)	Cl = 200 to 2 000 mg/L	-	Cl = 200 to 2 000 mg/L $\delta^{18}O$ > −13.0 ‰ V-SMOW
Brackish marine type (BrMarine)	Cl = 2 000 to 6 000 mg/L, Mg > 100 mg/L $\delta^{18}O$ at −11.5 to −8.6 ‰ V-SMOW	-	Cl = 2 000 to 6 500 mg/L, Mg >100 mg/L $\delta^{18}O$ at −13 to −7 ‰ V-SMOW
Brackish glacial type (BrGlacial)	-	Cl = 1 500 to 5 000 mg/L $\delta^{18}O$ < −12.0 ‰ V-SMOW	Cl = 1 500 to 8 500 mg/L $\delta^{18}O$ < −13.0 ‰ V-SMOW
Transition type (Transition)	Cl = 4 000 to 6 500 mg/L Mg = 25 to 100 mg/L	Cl = 2 500 to 6 000 mg/L $\delta^{18}O$ at −12.0 to −9.5 ‰ V-SMOW	Cl = 2 500 to 8 500 mg/L Mg = 25 to 100 mg/L $\delta^{18}O$ > −13.0 ‰ V-SMOW
Brackish non-marine type (BrNonMarine)	Cl = 4 000 to 10 000 mg/L Mg < 25 mg/L $\delta^{18}O$ at −16.0 to −10.5 ‰ V-SMOW	-	Cl = 4 000 to 8 500 mg/L Mg < 25 mg/L $\delta^{18}O$ at −13.0 to −10.5 ‰ V-SMOW
Deep saline groundwater type (DeepSaline)	Cl = 10 000 to 20 000 mg/L $\delta^{18}O$ at −13.8 to −12.9 ‰ V-SMOW	-	Cl = 8 500 to 20 000 mg/L $\delta^{18}O$ at −15 to −10.5 ‰ V-SMOW

The hydrogeochemical model representing the access volume is based on borehole information from only a few boreholes (cf Table 9-2). In this specific part of the SDM model, the upper bedrock (approximately 40 m) belongs to fracture domain FFM02 characterised by many water bearing fractures (cf Section 5.2.3 and Figure 8-4) and a generally high transmissivity resulting in a groundwater of mainly meteoric origin with some minor Littorina contribution. In contrast, fracture domain FFM01, located below FFM02, has a low fracture frequency with a small and successively decreasing number of minor deformation zones or rather single fractures down to about 300–400 m depth. In this depth range a minor and varying contribution of relict marine water from the Littorina stage seems to be present but to a much lesser extent than observed at similar depth in the major deformation zones (cf Figure 9-2). Further down (to −1 000 m elevation) within the lens, conductive fractures are generally very scarce or absent in most boreholes, and therefore there is a lack of hydrochemical data. However, increasing salinity and a gradually increasing brine signature is most probable.

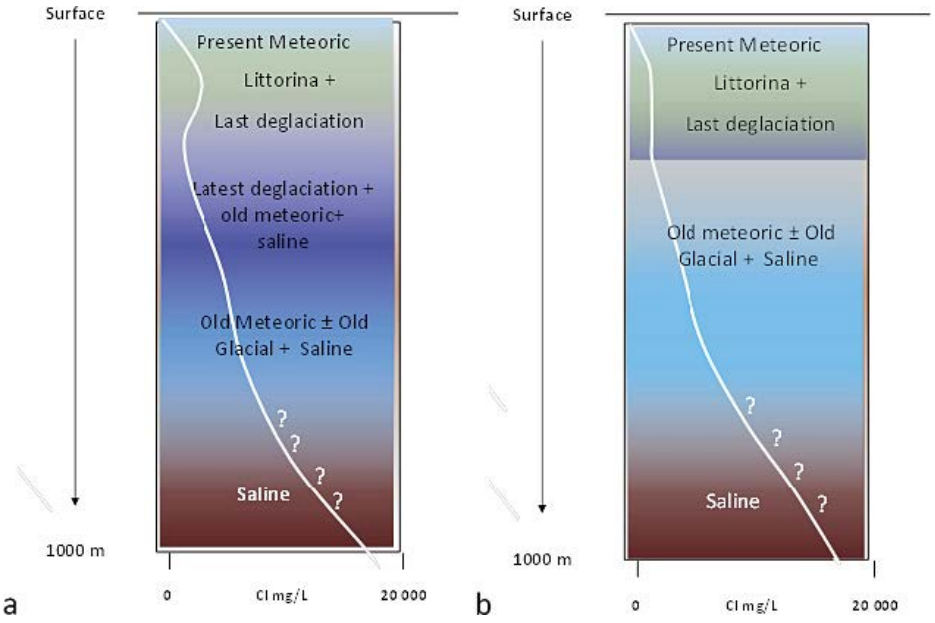

Figure 9-2. *Two alternative tentative sketches showing salinities and groundwater origins versus depth for the access volume in the present situation. The outlines are based on data from either one of the adjacent core drilled boreholes KFM08A a) and KFM01D b). In KFM01D waters of Littorina and glacial meltwater origin have not reached deeper than about –250 to –300 m elevation, probably due to lower transmissivity of the bedrock.*

9.2 Presentation of input data

9.2.1 Available data

Boreholes and borehole sections with groundwater data located within, or adjacent to, the access volume are listed in Table 9-2 and the locations of some of the borehole sections within, or very close to, the access volume are presented in Figure 9-3. Boreholes from earlier site investigations as well as the few new boreholes in Forsmark are included. It is mainly data from these sampling locations that will be used for the interpretations and modelling described in Section 9.3. However, additional information from SFR and the SFR-extension project (PSU) provides important supplementary input and additional knowledge and will also be considered. The brackish glacial groundwater type, which is quite frequently observed in samples from the SFR site, is present in for example the new borehole KFM24 and in borehole KFM08A close to KFM24. KFM08A was drilled and investigated during the site investigation for **SDM-Site**.

The ongoing monitoring programme in the percussion-drilled and the core-drilled boreholes has continued to produce hydrochemical data also after the completion of the site investigations for **SDM-Site** in 2007. Furthermore, extensive investigations (Complete Chemical Characterisation, CCC) have been performed in KFM08D in 2013 and in KFM01D in 2015. This means that sections in these two boreholes sampled during the site investigation have been resampled six and nine years after the first sampling, respectively. The new boreholes contribute with CCC data from borehole KFM24 drilled in the planned shaft position (cf Figure 9-3) and matrix porewater data from boreholes KFM22 and KFM23. These late data have not been evaluated before (quality categorisation/water type classification), see Sections 9.2.2 and 9.5 for explanation and discussion. The interpretations and discussions in this report consider basic water composition data, isotopes, and gases and give some comparisons of matrix porewater and fracture groundwater data.

Table 9-2. Boreholes and borehole sections with hydrochemical data, located inside or close to the access volume. Secup and Seclow = metres of borehole length (mbl) to the top and bottom of each packer section, Secmid = elevation at the mid-point of each section, ZFMxxxx/FFMxx = intersected zones or relevant fracture domains and available data, PDZ = possible deformation zone (water composition/isotopes, gas, matrix porewater).

Borehole	Secup (mbl)	Seclow (mbl)	Secmid (m elevation)	ZFMxxxx or FFMxx	Water composition + isotopes	Gas	Matrix pore-water
Boreholes drilled during the site investigation for SDM-Site							
HFM02*	38	48	−40	ZFM1203	Y		
HFM21	22	32	−19	FFM02	Y		
HFM27*	46	58	−46	ZFM1203	Y		
KFM01D*	194	195	−156	FFM01	Y		Y**
KFM01D*	314	320	−256	FFM01	Y	Y	Y**
KFM01D*	428	436	−342	FFM01	Y	Y	Y**
KFM01D*	568	575	−447	FFM01	Y	Y	Y**
KFM07A	Borehole included in Table 3-2, all chemical data acquired below −500 m elevation						
KFM08A	265	280	−228	ZFMENE1061A	Y	Y	
KFM08A	684	694	−551	PDZ	Y	Y	
KFM08D	660	680	−538	FFM06	Y	Y	
KFM08D	825	835	−662	FFM06	Y		
KFM09A	Borehole included in Table 3-2, all chemical data acquired below −500 m elevation						
New boreholes drilled and investigated after the site investigation for SDM-Site							
KFM22*	-	-	-	FFM02			Y**
KFM23*	-	-	-	FFM02			Y**
KFM24	191.5	198.6	−192.7	FFM01/ZFM1203	Y	Y	
KFM24	399.5	402.6	−397.1	FFM01	Y	Y	
KFM24	410.0	417.12	−409.5	FFM01	Y	Y	

* This borehole is not included in Table 3-2 but supplies useful hydrochemical data for the understanding of the access volume, see Figure 9-1.
** Several rock core samples are collected along the borehole and each one of them is rather short (15–20 cm).

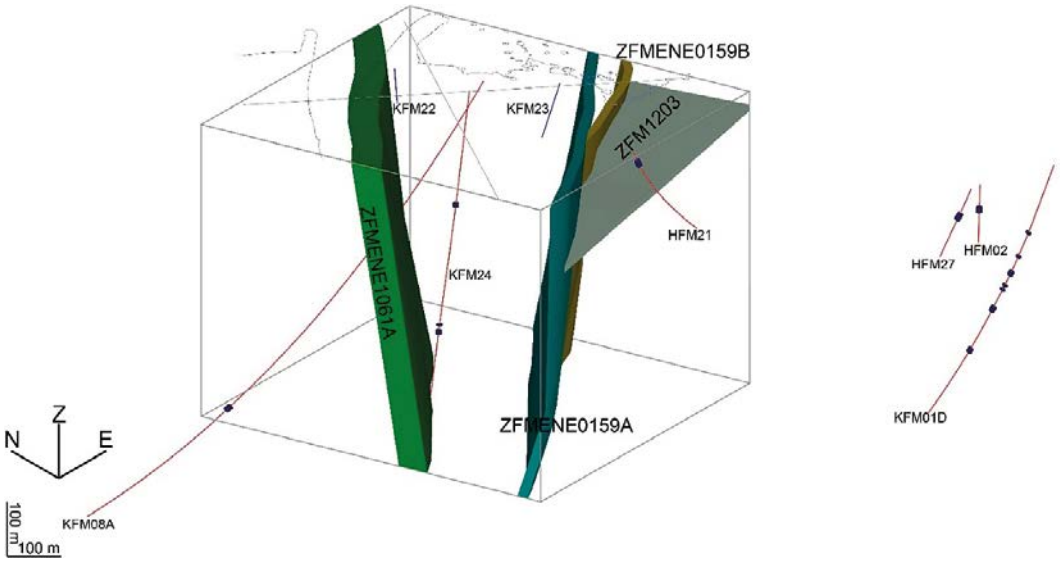

Figure 9-3. *3D visualisation of the access volume with deformation zones as interpreted in SDM-Site and boreholes with sampled borehole sections. Boreholes KFM22 and KFM23 (in blue) have matrix porewater data but no data for fracture groundwater. The shallow section of borehole KFM08A is located within the deformation zone ZFMENE1061A and does not show up in the figure.*

9.2.2 Quality categories

Groundwater samples collected before 2007 and used for **SDM-Site** are quality categorised according to categories 1 to 5, were 5 is allocated to samples of insufficient quality (Nilsson et al. 2011). The samples after 2007, however, have not been evaluated and lack quality categories so far. In the present report new and old data are generally used together with the only distinction that hydrochemical logging data (tube sampling, Tullborg et al. 2010) and high pH samples (> pH 9) are rejected (Nilsson and Sandberg 2017).

None of the sample series from the three borehole sections of KFM24 show completely stable water composition. An evaluation of the quality would therefore result in a lower but still acceptable quality for these new data. Pumping and sampling at low transmissivity such as in the section at −410 m elevation and to some extent also in the section at −399 m elevation result in a large pressure drawdown. The high stress on the packers may cause leakage between packer and borehole wall and the collected samples may consist of water from the borehole above or below the borehole section to be sampled. This may be an explanation to the trend in the sample series from −410 m towards the same groundwater compositions as at −397 m (cf Section 9.5.1). In addition, pumping of groundwater from a low transmissive bedrock may cause transport of water from long distances and the composition may change also because of that.

9.3 Evaluation and modelling

9.3.1 General evaluation and modelling strategy

The limited model scale and the few relevant data for the bedrock volume in question do not allow for an extensive and complete evaluation and modelling work according to previous SDM standard from the site investigation in Forsmark (Smellie et al. 2002). The focus in this report is to check if new data and findings after 2007 change the understanding of the groundwater conditions in this specific area. So-called explorative analyses constitute the initial and most comprehensive work and implies manual (x–y plots) and statistical evaluation of the dataset to understand and describe the data and the distribution of different hydrogeochemical properties in the bedrock volume.

The data from sampling locations relevant for the access volume, with or without quality categorisation (see Section 9.2.2) are compared and put into context of data from the entire Forsmark site considering water type and residence times, depth variations and distributions. Hydrogeological properties are important to explain residence times and water type distribution. The hydrogeochemistry within the access volume is discussed in relation to geological and/or hydrogeological structures and properties.

9.3.2 Groundwater composition and stable isotopes inside the access volume

The characteristics of the groundwater samples representing the bedrock within and close to the access volume are visualised together with all available data in two multivariate PCA-models and a number of x/y-plots. *The Ion Source Model* PCA-plot shows the relative contribution of different sources of dissolved ions to the water composition, similar to a Piper plot (Figure 9-4). *The Mixing Model* PCA-plot, on the other hand, reveals concentration gradients as well as deep saline, marine and glacial influences (Figure 9-6). Both PCA-models are based on the same dataset that includes all Forsmark and SFR data points. Average groundwater compositions are used for each sampling location. It should be noted that objects located close to each other in the plots show similarities regarding the chemical composition, which could be an indication of similar genesis, but not necessarily hydrological or structural connectivity.

The three sections of KFM24 (at −193, −397 and −410 m elevation) show marine and brine signatures according to the position on the marine-brine mixing line in Figure 9-4. The upper section at 193 metres depth shows both some marine influences and brine ion signatures similar to SFR (e.g. KFR02, 03, 13, 101, 105 at ca 150–240 metres depth) and the inland parts of Forsmark (e.g. KFM01D, 04A, 06C, 08A and –10A at ca 200–400 metres depth). The two deeper sections of KFM24 (397 and 410 metres depth, respectively) show very similar composition dominated by brine ion signatures comparable to adjacent boreholes at ca 500–600 metres depth (KFM06A, 08A, 08C, 08D, 11A), and KFM01D at 446 metres depth. The groundwater of the very shallow bedrock represented by HFM21 at 19 m, HFM02 at 40 m and HFM27 at 46 m show a mixed meteoric and marine origin (mixed brackish), which could be expected, since the fracture domain FFM02 is highly transmissive. All these shallow data points follow a mixing line between meteoric surface waters and towards the marine dominated part of the marine-brine mixing line.

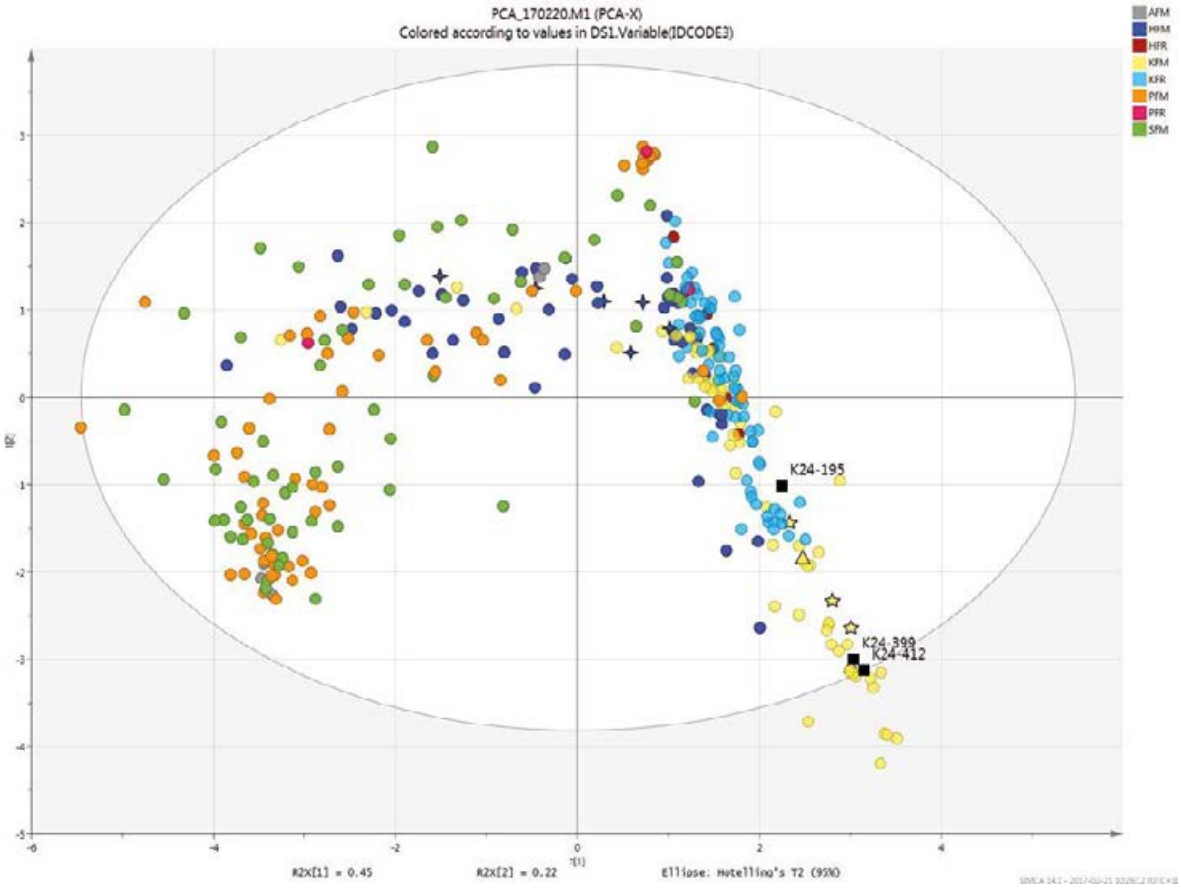

Figure 9-4. *Ion Source Model showing the main origins of the dissolved ions. The PCA-plot displays the relative distribution between cations (Na, K, Ca, Mg, Sr, Li) and anions (Cl, SO_4, HCO_3, Br, F), comparable to a so-called Piper plot. The model includes all hydrochemical data from Forsmark and SFR in Sicada and the data points represent the average value per object (id code and section). Data for KFM24 are marked by filled squares, whereas selected adjacent boreholes are marked by triangles (KFM08A), five armed stars (KFM01D) and four armed stars (HFM02, HFM21 and HFM27). The main panel shows scores for the two first principal components that comprise 67 % of the total variation. The inset panel show loadings for the same components. Three major ion sources could be identified: ions of brine origin, marine ions and ions originating from weathering of minerals, e.g. calcite in the regolith.*

The chloride distributions versus depth and magnesium to chloride ratios presented in x–y scatter plots in Figure 9-5a and b are other means to present the trends in salinity and marine–non-marine origins. The magnesium and also the sulphate concentrations in the deeper sections of KFM24 are unusually low (among the lowest measured in Forsmark) even for non-marine groundwaters. The different contributions from glacial meltwater to the samples cannot be elucidated from Figure 9-4, because glacial meltwater contributes to dilution rather than adding specific ions to the groundwater composition. However, the x–y plots including $\delta^{18}O$ (‰ V-SMOW) versus depth and versus chloride in Figure 9-5c and d reveal a clear glacial component (low values at ca −13‰ V-SMOW, or lower) in the three sampled sections of borehole KFM24 and this signature is most pronounced in the shallow section. The brackish-glacial signatures in the samples from the different sections of borehole KFM24 clearly resemble the two corresponding sections of borehole KFM08A rather than the groundwater of borehole KFM01D with its minor glacial imprints. The similarity with some of the boreholes in the SFR project is also evident.

Another observation regarding the groundwater in borehole KFM24 is the generally very high DOC concentrations for this depth range compared to most other boreholes. In this case, it is a condition in common with some sections of borehole KFM01D, see Figure 9-5e. This type of anomaly is still not fully understood. It will be an issue addressed in a coming data report, which will contain a more complete evaluation of organic contents and nitrogen compounds. Besides the high DOC concentration also the high $\delta^{34}S$ (‰ CDT) in sulphate show close resemblance to the ratios in groundwater sampled in KFM01D, see Figure 9-5f. This indicates/verifies sulphate reducing activity under closed system conditions. Taken together, the trends in sulphide, sulphate and $\delta^{34}S$ as well as DOC, in especially the deep section of KFM24, indicate sulphate reduction that decreases in the time series along with the trend in the overall water composition in the five samples.

In the Mixing Model, Figure 9-6, the upper section of KFM24 at 193 m depth plot in the area of the PCA characterised by cold temperature recharge, thus indicating significant glacial influence similar to Figure 9-5. According to the Ion Source Model, shallow groundwater ion signatures are absent in this upper section, and the rather dilute water could therefore most likely be explained by glacial dilution of groundwater of mainly brine origin, which shifts the observations to the left in the direction of the arrow. In contrast, the shallow percussion boreholes plot either close to fresh surface waters (HFM02 and HFM21) to the left or close to the marine signatures (HFM27) in the upper part of the plot, implying mainly meteoric origin or more of Littorina influences, respectively. The two deeper sections at 397 and 410 m show almost identical concentrations and significantly higher TDS (Total Dissolved Solids) than the shallow section. The rather low $\delta^{18}O$-signature in combination with a possible horizontal shift to the left of the brine mixing line for both observations implicate a significant glacial imprint also at this depth in KFM24.

Most groundwater observations in the bedrock from core drilled boreholes (KFM and KFR) plot along the marine-brine mixing line in Figure 9-4, implicating that the main ionic composition of these groundwaters could be explained by these two sources. Groundwater in the upper parts of the bedrock, often represented by percussion drilled boreholes (HFM and HFR), either show the same ion signatures as the core drilled boreholes, or signatures more like surface water and shallow groundwater in the regolith (PFM and SFM).

Observations of fresh surface water usually plot along the mixing line A, representing a gradual marine influence downstream the watersheds. It could also be concluded that examples of mixing between the deep groundwater and surface water are scarce among the sampled objects. From this plot, it is also evident that groundwater observations from SFR generally differ from groundwater observations inland when the apparent mixing lines B and C are compared. The deviating pattern for SFR reflects the stronger influence from (modern) marine ions, caused by drawdown due to the tunnel system of the SFR facility.

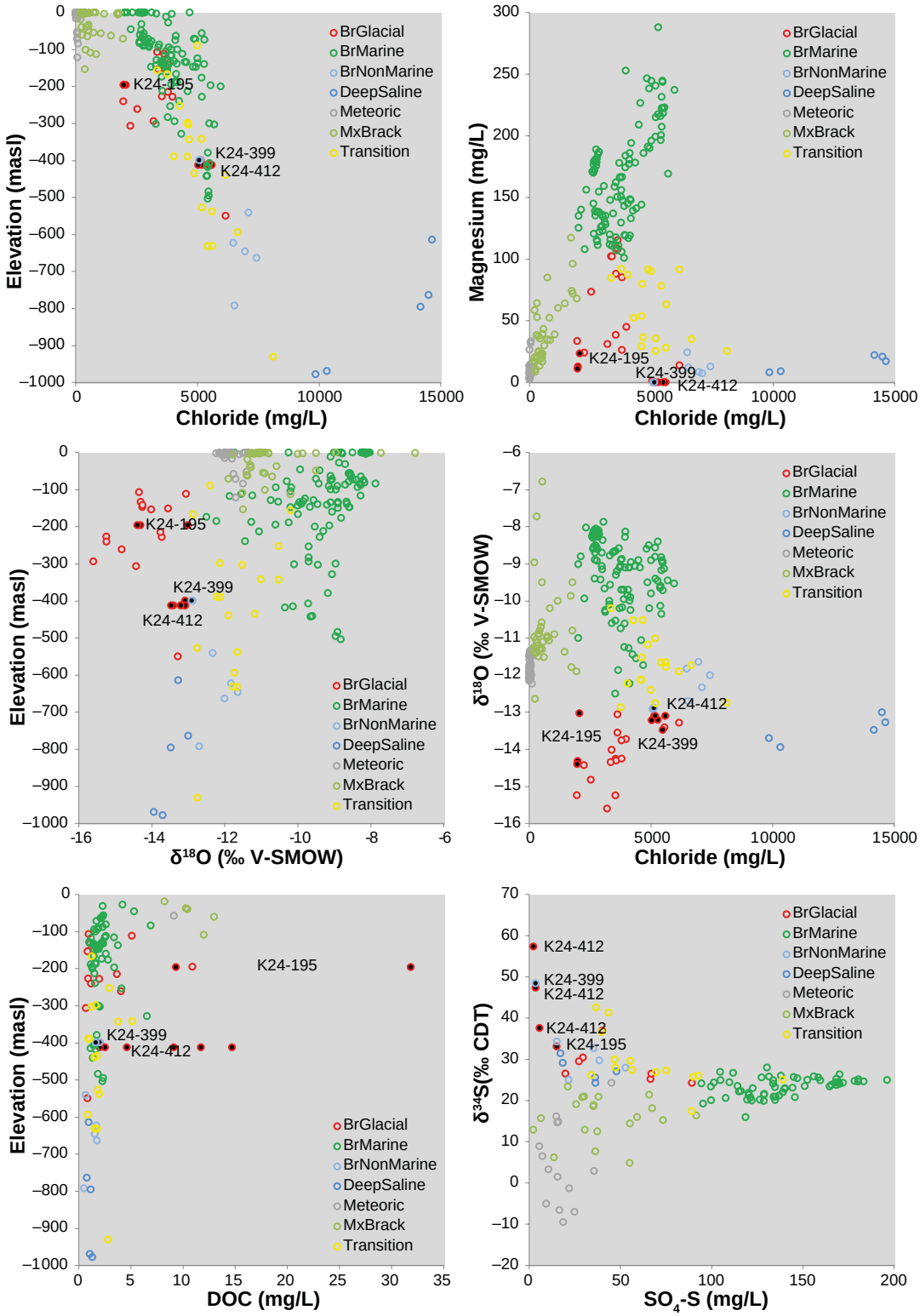

Figure 9-5. *a) Chloride versus elevation, b) Magnesium versus chloride, c) $\delta^{18}O$ (‰ V-SMOW) versus elevation, d) $\delta^{18}O$ (‰ V-SMOW) versus chloride, e) Dissolved Organic Carbon (DOC) versus elevation and f) SO_4^{2-} versus $\delta^{34}S$ (‰ CDT). The diagrams include all hydrochemical data from Forsmark and SFR in Sicada and the data points represent the average value per object (id code and section) except for KFM24 (all samples, filled with black); cf Table 9-1 for explanation of water types.*

The Mixing Model – PCA plot shown in Figure 9-6 is a complement to the Ion Source Model and reveals concentration gradients and mixing of different water types. This model is based on exactly the same data as the Ion Source Model (Figure 9-4) with the addition of $\delta^{18}O$ projected onto the model in order to display isotope signatures of the water. From this plot, little could be said about the surface water cluster other than it is characterised by low ion strength and low density.

The isotopic $\delta^{18}O$ signature projected onto the Mixing Model adds information of the origin of the water. High values (less negative) could be interpreted as warm climate meteoric signatures or evaporative signatures of lake and sea water. Low values (more negative) on the other hand reflect cold climate meteoric input, for example glacial water signatures. It is worth mentioning that low $\delta^{18}O$ signatures are also found for the observations that plot in the lowest part of the mixing line towards a strong brine signature. This implies that glacial meltwater may penetrate to such depth (around −1 000 m elevation). However, the sampling locations at depth are very few and represent deformation zones rather than low transmissive bedrock. Therefore, it is probably not a general truth that all deep groundwater is affected by glacial meltwater.

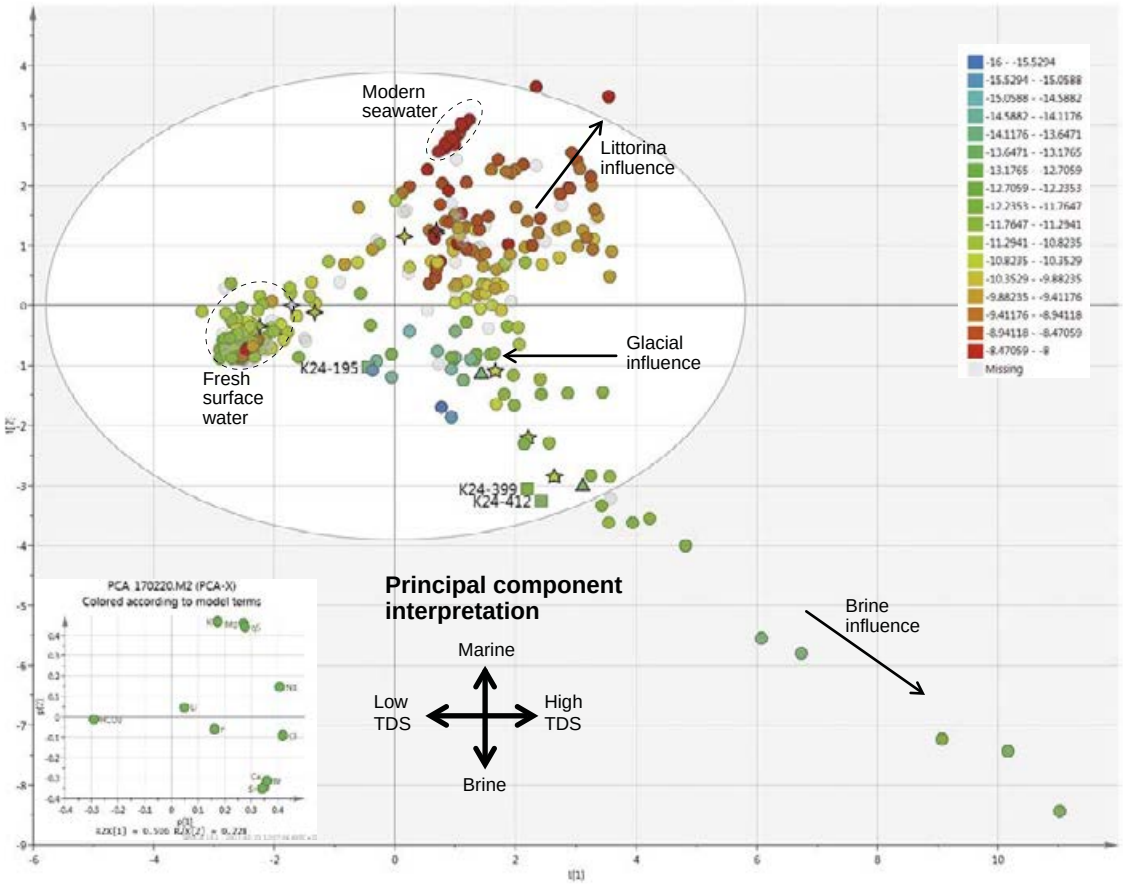

Figure 9-6. *The Mixing Model. The PCA-plot is based on concentrations of the major groundwater constituents (Na, K, Ca, Mg, Sr, Li, Cl, SO_4, HCO_3, Br, F). The model includes all hydrochemical data from Forsmark and SFR in Sicada and the data points represent the average value per object (id-code and section). Data for KFM24 are marked by filled squares, whereas selected adjacent boreholes are marked by triangles (KFM08A), five armed stars (KFM01D) and crosses (HFM02, HFM21 and HFM27). The main panel shows scores for the two first principal components that comprise 73 % of the total variation. The inset panel show loadings for the same components. The horizontal component could be interpreted as the total solid content or the density, whereas the vertical component discriminates between marine and brine influences.*

9.3.3 Dissolved gases, ^{36}Cl and residence times of groundwater in KFM24

Gas data from KFM24 are available from the two deepest sections in the borehole (−397.1 and −409.5 m elevation). Duplicate samples from −409.5 m were sent to different laboratories and therefore three analyses are presented. These results are interpreted together with the previous gas dataset from Forsmark and SFR (34 analyses). A thorough evaluation of the entire dataset is part of the data evaluation report that currently (2019) is under production. Here only helium and carbon dioxide/methane data are commented upon.

Helium is present in various amounts in the samples, ranging from 3 to 47 mL/L for the entire data set. The large variation is due to production of ^{4}He in the bedrock as a result of decay in the radioactive decay series of U and Th. Assuming all other parameters are equal, the longer the residence time in the bedrock the higher the helium content. Figure 9-7a shows helium plotted versus elevation. The trend is a general increase with depth, however, separating the different groundwater types gives an even better subdivision. The Saline to Brackish non-marine waters show the highest helium contents (oldest) and the Brackish marine waters show the lowest contents (youngest) in good agreement with the general understanding of the groundwater evolution of the area. No fresh groundwaters have been sampled and analysed for He. KFM24 −397.1 and −409.5 m elevation which are Brackish-glacial in type have contents from 9.5 to 13.1 mL/L helium, which are lower than the Brackish to Saline non-marine groundwaters but higher than the Brackish marine (Baltic Sea and Littorina) groundwaters.

Carbon dioxide generally shows a correlation with the bicarbonate content in the groundwater and CO_2-values are therefore higher in the Brackish-marine waters. All samples taken together, the measured CO_2 concentrations range from 0.02 to 4.6 mL/L in all samples. In KFM24, which is low in bicarbonate, the CO_2 values are also in the lower end showing values between 0.02 and 0.08 mL/L. Methane contents are below 1 mL/L in all samples except KFM01D: −446 m which has values of 4.6 to 4.8 mL/L (sampled the years 2006 and 2015). Figure 9-7b shows the CO_2/CH_4 ratio versus elevation. The brackish to saline non-marine waters generally show the lowest CO_2/CH_4 ratios, all of them below 3, whereas the Brackish marine waters have ratios higher than 8. The KFM24 samples have ratios between 0.1 and 0.4 that is, higher CH_4 than CO_2.

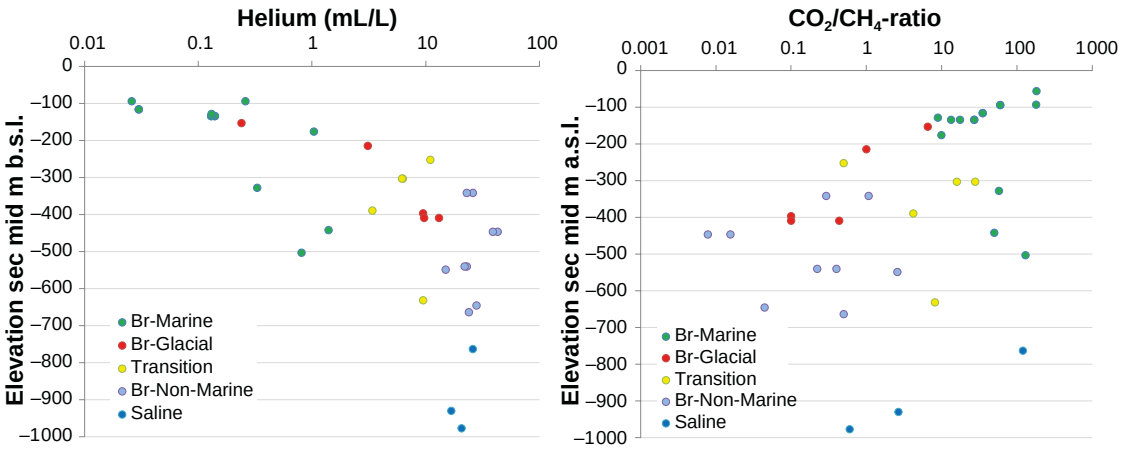

Figure 9-7. *a) Helium versus depth (left), b) CO_2/CH_4 ratio versus depth. The data from borehole KFM24 are encircled in red. The different groundwater types are indicated with a colour code.*

Chlorine-36 is produced in the atmosphere by two different spallation reactions: $^{40}Ar + p \rightarrow {}^{36}Cl + n + a$ and $^{36}Ar + n \rightarrow {}^{36}Cl + p$. The ^{36}C isotope enters the bedrock groundwater by recharge, where it decays to ^{36}S and ^{36}Ar through β-decay. The half-life is in the order of 300 000 years making this system suitable for detecting long residence times of the groundwaters. However, in contrast to tritium and ^{14}C, the subsurface production of ^{36}Cl in crystalline bedrock is not insignificant. A modelled equilibrium for the subsurface production can be calculated based on bedrock composition (mainly U and Th contents) together with porosity. Time scales exceeding 1.5 Ma are assumed to approach equilibria with the bedrock.

However, as an alternative one needs to consider the possibility that mixing of different waters have produced these values and therefore an independent parameter like helium is very useful for the interpretation of the residence times. For the Forsmark groundwater the present dataset with both helium and ^{36}Cl from the same section is limited and therefore only the ^{36}Cl versus Cl-content is shown here (Figure 9-8). The low marine contribution in KFM24 is supported by the ^{36}Cl data, which plot above the bedrock equilibrium line clearly separated from the brackish marine samples. For the sample from −403 m, the helium content of 9.7 to 13.1 mL/L is in line with a considerable residence time for the deeper sample although not as long as for e.g. the non-marine waters in KFM01D or KFM07A. No helium value is available for the upper sample at −193 m.

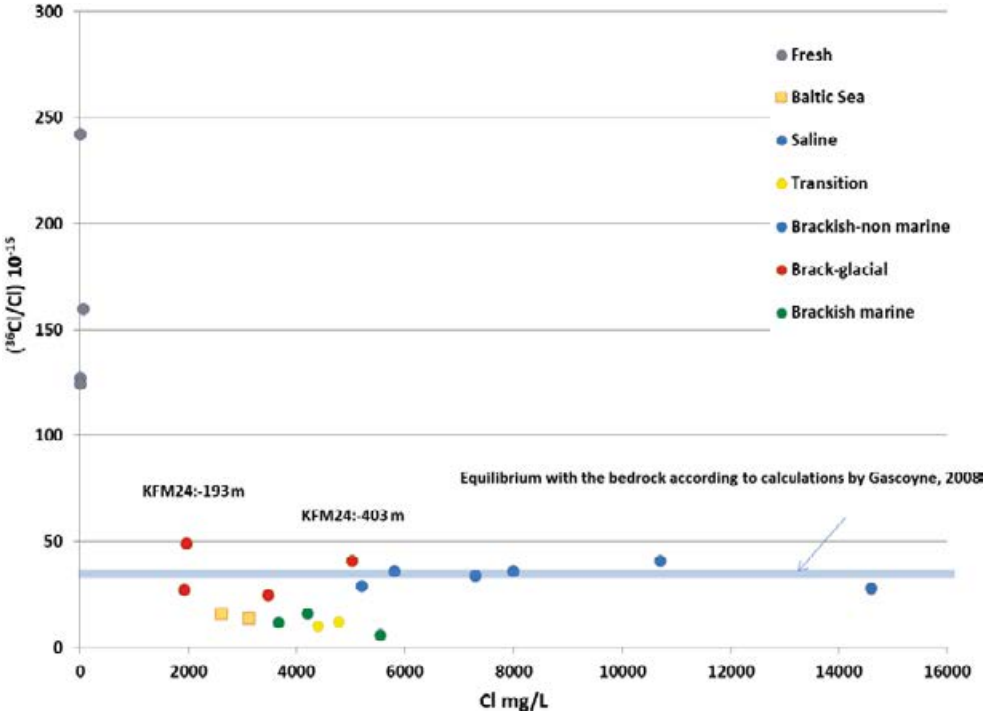

Figure 9-8. *($^{36}Cl/Cl$) 10^{-15} plotted versus Cl content for all samples from Forsmark and SFR.*

9.3.4 Interpretation of matrix porewater data in the access volume

Matrix porewater data are available from the two shallow boreholes KFM22 and KFM23 within the access volume. The porewater composition could be seen as a memory of previous groundwater regimes more or less overprinted by later groundwater regimes, for example recharging glacial melt water or Littorina sea water. Porewater Cl concentrations are generally lower than the groundwater concentrations at similar depths below −100 m elevation (Figure 9-9a). The variation in $\delta^{18}O$ is larger in porewater than groundwater (Figure 9-9b), especially in the upper range where there are no corresponding groundwater signatures (−7 to −2 ‰ V-SMOW).

When matrix porewater data are projected onto the Ion Source Model that describes the groundwater ion composition in the fracture zones, some similarities in ion composition are revealed (Figure 9-10). The uncertainties are very large for most of the components in the porewater experimental solutions (Waber et al. 2009). However, the representation still fits reasonable well with what could be expected (the unrealistically high *in-situ* concentrations of HCO_3 and F had to be changed to constant values of 150 mg/L and 1.5 mg/L, respectively, which only affects the distribution in the horizontal direction in the model). Data for $\delta^{18}O$, which reflect the water origin, is furthermore projected onto the Ion Source model as colours together with Cl concentrations as the size of the circles. $\delta^{18}O$ shows large variation along the brine-marine signature gradient. The main reason for the varying isotope signatures among otherwise similar ion signatures is the varying distances between the water bearing fracture and the porewater sample, which is the main factor controlling equilibrium concentrations due to diffusion.

The shallow porewater of KFM22 and KFM23 plots with the shallow fracture groundwater in the upper part of the mixing line between the marine and the brine signatures (in the marked cluster). This indicates that these porewaters are influenced by the Littorina intrusion. Fracture domain FFM02 in the upper bedrock is characterised by a high fracture frequency and high hydraulic transmissivity which favours equilibrium conditions and thereby similar water composition is expected in the porewater and the fracture groundwater, which is mainly of the marine type. A thorough evaluation of matrix porewater data will be an issue in the coming data evaluation report treating among others all Forsmark porewater data.

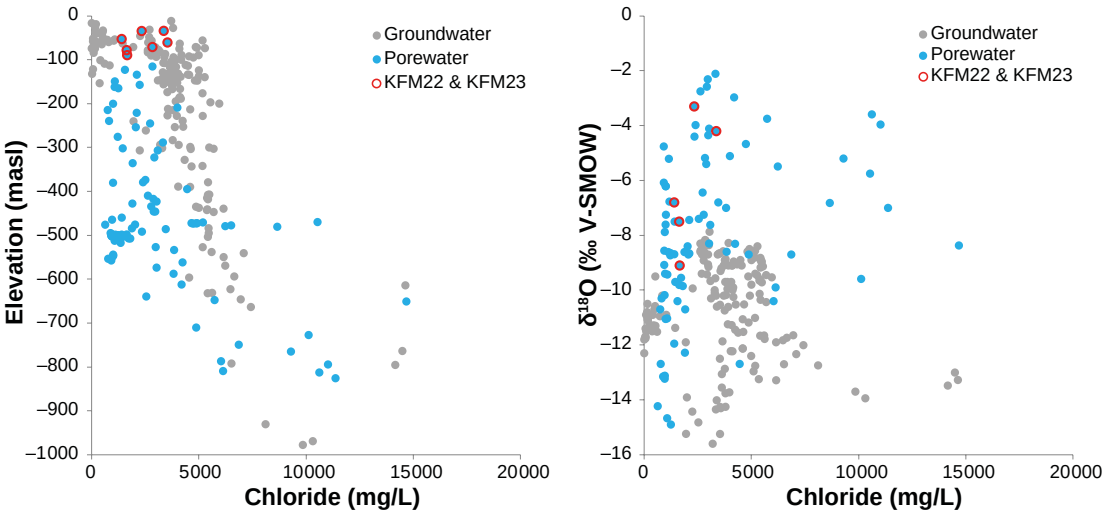

Figure 9-9. *a) Chloride versus elevation, b) $\delta^{18}O$ (‰ V-SMOW) versus chloride. Blue coloured dots represent porewater whereas grey dots represent the groundwater composition. The encircled area marks data from KFM22 and KFM23.*

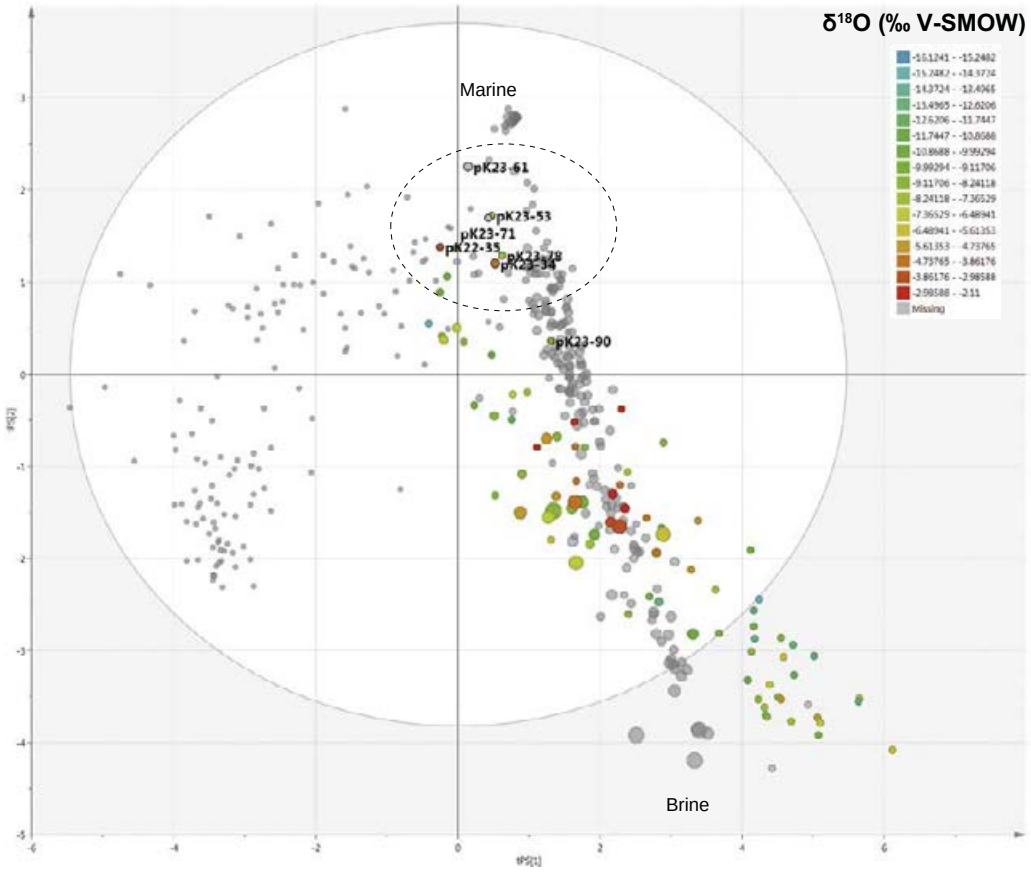

Figure 9-10. *Porewater data projected onto the Ion Source Model (cf Figure 9-4 for an explanation and interpretation of the Ion Source Model). Coloured dots represent porewater ion composition whereas grey dots represent the groundwater composition. The colour code shows the $\delta^{18}O$ isotope signature in each porewater sample. The size of the dot represents the Cl concentrations from low (small dot) to high concentrations. The encircled area marks the cluster that mainly contains data from KFM22 and KFM23.*

9.3.5 Prediction of surface water characteristics inside the access volume

Since there are no available surface water data from the access volume, no direct observations could be evaluated to describe surface water characteristics in the small ponds and shallow groundwater within the area close to the access facilities. Surface water characteristics in the Forsmark area are mainly governed by the specific conditions at the site, for example soil characteristics and the location in the landscape, and therefore data from similar surface water objects are used to predict the surface water characteristics inside the access volume.

The sea water sampling point in Asphällsfjärden (PFM0062) is representative for sea water close to the shoreline inside the access volume due to the inwards cooling water stream for the nuclear power plants. The small ponds adjacent to the shoreline are most probably similar to either the reference ponds (located higher in the landscape) or the artificial ponds (located lower in the landscape). Shallow groundwater inside the access volume is most probably similar to groundwater in monitoring wells located at recharge locations in the landscape (SFM0002, -05, -06, -08, -19, -56, -57, -59, -60, -61, cf classification in Werner et al. 2007). The ranges and mean values in the statistical compilation in Table 9-3 are probably representative for surface waters inside the access volume.

9.4 Resulting model

This section outlines the hydrogeochemical conditions inside the access volume according to present understanding. When new data and understanding after 2007 from early and new boreholes as well as from the SFR PSU modelling have been evaluated, the general description from Laaksoharju et al. (2008) remains unchallenged. However, as new data in the target volume are available, the presence of groundwater with clear glacial components at different locations in this rock volume has become more evident. The development of the groundwater in the upper section of KFM08A towards more of glacial contribution and the composition of the groundwater in the three sections of the new borehole KFM24 show that the glacial component is important in the groundwater evolution at the depth range around −200 to at least −500 m elevation inside the access volume. Furthermore, it may be a more frequently occurring component in the groundwater than what was outlined in the site investigations for **SDM-Site**.

Figure 9-11 shows a conceptual model outlining the sequence of different groundwaters along a cut plane (cf the NW-SE profile in Figure 9-1) through the access volume. The first 30–40 metres from the ground surface and downwards contain a groundwater mixture dominated by meteoric water including an increasing amount of a Littorina component with depth as indicated by data from borehole HFM21. The next depth range between −40 to −193 m elevation shows a decreasing meteoric/Littorina signature and increasing glacial and brine (non-marine) influences arriving at the composition in borehole KFM24 at −193 m elevation. Further down, the salinity increases with depth while the glacial signature decreases and possible minor remaining meteoric/Littorina contributions more or less disappear, resulting in compositions like the ones in borehole KFM24 at −397 m and −410 m elevation. It is likely that the successive salinity increase continues to the depth limit of the access volume arriving at a similar composition as in borehole KFM08A at −550 m elevation.

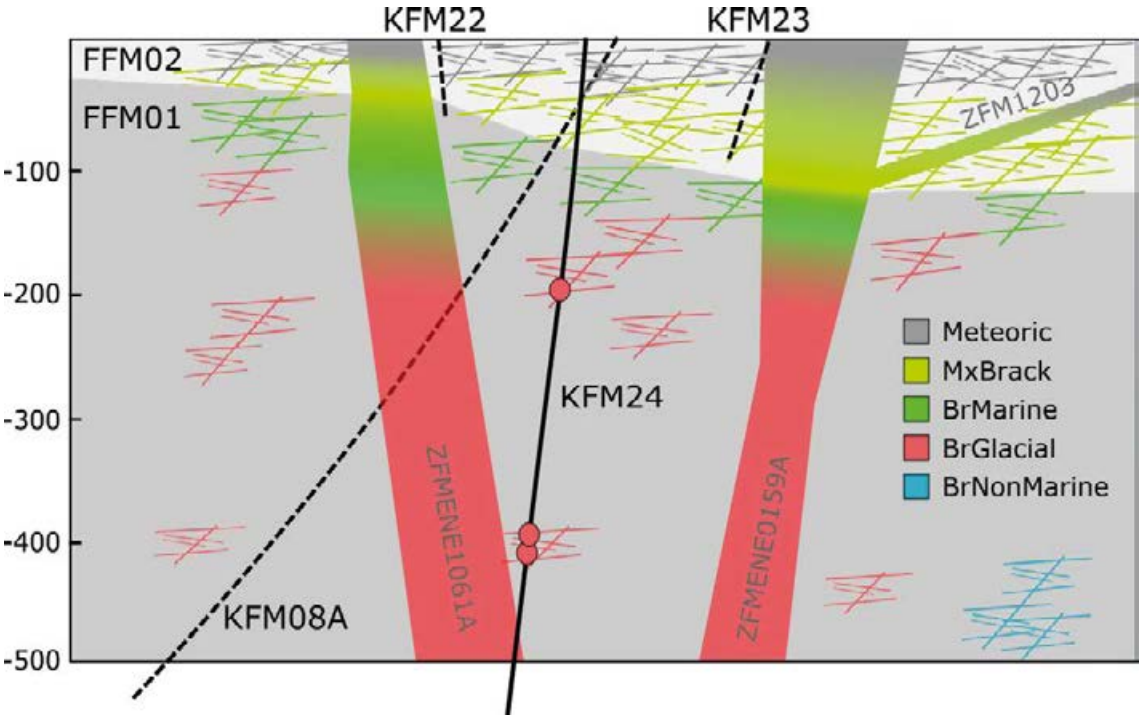

Figure 9-11. *Generalised cross section toward NE corresponding to "FPS-A profile NW-SE" in Figure 3-1. Hydrogeochemical sampling sections in borehole KFM24 at –193, –197, and –410 m elevation are marked by circles. Other boreholes projected onto the cross section are marked as dashed lines. Fracture domains FFM01 and FFM02 are marked as grey shades in the background. The colour marks the probable water type distribution within the fracture zones and the fractures at different depths as well as the water types in the sampled sections in borehole KFM24.*

Several observations from the groundwater collected in borehole KFM24 support the outline above and the interpreted long residence times especially in the sections at −397 and −410 m elevation:

- The very low concentrations of Mg and SO_4 indicate that there is hardly any marine contribution to the groundwater of the two deeper borehole sections. This together with the preserved glacial meltwater signatures in these groundwaters (KFM24: −397 and −410 m elevation) indicate very low groundwater fluxes.
- The relatively high He content is in line with pre-Holocene residence time for the two lowest sections. The low CO_2/CH_4 ratio is more indicative of the water type where the brackish glacial and especially the brackish non-marine water types are low in dissolved CO_2.
- The ^{36}Cl values (cf Section 9.3.3) support a low marine contribution to the groundwaters. Furthermore, ^{36}Cl in combination with the He concentration indicate a quite long residence time for the groundwater in the deepest section and very limited contribution, if any, of the Holocene water.
- High DOC, $\delta^{34}S$ in SO_4 and relatively high sulphate concentrations together with low SO_4 in the upper and the lower section indicate sulphate reduction at nearly closed conditions.
- The borehole section at −193 m elevation shows Mg, SO_4 and CO_2 concentration values which indicate some presence of marine components although the glacial component is very evident.

Table 9-3. Statistical compilation for sea water (2002–2014), natural small ponds (2008–2014), artificial ponds (2012–2014) and a selection of groundwater monitoring wells at recharge positions in the landscape (2002–2005). These data are not from the access area only.

		Conductivity mS/m	Sodium (Na) mg/L	Potassium (K) mg/L	Calcium (Ca) mg/L	Magnesium (Mg) mg/L	Bicarbonate (HCO_3) mg/L	Chloride (Cl) mg/L	Sulphate (SO_4) mg/L	Bromide (Br) mg/L	Silicon (Si) mg/L	Strontium (Sr) mg/L	Deuterium (δ^2H) ‰ dev SMOW	Oxygen-18 ($\delta^{18}O$) ‰ dev SMOW	Tritium (^3H) TU
Sea water	count	109	116	116	116	116	115	116	115	114	116	116	49	49	49
PFM0062	min	793	1280	48	64	157	63	2210	328	7	< 0.2	0.9	−85	−12	7
	mean	887	1477	57	75	179	77	2737	388	9	0.5	1.1	−63	−8	11
	max	959	1640	67	86	200	85	2981	494	16	1.3	1.3	−43	−5	16
	stddev	27	65	4	4	8	3	108	22	1	0.2	0.1	5	1	2
	CV (%)	3	4	6	5	4	4	4	6	12	48	7	−8	−10	21
Natural ponds	count	79	79	79	79	79	77	78	79	79	79	79			
PFM007442	min	17	2.2	0.5	28	1.9	77	2.1	0.3	< 0.2	1.0	0.04			
PFM007443	mean	30	4.5	1.8	56	3.3	166	6.7	6.3	0.1	5.2	0.07			
	max	70	11	4.8	151	5.8	432	21	31	0.4	16	0.13			
	stddev	9	1.4	0.7	20	0.8	63	3.6	7.5	0.03	2.7	0.02			
	CV (%)	30	31	40	36	23	38	54	119	32	52	25			
Arificial ponds	count	50	50	50	50	50	50	48	49	49	50	50			
PFM007445	min	33	12	2.5	29	5.0	44	18	3.3	< 0.2	< 0.03	0.07			
PFM007446	mean	64	56	4.6	56	12	173	82	44	0.3	5.9	0.13			
	max	154	231	10	100	27	390	370	163	1.1	17	0.22			
	stddev	25	42	2	15	5	71	67	42	0.2	3	0.04			
	CV (%)	40	76	37	26	44	41	81	96	73	59	30			
Monitoring wells	count	56	57	57	59	59	59	59	59	59	59	59	58	58	59
Recharge	min	46	5.4	1.6	54	4.2	226	4.4	8.1	< 1	3.0	0.08	−97	−13	< 0.8
positions	mean	110	79	7.5	124	12	356	139	73	0.5	5.3	0.21	−87	−12	9.3
	max	277	528	27	212	43	470	576	277	2.8	10	0.46	−80	−11	14
	stddev	70	151	7	39	7	61	178	78	0.6	2	0.10	4	1	4
	CV (%)	63	190	86	32	57	17	128	106	131	33	45	−5	−4	44

		pH	Ammonium nitrogen (NH_4-N) µg/L	Nitrate nitrogen (NO_3-N) µg/L	Particulate org nitrogen (PON) µg/l	Total nitrogen (TN) µg/L	Phosphate phosphorus (PO_4-P) µg/L	Particulate org. phosphorus (POP) µg/L	Total phosphorus (TP) µg/L	Dissolved organic carbon (DOC) mg/L	Particulate organic carbon (POC) mg/L	Total organic carbon (TOC) mg/L	Dissolved inorganic carbon (DIC) mg/L	Percent modern carbon (^{14}C) %	Carbon-13 (^{13}C) ‰ dev PDB
Sea water	count	114	115	115	109	114	115	114	114	115	109	114	115	9	9
PFM0062	min	7.4	0.3	< 0.3	7.9	218	< 0.5	0.6	7.2	1.4	73	1.5	0.4	103	−4.0
	mean	7.9	2.4	19	37	273	4.3	5.7	12	3.8	272	3.9	13	106	−2.0
	max	8.3	14	113	72	960	250	13	30	5.0	603	5.0	31	111	−0.3
	stddev	0.1	2	30	13	85	23	2	4	0.7	106	0.6	4	3	1.2
	CV	2	88	154	36	31	543	36	29	17	39	17	28	3	−59
Natural ponds	count	79	76	76		76	76		76	76		76	2		
PFM007442	min	6.7	3.1	0.3		579	< 0.5		4.0	18		19	25		
PFM007443	mean	7.6	114	10		1229	0.8		11	30		31	27		
	max	9.1	3370	79		5100	3.3		45	54		56	29		
	stddev	0.6	403	14		710	0.7		7	7		7	2		
	CV	8	354	147		58	91		68	23		23	9		
Arificial ponds	count	50	50	50		50	50		50	50		50			
PFM007445	min	6.5	1.5	0.5		687	< 0.5		7.0	18		19			
PFM007446	mean	7.4	38	13		1359	1.1		20	34		34			
	max	8.4	287	189		2260	3.9		44	58		58			
	stddev	0.5	70	32		406	0.9		8	9		9			
	CV	6	184	253		30	79		41	26		26			
Monitoring wells	count	59	46	45	5	42	46	4	42	45	5	46	44	24	36
Recharge	min	6.7	< 0.5	< 0.2	34	257	0.9	9	3	4	163	4	32	85	−16
positions	mean	7.2	35	130	41	624	4.4	32	23	12	525	11	56	93	−13
	max	8.1	260	850	55	1830	36	55	200	20	879	20	74	106	−10
	stddev	0.3	45	211	8	391	5	21	43	4	270	4	10	6	1
	CV	4	127	162	20	63	116	65	188	35	51	36	18	7	−11

9.5 Evaluation of uncertainties

Although the description of the groundwater composition inside the access volume down to about −500 m elevation is regarded as robust and reliable, there are still some uncertainties worth mentioning. They do not have an impact on the general picture and understanding but may be relevant when describing some of the data in greater detail.

9.5.1 Temporal stability and spatial variability

The sample series collected from the three sections of borehole KFM24 show variation in groundwater composition with pumped volumes, probably due to spatial variability, see Figure 9-12. Borehole KFM24 at −410 m elevation shows a clear trend in the sample series from a slightly more saline groundwater towards the composition of the section at −397 m elevation. The section at −397 m elevation also shows some spread in the three samples, however, not as large. The groundwater in the shallow section at −193 m elevation changes towards a more diluted glacial character and slightly more brine signature.

The low hydraulic transmissivity of the two deeper sections may obstruct the sampling of groundwater representative for the bedrock fractures close to the sampling location. It may be that an increasing amount of water, standing in the borehole above or below the packers delimiting the section, is drawn into the borehole section or that groundwater is drawn via the fracture system from a gradually increasing distance with time which thereby changes the groundwater character. The changes are neither large enough nor of such a kind that they alter the groundwater type assessment and the general understanding of the groundwater conditions.

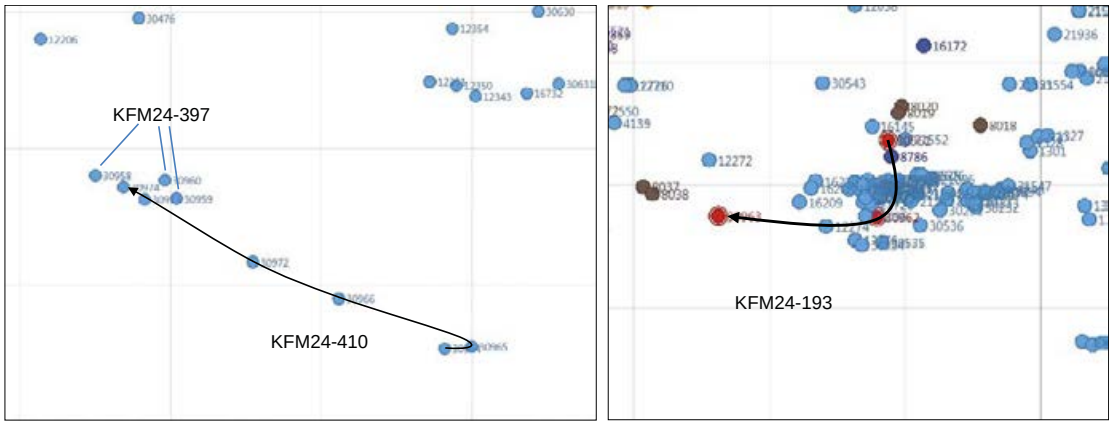

Figure 9-12. *Partial enlargements of the Mixing model in Figure 9-6 that shows the relative location of individual observations instead of averages in the original model. The numbers denote SKB sample numbers of the observations and the arrows show the sequential order of the samples taken. Each square in the left figure corresponds to 0.2 units in the original model, and 0.5 units in the right.*

9.5.2 Lack of data

No surface water data (lakes and streams) or groundwater data from shallow monitoring wells are available from the access area. The only possible sampling location is the shallow pond in the centre and close to the new borehole KFM24 in the shaft position. The water compositions of the different types of objects are estimated from the properties of similar objects at other locations outside this access volume. This may add some uncertainty, however, the expected variation within objects of the same type is not very large.

Furthermore, there are few groundwater data at and below repository depth. The scarcity of conductive fractures is typical for the bedrock within the lens in this depth range. This causes uncertainty about the groundwater composition trend towards depth, the residence times and the groundwater development in general. The only possible means to mitigate this uncertainty is to sample every sampling location/ conductive fracture wherever possible.

9.5.3 Corrosion problems and impacts on gas composition and pH

High pH values have been observed in several boreholes (Nilsson and Sandberg 2017). In addition, this phenomenon is accompanied by enhanced hydrogen gas content. The underlying causes are stray currents related to the Fenno-Skan cables to Finland and corrosion reactions in the vicinity of metal installations/structures/objects. Since pH is such an important parameter controlling the groundwater composition, the samples with clear artificial impacts (> pH 9) have been omitted from the interpretations and modelling. A few of the samples from the oldest borehole of interest inside the access volume, KFM08A, are affected.

There are some indications that also the groundwater of the new borehole KFM24 is subjected to this type of artificial impact. However, this has not been possible to verify or turn down. There is no sign of corrosion on the equipment and no clear enhancement of the hydrogen concentration has been observed. On the other hand, the magnesium and iron concentrations are generally very low (below detection limits) and pH is around nine, which is relatively high for groundwater. It cannot be excluded that some samples also from borehole KFM24 show a less representative composition due to a moderate artificial increase of pH. However, the glacial influences are obvious from the $\delta^{18}O$ values and a non-marine origin is most likely also from the general groundwater composition (the other components) and the very low groundwater flux.

9.5.4 The use of data without assessed quality categories

The sample quality categories used in **SDM-Site** and **SDM-PSU**, i.e. category 1 to 5 where 5 is the lowest quality and not used for modelling, have not been used in this report. Generally, all data are used except for samples having a pH > 9 (see 9.5.3) or collected from hydrochemical logging that

produces samples representing the water standing in the borehole rather than the fractures in the bedrock formation. The different sampling locations are generally represented by one average value instead of the evaluated most representative value. This evaluation approach is less time consuming and makes single deviating values less important but includes changes and may also cause small unwanted shifts of the data point positions in the PCA plots as well as in the common scatter plots.

9.5.5 Preliminary definition of groundwater types

The preliminary groundwater type assessment used in this report has been done with fixed limits and a simple automatic approach without a thorough evaluation of each sample and sampling location. Since there are continuous trends between the different types and no sharp and obvious limits, the water type definitions (exact limits) are set according to what was found most suitable from a visualisation point of view. The groundwater type definitions will probably be changed in the ongoing evaluation of the entire dataset.

10 Ecology and land use

The access area includes two shallow bays, three ponds, small wetlands and forest areas as well as large man-made areas, such as parking lots, roads and buildings (Figure 10-1). This area will be turned into an industrial site when the construction work for the spent fuel repository starts. Consequently, most of the ecosystems present today will disappear. The description of the access area is here focused on the presence of aquatic and terrestrial ecosystems and vegetation types found within this area today excluding the previously mentioned man-made areas. Few investigations have been done in this specific area to describe different ecosystem properties and the investigations made have mostly been done to evaluate nature values in case of their potential expropriation during the construction of the repository (e.g. Allmér 2011).

10.1 Status of site understanding and models

Below follows a general description taken from **SDM-PSU** (SKB 2013), which was based on Aquilonius (2010), Andersson (2010) and Löfgren (2010). These three publications are dedicated to descriptions of the marine, limnic and terrestrial ecosystems and did also underpin SDM-Site (SKB 2008). Nature values were not treated explicitly in the earlier SDM reports, which rather provided input data and description to the work carried out and reported within the framework of the environmental impact assessment (e.g. Hamrén and Collinder 2010, Allmér 2011). The following text is based on investigations of a larger area in Forsmark but is also valid for ecosystems identified inside the access area. It also includes a brief description of identified nature values in the Forsmark area based on Hamrén and Collinder (2010), Allmér (2011) and Berglund and Lindborg (2017).

10.1.1 Vegetation, habitats and land use

The largest part of the terrestrial area is today covered by temporary lodges for people working at the power plant, offices and associated parking lots. This also means that the surrounding areas are affected by different activities. Most of the forests are young and the only older trees are mainly found in the eastern part of the area in forests stands along the sea shoreline (Figure 10-1). Mixed forests with both deciduous and conifers are common in this costal environment. One forest stand was identified within the area as having nature values and is classified as lime influenced conifer dominated forest with deciduous trees (Figure 10-2). There are also similar forest areas in the south-east outside the access area and one such area was classified as a forest key habitat (Eklund 2004).

The three ponds are rather shallow (0.3–1 m). They are dominated by *Charophytes* and also by the species *Potamogeton pectinatus* in the two larger ones. The ponds can be classified as lime-rich oligomesotrophic ponds with benthic *Charophytes* (Hamrén and Collinder 2010). The most northerly located pond was not reproduced in the vegetation map, but the contour was illustrated in the map (Figure 10-1).

The man-made cooling-water inlet canal for the nuclear power plant is approximately 15 m deep. The water intake was recently increased by 20 % (2013–2015, Adill et al. 2014), with potential effects on the flora and fauna of the adjacent sea bay. The sea bays in the eastern part are shallow with boulder-covered bottoms and partly with fine sediments. In the most southerly located bay, a sewage water treatment plant was earlier active releasing water into the bay Söderviken, but this stopped in 2013 and the sewage water treatment plant was removed. Consequently, the bays are affected by changing processes (turbulent water and diminishing nitrogen release) that both have consequences in the short- and long-term development of biodiversity.

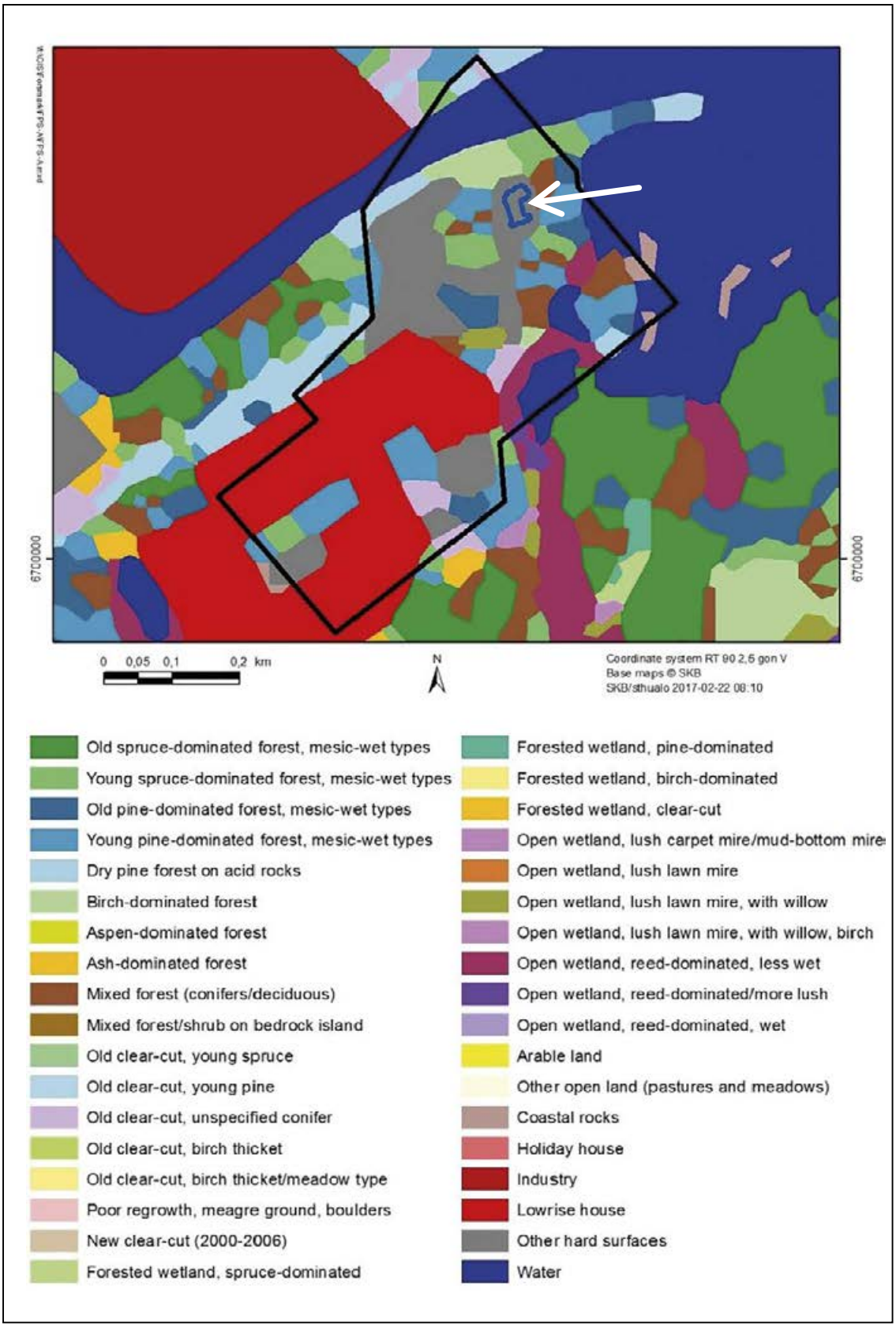

Figure 10-1. *Excerpt from the vegetation and land-use map of the Forsmark area, which is a partially updated version with regard to clear-cuts, and which is found in Löfgren (2010) and based on Boresjö Bronge and Wester (2003). The black line indicates the boundaries of the area of interest for the description of the access area. The white arrow indicates a pond that was not included in the vegetation and land-use map.*

10.1.2 Ecosystem descriptions

The terrestrial vegetation is strongly affected by topography, Quaternary deposits (QD) characteristics and human land use. Some three quarters of the land area in Forsmark is covered by forests, dominated by Scots pine (*Pinus sylvestris*) and Norway spruce (*Picea abies*) (Löfgren 2010). Due to the calcareous QD, the field layer is characterised by herbs, broad-leaved grasses and many orchid species. The area has a long history of forestry, with a large percentage of younger and older clear-cuts in different succession stages. Wetlands are frequent and cover more than 25 % of some sub-catchments. Most wetlands are coniferous forest swamps or open mires. Less mature wetlands consist of rich fens due to the high calcareous content of the QD.

The most common larger mammal species in the Forsmark area are roe deer (*Capreolus capreolus*) and moose (*Alces alces*). Altogether, 96 bird species have been found in the Forsmark area. The most common bird species in Forsmark are, as in the rest of Sweden, chaffinch (*Fringilla coelebs*) and willow warbler (*Phylloscopus trochilus*) (Löfgren 2010).

Modelling of the carbon dynamics for two conifer forests (i.e. the dominant vegetation type in Forsmark) and one forested wetland shows that the largest carbon flux in terrestrial ecosystems is the uptake of carbon by primary producers, and that the vegetation at all the investigated localities acts as a carbon sink (Löfgren 2010). This net primary production sets an upper limit on the potential uptake of different elements into biomass, which in turn limits the extent of further propagation up the food web. Eventually, biomass reaches the soil compartment as litter, where it is mineralised. The balance between litter production and heterotrophic respiration determines to what extent organic material (and incorporated elements) can be accumulated in the soil. Dynamic vegetation modelling shows that also other vegetation types (e.g. deciduous trees, meadows and arable land) are carbon sinks, with the exception of clear-cut forests that act as carbon sources.

The lakes in the Forsmark area are small and shallow. They are characterised as oligotrophic hardwater lakes, with high levels of calcium and low nutrient levels (Andersson 2010). This lake type is common along the coast of northern Uppland, but rare in the rest of Sweden (Brunberg et al. 2002, Hamrén and Collinder 2010). Shallow depths and moderate water colour permit photosynthesis in the entire benthic habitat, and the lake bottoms are covered by dense stands of macroalgae and a thick layer of microphytobenthos (microscopic algae and cyanobacteria). These two types of primary producers dominate the biomass and primary production, making phytoplankton biomass and production less important. All lakes are surrounded by reed belts, which are extensive especially around the smaller lakes. The fish community in the lakes of Forsmark is dominated by perch (*Perca fluviatilis*), roach (*Rutilis rutilus*), tench (*Tinca tinca*) and crucian carp (*Carassius carassius*), of which the two latter species are resistant to low oxygen concentrations during winter.

The streams in the Forsmark area are small and long stream stretches are dry during summer. However, some streams close to the coast carry water for most of the year and may function as passages for migrating spawning fish; extensive spawning migration has been observed between the sea and Lake Bolundsfjärden. The abundance of vegetation in the streams is heterogeneously distributed, varying between 0 and 100 % coverage of the stream bed, with some longer parts with intense growth (75–100 % coverage) (Andersson et al. 2011).

Both abiotic and biotic processes influence transport and accumulation of elements in limnic ecosystems. Modelling of carbon dynamics in limnic ecosystems shows that, contrary to typical Swedish lakes, primary production exceeds respiration in many lakes in the Forsmark area (Andersson 2010). In some of the larger lakes in the area (e.g. Bolundsfjärden and Eckarfjärden), the primary production involves large amounts of carbon compared with the amounts that are transported from the surrounding catchment area. Consequently, there is a large potential for carbon entering the lakes to be incorporated in the lake food web via primary producers. However, much of the primary produced carbon is circulated within the microbial food web and transferred back to abiotic pools or sequestered in sediments.

In the larger lakes, there is a relatively large accumulation in sediments, which can be a permanent sink for radionuclides and other pollutants. In smaller lakes, the amounts of carbon involved in primary production are small compared with the amounts transported from the surrounding catchment area. According to the ecosystems modelling, these lake systems function more as through flows. The chemical properties of the elements, the size of the lake and its location in the catchment area determine the fate of elements entering lake systems in the Forsmark area.

Due to upwelling along the coast, the marine ecosystems of the Forsmark area are rather productive in a region of otherwise fairly low primary production (Aquilonius 2010). The salinity of the seawater is low due to a large freshwater supply. The low salinity strongly affects the marine environment, as few organisms are adapted to such brackish conditions. Therefore, the fauna consists of a mix of freshwater and saltwater species. The marine biota in the area is dominated by benthic organisms such as microalgae, vascular plants and benthic microalgae. Both hard and soft bottom substrates are dominated by detrivores: snails and mussels feeding on dead material. The fish community is dominated by the marine species herring (*Clupea harengus*) in the pelagic zone, whereas limnic species (especially Eurasian perch, *Perca fluviatilis*) dominate in near-coastal areas and in secluded bays. Other investigations include vegetation mapping on the sea floor and mapping of reeds in shallow bays (Aquilonius et al. 2011, Strömgren and Lindgren 2011).

As for limnic ecosystems, both abiotic and biotic processes influence transport and accumulation of elements. However, modelling of carbon budgets shows that in marine ecosystems advective flux (water turnover) is often the dominating factor for transport and accumulation of elements, especially in open and more offshore basins. In comparison, biotic fluxes (i.e. transport from terrestrial areas) are less important. The modelling of the 28 delineated marine sub-basins based on the previous DEM shows that the whole marine area as an average has positive NEP (Net Ecosystem Production). Specifically, shallow areas near the coastline have positive NEP, whereas more offshore areas have negative NEP.

10.1.3 Nature values

The presence of rare species and their habitats that require protection or other measures is an important pre-condition for the assessment of the environmental consequences of any activity in Forsmark. Identified nature values inside the access area are therefore described below.

Habitats

The environmental impact statement produced for the spent fuel repository application (SKB 2011) describes the Forsmark area as having a wilderness character with high natural values due to an interaction of several factors, including the shoreline displacement, the flat topography, the calcite-rich regolith, and that the area is situated in a boundary zone between vegetation zones and also relatively undisturbed (outside the industrial areas). Much of the area around the nuclear power plant is of national interest for nature conservation and is surrounded by three Natura 2000 sites, two of which are also nature reserves (Natura 2000 is the EU network of nature protection areas and associated nature types).

Based on inventories performed as a part of the site investigations for the spent fuel repository, Hamrén and Collinder (2010) produced a map showing areas of conservational interest (Figure 10-2). The area south of the nuclear power plant was shown to contain numerous valuable environments, especially around Lake Bolundsfjärden. They mainly consist of different rich fen environments and calcite-rich ponds where red-listed species occur. There are also various kinds of coniferous forests on calcite-rich soil, some of which are of a natural forest character. Many of these environments, particularly the wetlands, are assessed to have very high natural values. Furthermore, some of these environments contain habitats covered by the EU Habitats Directive, and Sweden has pledged not to reduce their area.

Despite the influence of forestry, there are also older forest stands in Forsmark, some with such high natural values that they have been classified as key forest habitats or sites of natural value. Some of the lakes in the area, such as Lake Norra Bassängen and Lake Bolundsfjärden, are also of importance for spawning fish. All three ponds inside the specified access area were identified as valuable and so were the neighbouring wetlands. One forest stand was identified as having some older trees (Figure 10-2).

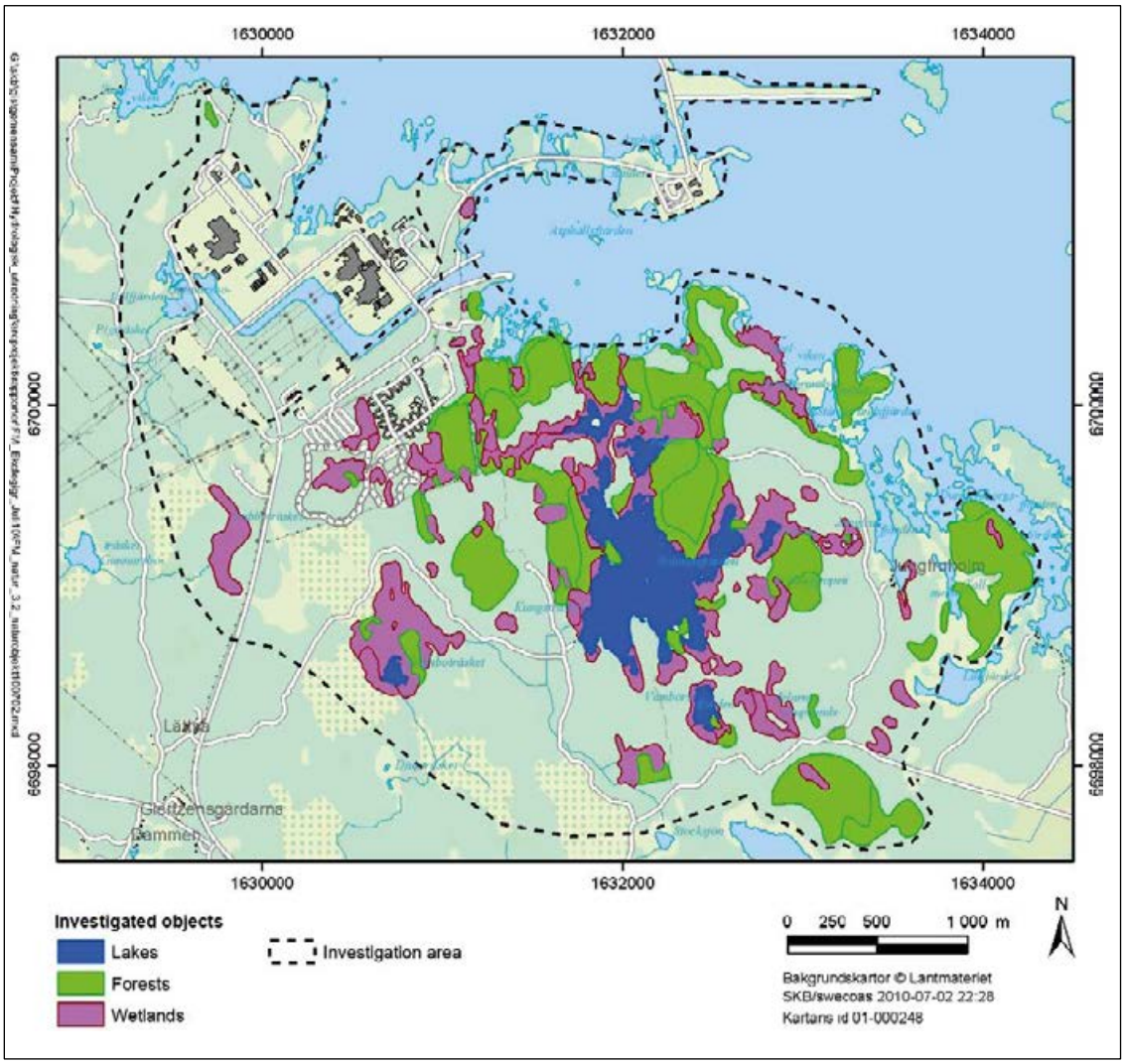

Figure 10-2. *The identified areas having nature values (from Hamrén and Collinder 2010).*

Species

During the inventories, red-listed species of mammals (Truvé 2012), birds (Green 2014), bats (de Jong and Gylje 2005), insects (Hamrén and Collinder 2010), amphibians (Hamrén and Collinder 2010), vascular plants (Göthberg and Wahlman 2006), mosses, fungi and fish have been encountered within the larger investigation area, including pool frog (*Rana lessonae*) and fen orchid (*Liparis loeselii*). In Sweden, the pool frog is only found along the northern coast of Uppland, and the environments south of Forsmark are an important part of the total habitat of pool frog in the country. In the two most northerly located ponds calling male pool frogs were noted early during the site investigations (Hamrén and Collinder 2010).

Several of the ponds also host an interesting dragonfly fauna (Hamrén and Collinder 2010). In the forest environments, more than 20 red-listed species of fungus have been encountered. The area around Forsmark is very rich in birds, including numerous red-listed species e.g. the white-tailed eagle (*Haliaeetus albicilla*) (Green 2014). The fen orchid has been described from several localities in the area and is monitored on a yearly basis since 2012 (Collinder and Zachariassen 2016).

10.2 Presentation of additional information

Most of the earlier activities that were coordinated by SKB at Forsmark were initiated in 2002 as a part of the site investigation related to the siting of a repository for spent nuclear fuel. The aims at that time were to increase the knowledge of the site and to detect whether the forthcoming increased activity at the site would affect the environment. Since then further needs have been identified, such as increasing the knowledge of habitats that potentially may be affected by the construction and operation of repositories at the site. This section introduces data gathered after **SDM-PSU,** which to large extent was based on earlier studies (Hamrén and Collinder 2010). The data shown in Table 10-1 and Table 10-2 are applicable to the area considered in this report (Figure 10-1).

Table 10-1. Investigations made in aquatic ecosystems with potential implications for the access area.

Activity	Reference
Marine inventory of vegetation	Wallin et al. 2014
Coastal bird monitoring*	Green 2017
Effects of nitrogen leakage	Hjerne 2016

* Part of a continuous monitoring programme.

Table 10-2. Investigations made in terrestrial ecosystems with potential implications for the access area.

Activity	Reference
Forestry plan	Internal document**
Terrestrial bird monitoring*	Green 2014
Pool frog monitoring*	Collinder and Zachariassen 2016
Great and Lesser crested newt monitoring*	Collinder and Zachariassen 2016
Bat inventory	de Jong 2017

* Part of a continuous monitoring programme.
** SKBdoc 1469099, SKB-internal document.

The Forsmark area has many shallow marine bays identified as being important for biodiversity and as habitat for spawning fish. Wallin et al. (2014) investigated several areas and among them the bay Söderviken in the eastern part of the access area (Figure 10-3), with the aim of further investigating the bottoms that will be affected by infilling during construction. They described the distribution and species composition on bottoms using transects in accordance with the national monitoring programme of the vegetation-covered substrates of the Baltic Sea, run by the Swedish Environmental Protection Agency (Naturvårdsverket 2000). Based on the field visits, the bays inside the access area were described as rather sparsely vegetated with low biodiversity.

In 2016, a coastal bird inventory started that included the bays close to the access area (Green 2017). They also used data from 2001 and 2011 and could consequently study trends between years. The aim of this study is to detect and describe effects on abundance and distribution in general of potential disturbances based on an increased activity in the harbour and associated boat traffic, but also effects on red-listed species (ArtDatabanken 2015) or species described in the EU Bird Directive. The bay Asphällsfjärden is already today the most affected bay with regard to such disturbances.

In 2016, work was made to describe potential future effects of nitrogen leakage from rock deposits in the bay Söderviken and distribution of drainage from subsurface facilities (Hjerne 2016). This work was based on a modelling approach using calculated water turnover times and biotic interactions. It was concluded that minor large-scale effects can be expected, whereas more significant effects could occur closer to the release points.

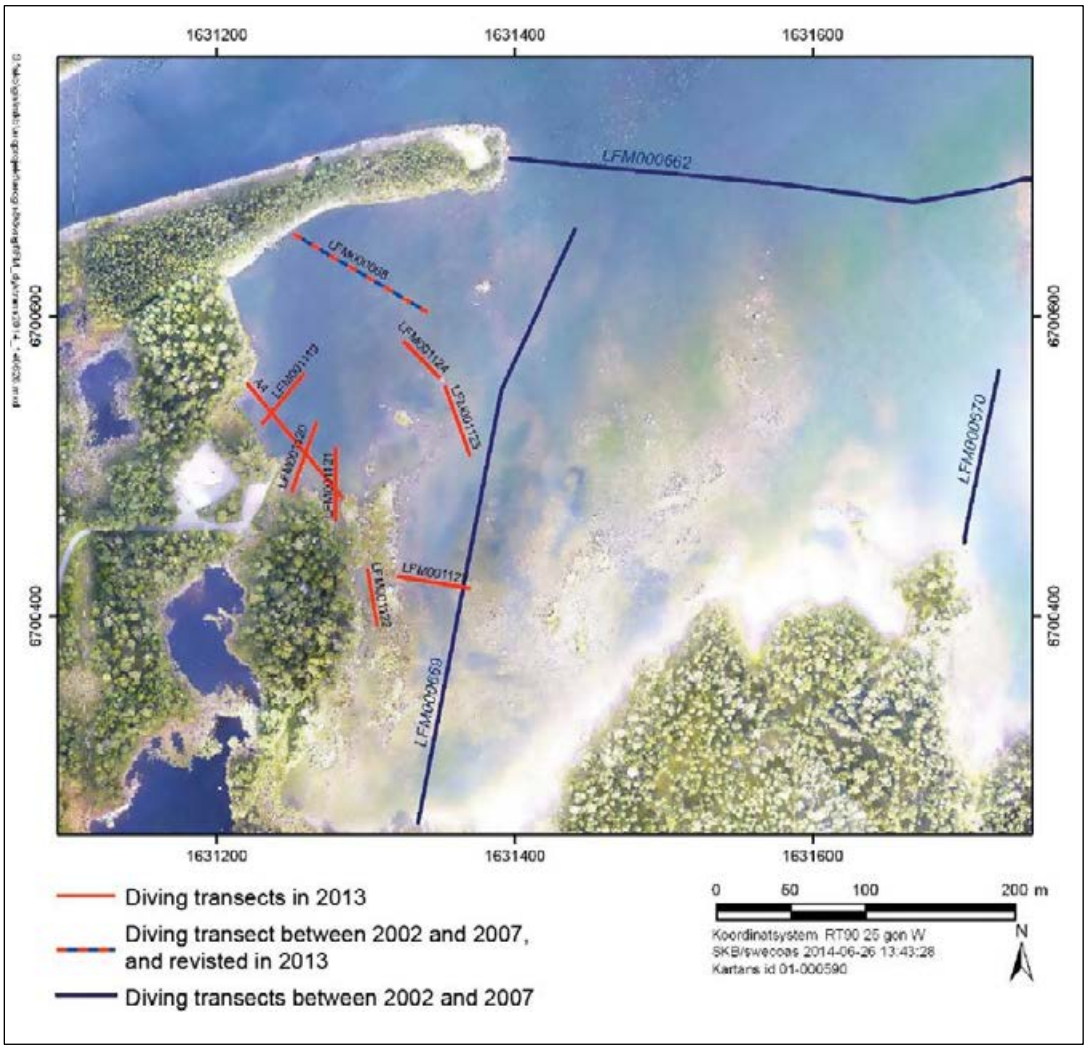

Figure 10-3. *The marine bottom investigations where red transects represent the investigation by Wallin et al. (2014) and blue those made by Borgiel (2005). The hatched blue/red line was visited in both investigations (map from Wallin et al. 2014).*

The forests have recently been included into a forestry management plan in order to develop their long-term nature values. Parts of the access area are included in this plan and these areas are characterised as young needle-leaved forests (northern and western parts) and old Norway spruce dominated forest on lime-influenced ground (eastern parts). This description is not completely consistent with the vegetation map but should be regarded as more correct than the partly outdated vegetation map. One reason for the discrepancy is the small-shattered land use pattern that possibly was difficult to interpret based on the satellite image with a 30 by 30 m^2 resolution.

Bird monitoring in terrestrial areas has been performed since 2002, see Berglund and Lindborg (2017) for an overview. Species of special interest, such as those found on the Swedish red-list (ArtDatabanken 2015), have been monitored on a yearly basis in those areas regarded as potential breeding habitats for these species, but such areas have not been found inside the access area. However, the monitoring using line transects and point counts has been performed during 2002–2004, 2007 and 2013. One such transect is found inside the access area and would consequently add data concerning breeding birds in this area (Figure 10-4).

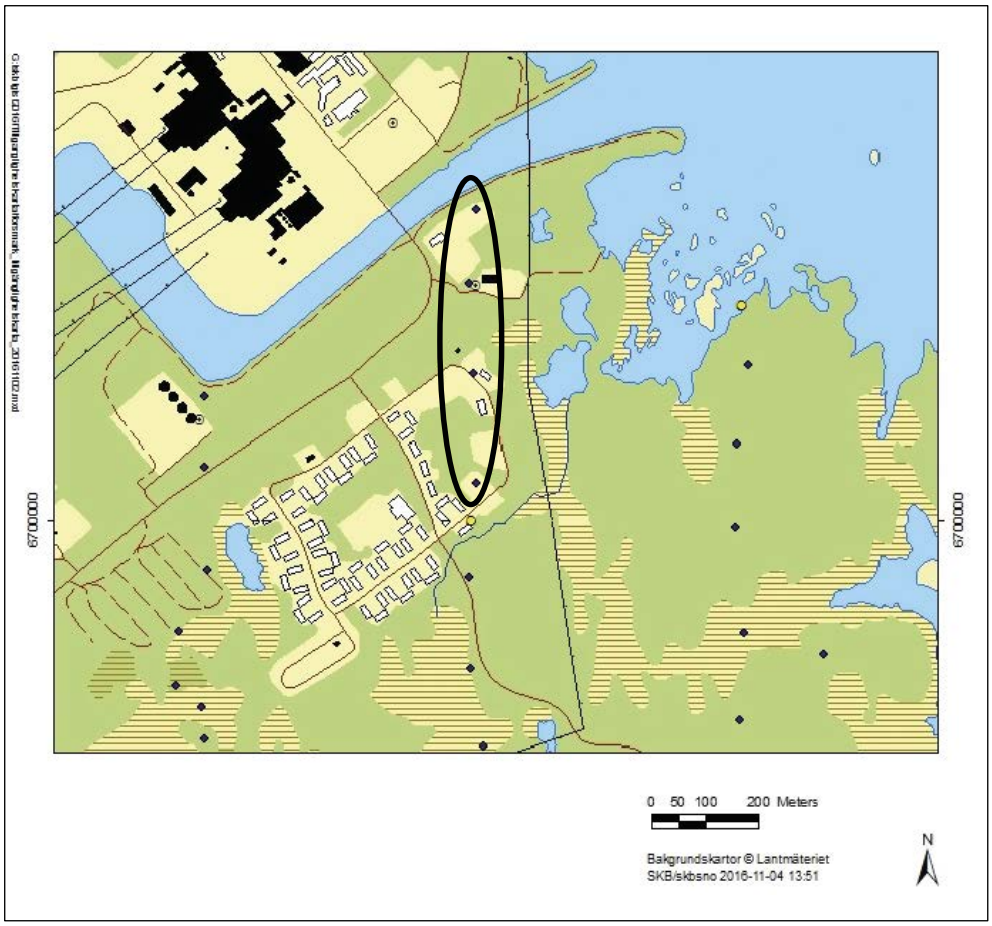

Figure 10-4. *Illustration of the line transects that are monitored for birds on a regular basis. These transects are used both for continuous monitoring along the transect, but also using points for counting during a certain period of time. This method gives both a good estimate of the number of species and the individuals. The ellipse shows the four points that falls inside the access area.*

Pool frog and great crested newt are both protected according to the EU Habitats Directive and are found in similar, shallow surface-water habitats. The pool frog has been monitored annually since 2011 in the Forsmark area. The great crested newt has been monitored since 2012 and the common newt (*Lissotriton vulgaris*) was also included in the 2013 inventory (Collinder 2014). Both the pool frog and the great crested newt have large populations in the most northerly located pond, whereas the other two ponds may only host occasional individuals of both species (Collinder and Zachariassen 2016). This seems to be the case also for the common newt, but with fewer individuals. The two larger ponds both have resident fish populations, which make these ponds less suitable for reproduction of both frogs and newts. Based on the information that the most northerly pond has a large resident pool frog and a great crested newt population, it is regarded as the most valuable of the three ponds.

A second bat inventory was performed in 2016 in order to compare results with the earlier one made in 2004 (de Jong and Gylje 2005). The bat inventory included a locality within the access area, where a so called autobox with 6 hours of continuous recording of bat sounds was placed for one night. Among the 24 recordings that were made in the larger investigation area this locality resulted in the second lowest number of identified bat individuals, consisting of two common species (de Jong 2017). The conclusion from this inventory and the earlier one was that the access area is trivial in terms of habitats and potential breeding ground for bats, and that the most interesting localities are found elsewhere in the larger area around Forsmark, e.g. in the Forsmark village and Storskäret (de Jong and Gylje 2005, de Jong 2017).

10.3 Evaluation of uncertainties

Monitoring and specific species inventories are always associated with errors. In this case the risk of missing species indicating large nature values is the most important one. When searching for specific species, the distribution of suitable habitats is always used to narrow down the potential area that has to be visited. The access area is small and well documented in terms of vegetation types, and the habitats and species of most importance are well known from the area, making the description of the access area reliable.

11 Current understanding of the access area/volume

11.1 Overview of undertaken work

Below, the current understanding of the findings of each discipline contributing to the multidisciplinary description of the access area/volume is summarised. The following aspects of the geoscientific and ecological conditions in the access area/volume are addressed in this document:

- Surface system – topography, regolith geology, climate, hydrology, near-surface hydrogeology and hydrochemistry, ecology and land use.
- Bedrock system – bedrock geology, thermal, mechanical and transport properties, hydrogeology and hydrogeochemistry.

11.2 Topography and regolith geology

The end product of geometric modelling of topographic data is a digital elevation model (DEM), which is based on interpolated point measurements of elevation. The resolution and accuracy of a DEM is a function of point density and type of measurement. The DEM for the access area presented in this document is an excerpt of a larger DEM covering a regional scale of the Forsmark area.

Regolith refers to all unconsolidated deposits which overlay the bedrock. In the Forsmark area, all regolith was deposited during the Quaternary period and is therefore often referred to as Quaternary deposits (QD). The term regolith also includes man-made deposits, in the Forsmark area mainly artificial fill. In the terrestrial areas, the upper part of the regolith that has been affected by climate and vegetation is referred to as soil.

Modelling of regolith thickness data has resulted in a regolith depth model (RDM), including elevation of the bedrock surface and depth distribution of the most commonly occurring regolith types. The high occurrence of large boulders near the real bedrock surface in Forsmark can locally lead to an underestimation of the regolith depth. Conversely, large, sediment filled fractures can locally lead to an overestimation of the regolith depth. No sediment filled fractures have been detected as part of the work for this document.

The topography of the bedrock surface inside the access area is uneven on a small scale (< 10 m) but has a low relief on larger scales. Inside the access area, the mean thickness of the regolith is ca 4 m, which is less than the overall mean thickness of the regolith in Forsmark, 6.7 m (Sohlenius et al. 2013). Since no thick clay deposits are present inside the access area, the maximum regolith thickness, approximately 10 m, is also much smaller than the maximum regolith thickness in the Forsmark **SR-PSU** area where nearly 50 m of Quaternary deposits have been recorded in the deeper trenches. The distribution of different types of deposits is also somewhat different. The major difference is the high abundance of artificial fill on the surface inside the access area compared to the area in general. This is due to the many construction projects that have been taking place within this area. The Quaternary deposits in the access area are dominated by till.

11.3 Bedrock geology

11.3.1 Rock domains

The access area consists of two rock domains (RFM): RFM029 and RFM045. The dominating rock type in rock domain RFM029 is a medium-grained and clearly deformed meta-granite. Subordinate rock types include pegmatite to pegmatitic granite, fine- to medium-grained meta-granitoid and amphibolite.

The subordinated rock domain RFM045 consists of an albitised (Na-K altered) medium-grained meta-granite together with aplitic meta-granite and lesser amount pegmatitic granite and amphibolite. Fresh rock types are common, thus the albitisation is not pervasive in this domain.

11.3.2 Deformation zones

Most of the deformation zones modelled deterministically in 3D for **SDM-Site** have surface trace lengths greater or equal to 1 000 m. Deformation zones with shorter trace lengths were regarded as minor deformation zones and denoted by MDZ. Six deformation zones transect the access volume (Figure 5-3c). Three of these zones are MDZ. One of the minor deformation zones was not modelled by Stephens et al. (2007) or Stephens and Simeonov (2015) but inferred in the data assessment for this document. The orientation pattern of the deformation zones inside the access volume is coherent with the orientation pattern of all deformation zones modelled in **SDM-Site** and in Stephens and Simeonov (2015).

It is noted that according to the deformation zone model for **SDM-Site** the ending of the trajectory of borehole KFM24 intersects one of the deformation zones which has a surface trace length greater or equal to 1 000 m. This notion assumes that the thickness of the zone is uniform. However, no deformation zone type properties were observed in the geoscientific single-hole interpretation of borehole KFM24.

11.3.3 Fracture domains

Three fracture domains occupy the access volume, where FFM02 overlies both FFM01 and FFM06. The latter is only present in rock domain RFM045 and obscured by FFM02. The upper metres of FFM02 are characterised by long and persistent undulating subhorizontal sheet joints, with locally large apertures (up to a couple of decimetres). These are often filled with silty to clayey, in places layered, sediments. The current understanding is that these slabs of bedrock were formed due to stress relief during thawing of large ice sheets.

11.3.4 Geological observations for the access volume

The rock composition both inside and outside the access volume is dominated by granite to granodiorite. Observations of minor rock occurrences (less than one metre occurrence in cored boreholes) show that amphibolites are less common and the pegmatites are more common inside the access volume compared to data in **SDM-Site** local model.

Albitisation is the most common alteration type, and it is more common inside than outside the access volume. In particular, rock domain RFM045 is characterised by this type of alteration, whereas both oxidation and quartz dissolution are more common outside the access volume. Quartz dissolution intervals are found in boreholes KFM08A and KFM08C but are less common inside the access volume than in the rest of the **SDM-Site** investigation area.

The fracture pattern of open fractures within fracture domains FFM01 and FFM02 is characterised north-easterly striking and subhorizontal fractures, which is evident both inside and outside of the access volume. In comparison, the open fracture population in FFM02 displays a stronger influence of a sub-horizontal fractures than in FFM01.

The sealed fracture orientations in FFM01 are dominated by a steep north-easterly striking set, whereas there is only a minor component of sub-horizontal fractures. The sealed fracture pattern inside the access volume is similar to that in **SDM-Site**.

Fracture intensity has been analysed as the averaged fracture frequency (P_{10}) values for every vertical 10 m section inside and outside the access volume. With the addition of the KFM24 to the **SDM-Site** data, open fracture intensity (based on Terzaghi corrected P_{10} observations) in the deeper parts of the bedrock (FFM01) is higher inside the access volume than concluded for the **SDM-Site** model area in general. However, this is consistent with what was observed in the **SDM-Site** data looking at the access area alone.

The intensity of open fractures decreases with depth regardless of fracture domain. However, the fracture intensity of open fractures in FFM01 appears to be higher at depth inside the access volume than outside. Observations in the upper parts of FFM02, show similar open fracture intensity inside the access volume as observed outside the access volume.

The sealed fracture intensity in FFM01 is also higher inside the access volume than outside. This indicates that the bedrock is also somewhat more fractured in terms of sealed fractures at depth. Sealed fracture intensity in the upper parts of the bedrock, i.e. FFM02, is in line with observations made outside the access volume.

11.4 Bedrock thermal properties and rock mechanics

The core-drilled borehole KFM24 is logged with acoustic televiewer. This enables the study of borehole breakouts in the borehole wall, which can be used to interpret the orientation of the *in-situ* stress. A similar analysis was used also for **SDM-Site** based on the available acoustic logger data at that time, see Glamheden et al. (2008). Two small "classical" breakouts are found in KFM24, at 127 m and at 399 m borehole length, respectively. Very few areas for so called "micro-fallout" are identified. The borehole breakouts are in line with previous results reported in **SDM-Site** (SKB 2008).

No new data are available for the bedrock volume inside the access volume for a detailed analysis and description of the bedrock thermal properties and rock mechanics. Hence, the description of bedrock thermal properties and the rock mechanics model developed for **SDM-Site** are both considered relevant models also for the access volume.

11.5 Climate, hydrology and near-surface hydrogeology

The findings from the evaluation of monitoring data gathered subsequent to **SDM-Site**, inside and outside the access area, do not contradict overall **SDM-Site** findings related to the hydrology and near-surface hydrogeology of the Forsmark area. A potentially important characteristic of the access area and its environs is the occurrence of coarse-grained, easily-drained artificial fill. This may cause local deviations from overall Forsmark characteristics, for instance in terms of relations between groundwater levels, topography and surface-water levels.

Data evaluations indicate that groundwater flow is directed both from inland areas towards the coastline, but also from regolith to bedrock. There is little or no correlation between the groundwater level in the upper part of the bedrock and the local topography, likely due to near-surface sub-horizontal fractures standing in hydraulic contact with the sea. That is, the sub-horizontal fractures act as a "drain" boundary condition for groundwater levels in the bedrock within the tectonic lens. It is noted that the average groundwater level in one of the percussion-drilled boreholes (HFM41), located north of the cooling-water canal, is ca 0.5 m below sea level, possibly due to the groundwater drainage below the reactor buildings of the Forsmark nuclear power plant.

11.6 Bedrock hydrogeology

The total borehole transmissivities of about 20 short boreholes penetrating the uppermost 100–150 m of rock inside the access area were determined by single-hole pumping tests. The transmissivity data vary about three orders of magnitude with most data centred on 1×10^{-4} m^2/s. The geometric mean of the total borehole transmissivities is approximately 5×10^{-5} m^2/s. There is no correlation between the total borehole transmissivity data and the total borehole depths below ground surface. A division of the total borehole transmissivities into 20 m intervals (T_{20m}) reveals a significant spatial variability over short distances both vertically and laterally.

The results from the difference flow logging with the Posiva Flow Log (PFL) in the new borehole KFM24, which is drilled near the planned skip shaft, reveal 34 flowing fractures. The number and spatial distribution of the flowing fractures observed in borehole KFM24 resemble the number and spatial distribution of flowing fractures observed in boreholes KFM01A, KFM01D, KFM08A and KFM08C. It is noted that many of the flowing fractures in boreholes KFM08A and KFM08C, which are situated closest to KFM24, were interpreted to coincide with possible deformation zones (PDZ) in the geological single-hole interpretations for **SDM-Site**. However, the single-hole interpretation of borehole KFM24 did not identify any intervals with possible deformation zone type properties.

Hence, the flowing fractures in borehole KFM24 are currently associated with the rock between possible deformation zones. As geological single-hole interpretation is not taking other data into account than the geological data observed in the borehole in focus, the interpretation of the PFL results are preliminary pending the outcome of the ultimate 3D geological deformation zone model.

A preliminary analysis of the orientation of the flowing fractures in borehole KFM24 identified with the PFL method suggests two dominant flowing fracture sets; one SE dipping sub-horizontal set and one NE striking steeply dipping set. This is coherent with the understanding of data acquired for **SDM-Site**. Borehole KFM24 has a steel casing in its uppermost ca 35 m, which prohibits hydraulic investigations of fracture domain FFM02. Thus, all flowing fractures detected with the PFL method in borehole KFM24 are situated in fracture domain FFM01.

Borehole KFM24 was pumped in conjunction with reaming and cleaning activities. During these activities hydraulic cross-hole interferences were observed in the uppermost 100 m of bedrock in the nearby boreholes KFM08A, KFM08B, KFM13, KFM14, KFM16, KFM17, KFM21, KFM22, KFM23 and HFM22 (cf Figure 3-3 and Figure 3-4). Likewise, hydraulic cross-hole interferences were observed in the nearby boreholes KFM08A–C during the difference flow logging of borehole KFM24 (here the pumped borehole acted as a line sink). The maximum depths of responding monitoring intervals in KFM08A–C are about −240 m elevation (cf Figure 3-5 and Figure 3-6). The results from the cross-hole observations during the difference flow logging are corroborated by conventional pumping tests between packers. Interpreted cross-hole transmissivities are low och moderate in magnitude, 5×10^{-9} to 5×10^{-7} m^2/s.

Noteworthy, the interval −184 to −194 m elevation contains five flowing fractures and is the most conductive interval of KFM24. The largest transmissivity value, 3.1×10^{-7} m^2/s, occurs at −184 m elevation and the second largest, 1.6×10^{-7} m^2/s, occurs at −194 m elevation. The five fractures are gently dipping. One of the subhorizontal zones modelled for **SDM-Site**, ZFM1203, is present in the access area. ZFM1203 was assumed to terminate against ZFMENE0159A (Figure 5-3). If ZFM1203, or single fractures of the same orientation as ZFM1203 crosses ZFMENE0159A it would intersect borehole KFM24 at about −190 m elevation. Borehole HFM21 is situated on opposite (eastern) side of ZFMENE0159A and intersects ZFM1203 (Stephens and Simeonov 2015). The hydraulic responses observed in borehole HFM21 during the difference flow logging of KFM24 (Odén and Follin 2016) and the pumping between packers in KFM24 (Harrström et al. 2017) do not support this speculation, however.

11.7 Hydrogeochemistry

In fracture domain FFM02, i.e. in the uppermost ca 40 m of the bedrock, the groundwater composition changes from young meteoric (in the first 10–15 m) to a mixed brackish character, which includes a young meteoric component mixed with varying proportions of a marine component, either from the Baltic Sea or the previous intrusion of Littorina Sea water during Holocene. The chloride concentration of the mixed brackish water is in the range 200 to 2 000 mg/L.

In fracture domain FFM01, i.e. between −40 to −500 m elevation, the contribution of an older glacial signature, indicated by $\delta^{18}O$ (‰ V-SMOW) values, is significant. Here, the minor marine component decreases further with depth whereas the influence of brine water increases with depth, as interpreted from the ionic composition. The chloride concentration is typically between 4 000 and 6 000 mg/L at repository depth within the access area.

11.8 Transport properties

In the site investigations underpinning **SDM-Site** and **SDM-PSU**, only very little transport properties data were acquired within the access area. Thus, no access area-specific description or comparison with the **SDM-Site** model, similar to those in Chapters 4 through 10, was produced for transport in this work. However, transport data are included in Chapter 3 (Table 3-2 and Table 3-4), and the present section provides a brief summary of these data and needs for additional information for potential future modelling of the access area.

As indicated in Table 3-2, sampling for laboratory measurements of transport parameters has been performed in KFM07A, KFM08A, KFM08C och KFM09A (Selnert et al. 2008, Crawford 2008). In total from these boreholes, 15 samples were subject to porosity measurements by water saturation, seven samples to through-diffusion measurements, four to electrical formation factor measurements (also diffusion), whereas batch sorption measurements were performed on one sample (from KFM07A). Furthermore, in situ formation factor logging to obtain diffusion parameters was carried out in three of the boreholes (KFM07A, KFM08A and KFM08C).

It should be noted that the limited availability of transport data from the access area, or any other particular area or location, is not necessarily a problem for the transport modelling. This is because the modelling methodology (as explained in Section 2.2.4 for the surface system and in Section 2.3.14 for the bedrock system) is based on identification and parameterisation of different geological materials and (for the bedrock) site-typical structures. This means that data from measurements on a particular regolith or rock type can be used wherever this material is present and together with all other data on this material.

The **SDM-Site** data collection and modelling of the bedrock were focused on rock domains RFM029 and RFM045, with rock type 101057 (dominant in RFM029, see Chapter 5) being the most well-represented rock type in the transport database (e.g. Crawford 2008), which also includes several less abundant rock types and materials associated with structures. Given the overall modelling methodology, the validity of the existing transport description for modelling the access area depends on whether the intended modelling volume contains geological materials or structures not represented in the descriptive model.

Transport modelling of bedrock and/or regolith within the access area could be needed to support the evaluation of monitoring data from the accesses and their vicinity and from more distant areas containing wetlands and ponds of high nature values. At some point in the future, also modelling of post-closure transport in the bedrock volume containing the sealed accesses could be required. For these and other potential modelling activities that involve lateral transport in the near-surface realm and/or transport from bedrock to regolith or vice versa, the description of the upper bedrock and the regolith-rock interface is crucial and needs to be improved (e.g. Section 2.3.8 and Section 4.1). Based on complementary geological modelling of the uppermost rock it could be judged whether structures and fracture-filling materials not represented in the present transport model exist and need to be investigated and described.

11.9 Ecology and land use

Supplementing information has been added since the first description to cover potential gaps in the knowledge or to answer specific questions. The added information has shown that the most northerly located pond in the access area is the most valuable from a conservational point of view. Much suggests that the other two ponds are non-important in the respect that they do not provide habitats for reproduction for the pool frog and the great crested newt. The populations inside the access area seem to be quite isolated in terms of barriers (sea) and suitable neighbouring habitats, which mainly are found further south around Lake Bolundsfjärden. Moreover, the shallow sea bays in the eastern part of the access area have been shown to have low biodiversity, which potentially is an effect of the cooling-water intake and the earlier sewage water treatment plant. Most other information has strengthened the earlier suggested patterns.

11.10 Other processes and characteristics of the access area

Earth currents have caused problems with corrosion on monitoring equipment in some of the boreholes at Forsmark, including boreholes within the access area (Section 9.5.3). Access area boreholes where corrosion damages to instrumentation have been observed include some of the KFM07- and KFM08-boreholes (Nilsson and Sandberg 2017). This implies that earth currents and their effects need to be considered in the planning and design of underground constructions and measurement equipment. To this end, a brief description and some references are given below.

The main underlying source to earth currents at Forsmark has been shown to be the return current electrode of the Fenno-Skan high voltage direct current (HVDC) link connecting the Swedish and Finnish power grids (e.g. Pedersen et al. 2013). The electrode is located at Fågelsundet, about 25 km north of Forsmark. Measurements of potential gradients caused by earth currents have been carried out in several projects; earlier investigations are compiled and discussed in Thunehed (2017). An extensive field investigation addressing some of the knowledge gaps related to earth currents was performed in 2017 (reported in Thunehed 2018). This investigation included electric potential surface mapping and measurements along the KFM07A and KFM24 boreholes, as well as cross-hole resistivity measurements in the access area.

Starting from the hydrochemical side of the problem, Nilsson and Sandberg (2017) compiled and evaluated occurrences of very high pH values in the SKB Sicada database. For Forsmark, they found that high pH values most probably were caused by corrosion due to earth currents. Furthermore, potential implications of earth currents and associated corrosion of engineered barriers for the long-term safety of planned nuclear waste repositories at Forsmark have been investigated through numerical modelling (e.g. Löfgren and Sidborn 2018).

References

SKB's (Svensk Kärnbränslehantering AB) publications can be found at www.skb.com/publications. SKBdoc documents will be submitted upon request to document@skb.se.

Adill A, Heimbrand Y, Sevastik S, 2014. Biologisk recipientkontroll vid Forsmarks kärnkraftverk. Årsrapport för 2013. Aqua reports 2014:5, Sveriges lantbruksuniversitet, Öregrund. (In Swedish.)

Allmér J, 2011. Konsekvensbedömning av påverkan på naturvärden av anläggande och drift av slutförvar för använt kärnbränsle i Forsmark. SKB P-10-15, Svensk Kärnbränslehantering AB. (In Swedish.)

Andersson C, 2013. Meteorological monitoring at Forsmark during January–December 2012. SMHI. SKBdoc 1392293 ver 1.0, Svensk Kärnbränslehantering AB.

Andersson C, Jones J, 2009. Forsmark site investigation. Meteorological monitoring at Forsmark, January 2008 until December 2008. SKB P-09-04, Svensk Kärnbränslehantering AB.

Andersson C, Jones J, 2010. Forsmark site investigation. Meteorological monitoring at Forsmark, January–December 2009. SKB P-10-05, Svensk Kärnbränslehantering AB.

Andersson C, Jones J, 2011. Monitoring Forsmark. Meteorological monitoring at Forsmark, January–December 2010. SKB P-11-11, Svensk Kärnbränslehantering AB.

Andersson C, Jones J, 2012. Meteorological monitoring at Forsmark, January–December 2011. SKBdoc 1405037 ver 1.0, Svensk Kärnbränslehantering AB.

Andersson C, Jones J, 2014. Monitering Forsmark. Meteorological monitoring at the Högmasten station in Forsmark during January–December 2013. SMHI. SKBdoc 1439628 ver 2.0, Svensk Kärnbränslehantering AB.

Andersson E, 2010. The limnic ecosystems at Forsmark and Laxemar-Simpevarp. SKB TR-10-02, Svensk Kärnbränslehantering AB.

Andersson E, Aquilonius K, Sivars Becker L, Borgiel M, 2011. Site investigation SFR. Vegetation in streams in the Forsmark area. SKB P-11-18, Svensk Kärnbränslehantering AB.

Aquilonius K (ed), 2010. The marine ecosystems at Forsmark and Laxemar-Simpevarp. SR-Site Biosphere. SKB TR-10-03, Svensk Kärnbränslehantering AB.

Aquilonius K, Qvarfordt S, Borgiel M, 2011. Validation of the marine vegetation model in Forsmark. SFR-Site Forsmark. SKB P-11-10, Svensk Kärnbränslehantering AB.

ArtDatabanken, 2015. Rödlistade arter i Sverige 2015. Uppsala: ArtDatabanken SLU. (In Swedish.)

Back P-E, Wrafter J, Sundberg J, Rosén L, 2007. Thermal properties. Site descriptive modelling Forsmark – stage 2.2. SKB R-07-47, Svensk Kärnbränslehantering AB.

Berglund S, Lindborg T (eds), 2017. Monitoring Forsmark – evaluation and recommendations for programme update. SKB TR-15-01, Svensk Kärnbränslehantering AB.

Boresjö Bronge L, Wester K, 2003. Vegetation mapping with satellite data of the Forsmark, Tierp and Oskarshamn regions. SKB P-03-83, Svensk Kärnbränslehantering AB.

Borgiel M, 2005. Forsmark site investigation. Benthic vegetation, plant associated macrofauna and benthic macrofauna in shallow bays and shores in the Grepen area, Bothnian Sea. Results from sampling 2004. SKB P-05-135, Svensk Kärnbränslehantering AB.

Bosson E, Gustafsson L-G, Sassner M, 2008. Numerical modelling of surface hydrology and near-surface hydrogeology at Forsmark. Site descriptive modelling, SDM-Site Forsmark. SKB R-08-09, Svensk Kärnbränslehantering AB.

Brunberg A-K, Carlsson T, Blomqvist P, Brydsten L, Strömgren M, 2004. Forsmark site investigation. Identification of catchments, lake-related drainage parameters and lake habitats. Revised December 2007. SKB P-04-25, Svensk Kärnbränslehantering AB.

Brunberg A-K, Nilsson E, Blomqvist P, 2002. Characteristics of oligotrophic hardwater lakes in a postglacial land-rise area in mid-Sweden. Freshwater Biology 47, 1451–1462.

Byegård J, Selnert E, Tullborg E-L, 2008. Bedrock transport properties. Data evaluation and retardation model. Site descriptive modelling, SDM-Site Forsmark. SKB R-08-98, Svensk Kärnbränslehantering AB.

Carlsson A, 1979. Characteristic features of a superficial rock mass in southern central Sweden: horizontal and sub-horizontal fractures and filling material. Uppsala: Societas Upsaliensis pro geologia quaternaria. (Striae 11.)

Collinder P, 2014. Inventering av gölgroda, större vattensalamander och gulyxne i Forsmark 2013. SKB P-14-02, Svensk Kärnbränslehantering AB. (In Swedish.)

Collinder P, Zachariassen E, 2016. Inventering av gölgroda, större vattensalamander och gulyxne i Forsmark 2015. SKB P-16-01, Svensk Kärnbränslehantering AB. (In Swedish.)

Crawford J, 2008. Bedrock transport properties Forsmark. Site descriptive modelling, SDM-Site Forsmark. SKB R-08-48, Svensk Kärnbränslehantering AB.

Crawford J, 2010. Bedrock K_d data and uncertainty assessment for application in SR-Site geosphere transport calculations. SKB R-10-48, Svensk Kärnbränslehantering AB.

Curtis P, Markström I, Petersson J, Triumf C-A, Isaksson H, Mattsson H, 2011. Site investigation SFR. Bedrock geology. SKB R-10-49, Svensk Kärnbränslehantering AB.

Curtis P, Runslätt E, Vestgård J, Bergkvist L, Mærsk Hansen L, Olsson A, Ergun F, 2012. SFK Byggundersökningar. Detaljerad sprickkartering i diken i Söderviken. SKBdoc 1338599 ver 1.0, Svensk Kärnbränslehantering AB. (In Swedish.)

Dahlin P, Maskenskaya O, 2017. Boremap mapping of core drilled borehole KFM24. SKB P-16-28, Svensk Kärnbränslehantering AB.

Dahlin P, Petersson J, Mattsson H, 2017. Geological single-hole interpretation of KFM24. SKB P-16-29, Svensk Kärnbränslehantering AB.

de Jong J, 2017. Inventering av fladdermöss vid Forsmark. SKB P-16-30, Svensk Kärnbränslehantering AB. (In Swedish.)

de Jong J, Gylje S, 2005. Forsmark site investigation. Abundance and distribution of bat (Chiroptera) species in the Forsmark area. SKB P-05-61, Svensk Kärnbränslehantering AB.

Eklund S, 2004. Nyckelbiotoper och högre naturvärden inom prioriterade områden i Uppsala län. Sammanställning av inventeringsresultat samt fördjupad inventering i Forsmark. SKB P-04-33, Svensk Kärnbränslehantering AB. (In Swedish.)

Follin S, 2008. Bedrock hydrogeology Forsmark. Site descriptive modelling, SDM-Site Forsmark. SKB R-08-95, Svensk Kärnbränslehantering AB.

Follin S, Hartley L, 2014. Approaches to confirmatory testing of a groundwater flow model for sparsely fractured crystalline rock, exemplified by data from the proposed high-level nuclear waste repository site at Forsmark, Sweden. Hydrogeology Journal 22, 333–349.

Follin S, Johansson P-O, Hartley L, Jackson P, Roberts D, Marsic N, 2007a. Hydrogeological conceptual model development and numerical modelling using CONNECTFLOW, Forsmark modelling stage 2.2. SKB R-07-49, Svensk Kärnbränslehantering AB.

Follin S, Levén J, Hartley L, Jackson P, Joyce S, Roberts D, Swift B, 2007b. Hydrogeological characterisation and modelling of deformation zones and fracture domains, Forsmark modelling stage 2.2. SKB R-07-48, Svensk Kärnbränslehantering AB.

Follin S, Hartley L, Jackson P, Roberts D, Marsic N, 2008. Hydrogeological conceptual model development and numerical modelling using CONNECTFLOW, Forsmark modelling stage 2.3. SKB R-08-23, Svensk Kärnbränslehantering AB.

Follin S, Hartley L, Rhén I, Jackson P, Joyce S, Roberts D, Swift, B. 2014. A methodology to constrain the parameters of a hydrogeological discrete fracture network model for sparsely fractured crystalline rock, exemplified by data from the proposed high-level nuclear waste repository site at Forsmark, Sweden. Hydrogeology Journal 22, 313-331.

Forssberg O, Mærsk Hansen L M, Koyi S, Vestgård J, Öhman J, Petersson J, Albrecht J, Hedenström A, Gustavsson J, 2007. Forsmark site investigation. Detailed fracture and bedrock mapping, Quaternary investigations and GPR measurements at excavated outcrop AFM001264. SKB P-05-269, Svensk Kärnbränslehantering AB.

Glamheden R, Fredriksson A, Röshoff K, Karlsson J, Hakami H, Christiansson R, 2007a. Rock mechanics Forsmark. Site descriptive modelling, Forsmark stage 2.2. SKB R-07-31, Svensk Kärnbränslehantering AB.

Glamheden R, Mærsk Hansen L M, Fredriksson A, Bergkvist L, Markström I, Elfström M, 2007b. Mechanical modelling of the Singö deformation zone. Site descriptive modelling, Forsmark stage 2.1. SKB R-07-06, Svensk Kärnbränslehantering AB.

Glamheden R, Lanaro F, Karlsson J, Lindberg U, Wrafter J, Hakami H, Johansson M, 2008. Rock mechanics Forsmark. Modelling stage 2.3. Complementary analysis and verification of the rock mechanics model. SKB R-08-66, Svensk Kärnbränslehantering AB.

Green M, 2014. Fågelövervakning i Forsmark 2013. SKB R-14-16, Svensk Kärnbränslehantering AB. (In Swedish.)

Green M, 2017. Fågelövervakning i Forsmark 2016. SKB P-16-26, Svensk Kärnbränslehantering AB. (In Swedish.)

Göthberg A, Wahlman H, 2006. Forsmark site investigation. Inventory of vascular plants and classification of calcareous wetlands in the Forsmark area. SKB P-06-115, Svensk Kärnbränslehantering AB.

Hakami E, 2011. Rock stress orientation measurements using induced thermal spalling in slim boreholes. SKB R-11-12, Svensk Kärnbränslehantering AB.

Hamrén U, Collinder P, 2010. Vattenverksamhet i Forsmark. Ekologisk fältinventering och naturvärdesklassificering samt beskrivning av skogsproduktionsmark. SKB R-10-16, Svensk Kärnbränslehantering AB. (In Swedish.)

Harrström J, Sjöberg O, Öhman J. 2017. Evaluation of hydraulic interference tests in Forsmark with KFM24 as pumping borehole. SKB P-17-17, Svensk Kärnbränslehantering AB.

Hedenström A, 2004. Forsmark site investigation. Investigation of marine and lacustrine sediments in lakes. Stratigraphical and analytical data. SKB P-04-86, Svensk Kärnbränslehantering AB.

Hedenström A, Sohlenius G, 2008. Description of the regolith at Forsmark. Site descriptive modelling, SDM-Site Forsmark. SKB R-08-04, Svensk Kärnbränslehantering AB.

Hedenström A, Sohlenius G, Strömgren M, Brydsten L, Nyman H, 2008. Depth and stratigraphy of regolith at Forsmark. Site descriptive modelling. SDM-Site Forsmark. SKB R-08-07, Svensk Kärnbränslehantering AB.

Helgstedt M D, 1997. An assessment of the in-situ shear strength of rock masses and discontinuities. MSc thesis. Luleå University of Technology, Sweden.

Hellgren S, 2010. Rapport Geoteknisk Undersökning, RGEO Forsmark – Projekt Kärnbränsleförvaret. Jord-bergsondering, etapp 1. Östhammars kommun. Tyréns. SKBdoc 1325135 ver 1.0, Svensk Kärnbränslehantering AB. (In Swedish.)

Hellgren S, 2011. Rapport Geoteknisk Undersökning, RGEO Forsmark – Projekt Kärnbränsleförvaret. Byggförberedande undersökningar, etapp 2a och 2b. Östhammars kommun. Tyréns. SKBdoc 1325128 ver 1.0, Svensk Kärnbränslehantering AB. (In Swedish.)

Henriksson H, 2016. Fältrapport/Geoteknik. Fältrapport. Slutrapport 2016-05-20.Tyréns. SKBdoc 1551182 ver 1.0, Svensk Kärnbränslehantering AB. (In Swedish.)

Hermansson T, Stephens M B, Corfu F, Andersson J, Page L, 2007. Penetrative ductile deformation and amphibolite-facies metamorphism prior to 1851 Ma in the western part of the Svecofennian orogen, Fennoscandian Shield. Precambrian Research 153, 29–45.

Hermansson T, Stephens M B, Corfu F, Page L M, Andersson J, 2008. Migratory tectonic switching, western Svecofennian orogen, central Sweden: Constraints from U/Pb zircon and titanite geochronology. Precambrian Research 161, 250–278.

Hjerne O, 2016. Effekter av kväveutsläpp i Forsmark. SKB R-16-11, Svensk Kärnbränslehantering AB.

Hurmerinta E, 2017. Forsmark site investigations. Difference flow logging in borehole KFM24. SKB P-16-27, Svensk Kärnbränslehantering AB.

INSIGHT, 2014. Manual SubsurfaceViewer XL and SubsurfaceViewer MX 6.0. INSIGHT Geologische Softwaresysteme GmbH, Cologne, Germany.

Ising J, 2005. Forsmark site investigation. Mapping of Quaternary deposits on the bottom of shallow bays outside Forsmark. SKB P-06-88, Svensk Kärnbränslehantering AB.

Johansson P-O, 2008. Description of surface hydrology and near-surface hydrogeology at Forsmark. Site descriptive modelling, SDM-Site. SKB R-08-08, Svensk Kärnbränslehantering AB.

Johansson P-O, Öhman J, 2008. Presentation of meteorological, hydrological and hydrogeological monitoring data from Forsmark. Site descriptive modelling, SDM-Site Forsmark. SKB R-08-10, Svensk Kärnbränslehantering AB.

Jones J, Kindell S, 2015. Meteorological monitoring at the Högmasten station in Forsmark during January–December 2014. SMHI. SKBdoc 1520333 ver 1.0, Svensk Kärnbränslehantering AB.

Jones J, Kindell S, 2016. Meteorological monitoring at the Högmasten and Labbomasten stations in Forsmark during January–December 2015. SMHI. SKBdoc 1540483 ver 1.0, Svensk Kärnbränslehantering AB.

Joyce S, Simpson T, Hartley L, Applegate D, Hoek J, Jackson P, Swan D, Marsic N, Follin S, 2010. Groundwater flow modelling of periods with temperate climate conditions – Forsmark. SKB R-09-20, Svensk Kärnbränslehantering AB.

Jönsson J, Hjerne C, Ludvigson J-E, 2005. Forsmark site investigation. Pumping tests and flow logging. Boreholes HFM20, HFM21 and HFM22. SKB P-05-14, Svensk Kärnbränslehantering AB.

Jönsson S, 2011. Flödesloggningar i projekt SFK byggundersökningar. Geosigma. SKBdoc 1321424 ver 1.0, Svensk Kärnbränslehantering AB. (In Swedish.)

Jönsson S, Ludvigson J-E, 2006. Forsmark site investigation. Pumping tests and flow logging boreholes HFM23, HFM27 and HFM28. SKB P-06-191, Svensk Kärnbränslehantering AB.

Laaksoharju M, Smellie J, Tullborg E-L, Gimeno M, Hallbeck L, Molinero J, Waber N, 2008. Bedrock hydrogeochemistry Forsmark. Site descriptive modelling. SDM-Site Forsmark. SKB R-08-47, Svensk Kärnbränslehantering AB.

Lindroos H, Isaksson H, Thunehed H, 2004. The potential for ore and industrial minerals in the Forsmark area. SKB R-04-18, Svensk Kärnbränslehantering AB.

Lundgren M, 2017. OPTV-loggning i KFM024. SKBdoc 1588473 ver 1.0, Svensk Kärnbränslehantering AB. (In Swedish.)

Löfgren A (ed), 2010. The terrestrial ecosystems at Forsmark and Laxemar-Simpevarp. SR-Site Biosphere. SKB TR-10-01, Svensk Kärnbränslehantering AB.

Löfgren M, Sidborn M, 2010. Statistical analysis of results from the quantitative mapping of fracture minerals in Forsmark. Site descriptive modelling – complementary studies. SKB R-09-30, Svensk Kärnbränslehantering AB.

Löfgren M, Sidborn M, 2018. Modelling of bounding corrosion rates of reactor pressure vessels in SFR due to earth currents. SKB R-16-14, Svensk Kärnbränslehantering AB.

Martin C D, 2007. Quantifying in situ stress magnitudes and orientations for Forsmark. Forsmark stage 2.2. SKB R-07-26, Svensk Kärnbränslehantering AB.

Mattsson H, 2011. Geofysiska undersökningar i projekt SFK byggundersöningar. Försöksrapport/ Fält. SKBdoc 1318988 ver 1.0, Svensk Kärnbränslehantering AB. (In Swedish.)

Naturvårdsverket, 2000. Bedömningsgrunder för miljökvalitet. Kust och Hav. Rapport 4914, Naturvårdsverket. (In Swedish.).

Nilsson A-C, Sandberg B, 2017. Elevated pH values in groundwater. Observations from SKB investigations 1976-2014 and possible causes. SKB R-16-04, Svensk Kärnbränslehantering AB.

Nilsson A-C, Tullborg E-L, Smellie J, Gimeno M J, Gómez J B, Auqué L F, Sandström B, Pedersen K, 2011. SFR site investigation. Bedrock Hydrogeochemistry. SKB R-11-06, Svensk Kärnbränslehantering AB.

Nilsson G, 2013. Borrningens genomförande och tekniska data för kärnborrhålen KFM13–KFM23 samt för hammarborrhålen HFM39, HFM40 och HFM41 vid Söderviken inom Forsmarks platsundersökningsområde. SKBdoc 1338601 ver 1.0, Svensk Kärnbränslehantering AB. (In Swedish.)

Nilsson G, 2017. Steered core drilling of borehole KFM24. SKB P-16-32, Svensk Kärnbränslehantering AB.

Nordén S, Avila R, de la Cruz I, Stenberg K, Grolander S, 2010. Element-specific and constant parameters used for dose calculations in SR-Site. SKB TR-10-07, Svensk Kärnbränslehantering AB.

Nyberg G, Wass E, 2008a. Forsmark site investigation. Snow depth, snow water content and ice cover during the winter 2007/2008. SKB P-08-92, Svensk Kärnbränslehantering AB.

Nyberg G, Wass E, 2008b. Forsmark site investigation. Hydro monitoring program. Report for April 2007 – April 2008. P-08-72, Svensk Kärnbränslehantering AB.

Nyberg G, Wass E, 2009a. Forsmark site investigation. Snow depth, snow water content and ice cover during the winter 2008/2009. SKB P-09-70, Svensk Kärnbränslehantering AB.

Nyberg G, Wass E, 2009b. Forsmark site investigation. Hydro monitoring program. Report for May 2008 – April 2009. SKB P-09-42, Svensk Kärnbränslehantering AB.

Nyberg G, Wass E, 2010a. Forsmark site investigation. Snow depth, snow water content and ice cover during the winter 2009/2010. SKB P-10-45, Svensk Kärnbränslehantering AB.

Nyberg, G, Wass E, 2010b. Hydro Monitoring Program May 2009 May 2010. Forsmark site investigation. Report for May 2009 – May 2010. SKBdoc 1319765 ver 1.0, Svensk Kärnbränslehantering AB.

Nyberg J, Elhammer A, Sohlenius G, Kjellin B, Nordgren P, 2011. Results from marine geological investigations outside Forsmark. SKB P-11-39, Svensk Kärnbränslehantering AB.

Odén M, Follin S, 2016. Hydrauliska responser i närliggande borrhål vid hammarborrning och differensflödesloggning av teleskopborrhål KFM24. SKBdoc 1529352 ver 1.0, Svensk Kärnbränslehantering AB. (In Swedish.)

Olofsson I, Simeonov A, Stephens M, Follin S, Nilsson A-C, Röshoff K, Lindberg U, Lanaro F, Fredriksson A, Persson L, 2007. Site descriptive modelling Forsmark, stage 2.2. A fracture domain concept as a basis for the statistical modelling of fractures and minor deformation zones, and interdisciplinary coordination. SKB R-07-15, Svensk Kärnbränslehantering AB.

Pedersen L B, Shan C, Dynesius L, 2013. Forsmark. Measurements of electrical potential gradients in the Forsmark area autumn 2013. SKB P-13-49, Svensk Kärnbränslehantering AB.

Petersson J, Skogsmo G, Vestgård J, Albrecht J, Hedenström A, Gustavsson J, 2007. Forsmark site investigation. Bedrock mapping and magnetic susceptibility measurements, Quaternary investigations and GPR measurements in trench AFM001265. SKB P-06-136, Svensk Kärnbränslehantering AB.

Petersson J, Kvartsberg S, Vestgård J, Andersson T, Åkerström K, 2010. Berggrundskartering av avrymningarna AFM001393 och AFM001394 belägna vid Söderviken, Forsmark. SKBdoc 1338506 ver 1.0, Svensk Kärnbränslehantering AB. (In Swedish.)

Petrone J, 2017. PM tillhörande AP SFK-16-031. SKBdoc 1564669 ver 1.0, Svensk Kärnbränslehantering AB. (In Swedish.)

Ringgaard J, 2007a. Forsmark site investigation. Mapping of borehole breakouts. Processing of acoustical televiewerdata from KFM08A, KFM08C, KFM09A, KFM09B and KFM90B. SKB P-07-166, Svensk Kärnbränslehantering AB.

Ringgaard J, 2007b. Forsmark site investigation. Mapping of borehole breakouts. Processing of acoustical televiewerdata from KFM01A, KFM01B, KFM02A, KFM03A, KFM03B, KFM04A, KFM05A, KFM06A and KFM07C. SKB P-07-07, Svensk Kärnbränslehantering AB.

Sandström B, Tullborg E-L, 2006. Forsmark site investigation. Fracture mineralogy. Results from KFM06B, KFM06C, KFM07A, KFM08A, KFM08B. SKB P-06-226, Svensk Kärnbränslehantering AB.

Selnert E, Byegård J, Widestrand H, 2008. Forsmark site investigation. Laboratory measurements within the site investigation programme for the transport properties of the rock. Final report. SKB P-07-139, Svensk Kärnbränslehantering AB.

Sheppard S, Long J, Sanipelli B, Sohlenius G, 2009. Solid/liquid partition coefficients (Kd) for selected soils and sediments at Forsmark and Laxemar-Simpevarp. R-09-27, Svensk Kärnbränslehantering AB.

Sheppard S, Sohlenius G, Omberg L-G, Borgiel M, Grolander S, Nordén S, 2011. Solid/liquid partition coefficients (K_d) and plant/soil concentration ratios (CR) for selected soils, tills and sediments at Forsmark. SKB R-11-24, Svensk Kärnbränslehantering AB.

SKB, 2005. Preliminary site description Forsmark area – version 1.2. SKB R-05-18, Svensk Kärnbränslehantering AB.

SKB, 2008. Site description of Forsmark at completion of the site investigation phase. SDM-Site Forsmark. SKB TR-08-05, Svensk Kärnbränslehantering AB.

SKB, 2011. Environmental Impact Statement. Interim storage, encapsulation and final disposal of spent nuclear fuel. Svensk Kärnbränslehantering AB.

SKB, 2013. Site description of the SFR area at Forsmark at completion of the site investigation phase. SDM-PSU Forsmark. TR-11-04, Svensk Kärnbränslehantering AB.

SKB, 2015. Safety analysis for SFR. Long-term safety. Main report for the safety assessment SR-PSU. Revised edition. SKB TR-14-01, Svensk Kärnbränslehantering AB.

SKB, 2018. Detailed site investigation programme for the construction and operation of the Repository for spent nuclear fuel. SKB R-17-16, Svensk Kärnbränslehantering AB.

Smellie J, Laaksoharju M, Tullborg E-L, 2002. Hydrogeochemical site descriptive model – a strategy for the model development during site investigations. SKB R-02-49, Svensk Kärnbränslehantering AB.

Sohlenius G, Hedenström A, 2009. Platsundersökning Forsmark. Stratigrafiska undersökningar i våtmarksobjekt. SKB P-09-18, Svensk Kärnbränslehantering AB. (In Swedish.)

Sohlenius G, Strömgren M, Hartz F, 2013. Depth and stratigraphy of regolith at Forsmark. SR-PSU Biosphere. SKB R-13-22, Svensk Kärnbränslehantering AB.

Stephens M B, Fox A, La Pointe P R, Simeonov A, Isaksson H, Hermanson J, Öhman J, 2007. Geology Forsmark. Site descriptive modelling, Forsmark stage 2.2. SKB R-07-45, Svensk Kärnbränslehantering AB.

Stephens M B, Bergman T, Isaksson H, Petersson J, 2008. Bedrock geology Forsmark. Modelling stage 2.3. Description of the bedrock geological map at the ground surface. SKB R-08-128, Svensk Kärnbränslehantering AB.

Stephens M B, Simeonov A, 2015. Description of deformation zone model version 2.3, Forsmark. SKB R-14-28, Svensk Kärnbränslehantering AB.

Strömgren M, Brydsten L, 2008. Digital elevation models of Forsmark. Site-descriptive modelling. SDM-Site Forsmark. SKB R-08-62, Svensk Kärnbränslehantering AB.

Strömgren M, Lindgren F, 2011. Mapping of reed in shallow bays. SFR-Site Forsmark. SKB P-11-09, Svensk Kärnbränslehantering AB.

Strömgren M, Brydsten L, 2013. Digital elevation model of Forsmark. Site descriptive modelling. SR-PSU biosphere. SKB R-12-03, Svensk Kärnbränslehantering AB.

Sundberg J, Wrafter J, Ländell M, Back P-E, Rosén L, 2008. Thermal properties Forsmark. Modelling stage 2.3. Complementary analysis and verification of the thermal bedrock model, stage 2.2. SKB R-08-65, Svensk Kärnbränslehantering AB.

Söderbäck B (ed), 2008. Geological evolution, palaeoclimate and historical development of the Forsmark and Laxemar-Simpevarp areas. Site descriptive modelling. SDM-Site. SKB R-08-19, Svensk Kärnbränslehantering AB.

Thunehed H, 2017. Compilation and evaluation of earth current measurements in the Forsmark area. SKB R-14-34, Svensk Kärnbränslehantering AB.

Thunehed H, 2018. Measurements of potential fields caused by earth currents and estimation of the bulk electric resistivity between deep boreholes at Forsmark. SKB P-18-06, Svensk Kärnbränslehantering AB.

Truvé J, 2012. Inventering av däggdjur i Forsmark och Hållnäs. SKB P-12-20, Svensk Kärnbränslehantering AB. (In Swedish.)

Tröjbom M, Nordén S, 2010. Chemistry data from surface ecosystems in Forsmark and Laxemar-Simpevarp. Site specific data used for estimation of CR and K_d values in SR-Site. SKB R-10-28, Svensk Kärnbränslehantering AB.

Tröjbom M, Grolander S, Rensfeldt V, Nordén S, 2013. K_d and CR used for transport calculations in the biosphere in SR-PSU. SKB R-13-01, Svensk Kärnbränslehantering AB.

Tullborg E-L, Smellie J, Nilsson A-C, Gimeno M J, Auqué L F, Brüchert V, Molinero J, 2010. SR-Site – sulphide content in the groundwater at Forsmark. SKB TR-10-39, Svensk Kärnbränslehantering AB.

Waber H N, Smellie J A T, 2012. Forsmark site characterisation. Borehole KFM22 and KFM23: Derivation of porewater data by diffusion experiments. SKB P-12-18, Svensk Kärnbränslehantering AB.

Waber H N, Gimmi T, Smellie J A T, 2009. Porewater chemistry in the rock matrix. Site descriptive modelling, SDM Site Forsmark. SKB R-08-105, Svensk Kärnbränslehantering AB.

Walger E, Jönsson S, Ludvigson J-E, 2007. Forsmark site investigation. Pumping tests and flow logging. Boreholes HFM36, HFM37 and HFM38. SKB P-07-22, Svensk Kärnbränslehantering AB.

Walger E, Ludvigson J-E, Olofsson C, Harrström J, 2012. Evalutation of hydraulic interference tests in the Forsmark Site investigation area with KFM16 and KFM23 as pumping boreholes. SKBdoc 1338614 ver. 1.0, Svensk Kärnbränslehantering AB.

Wallin A, Qvarfordt S, Borgiel M, 2014. Marin inventering av vegetation i Söderviken, Asphällsfjärden, Forsmark 2013. Sveriges Vattenekologer AB. SKBdoc 1438182 ver 2.0, Svensk Kärnbränslehantering AB. (In Swedish.)

Wass E, 2011. Monitoring Forsmark. Snow depth, snow water content and ice cover during the winter 2010/2011. Forsmark site investigation. SKB P-11-13, Svensk Kärnbränslehantering AB.

Wass E, 2012. Snow depth, snow water content and ice cover during the winter 2011/2012. Monitering Forsmark. SKBdoc 1352966 ver 1.0, Svensk Kärnbränslehantering AB.

Wass E, 2013a. Snow depth, snow water content and ice cover during the winter 2012/2013. SKBdoc 1390374 ver 1.0, Svensk Kärnbränslehantering AB.

Wass E, 2013b. Hydro Monitoring Program. Report for June 2010 – May 2011. Monitering Forsmark. SKBdoc 1406235 ver 1.0, Svensk Kärnbränslehantering AB.

Wass E, 2014a. Snow depth and ice cover during the winter 2013/2014. SKBdoc 1435895 ver 1.0, Svensk Kärnbränslehantering AB.

Wass E, 2014b. Monitoring Forsmark. Hydro monitoring program report for June 2012 – May 2013. SKBdoc 1435248 ver 1.0, Svensk Kärnbränslehantering AB.

Wass E, 2015a. Snow depth and ice cover during the winter 2014/2015. SKBdoc 1483084 ver 1.0, Svensk Kärnbränslehantering AB.

Wass E, 2015b. Monitering Forsmark. Hydro monitoring program. Report for June 2011 – May 2012. SKBdoc 1407350 ver 2.0, Svensk Kärnbränslehantering AB.

Wass E, 2015c. Monitoring Forsmark. Hydro monitoring program. Report for June 2013 – May 2014. SKBdoc 1478011 ver 1.0, Svensk Kärnbränslehantering AB.

Wass E, 2016a. Snow depth and ice cover during the winter 2015/2016. SKBdoc 1549190 ver 1.0, Svensk Kärnbränslehantering AB.

Wass E, 2016b. Monitoring Forsmark. Hydro monitoring program. Report for June 2014 – May 2015. SKBdoc 1683293 ver 1.0, Svensk Kärnbränslehantering AB.

Wass E, 2018. Monitoring Forsmark. Hydro monitoring program. Report for June 2015 – September 2017. SKBdoc 1685312 ver 1.0, Svensk Kärnbränslehantering AB.

Wern L, Jones J, 2007. Forsmark site investigation. Meteorological monitoring at Forsmark, October 2006 until June 2007. SKB P-07-175, Svensk Kärnbränslehantering AB.

Wern L, Jones J, 2008. Forsmark site investigation. Meteorological monitoring at Forsmark July 2007 – December 2007. SKB P-08-100, Svensk Kärnbränslehantering AB.

Werner K, 2018. Data compilation and analysis for the description of the access area of the planned spent fuel repository in Forsmark – meteorology, hydrology and near-surface hydrogeology. SKB P-17-19, Svensk Kärnbränslehantering AB.

Werner K, Johansson P-O, Brydsten L, Bosson E, Berglund S, Tröjbom M, Nyman H, 2007. Recharge and discharge of near-surface groundwater in Forsmark. Comparison of classification methods. SKB R-07-08, Svensk Kärnbränslehantering AB.

Werner K, Sassner M, Johansson E, 2013. Hydrology and near-surface hydrogeology at Forsmark – synthesis for the SR-PSU project. SR-PSU Biosphere. SKB R-13-19, Svensk Kärnbränslehantering AB.

Werner K, Norville J, Öhman J, 2014. Meteorological, hydrological and hydrogeological monitoring data from Forsmark – compilation and analysis for the SR-PSU project. SR-PSU Biosphere. SKB R-13-20, Svensk Kärnbränslehantering AB.

Widestrand H, Byegård J, Ohlsson Y, Tullborg E-L, 2003. Strategy for the use of laboratory methods in the site investigations programme for the transport properties of the rock. SKB R-03-20, Svensk Kärnbränslehantering AB.

Winell S, 2012. Boremap-kartering av kärnborrhålen KFM13–23 och hammarborrhålen HFM39–41. SKBdoc 1327873 ver 1.0, Svensk Kärnbränslehantering AB. (In Swedish.)

Appendix A

Maps of the access area of the planned repository for spent nuclear fuel

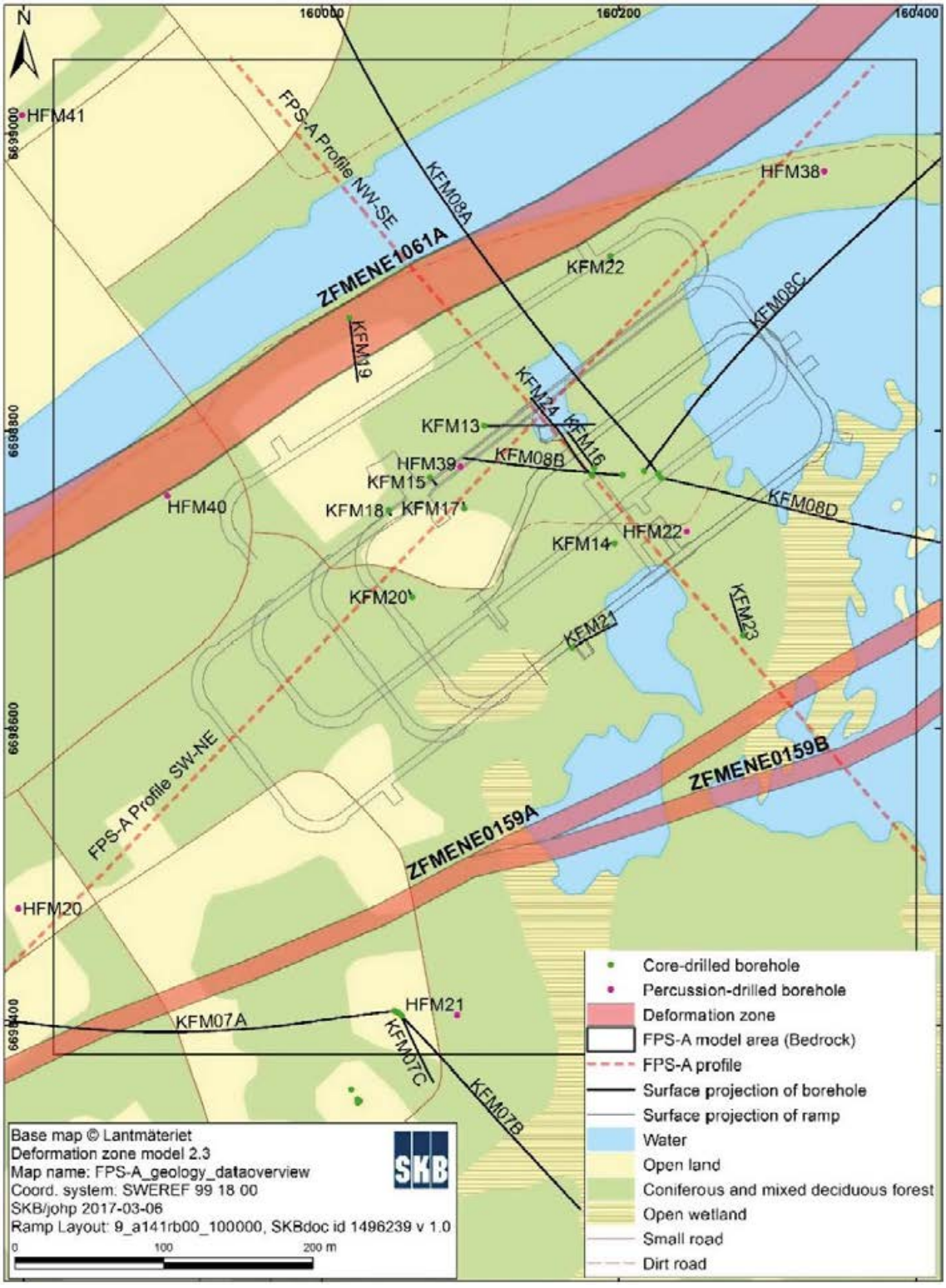

Figure A1-1. *Map showing steeply dipping deformation zones and bedrock boreholes considered in the geoscientific descriptions of the bedrock in proximity of the ramp and shafts of the planned repository for spent nuclear fuel (solid black line).*

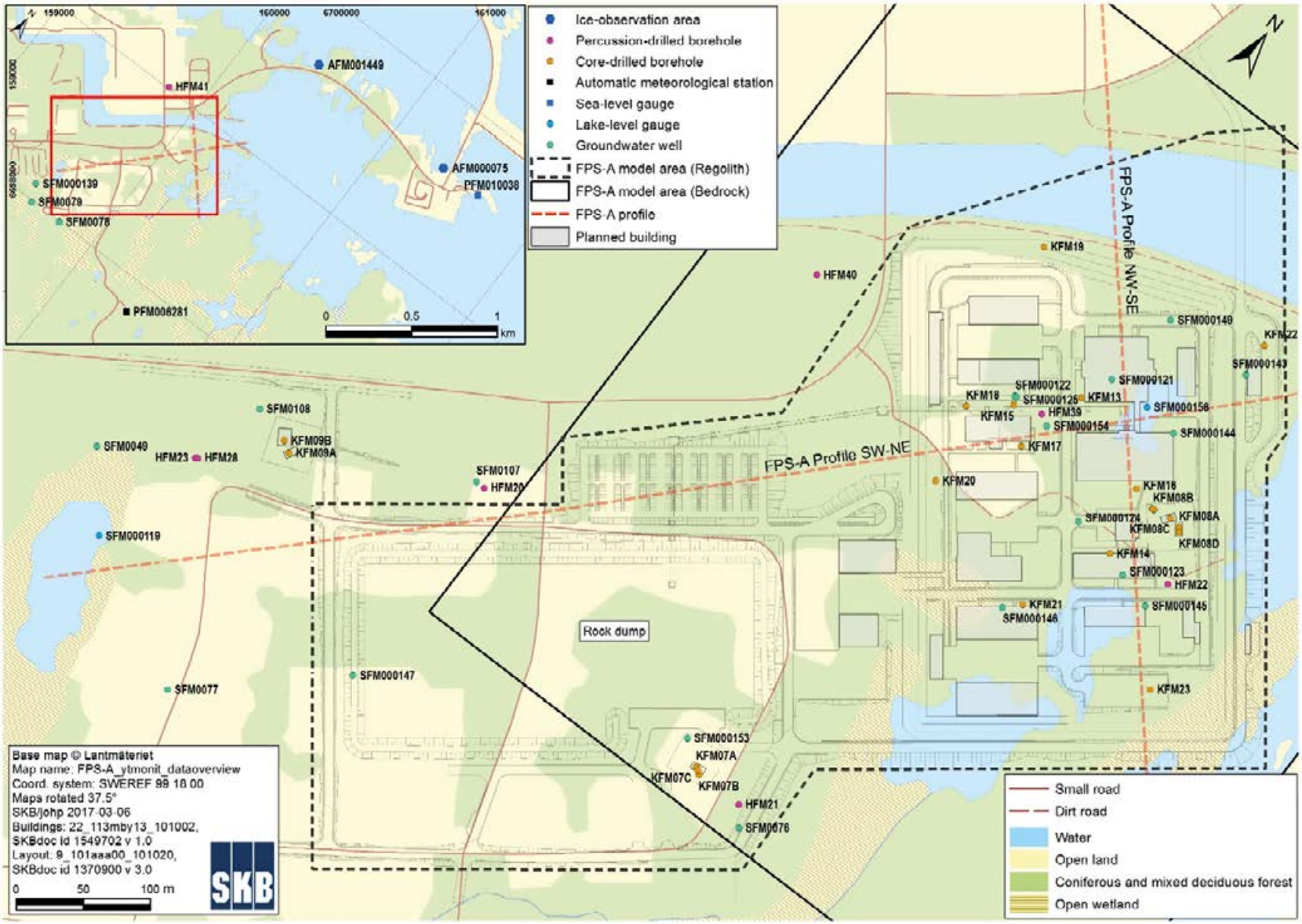

Figure A1-2. *Map showing planned buildings and rock dump together with the present-day land use and boreholes used for monitoring of groundwater levels. The solid and dashed black lines represent the model areas considered in the geoscientific descriptions of the bedrock and the regolith, respectively.*

Appendix B

WellCAD plots for boreholes KFM07A–7C, KFM08A–8D, KFM09A–9B, HFM20–23, HFM28 and HFM38

KFM07A – 1/6

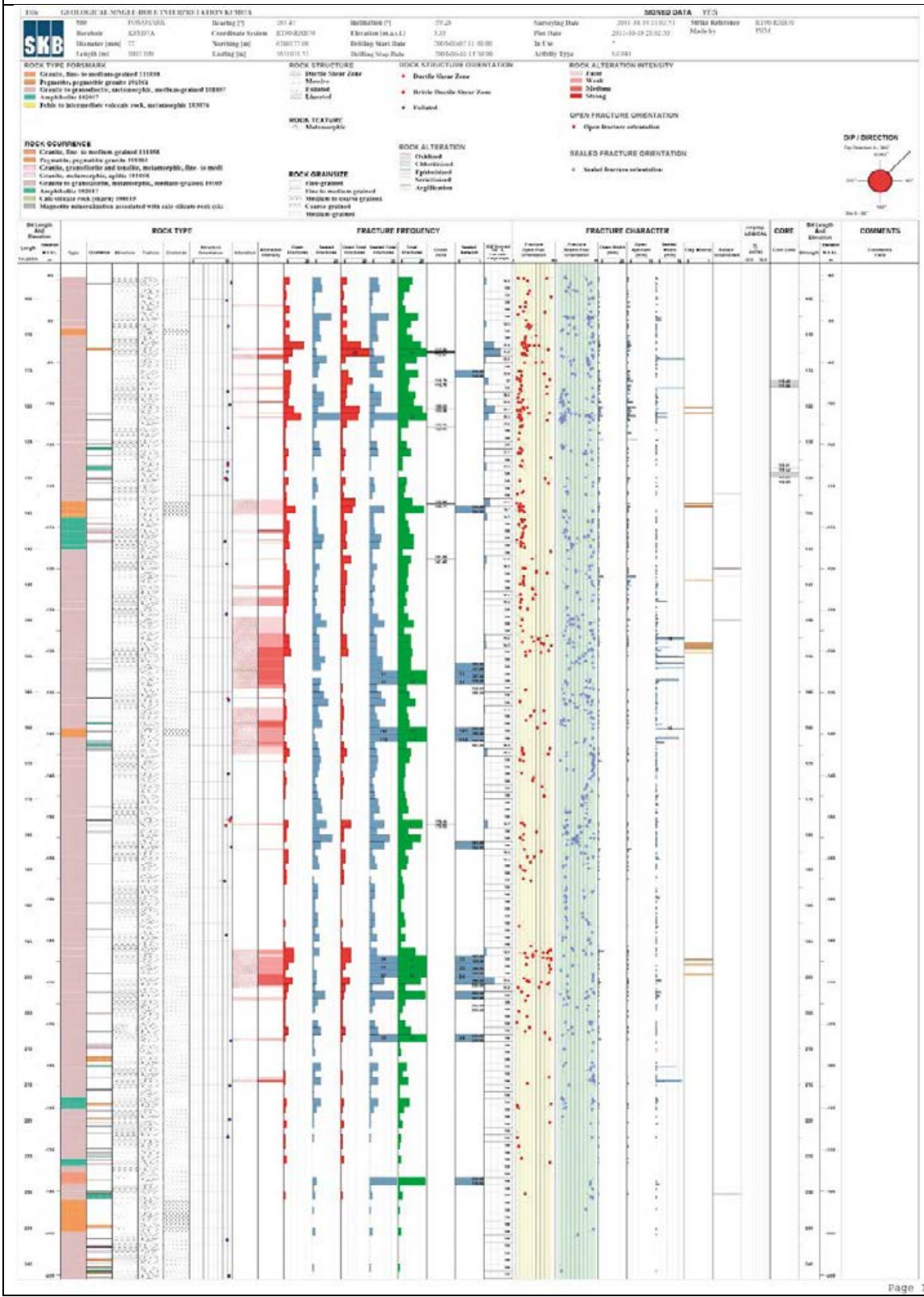

KFM07A – 2/6

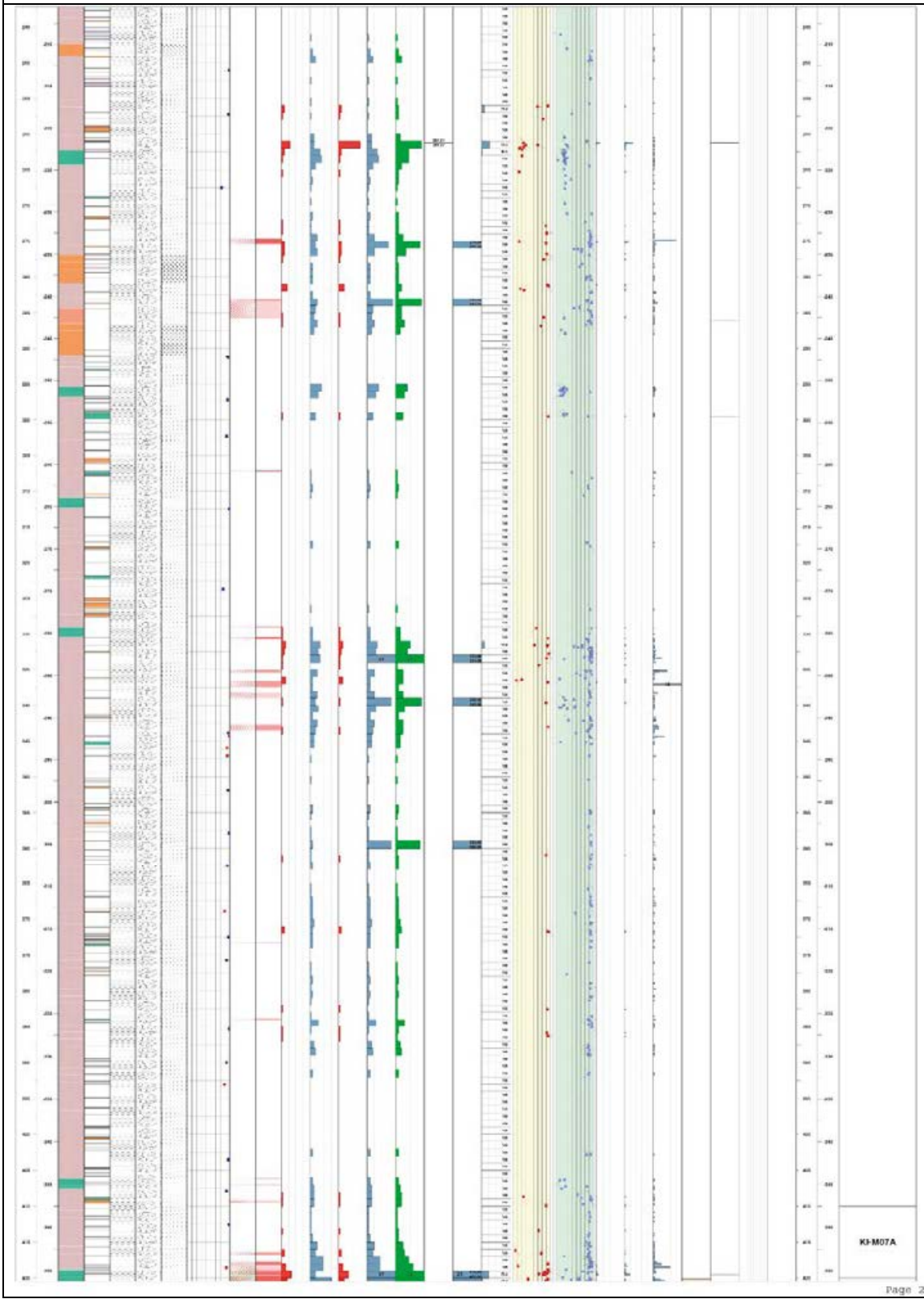

KFM07A – 3/6

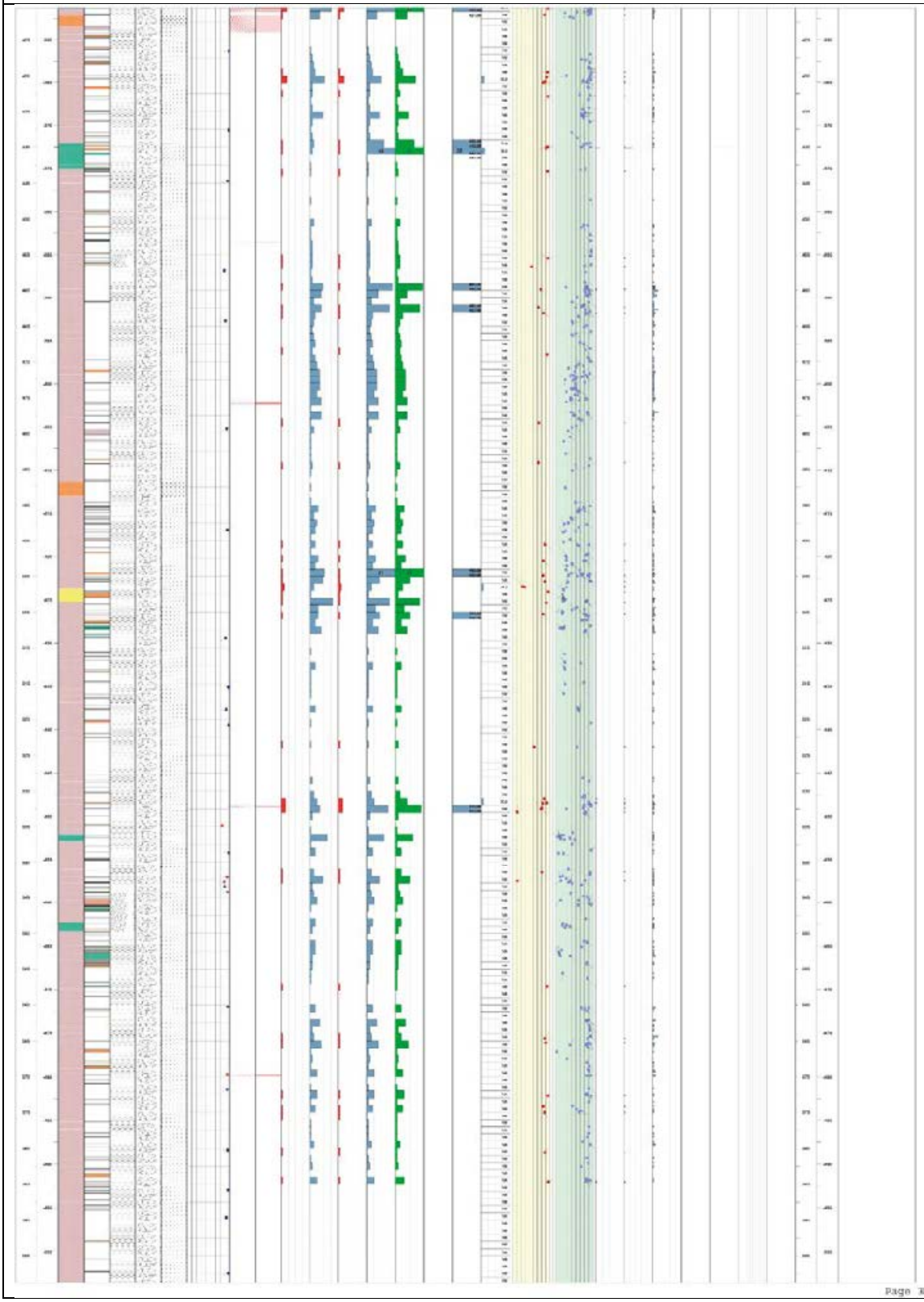

KFM07A – 4/6

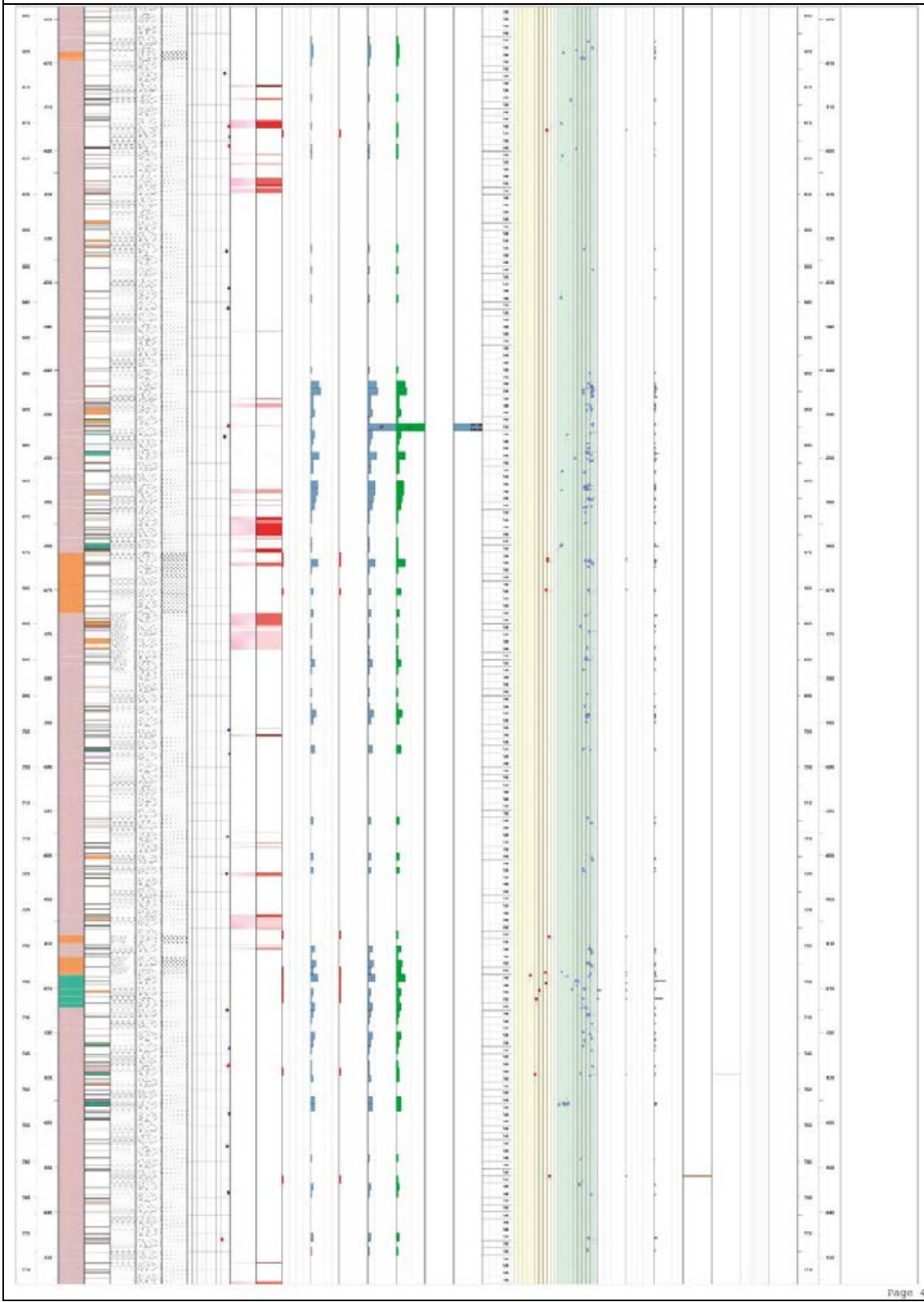

KFM07A – 5/6

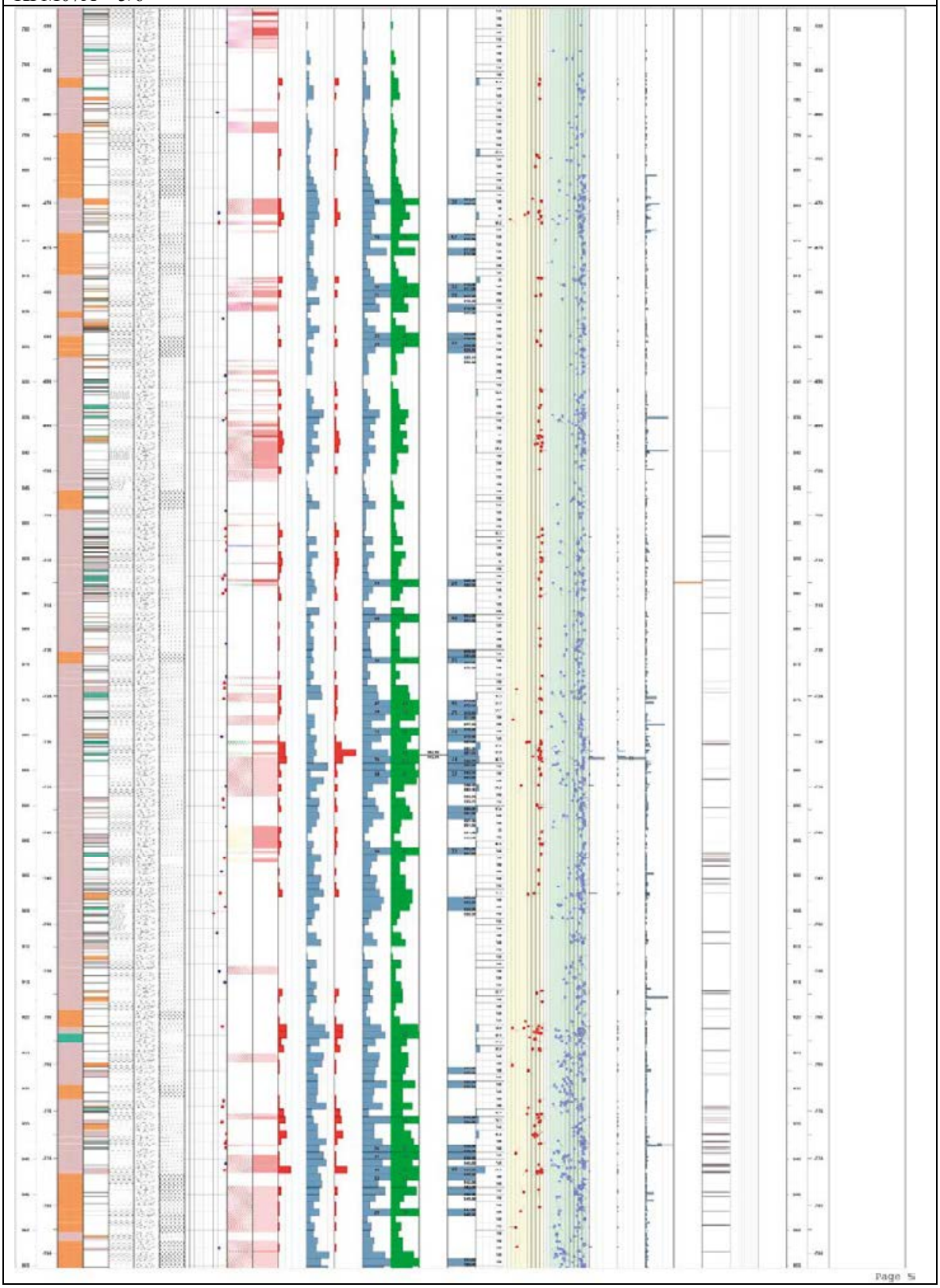

KFM07A – 6/6

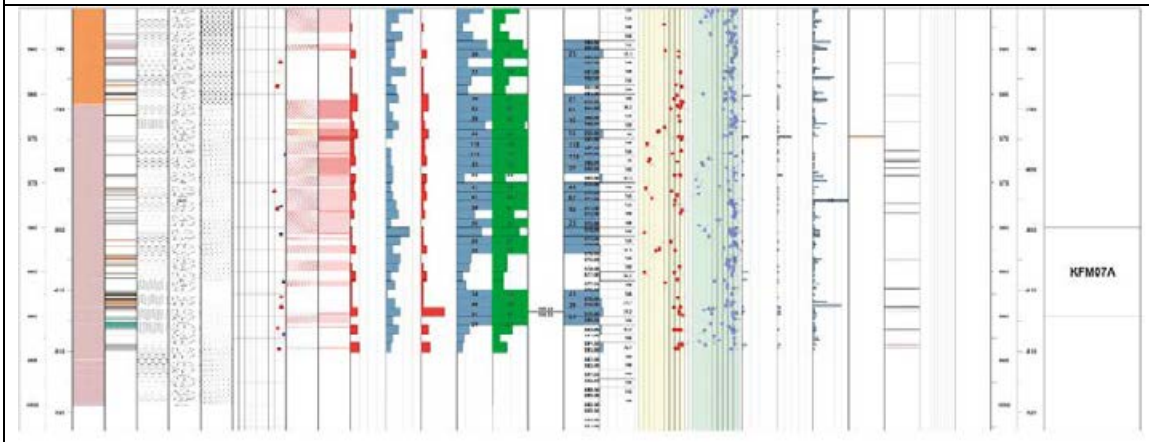

KFM07B – 1/2

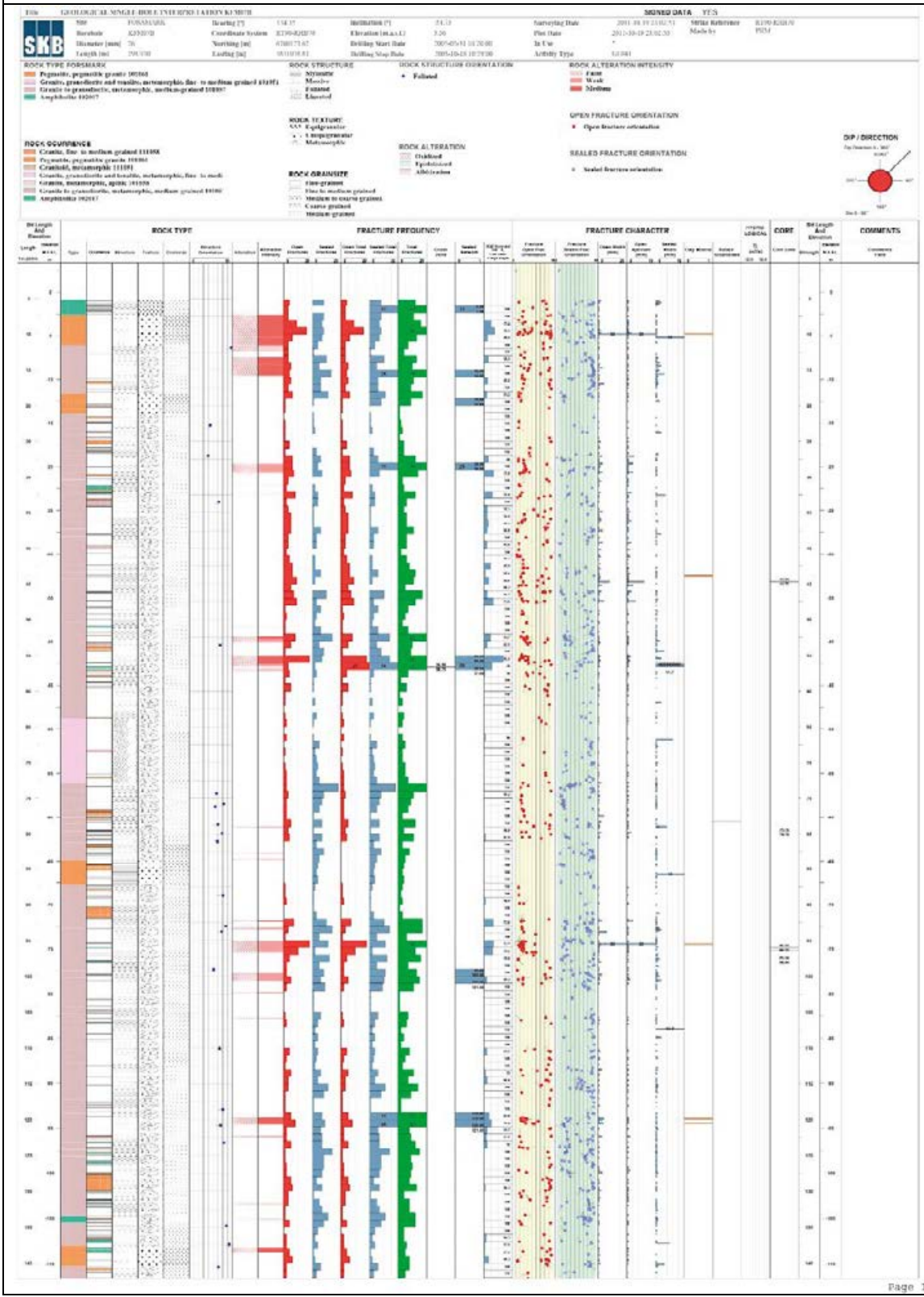
SKB
ROCK TYPE
FRACTURE FREQUENCY
FRACTURE CHARACTER
CORE
COMMENTS
Page 1

KFM07B – 2/2

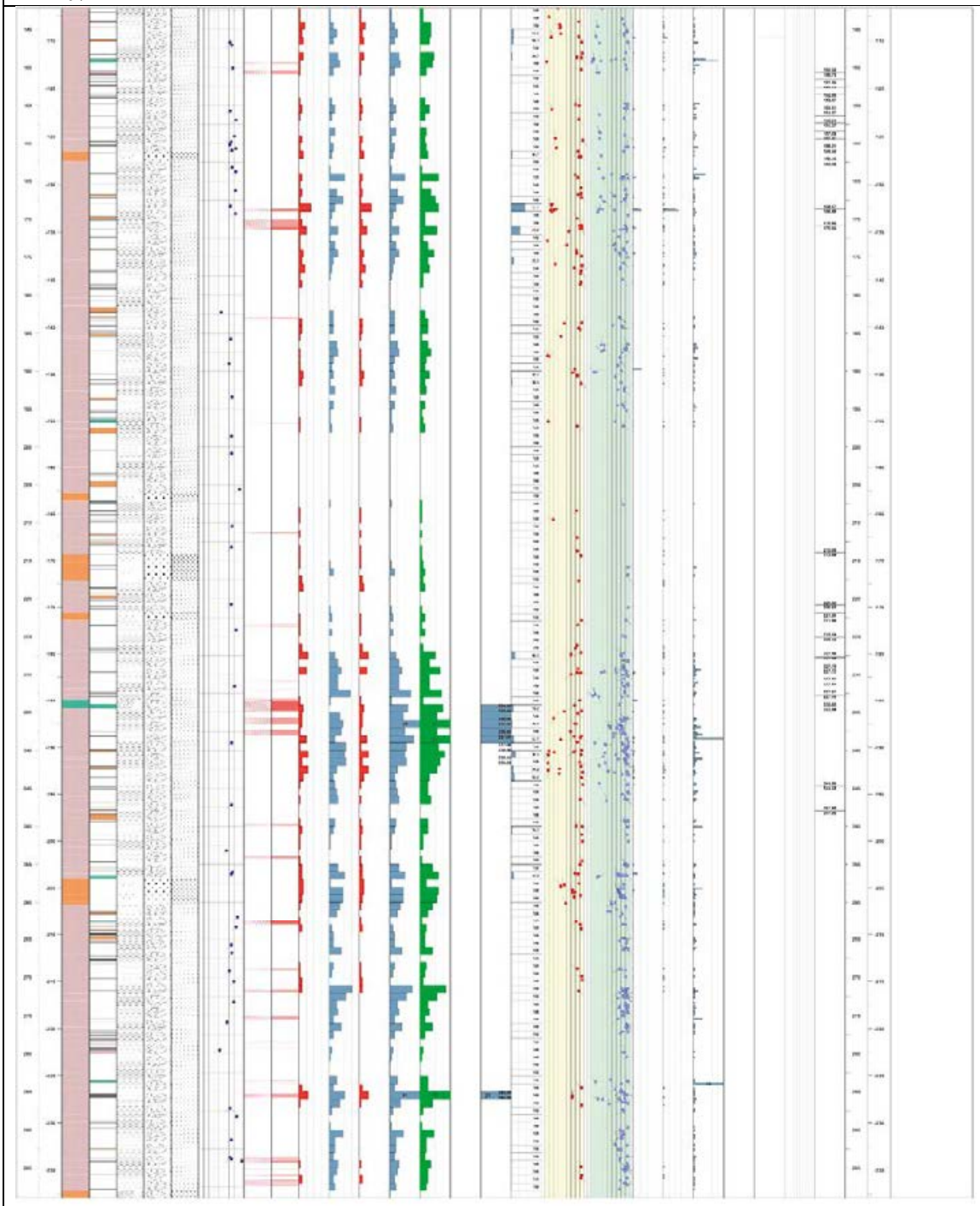

Page 2

KFM07C – 1/3

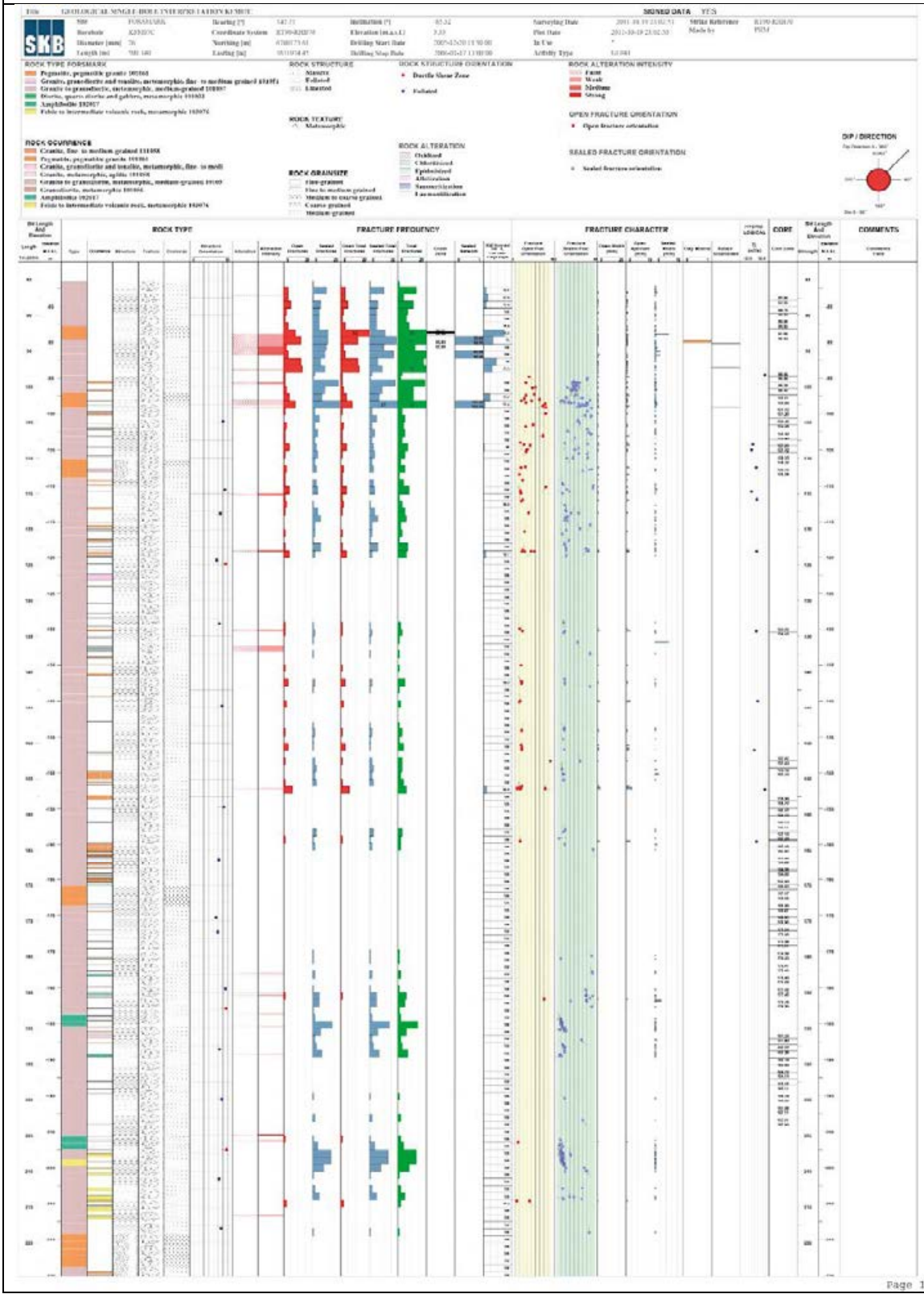
SKB
SIGNED DATA
ROCK TYPE FORSMARK
ROCK STRUCTURE
ROCK STRUCTURE ORIENTATION
ROCK ALTERATION INTENSITY
OPEN FRACTURE ORIENTATION
SEALED FRACTURE ORIENTATION
DIP / DIRECTION
ROCK TEXTURE
ROCK GRAINSIZE
ROCK ALTERATION
ROCK OCCURRENCE
ROCK TYPE
FRACTURE FREQUENCY
FRACTURE CHARACTER
CORE
COMMENTS
Page 1

KFM07C – 2/3

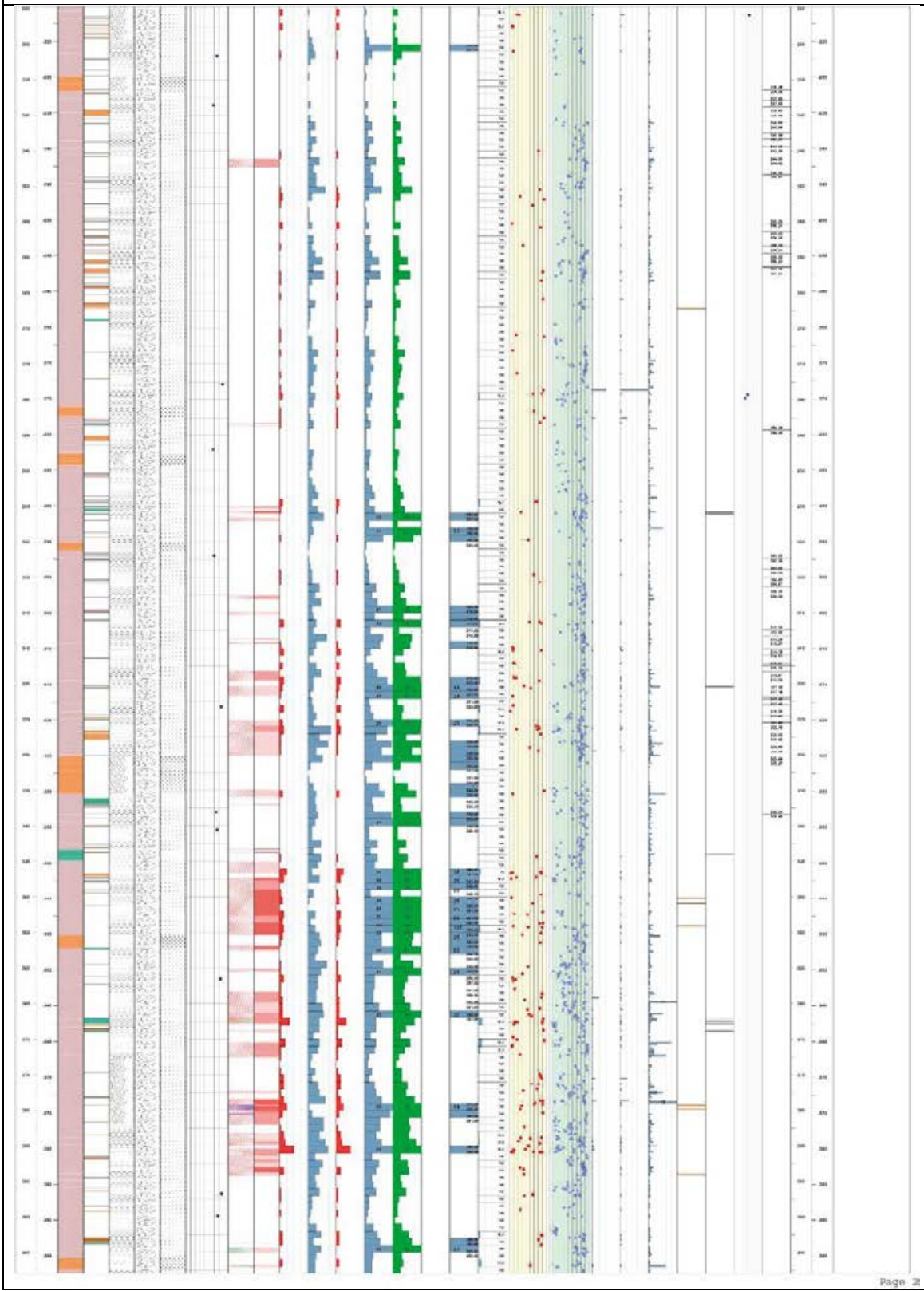

KFM07C – 3/3

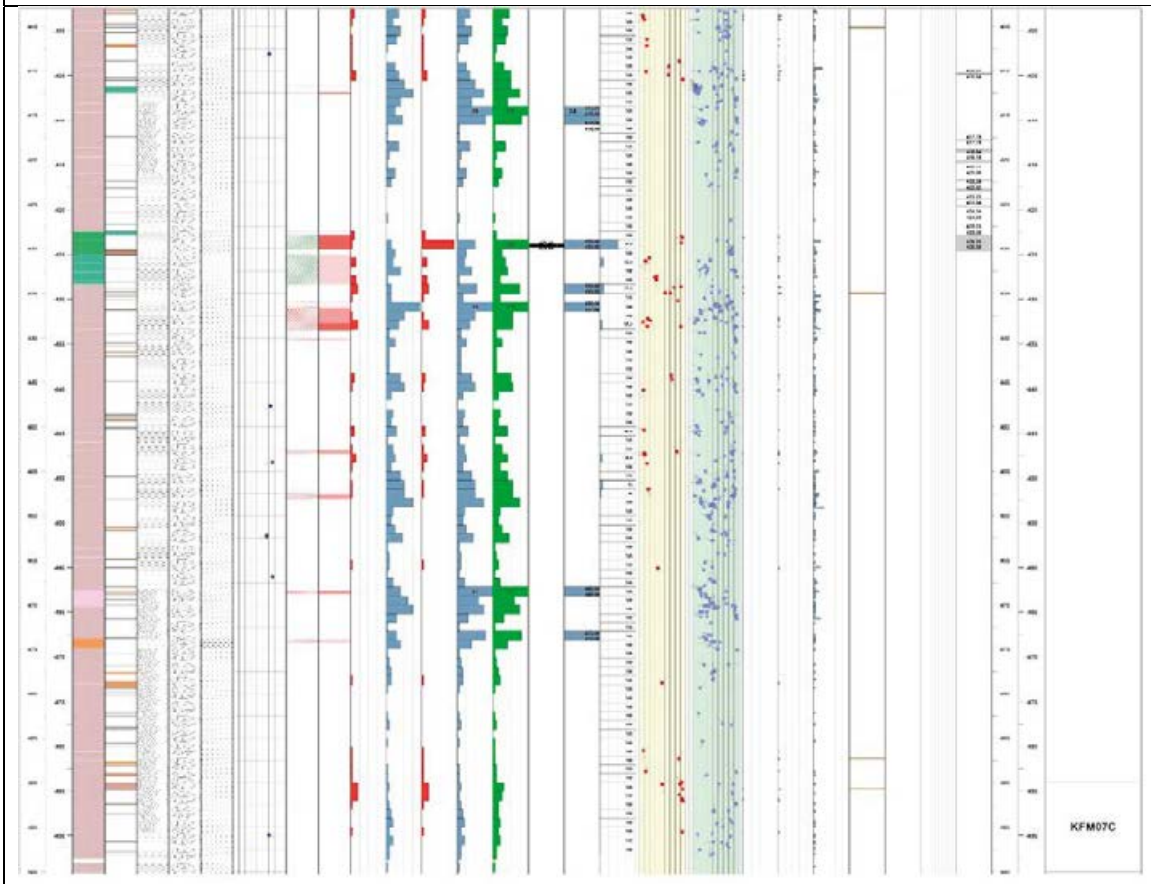

KFM08A – 1/6

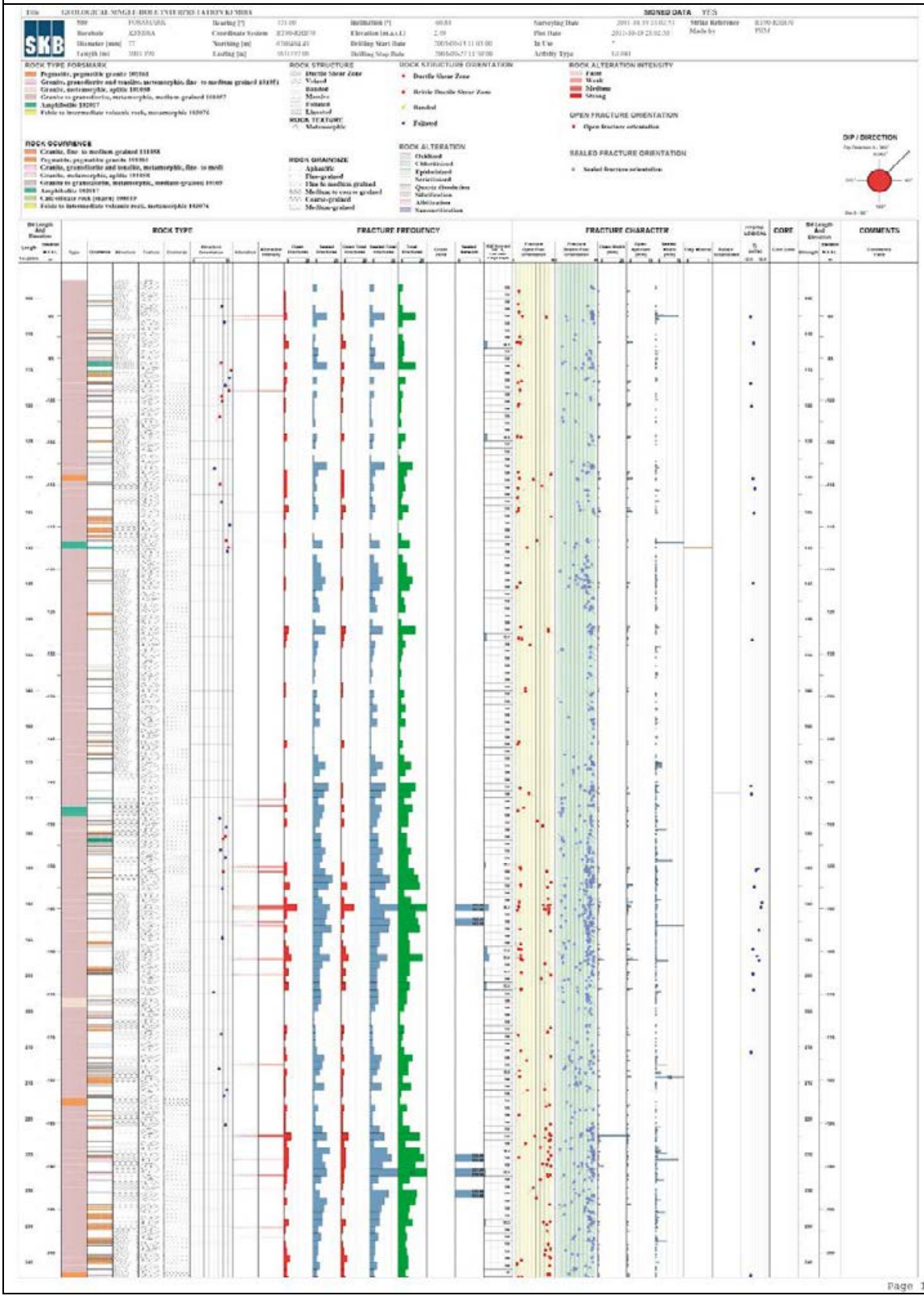
SKB
SIGNED DATA YES
ROCK TYPE FORSMARK
ROCK STRUCTURE
ROCK STRUCTURE ORIENTATION
ROCK ALTERATION INTENSITY
OPEN FRACTURE ORIENTATION
SEALED FRACTURE ORIENTATION
DIP / DIRECTION
ROCK OCCURRENCE
ROCK TEXTURE
ROCK GRAINSIZE
ROCK ALTERATION
ROCK TYPE
FRACTURE FREQUENCY
FRACTURE CHARACTER
CORE
COMMENTS
Page 1

KFM08A – 2/6

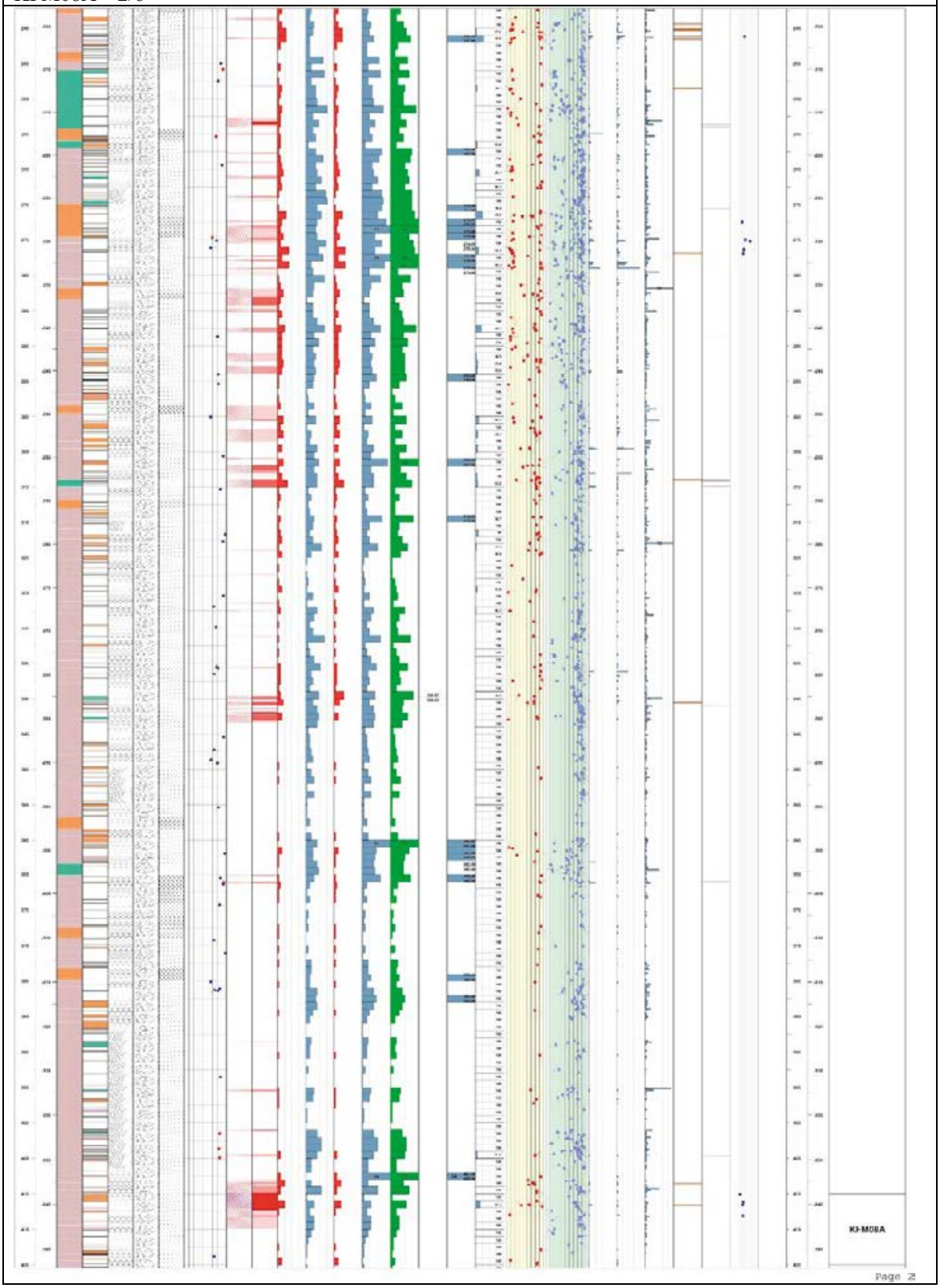

KFM08A – 3/6

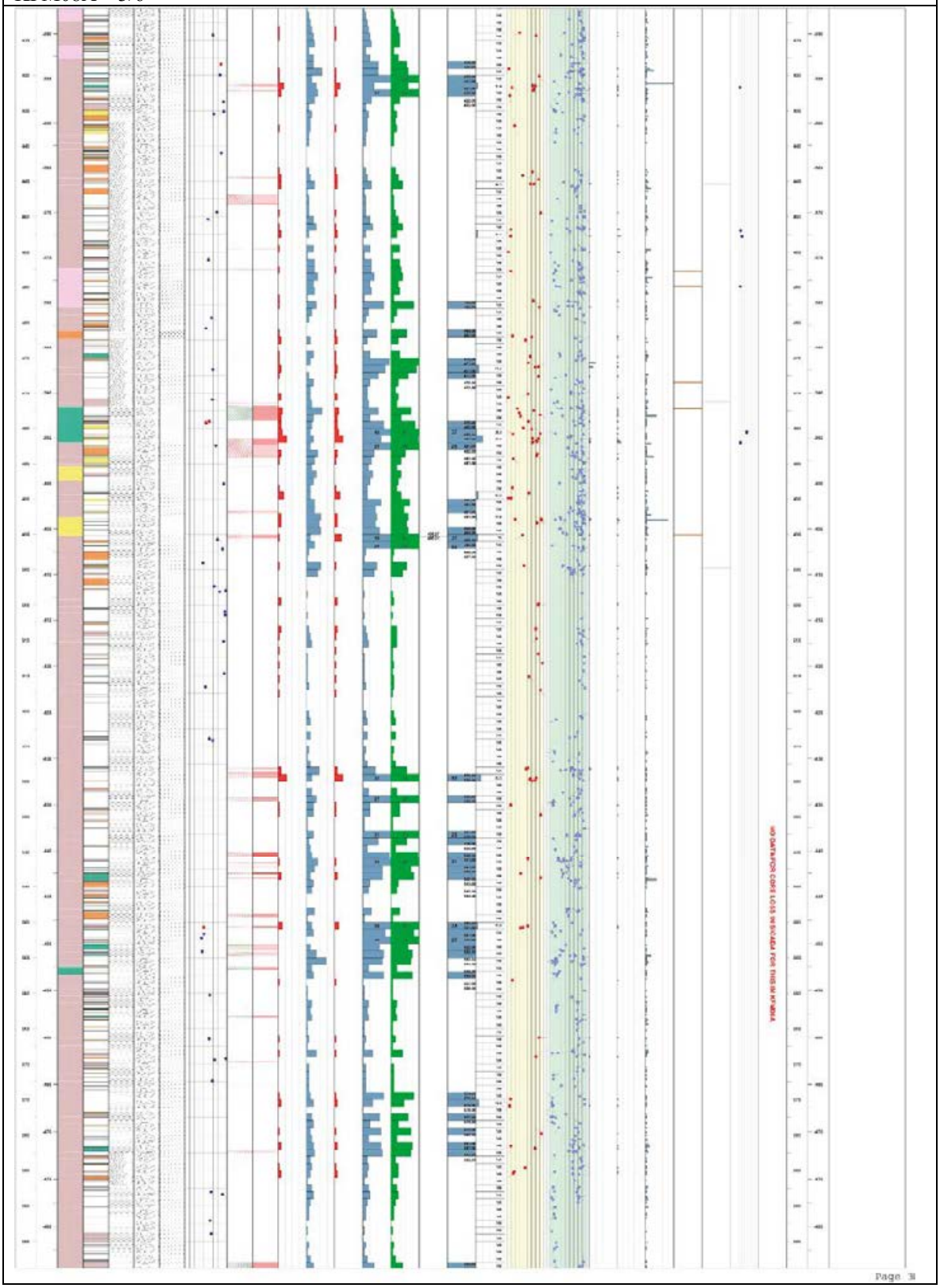

KFM08A – 4/6

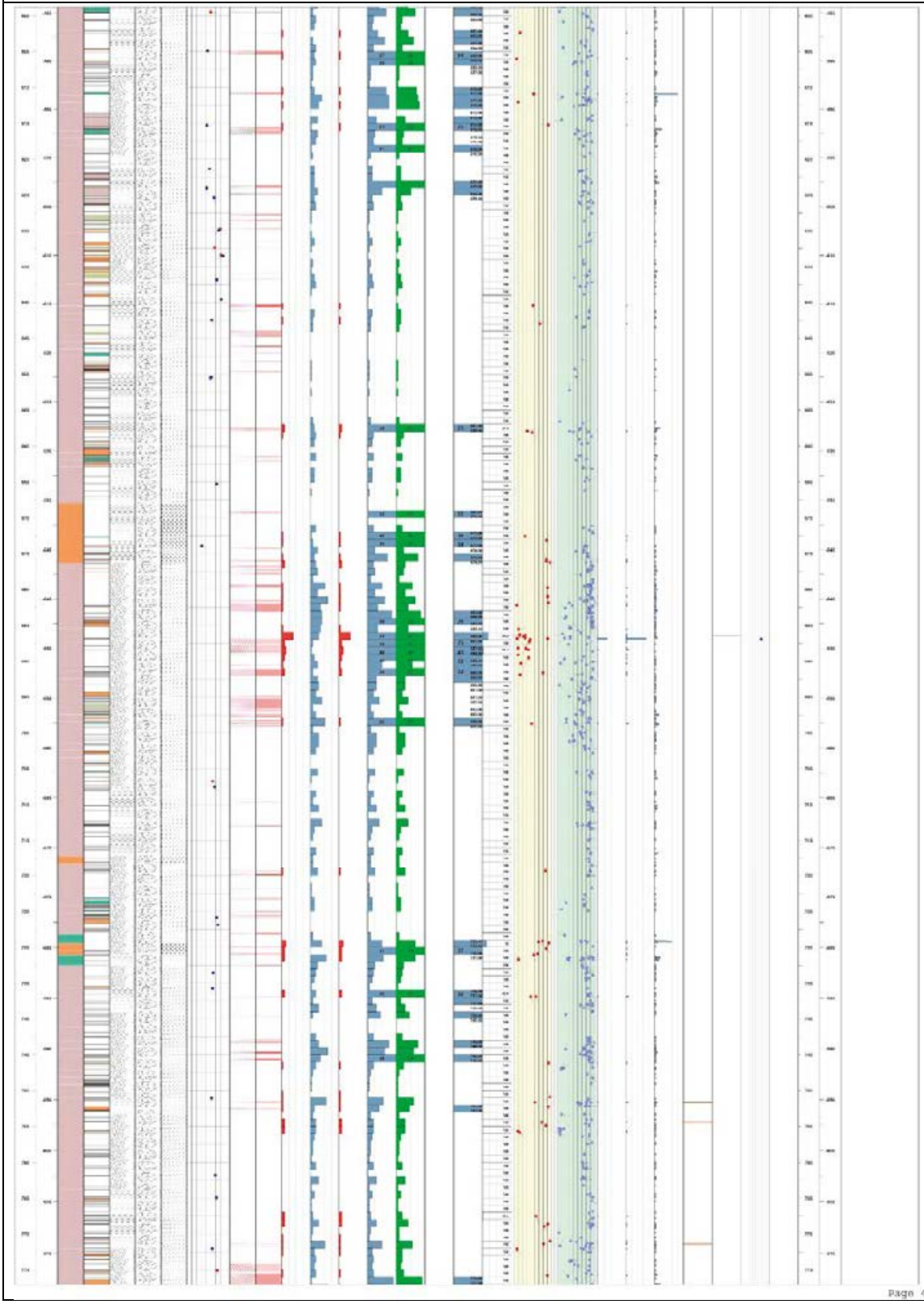

KFM08A – 5/6

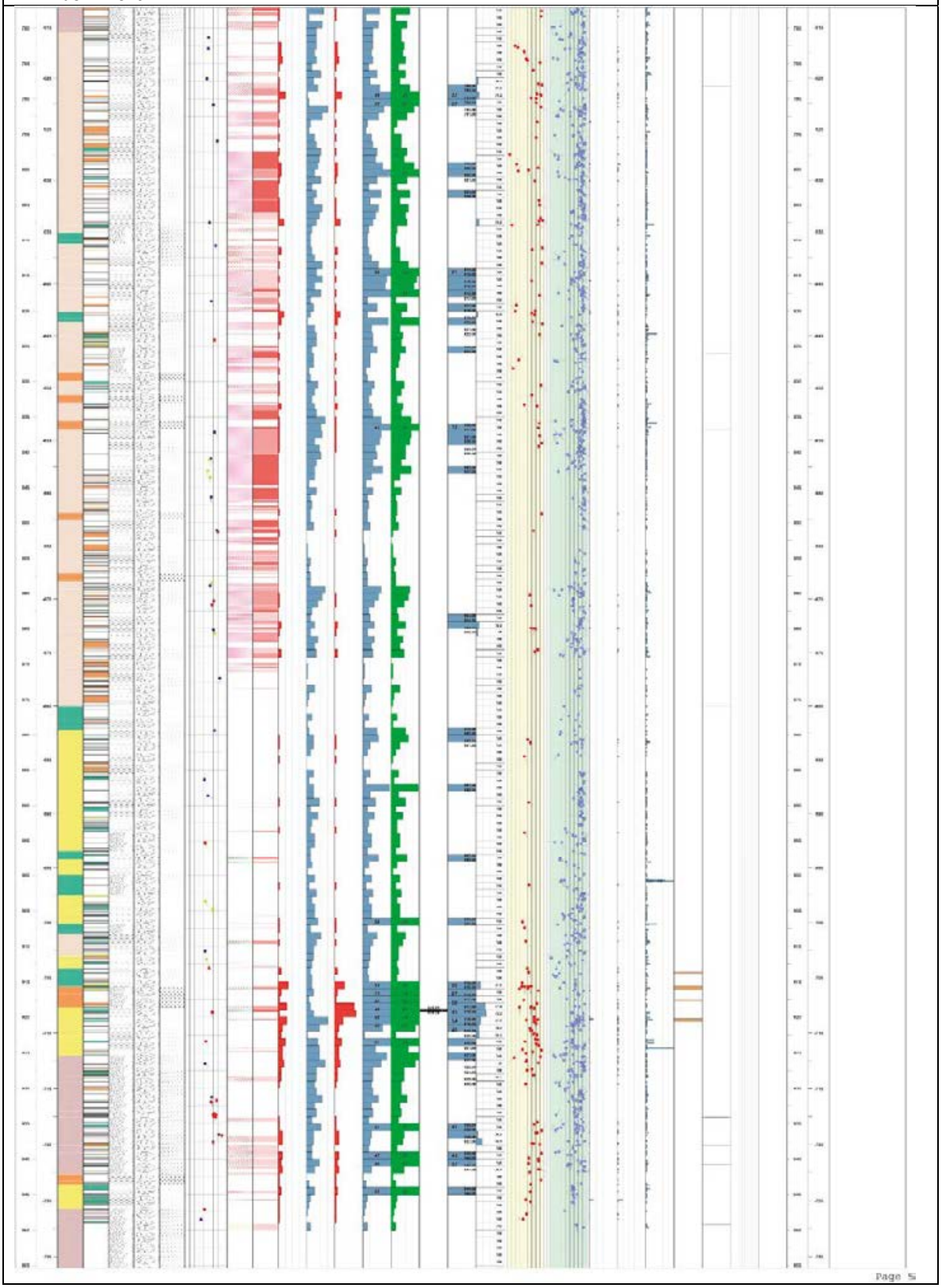

KFM08A – 6/6

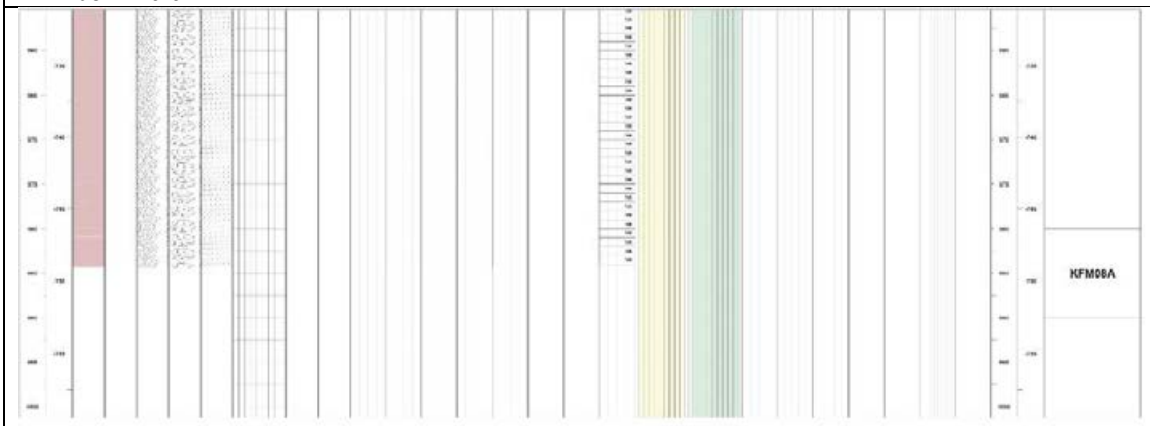

KFM08B – 1/2

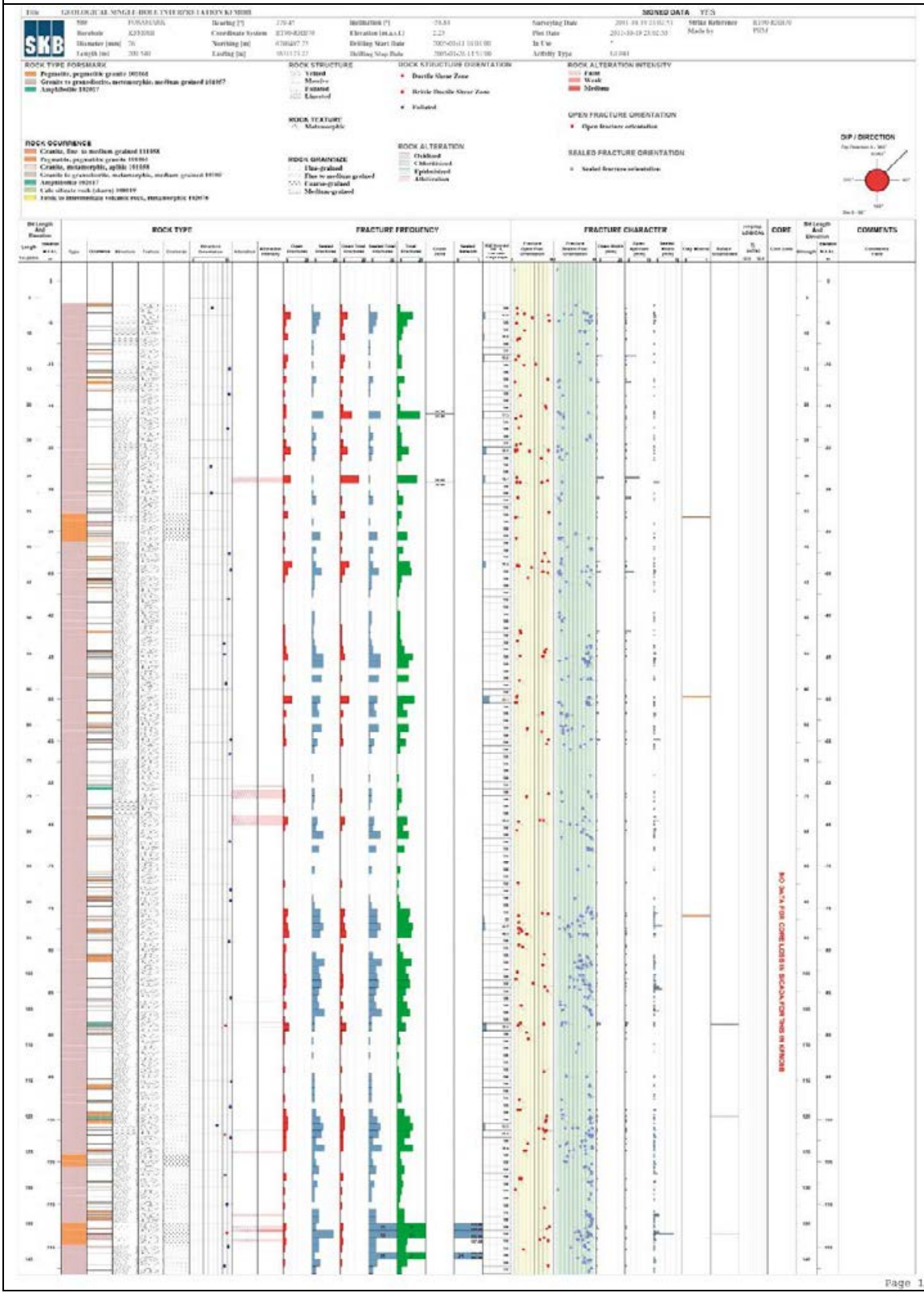
SKB
SIGNED DATA YES
ROCK TYPE FORSMARK
ROCK STRUCTURE
ROCK STRUCTURE ORIENTATION
ROCK ALTERATION INTENSITY
ROCK TEXTURE
OPEN FRACTURE ORIENTATION
ROCK OCCURRENCE
ROCK GRAINSIZE
ROCK ALTERATION
SEALED FRACTURE ORIENTATION
DIP / DIRECTION
ROCK TYPE
FRACTURE FREQUENCY
FRACTURE CHARACTER
CORE
COMMENTS
Page 1

KFM08B – 2/2

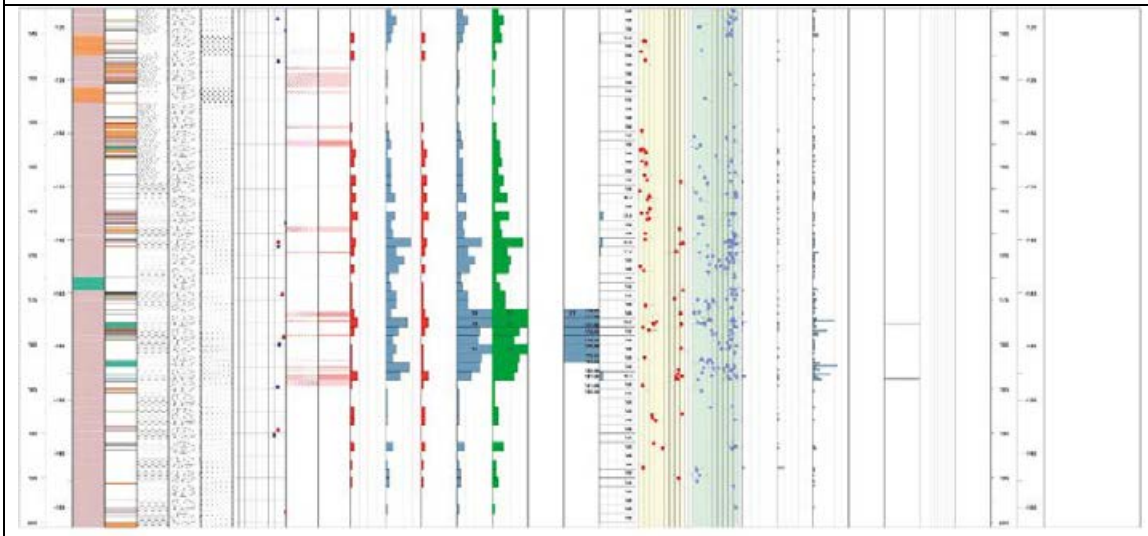

KFM08C – 1/5

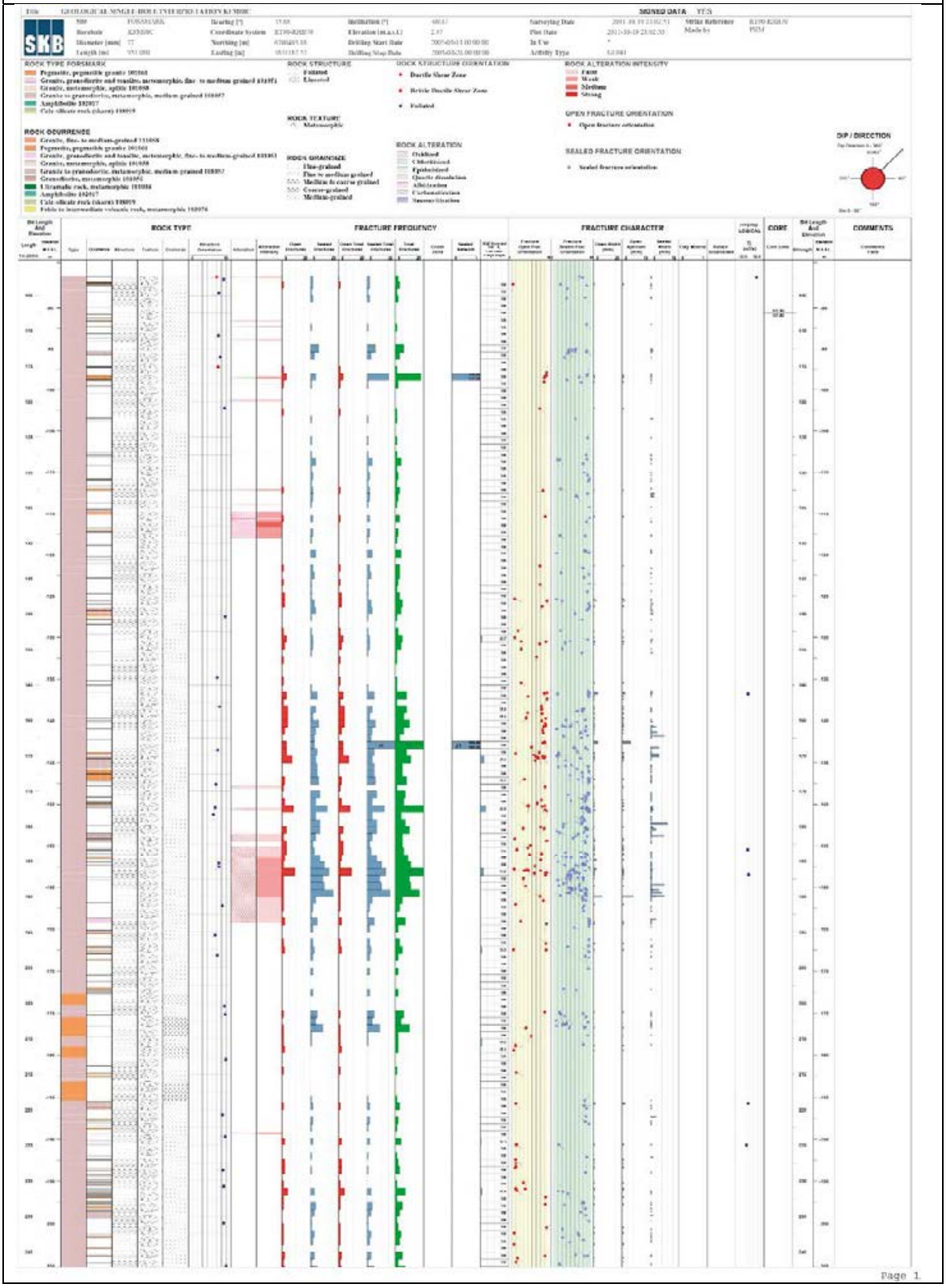
SKB
SIGNED DATA YES
ROCK TYPE FORSMARK
ROCK OCCURRENCE
ROCK STRUCTURE
ROCK STRUCTURE ORIENTATION
ROCK ALTERATION INTENSITY
OPEN FRACTURE ORIENTATION
SEALED FRACTURE ORIENTATION
DIP / DIRECTION
ROCK TEXTURE
ROCK GRAINSIZE
ROCK ALTERATION
ROCK TYPE
FRACTURE FREQUENCY
FRACTURE CHARACTER
CORE
COMMENTS
Page 1

KFM08C – 2/5

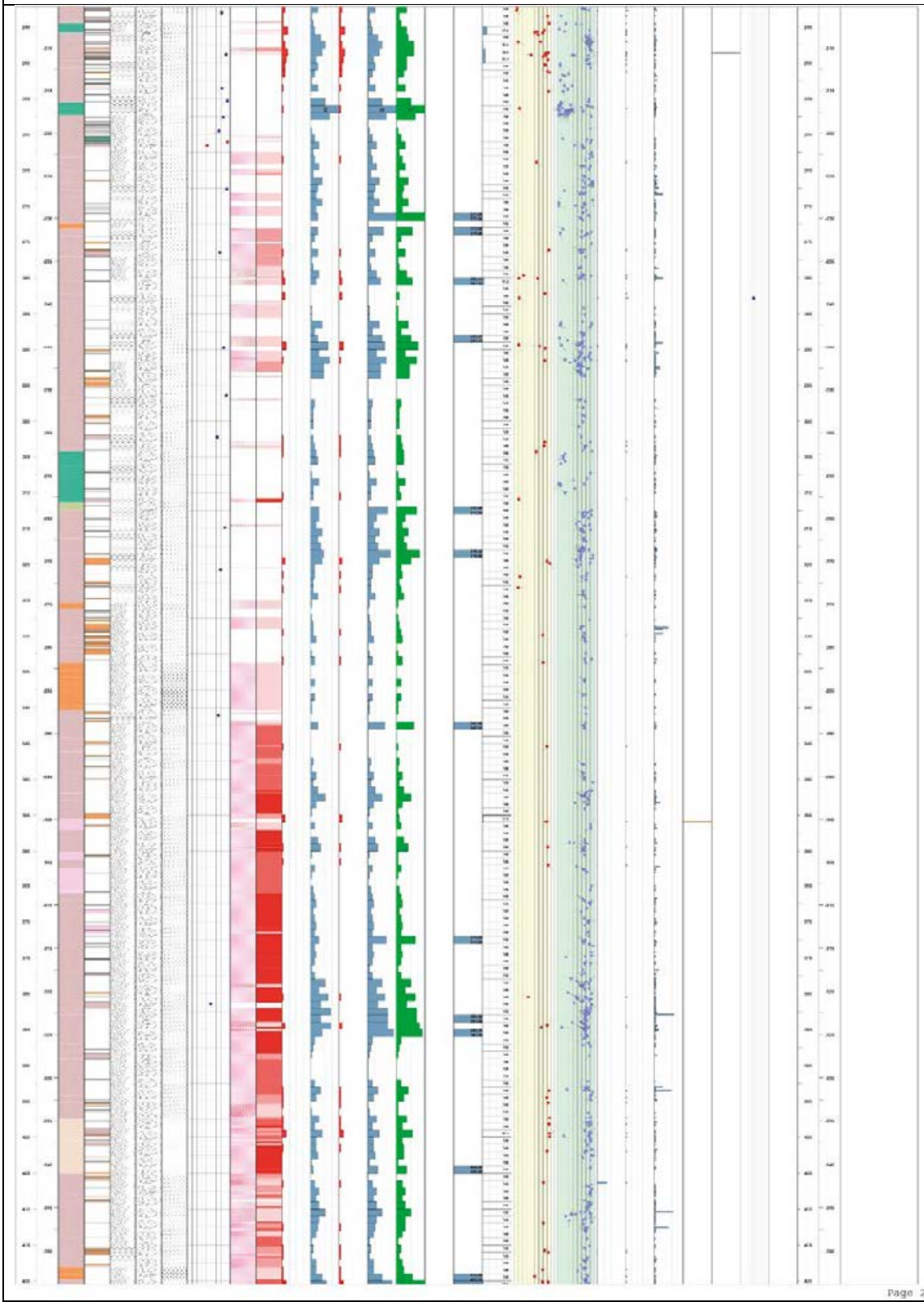

KFM08C – 3/5

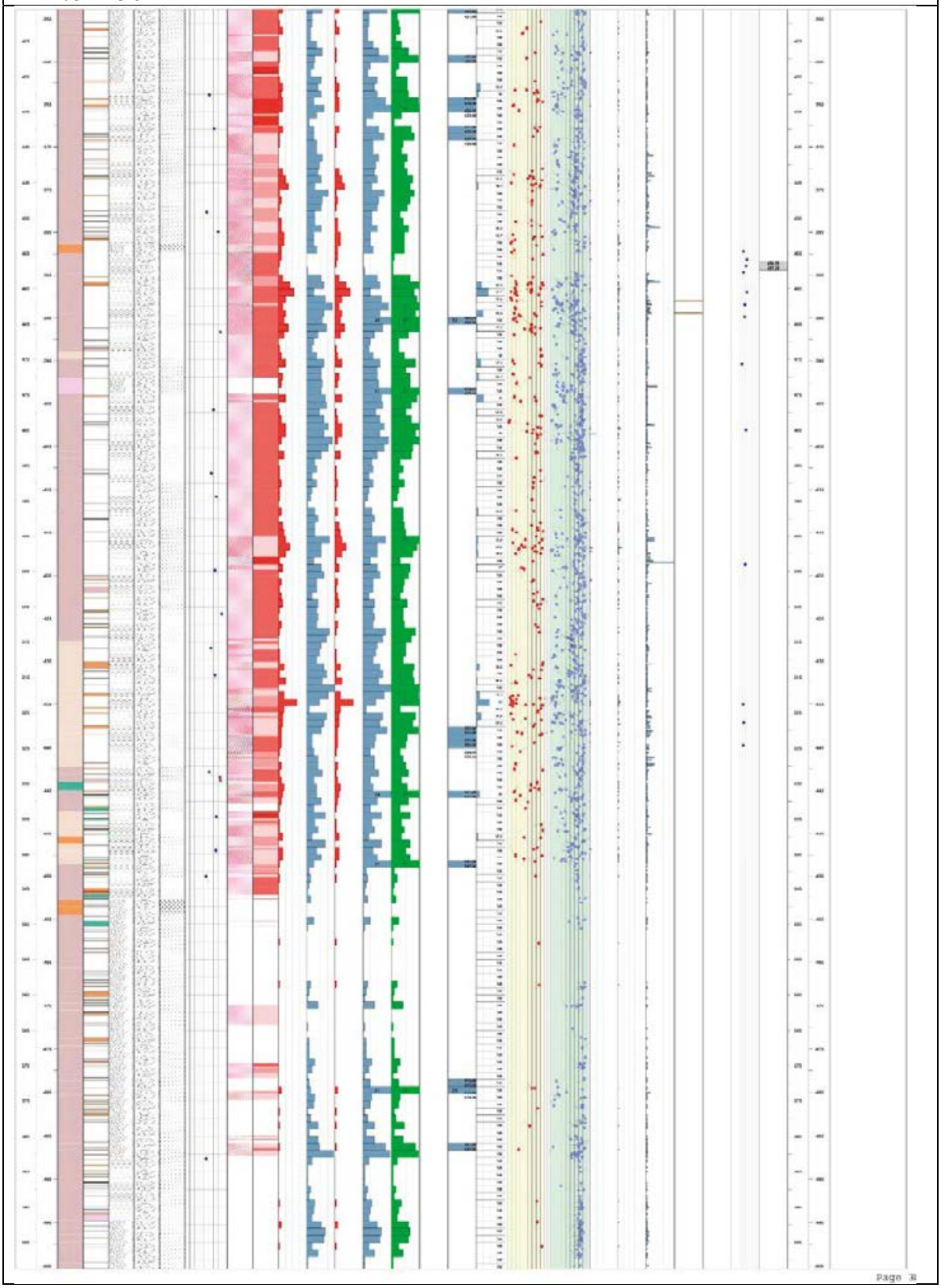

KFM08C – 4/5

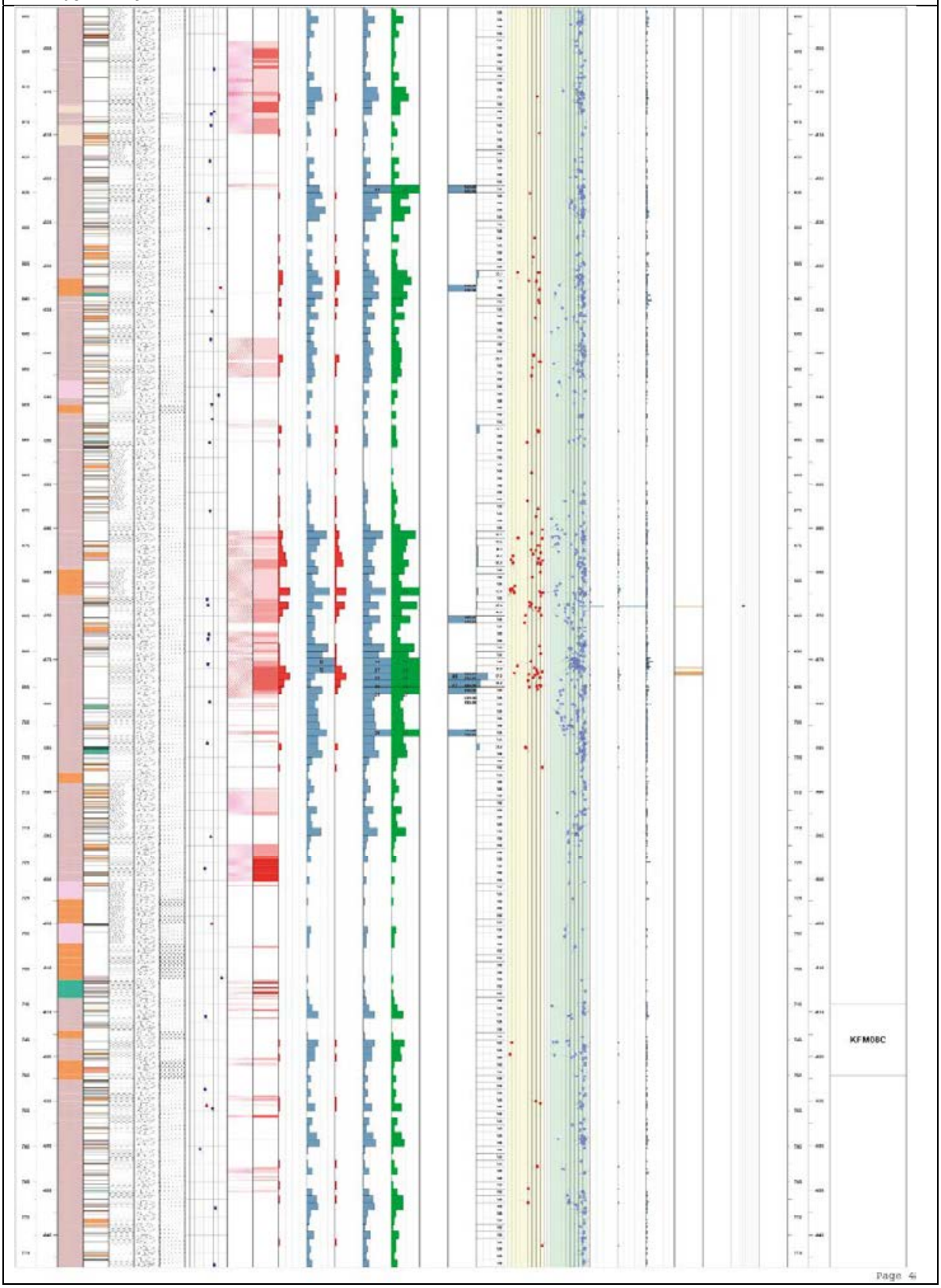

KFM08C – 5/5

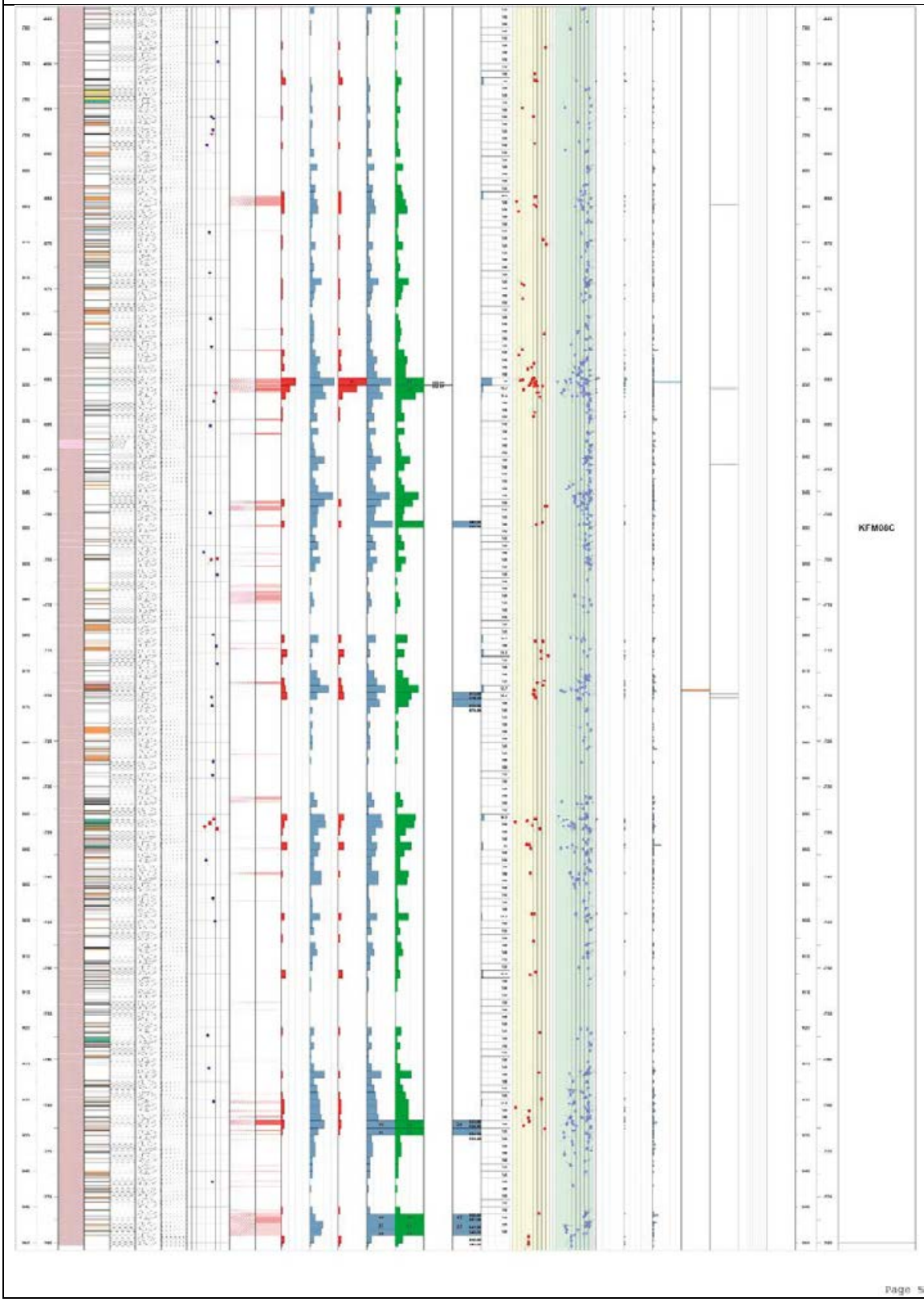

KFM08D – 1/6

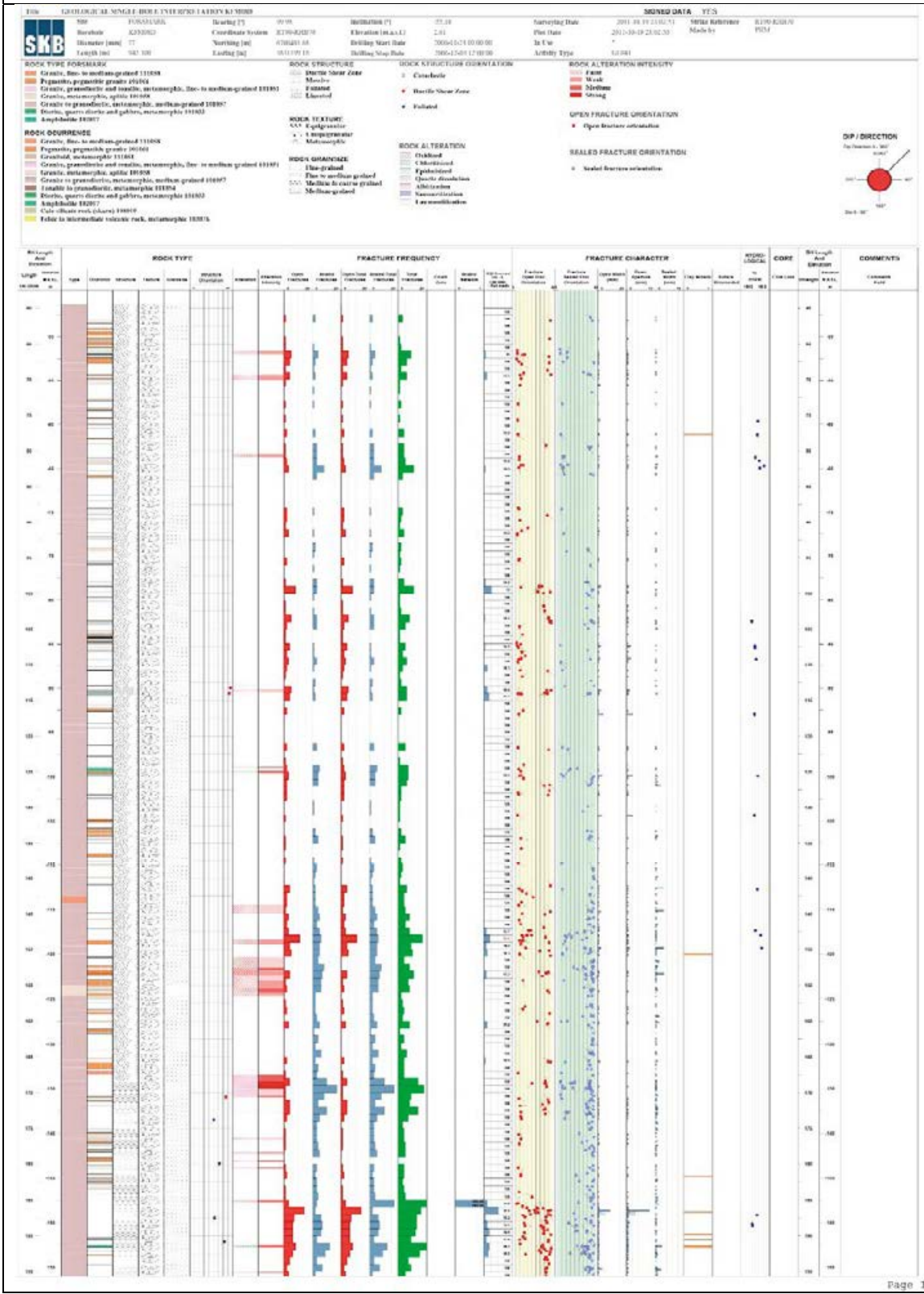
SKB
ROCK TYPE FORSMARK
ROCK OCCURRENCE
ROCK STRUCTURE
ROCK TEXTURE
ROCK GRAINSIZE
ROCK STRUCTURE ORIENTATION
ROCK ALTERATION
ROCK ALTERATION INTENSITY
OPEN FRACTURE ORIENTATION
SEALED FRACTURE ORIENTATION
DIP / DIRECTION
ROCK TYPE
FRACTURE FREQUENCY
FRACTURE CHARACTER
CORE
COMMENTS
Page 1

KFM08D – 2/6

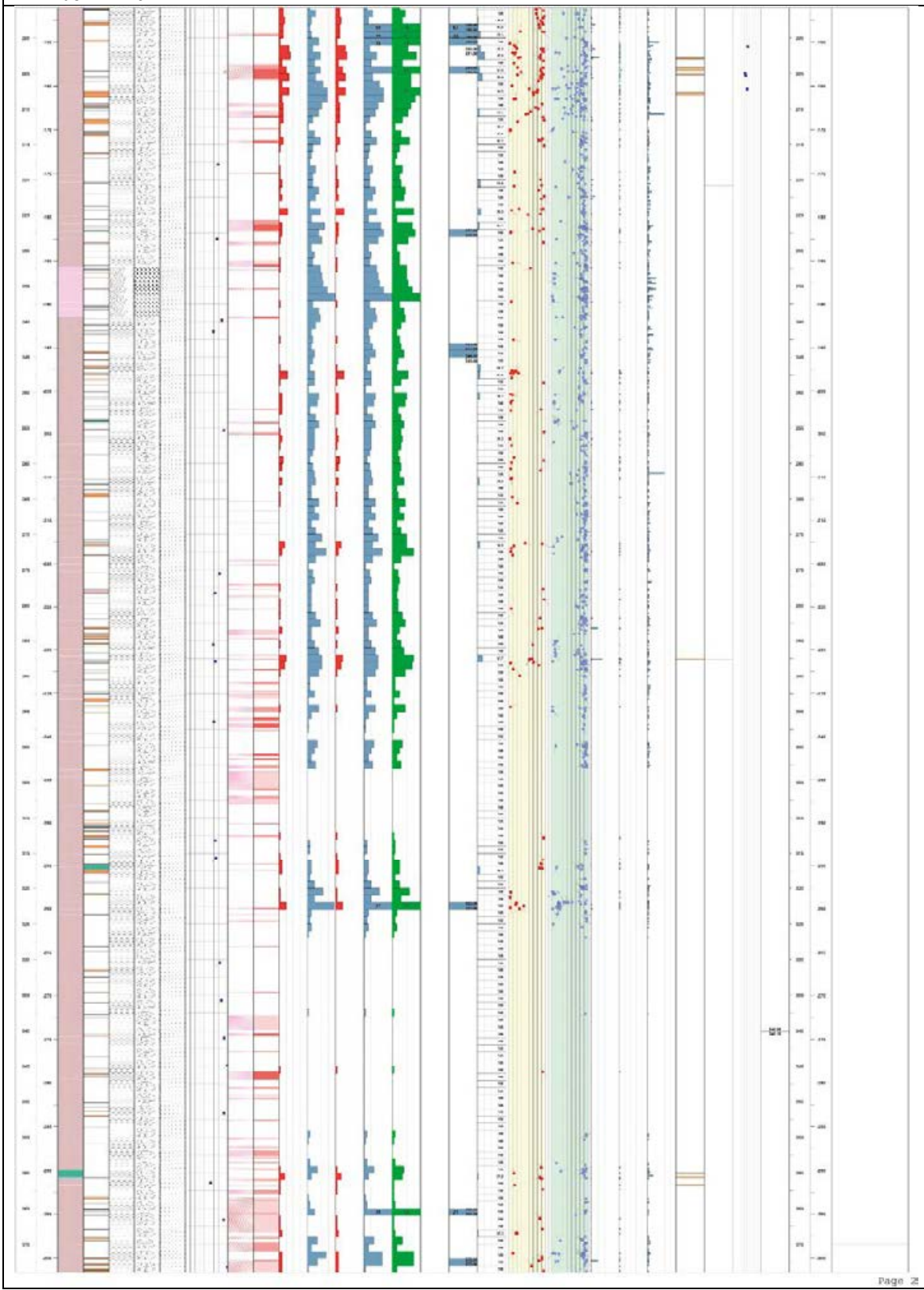

KFM08D – 3/6

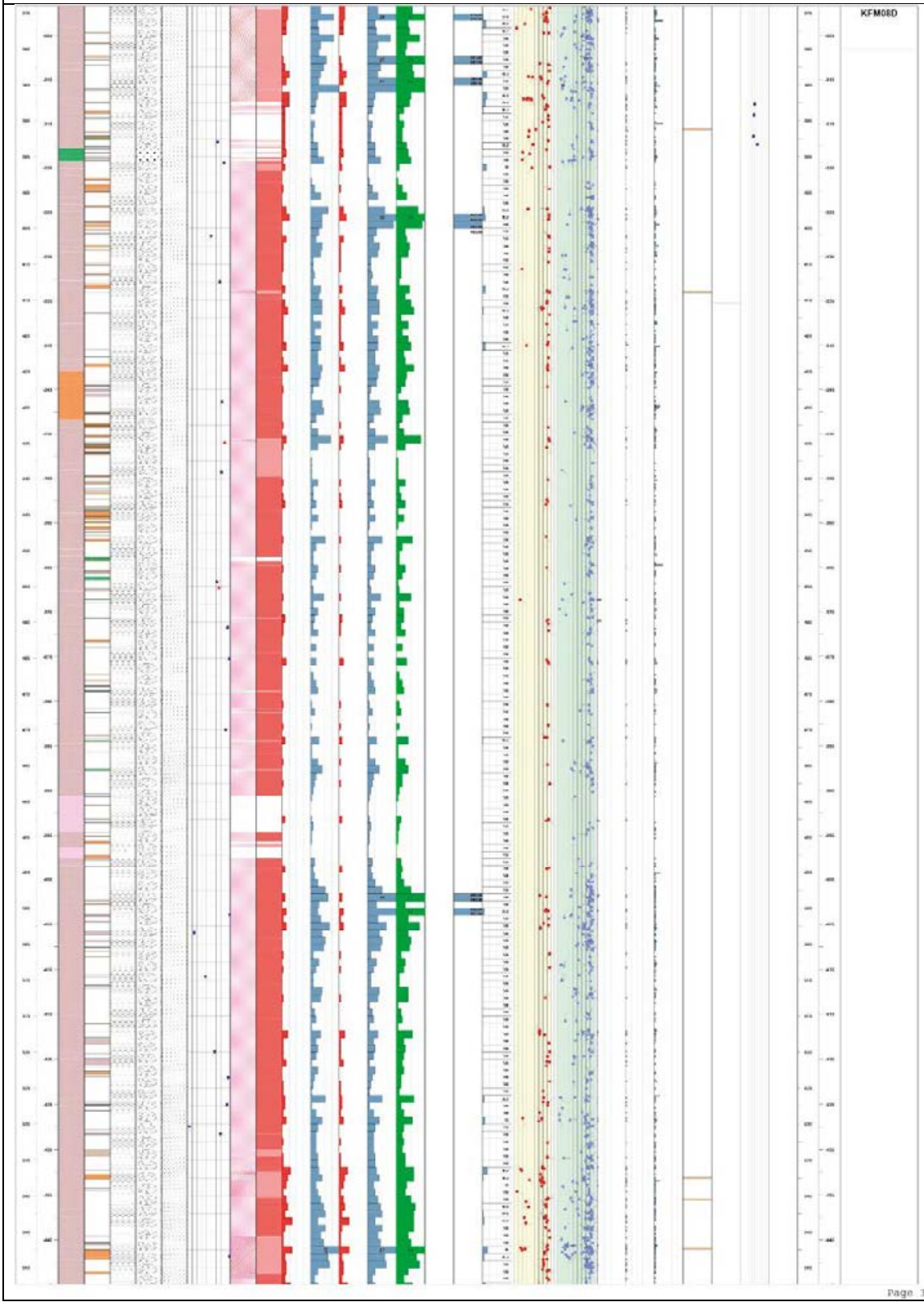

KFM08D – 4/6

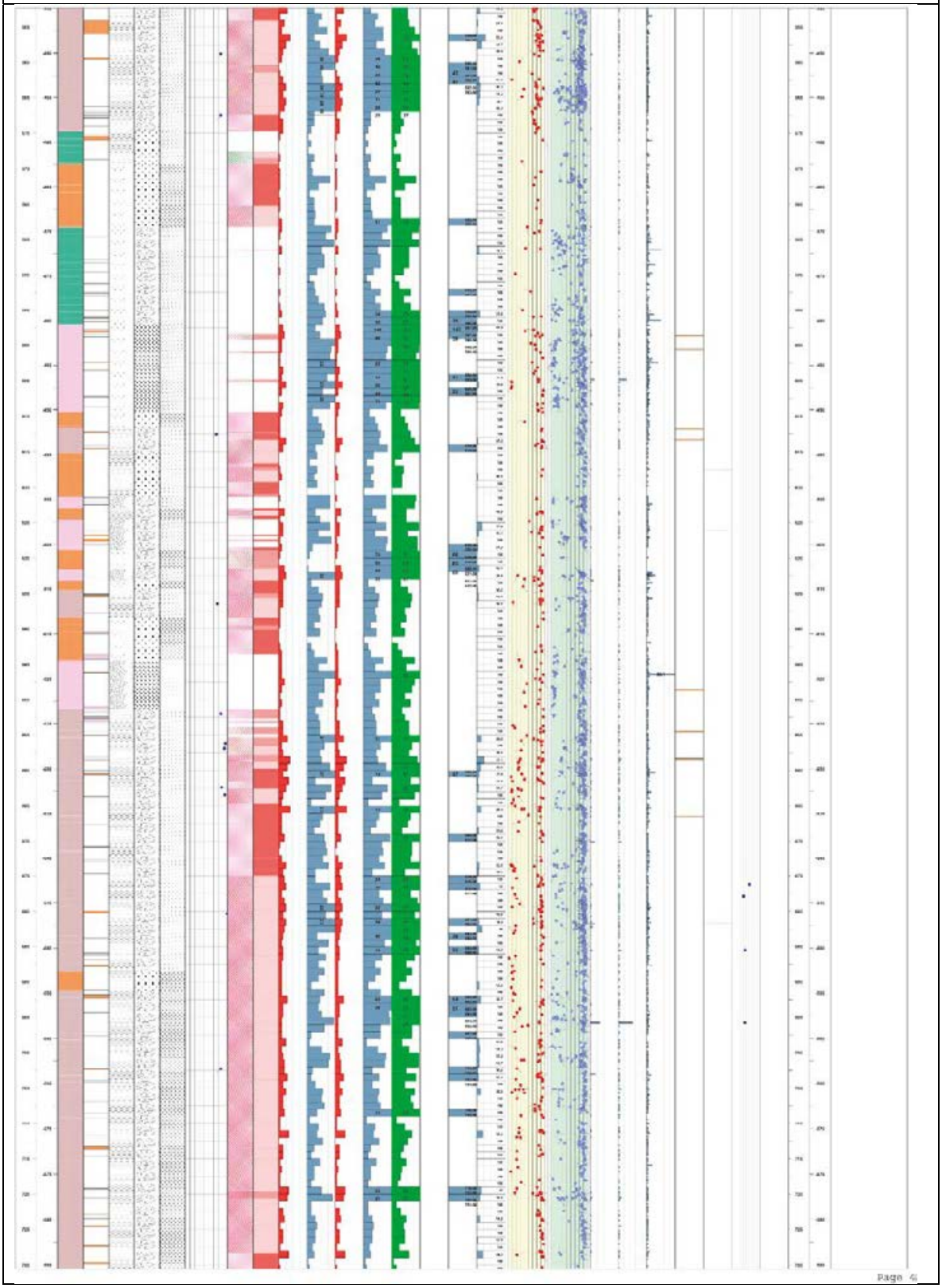

KFM08D – 5/6

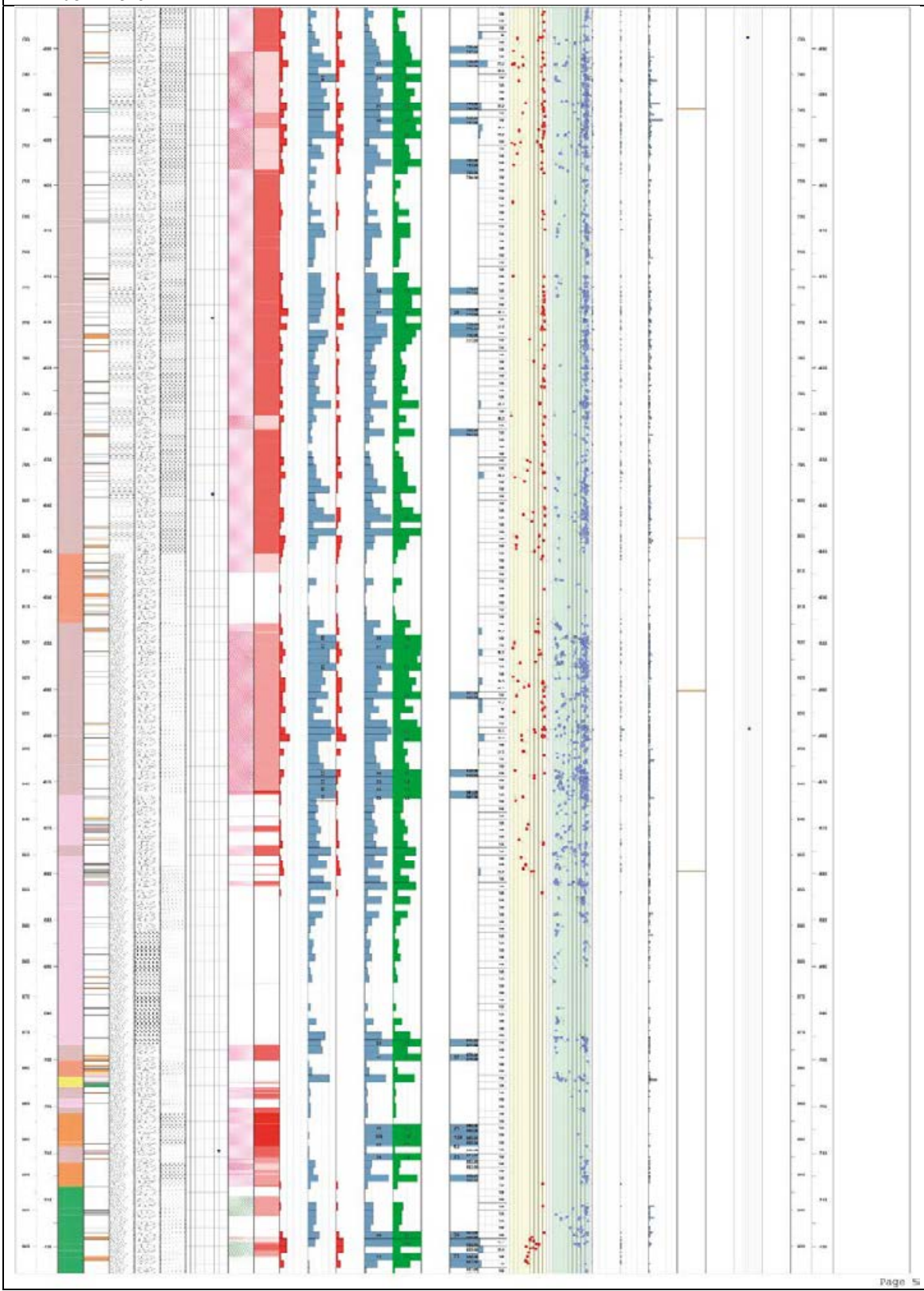

KFM08D – 6/6

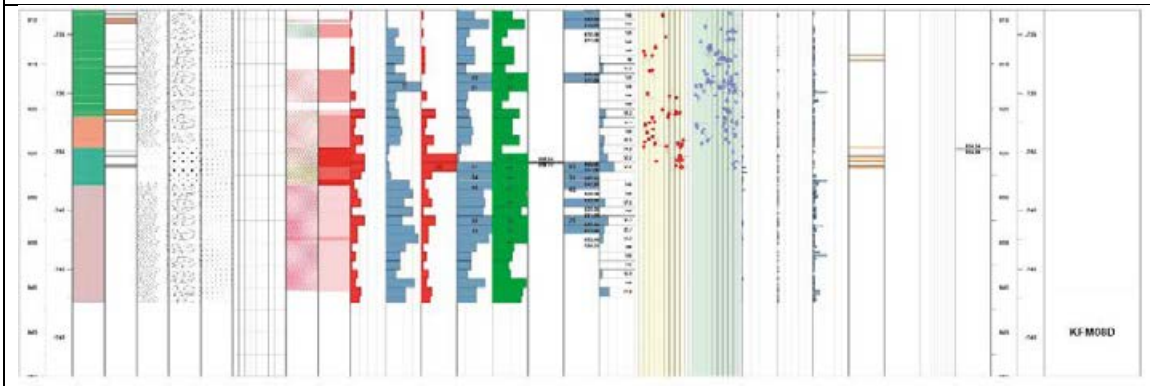

KFM09A – 1/5

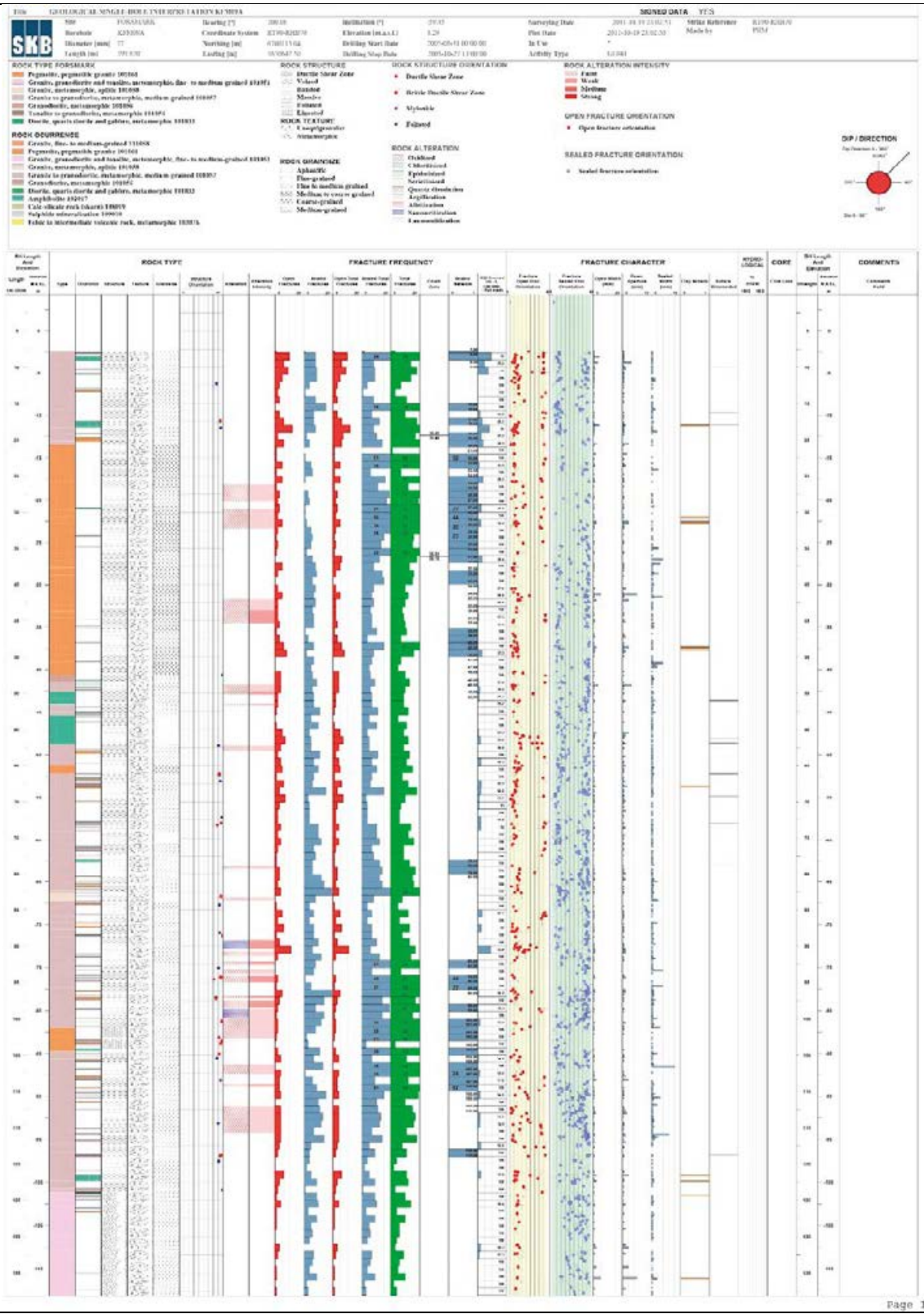
SKB
SIGNED DATA
ROCK TYPE FORSMARK
ROCK OCCURRENCE
ROCK STRUCTURE
ROCK ALTERATION
ROCK ALTERATION INTENSITY
OPEN FRACTURE ORIENTATION
SEALED FRACTURE ORIENTATION
DIP / DIRECTION
ROCK TYPE
FRACTURE FREQUENCY
FRACTURE CHARACTER
CORE
COMMENTS
Page 1

KFM09A – 2/5

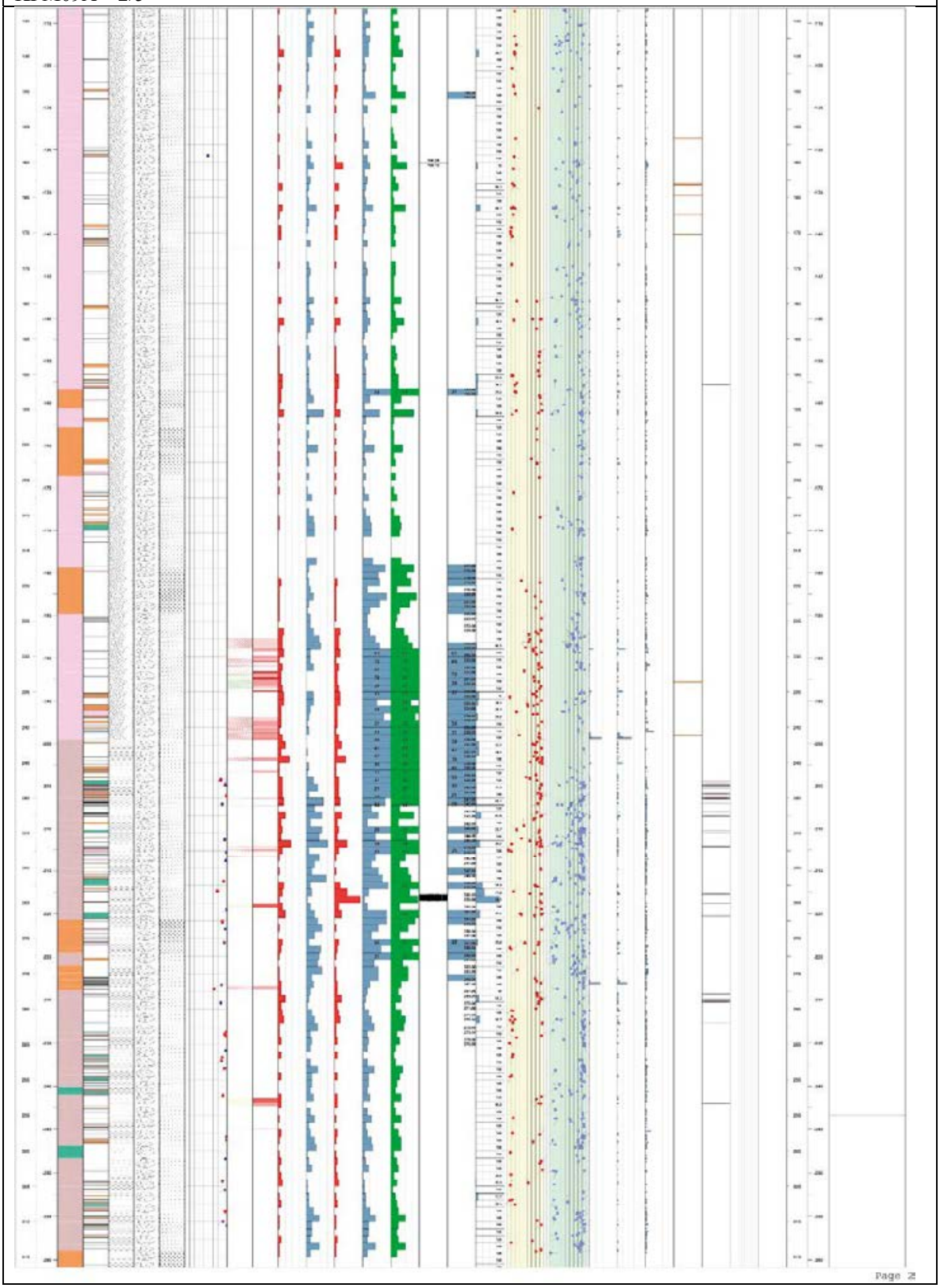

KFM09A – 3/5

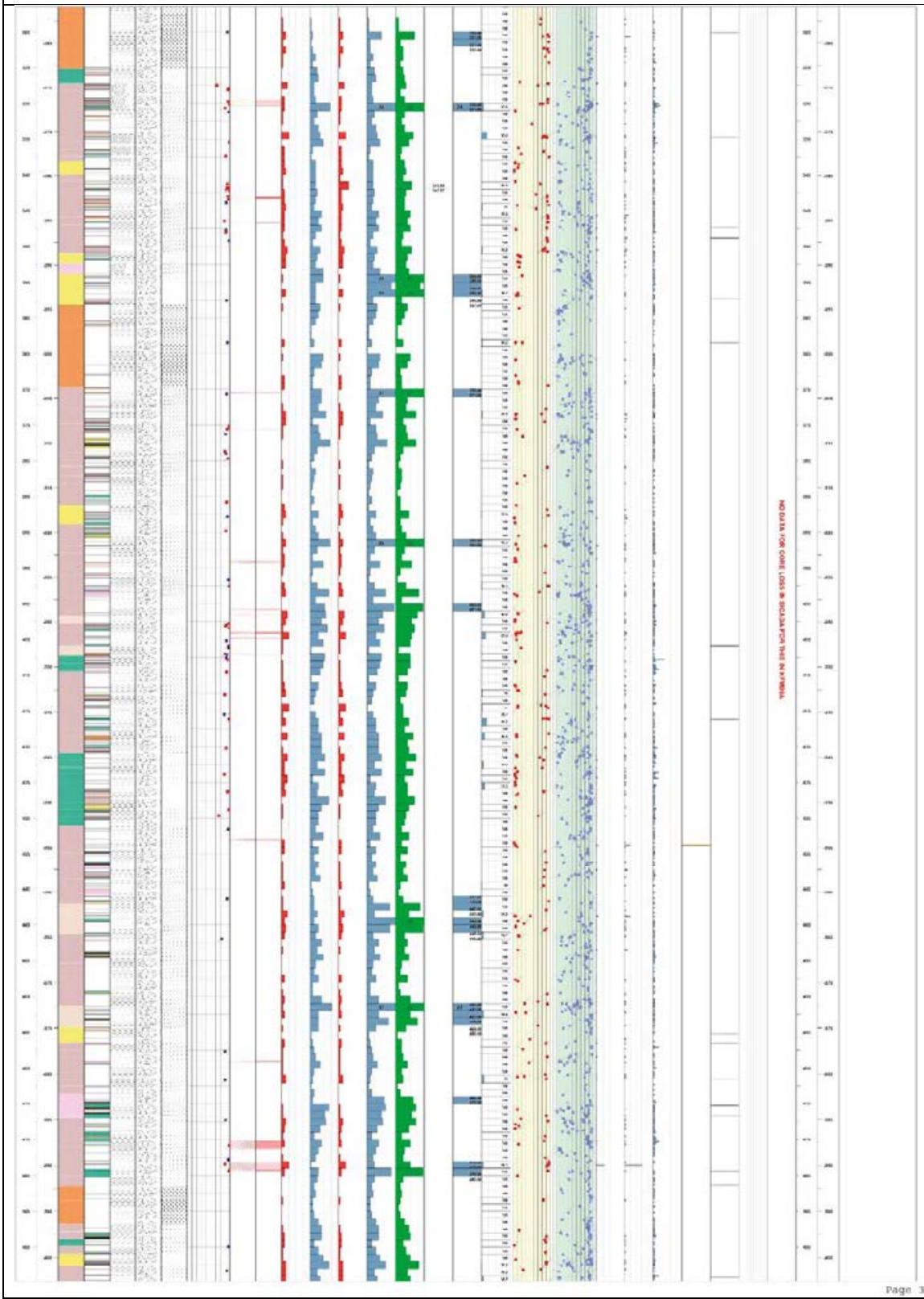

KFM09A – 4/5

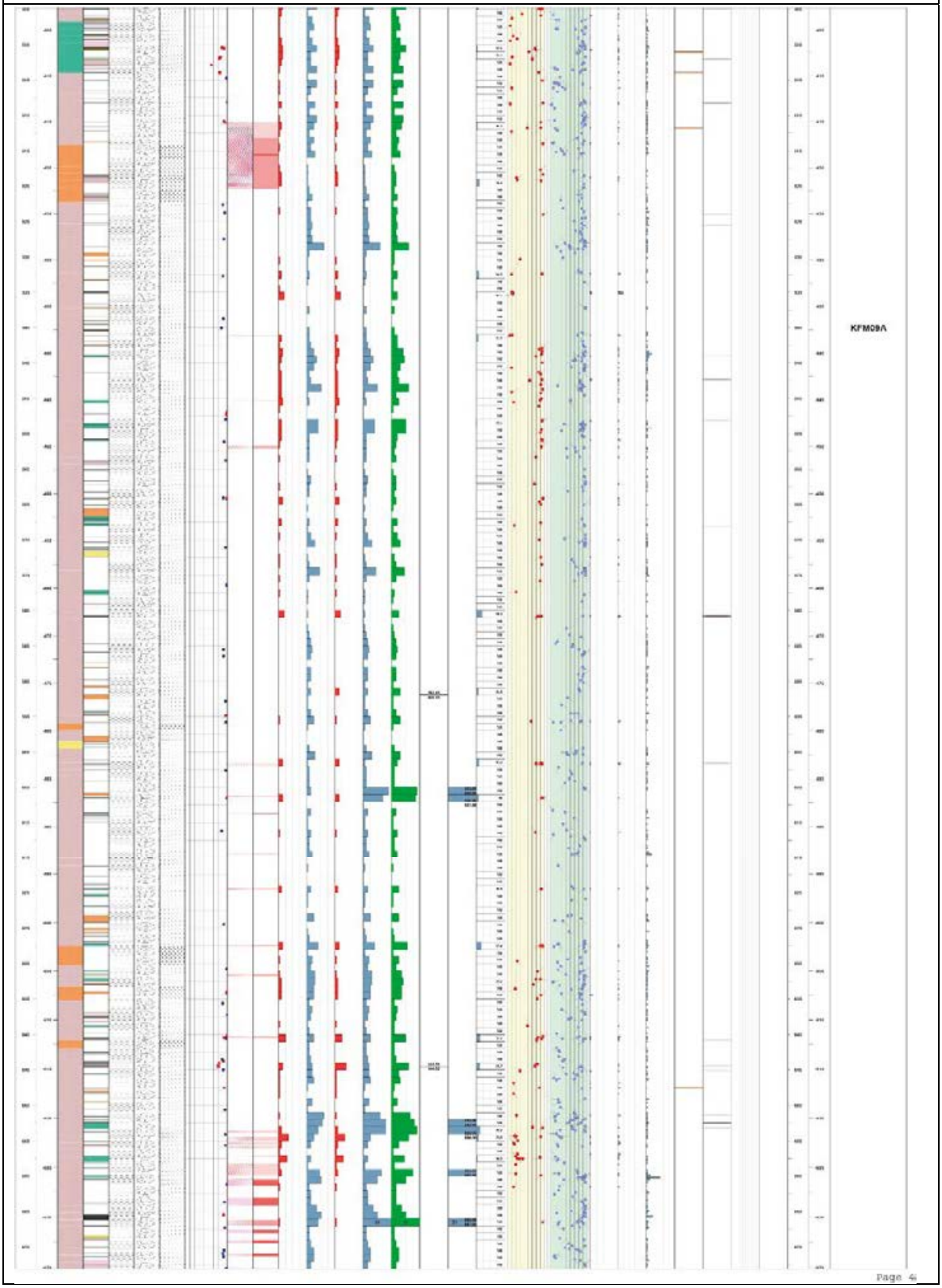

KFM09A – 5/5

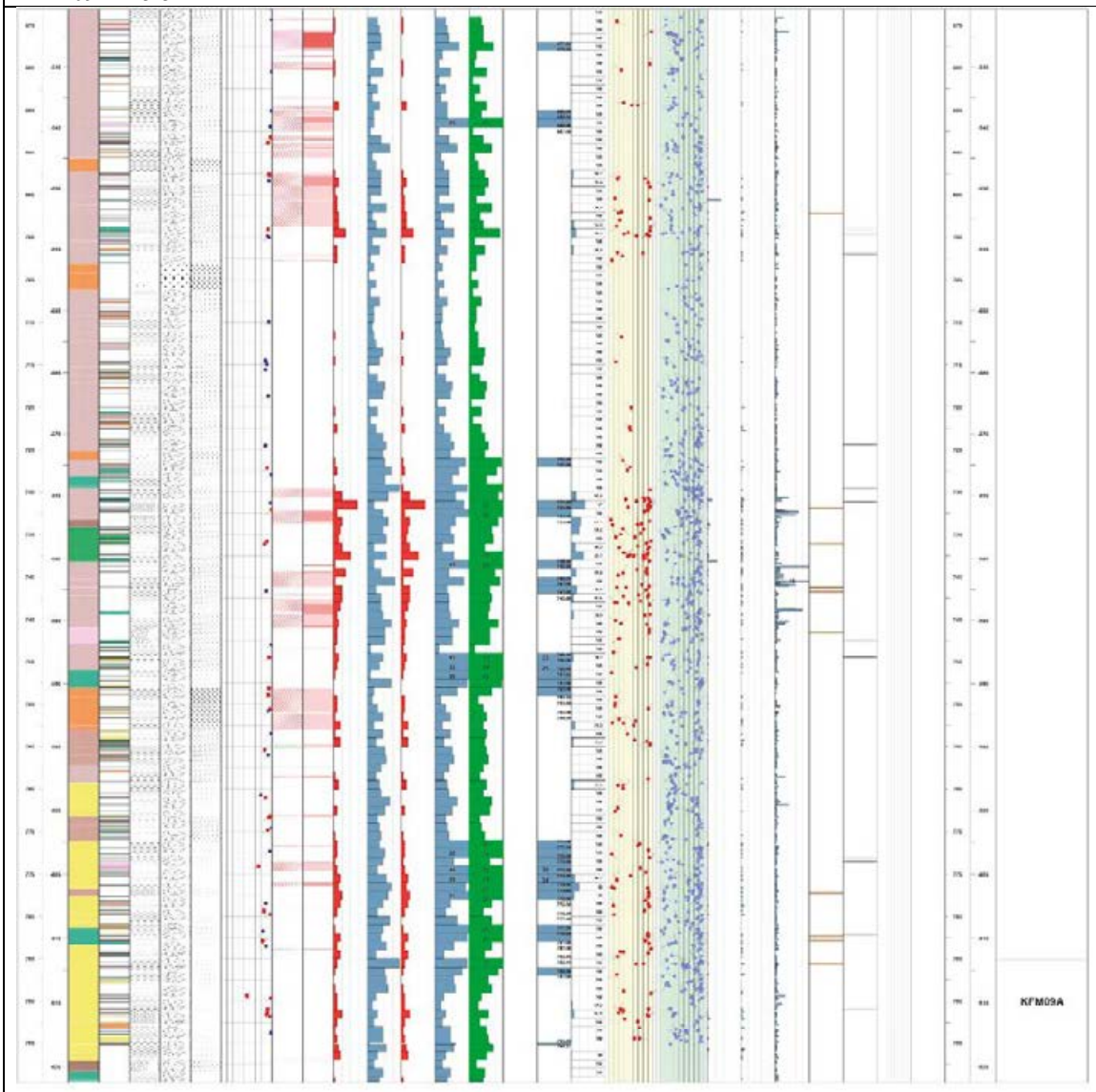

Page 5

KFM09B – 1/4

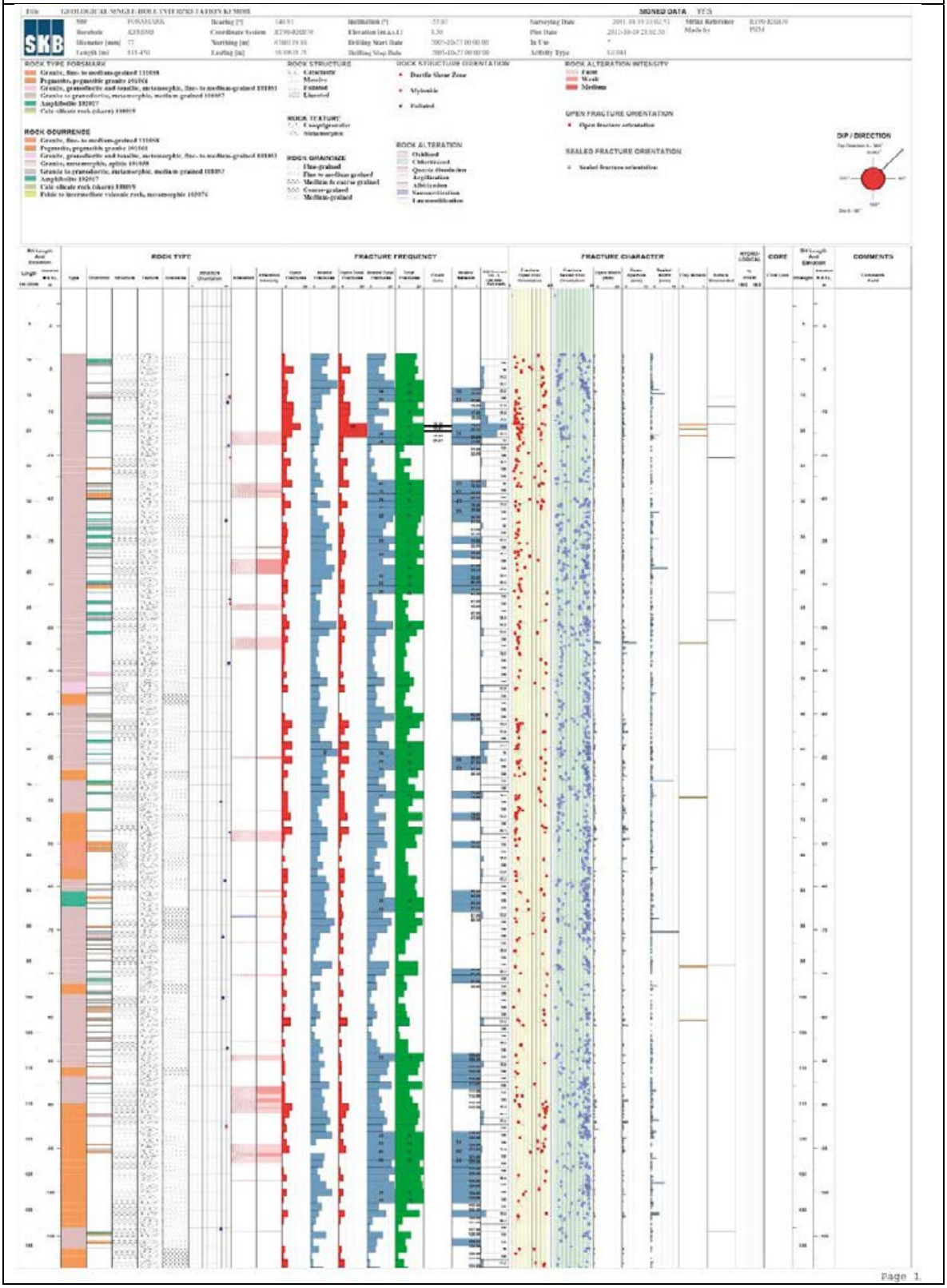
SKB
SIGNED DATA YES
ROCK TYPE FORSMARK
ROCK OCCURRENCE
ROCK STRUCTURE
ROCK STRUCTURE ORIENTATION
ROCK ALTERATION INTENSITY
OPEN FRACTURE ORIENTATION
SEALED FRACTURE ORIENTATION
ROCK TEXTURE
ROCK GRAINSIZE
ROCK ALTERATION
DIP / DIRECTION
ROCK TYPE
FRACTURE FREQUENCY
FRACTURE CHARACTER
HYDRO-LOGICAL
CORE
COMMENTS
Page 1

KFM09B – 2/4

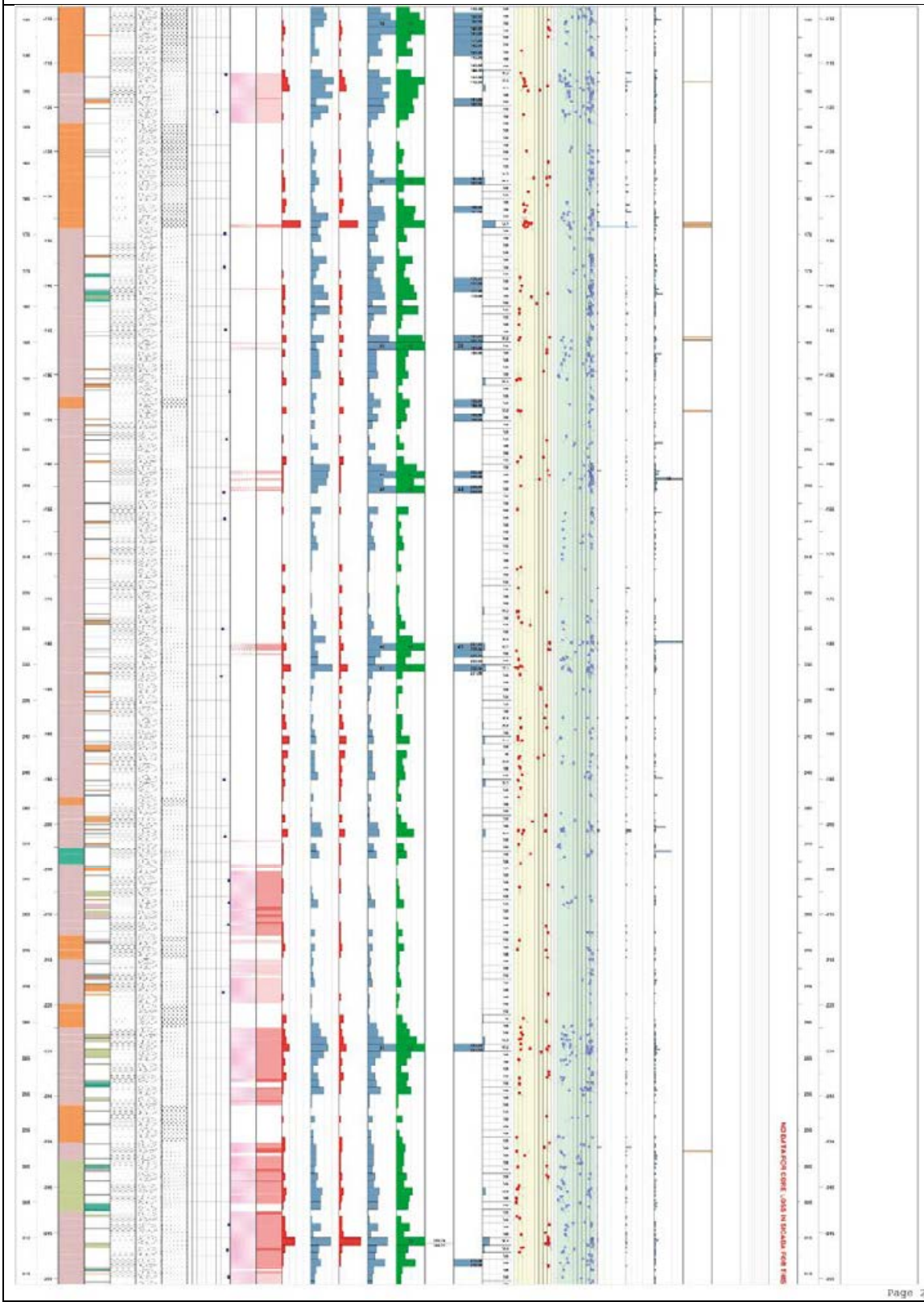

KFM09B – 3/4

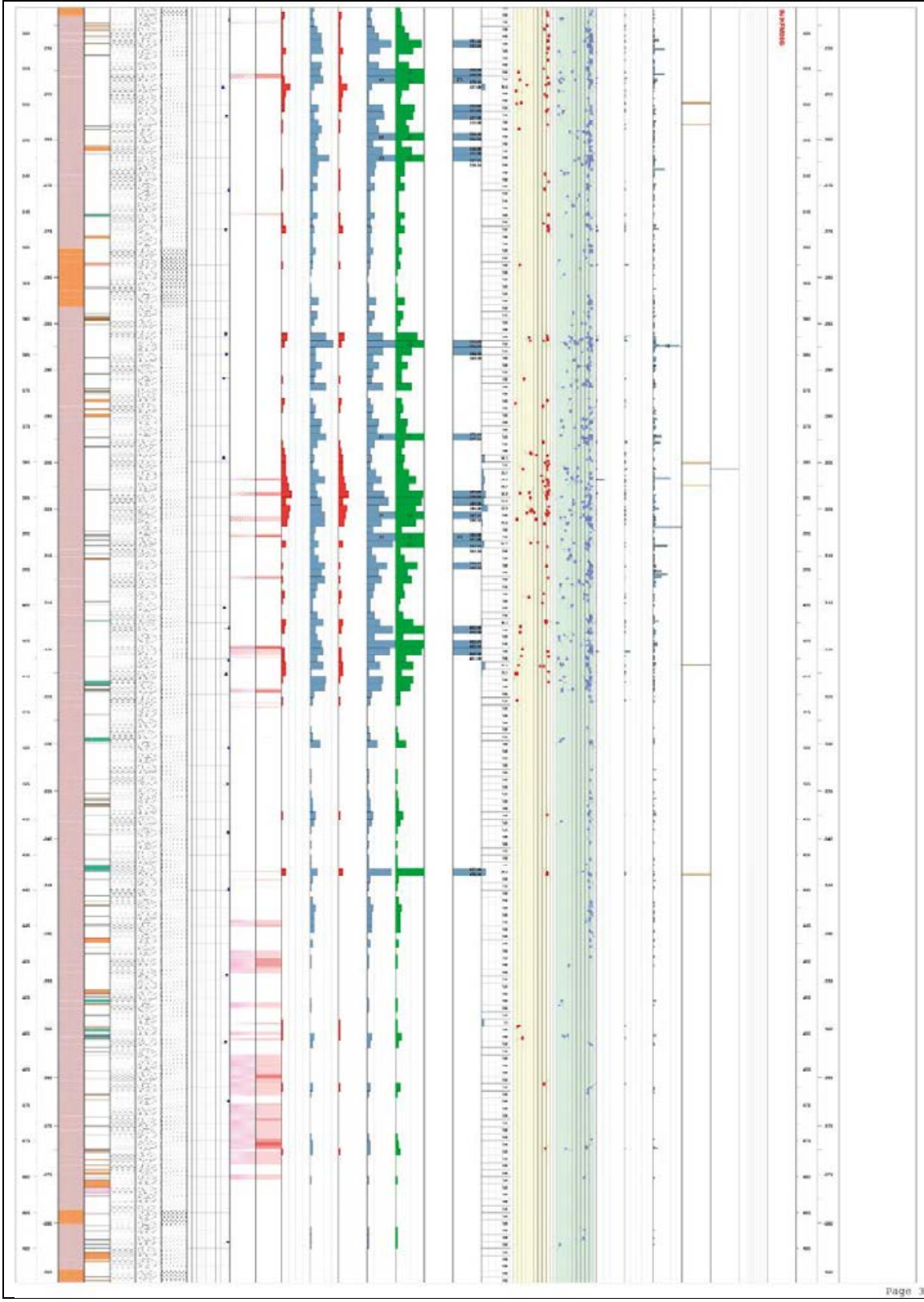

KFM09B – 4/4

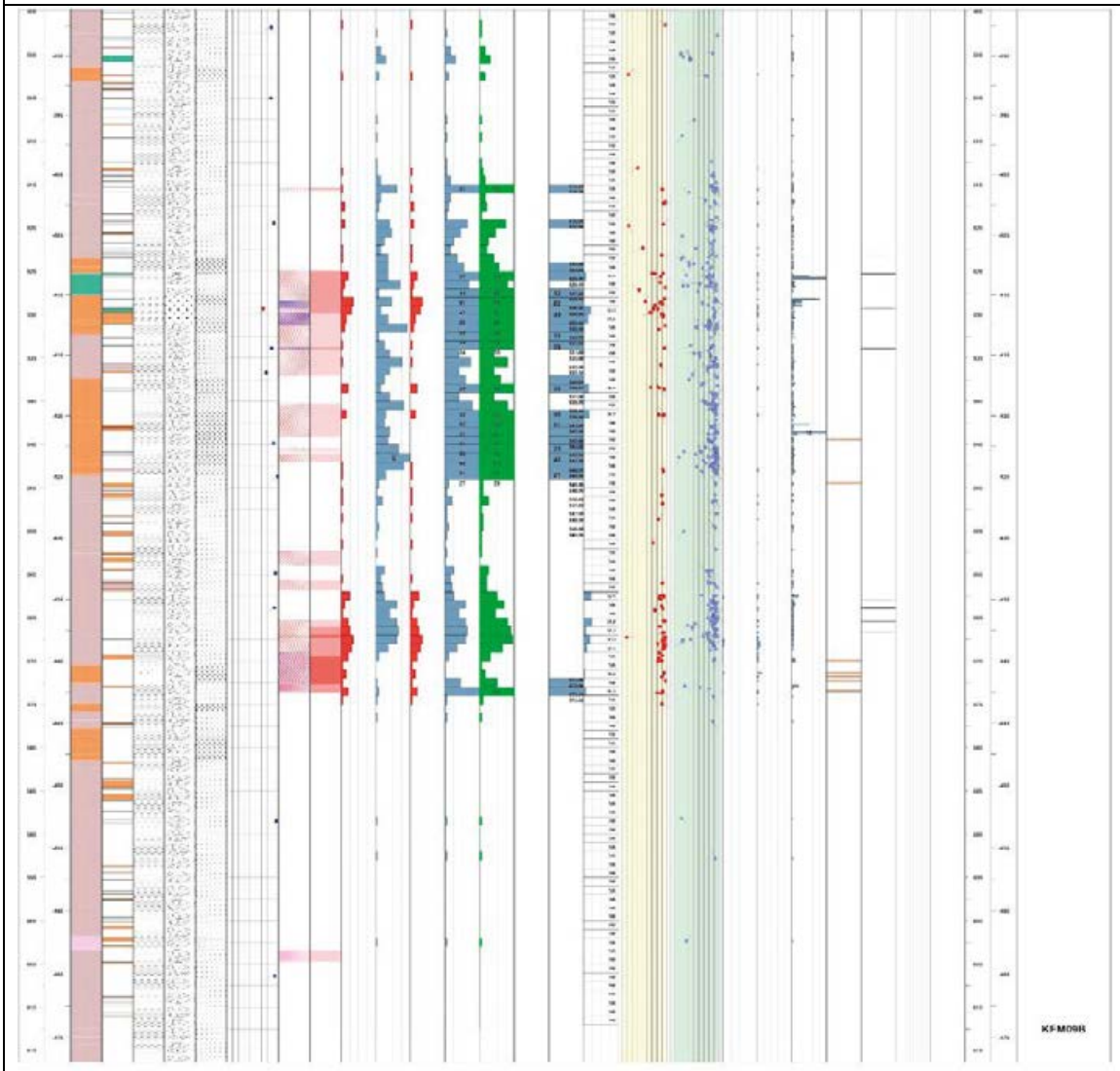

HFM20 – 1/2

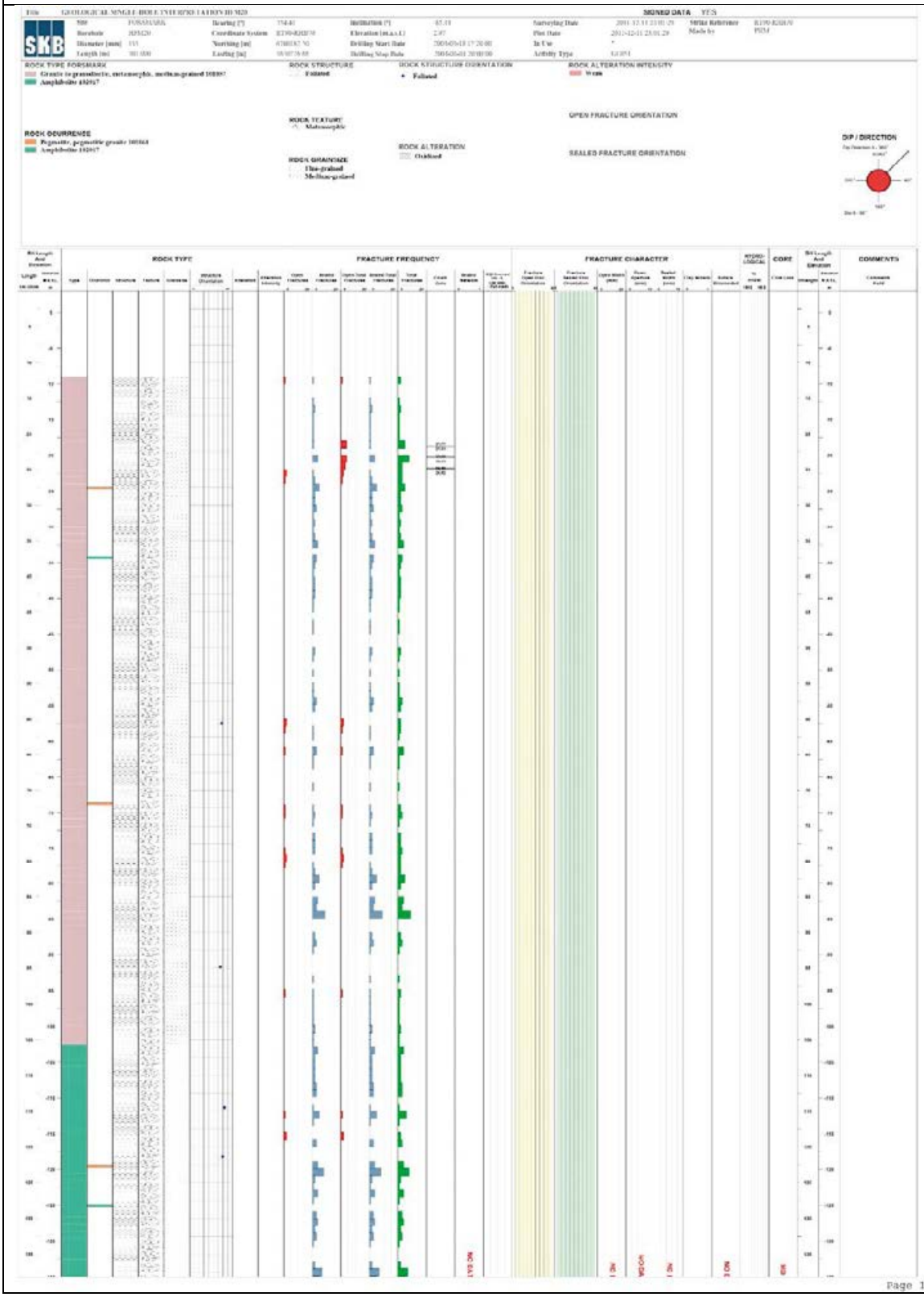
SKB
SIGNED DATA YES
ROCK TYPE FORSMARK
ROCK OCURRENCE
ROCK STRUCTURE
ROCK STRUCTURE ORIENTATION
ROCK ALTERATION INTENSITY
ROCK TEXTURE
ROCK ALTERATION
OPEN FRACTURE ORIENTATION
SEALED FRACTURE ORIENTATION
ROCK GRAINSIZE
DIP / DIRECTION
ROCK TYPE
FRACTURE FREQUENCY
FRACTURE CHARACTER
CORE
COMMENTS
Page 1

HFM20 – 2/2

HFM21 – 1/2

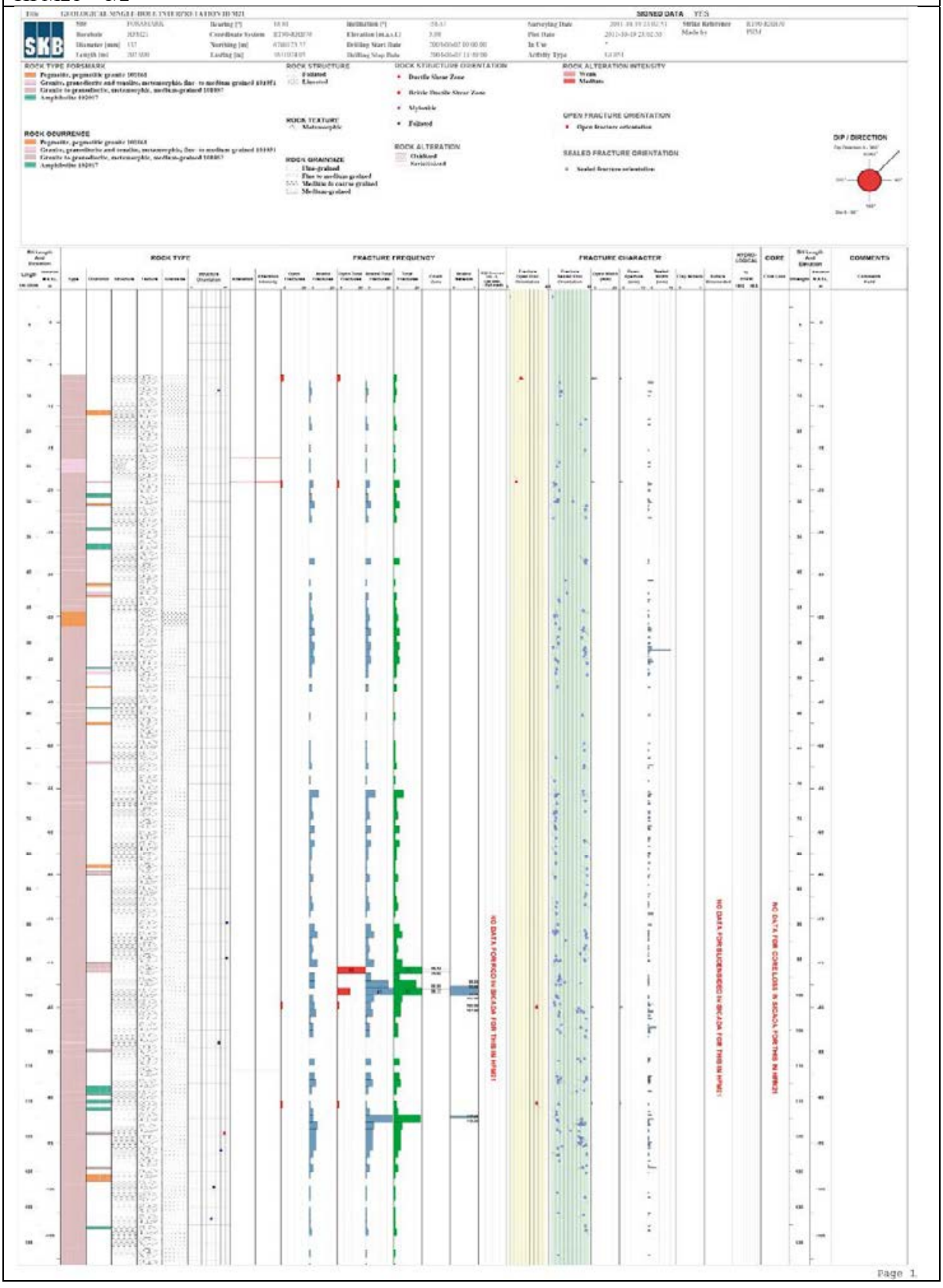
SKB
SIGNED DATA YES
ROCK TYPE FORSMARK
ROCK OCCURRENCE
ROCK STRUCTURE
ROCK STRUCTURE ORIENTATION
ROCK ALTERATION INTENSITY
ROCK TEXTURE
ROCK GRAINSIZE
ROCK ALTERATION
OPEN FRACTURE ORIENTATION
SEALED FRACTURE ORIENTATION
DIP / DIRECTION
ROCK TYPE
FRACTURE FREQUENCY
FRACTURE CHARACTER
CORE
COMMENTS
NO DATA FOR ROCK IN SICADA FOR THIS IN HFM21
NO DATA FOR BOREHOLE IN SICADA FOR THIS IN HFM21
NO DATA FOR CORE LOSS IN SICADA FOR THIS IN HFM21
Page 1

HFM21– 2/2

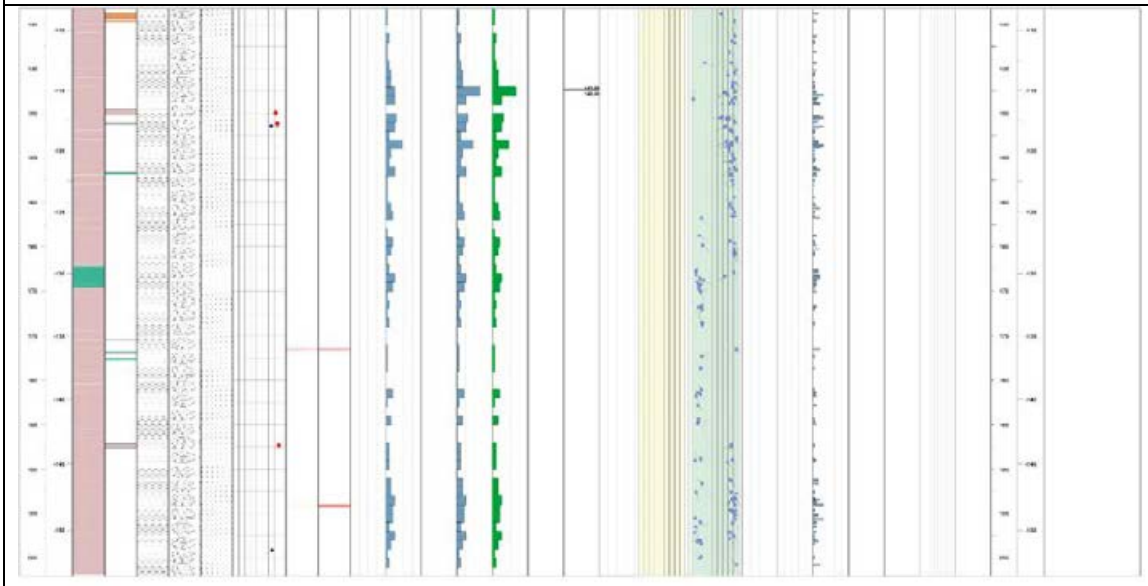

HFM22 – 1/2

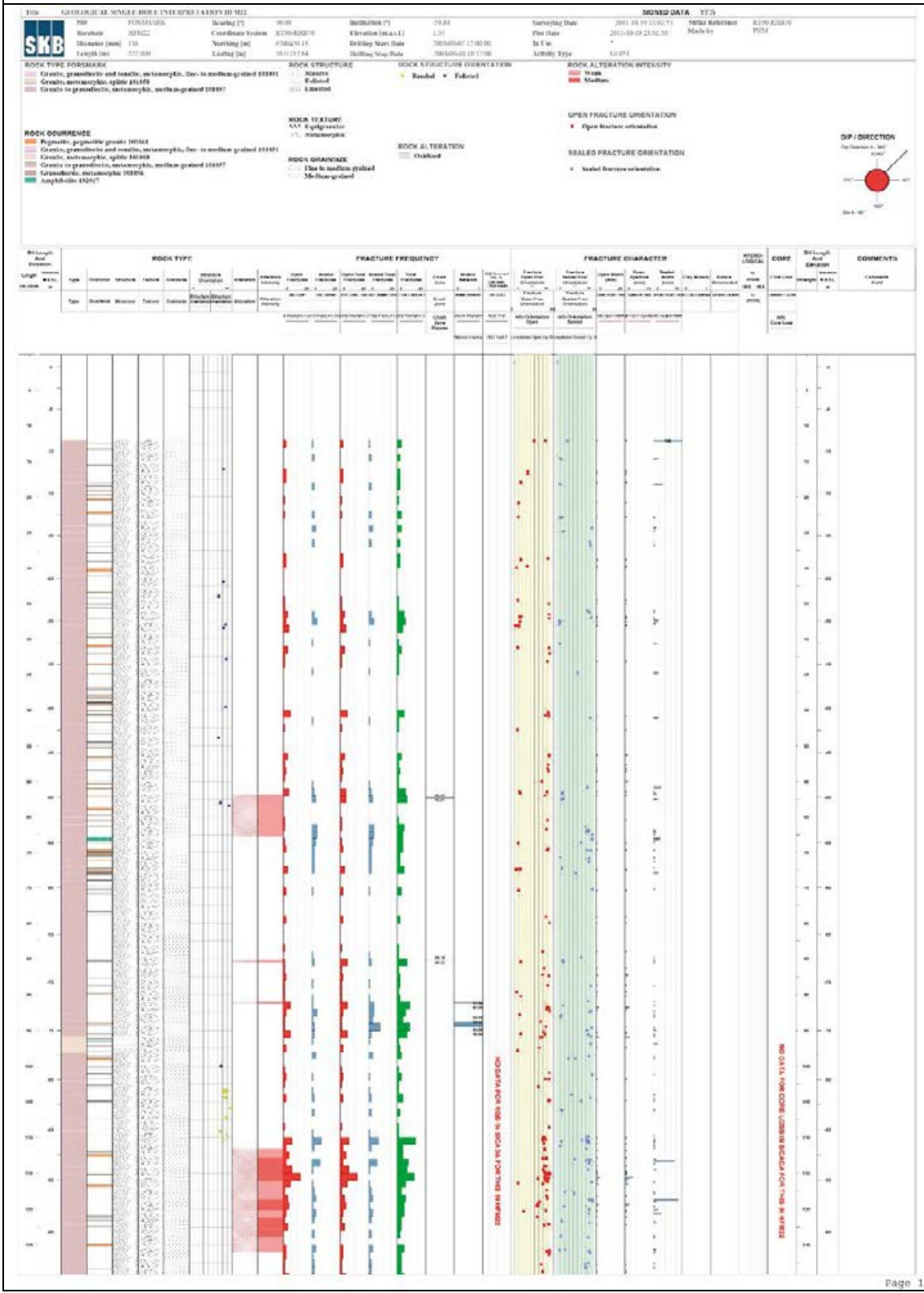
SKB
SIGNED DATA YES
ROCK TYPE FORSMARK
ROCK OCCURRENCE
ROCK STRUCTURE
ROCK STRUCTURE ORIENTATION
ROCK ALTERATION INTENSITY
ROCK TEXTURE
ROCK ALTERATION
ROCK GRAINSIZE
OPEN FRACTURE ORIENTATION
SEALED FRACTURE ORIENTATION
DIP / DIRECTION
ROCK TYPE
FRACTURE FREQUENCY
FRACTURE CHARACTER
CORE
COMMENTS
Page 1

HFM22 – 2/2

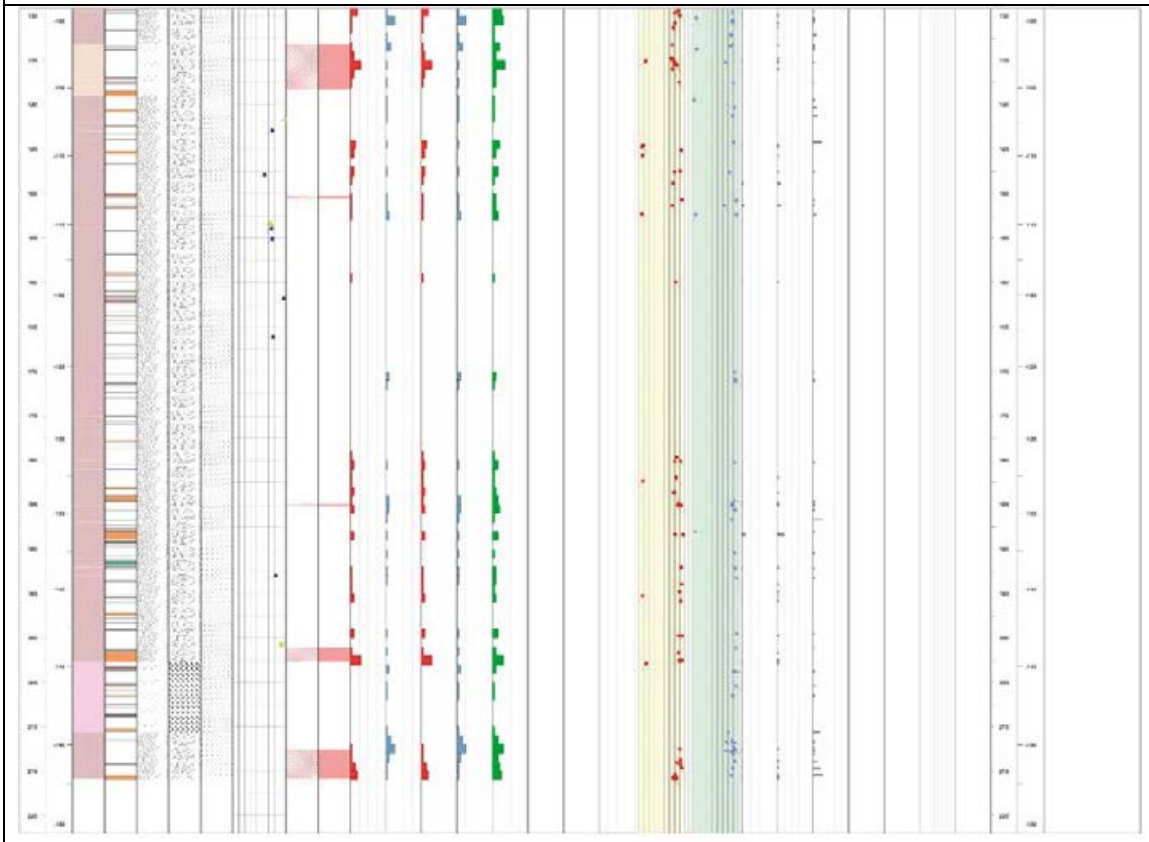

HFM23 – 1/2

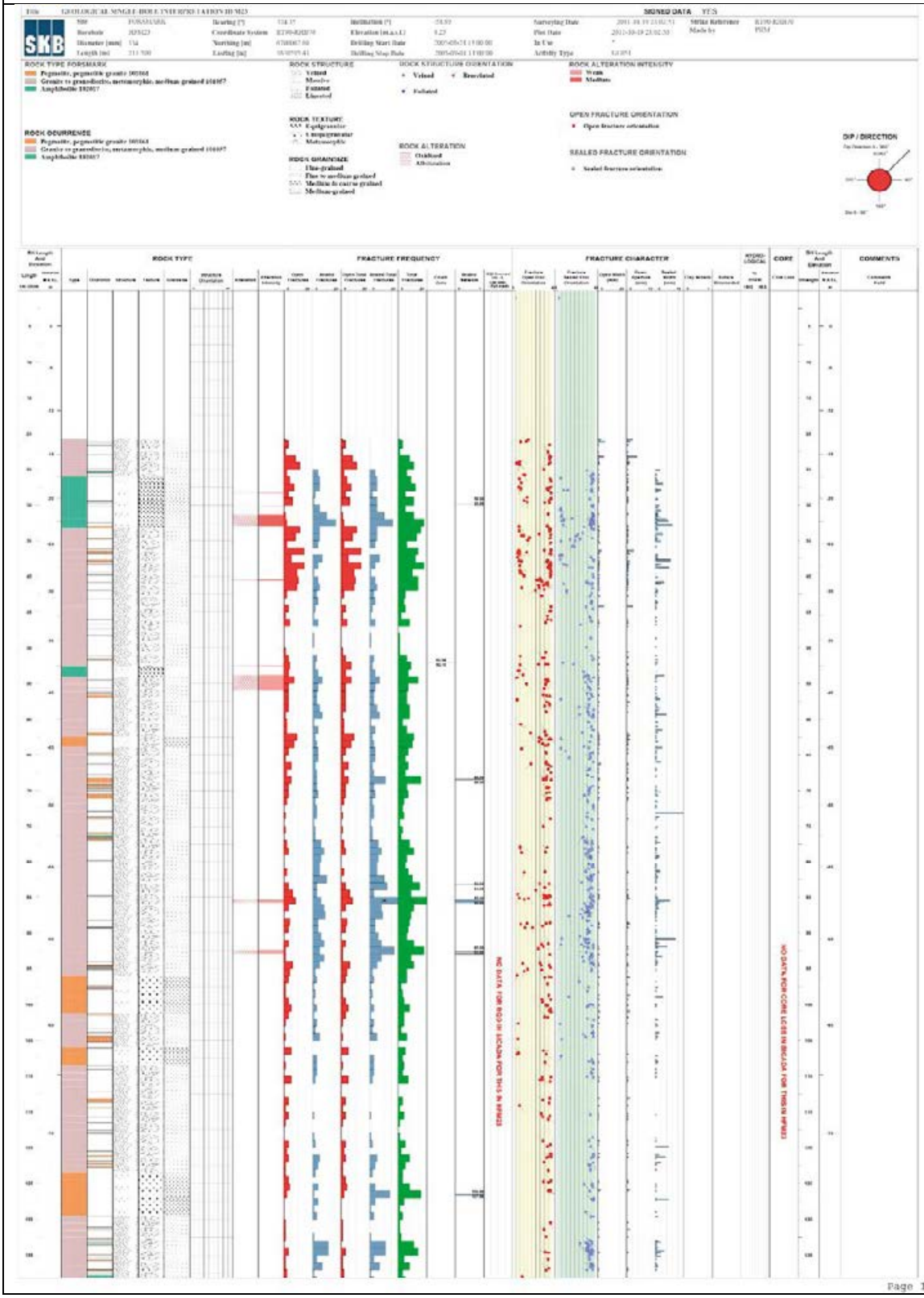
SKB
SIGNED DATA YES
ROCK TYPE FORSMARK
ROCK OCCURRENCE
ROCK STRUCTURE
ROCK STRUCTURE ORIENTATION
ROCK ALTERATION INTENSITY
OPEN FRACTURE ORIENTATION
SEALED FRACTURE ORIENTATION
ROCK TEXTURE
ROCK GRAINSIZE
ROCK ALTERATION
DIP / DIRECTION
ROCK TYPE
FRACTURE FREQUENCY
FRACTURE CHARACTER
CORE
COMMENTS
NO DATA FOR BOREHOLE SECTION FOR THIS IN HFM23
NO DATA FOR CORE LOGGING FOR THIS IN HFM23
Page 1

HFM23 – 2/2

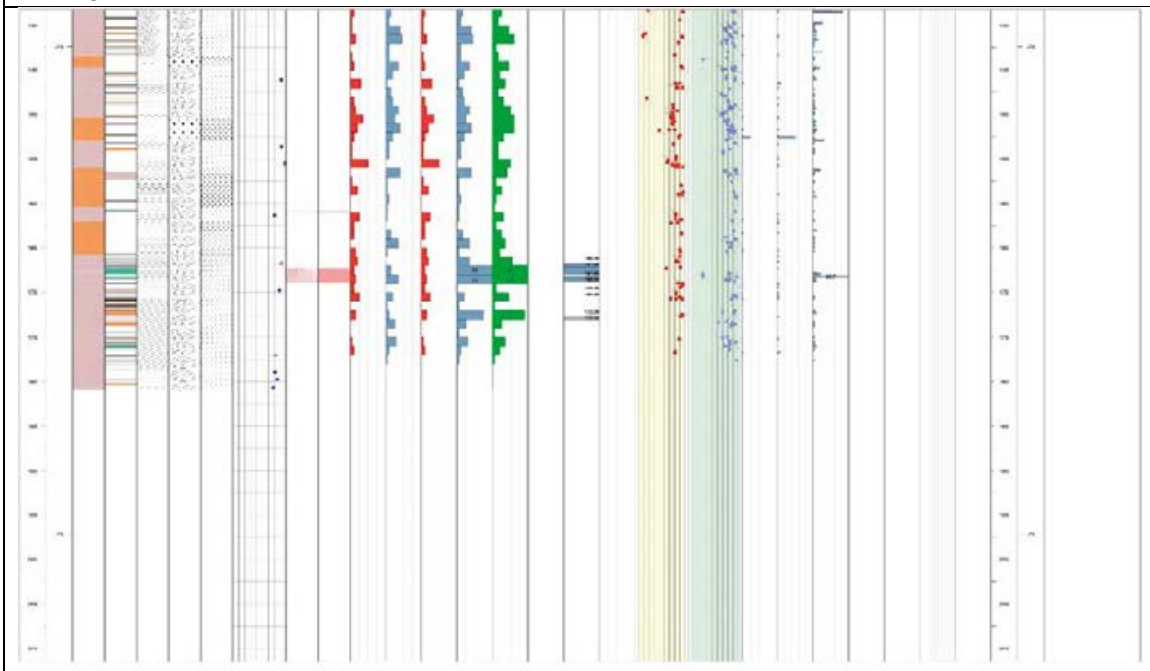

HFM28 – 1/2

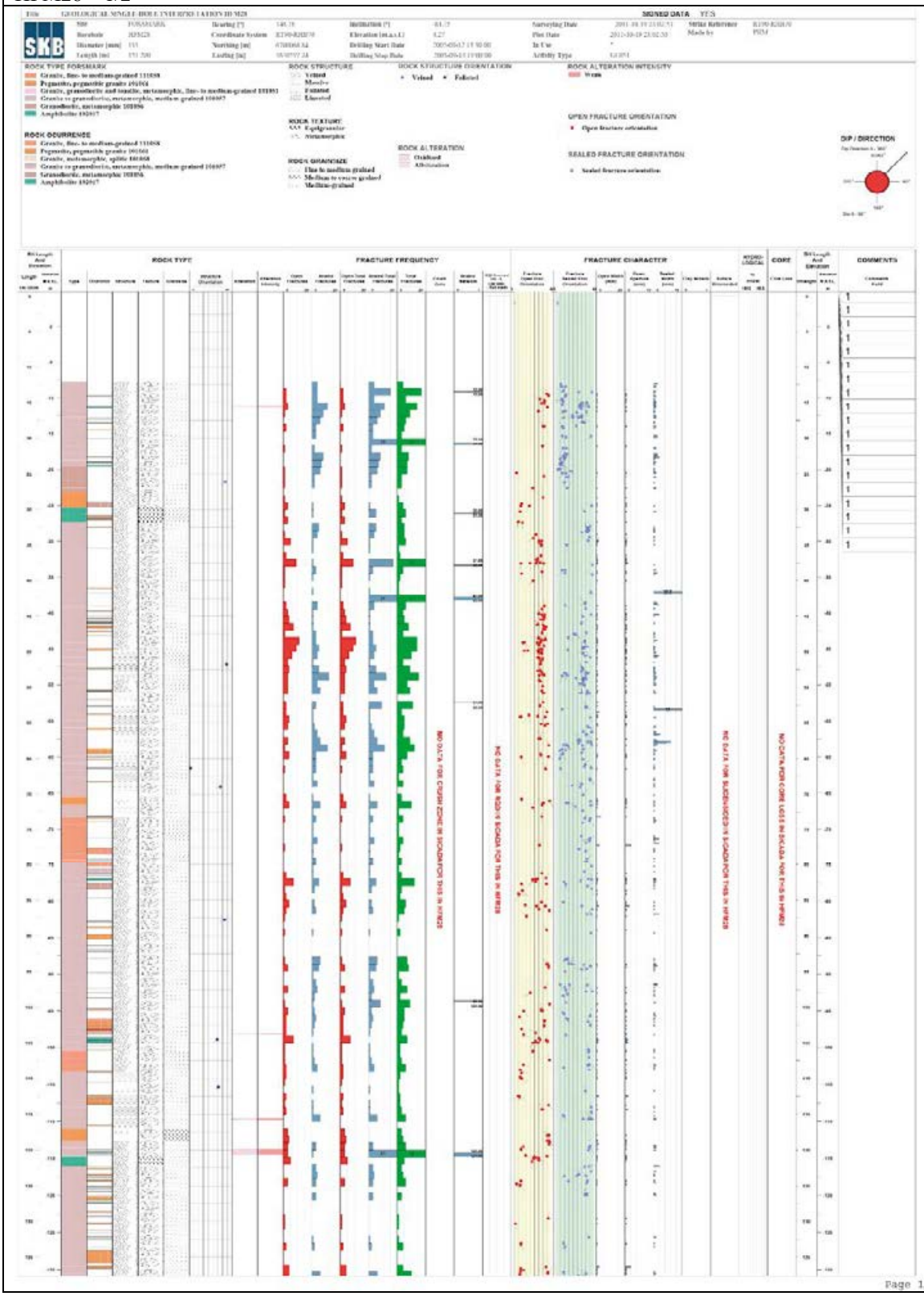
SKB
SIGNED DATA YES
ROCK TYPE FORSMARK
ROCK OCCURRENCE
ROCK STRUCTURE
ROCK STRUCTURE ORIENTATION
ROCK ALTERATION INTENSITY
ROCK TEXTURE
ROCK ALTERATION
ROCK GRAINSIZE
OPEN FRACTURE ORIENTATION
SEALED FRACTURE ORIENTATION
DIP / DIRECTION
ROCK TYPE
FRACTURE FREQUENCY
FRACTURE CHARACTER
CORE
COMMENTS
Page 1

HFM28 – 2/2

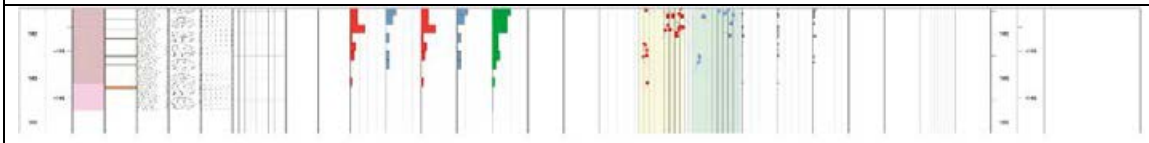

HFM38 – 1/2

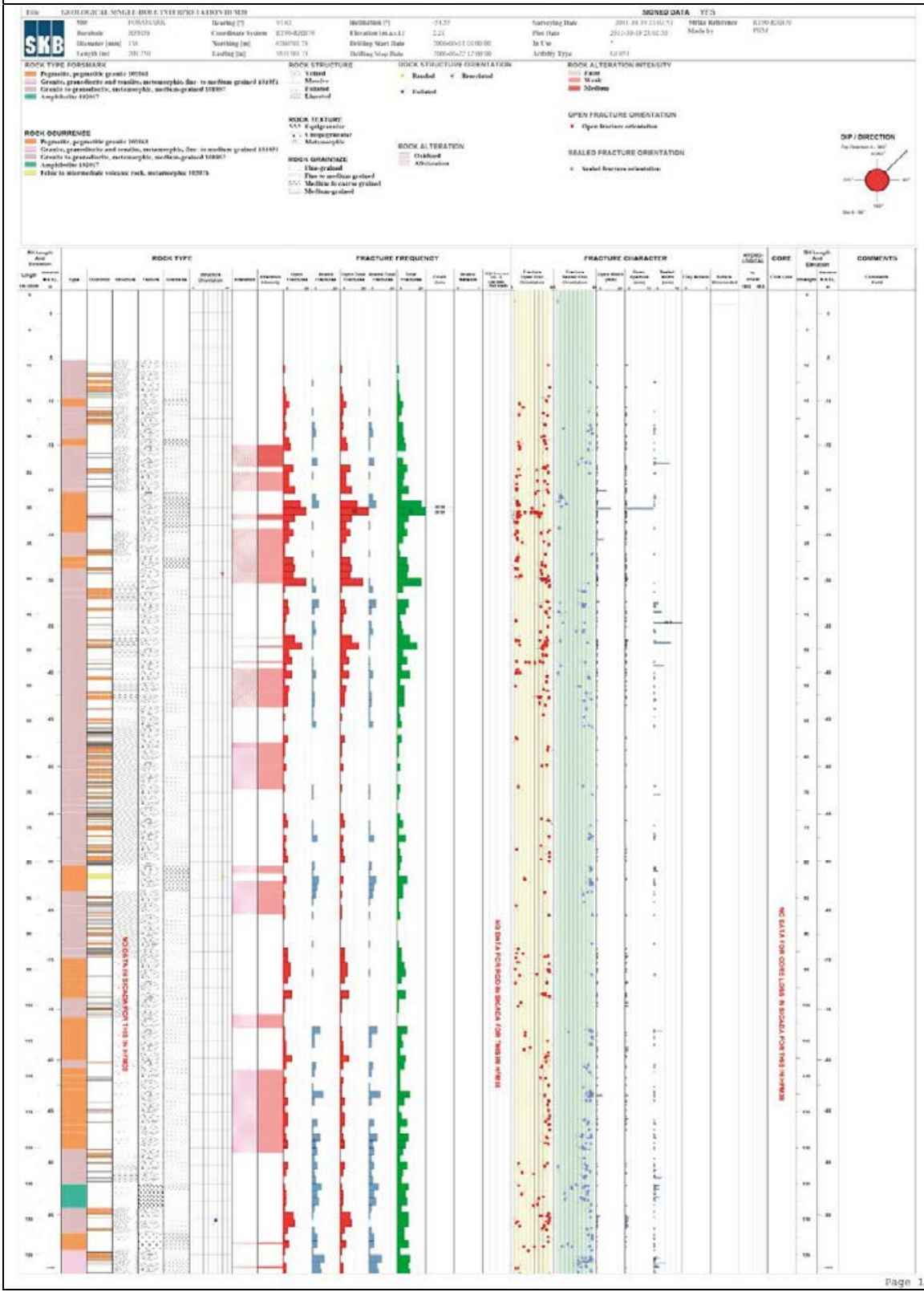
SKB
SIGNED DATA YES
ROCK TYPE FORSMARK
ROCK OCCURRENCE
ROCK STRUCTURE
ROCK STRUCTURE ORIENTATION
ROCK ALTERATION INTENSITY
OPEN FRACTURE ORIENTATION
SEALED FRACTURE ORIENTATION
ROCK TEXTURE
ROCK GRAINSIZE
ROCK ALTERATION
DIP / DIRECTION
ROCK TYPE
FRACTURE FREQUENCY
FRACTURE CHARACTER
CORE
COMMENTS
Page 1

HFM38 – 2/2

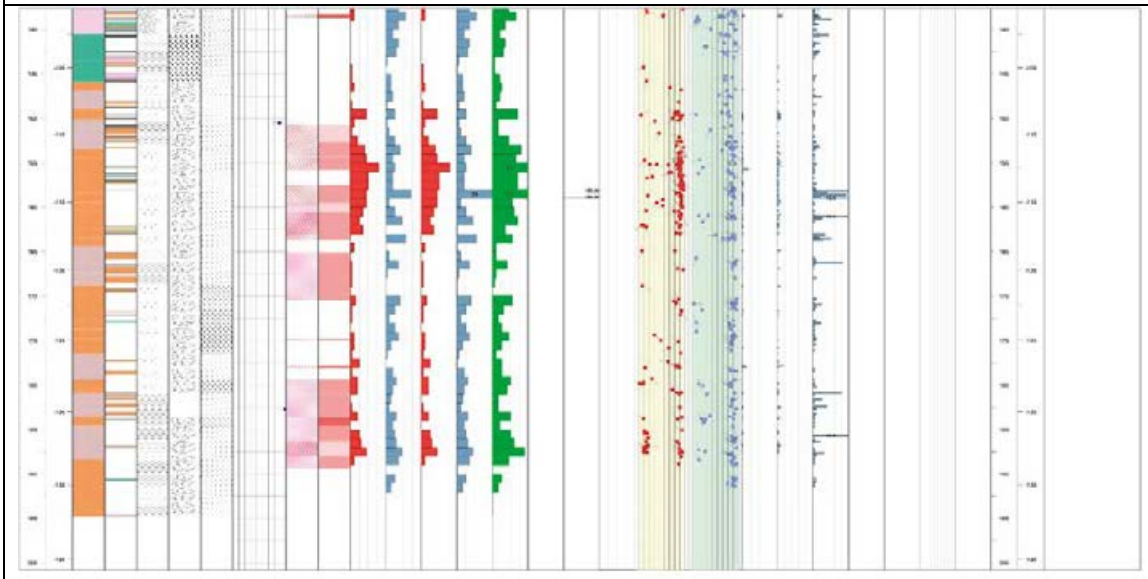

Appendix C

WellCAD plots for boreholes KFM13–24 and HFM39–41

KFM13 – 1/2

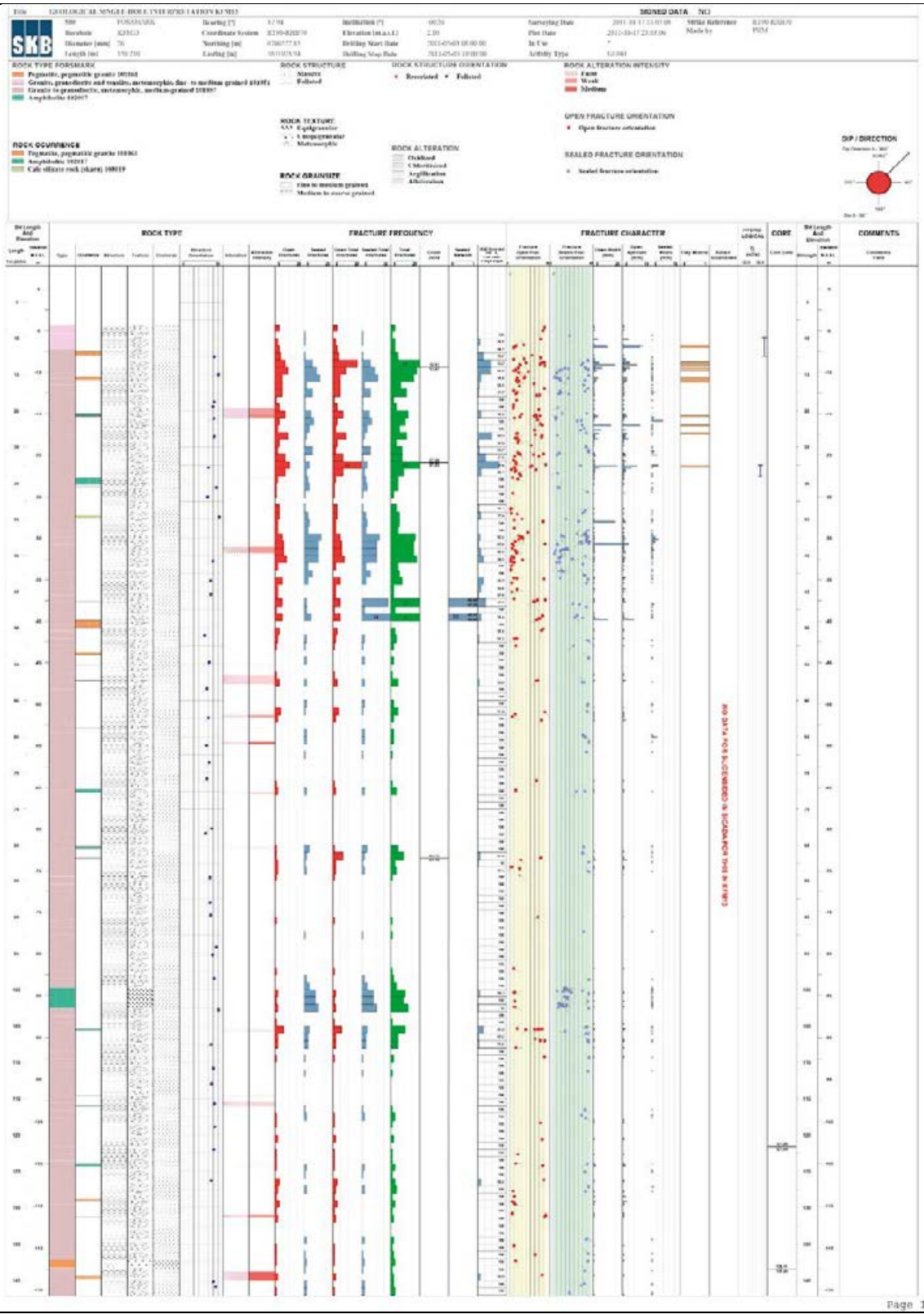

KFM13 – 2/2

KFM14 – 1/1

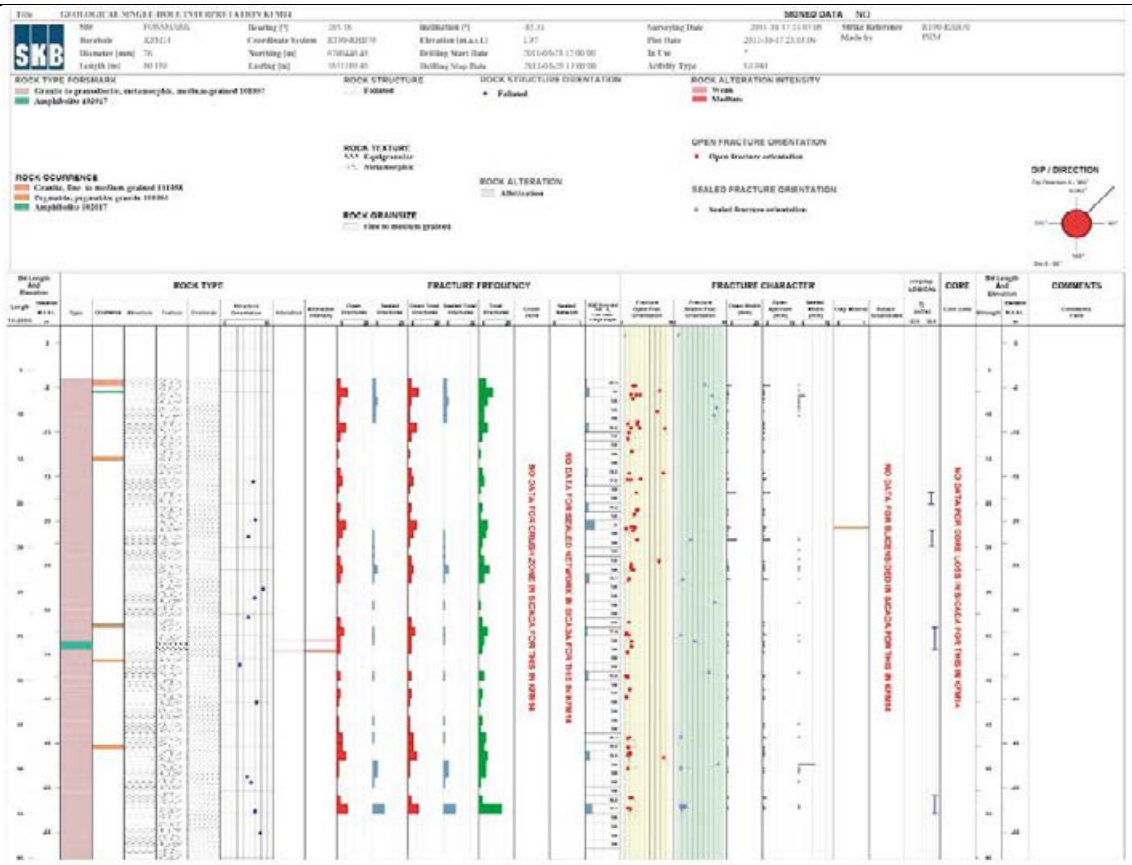
SKB
SIGNED DATA NO
ROCK TYPE FORSMARK
ROCK STRUCTURE
ROCK STRUCTURE ORIENTATION
ROCK ALTERATION INTENSITY
ROCK TEXTURE
ROCK OCCURRENCE
ROCK ALTERATION
ROCK GRAINSIZE
OPEN FRACTURE ORIENTATION
SEALED FRACTURE ORIENTATION
DIP / DIRECTION
ROCK TYPE
FRACTURE FREQUENCY
FRACTURE CHARACTER
CORE
COMMENTS
NO DATA FOR CRUSH ZONE IN SICADA FOR THIS IN KFM14
NO DATA FOR SEALED NETWORK IN SICADA FOR THIS IN KFM14
NO DATA FOR BLOCKS-DEG IN SICADA FOR THIS IN KFM14
NO DATA FOR CORE LOSS IN SICADA FOR THIS IN KFM14

KFM15 – 1/1

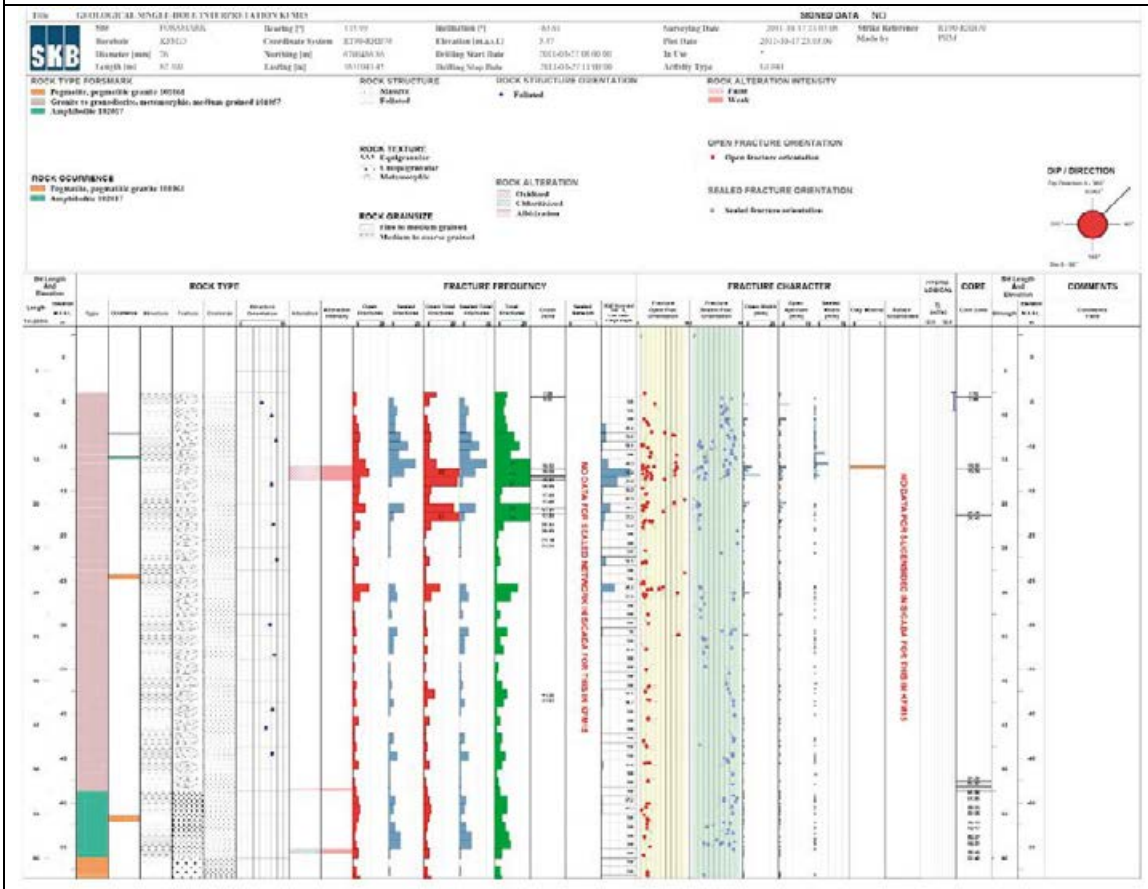
SKB
ROCK TYPE FORSMARK
ROCK OCCURRENCE
ROCK STRUCTURE
ROCK STRUCTURE ORIENTATION
ROCK ALTERATION INTENSITY
ROCK TEXTURE
ROCK ALTERATION
ROCK GRAINSIZE
OPEN FRACTURE ORIENTATION
SEALED FRACTURE ORIENTATION
DIP / DIRECTION
ROCK TYPE
FRACTURE FREQUENCY
FRACTURE CHARACTER
CORE
COMMENTS

KFM16 – 1/1

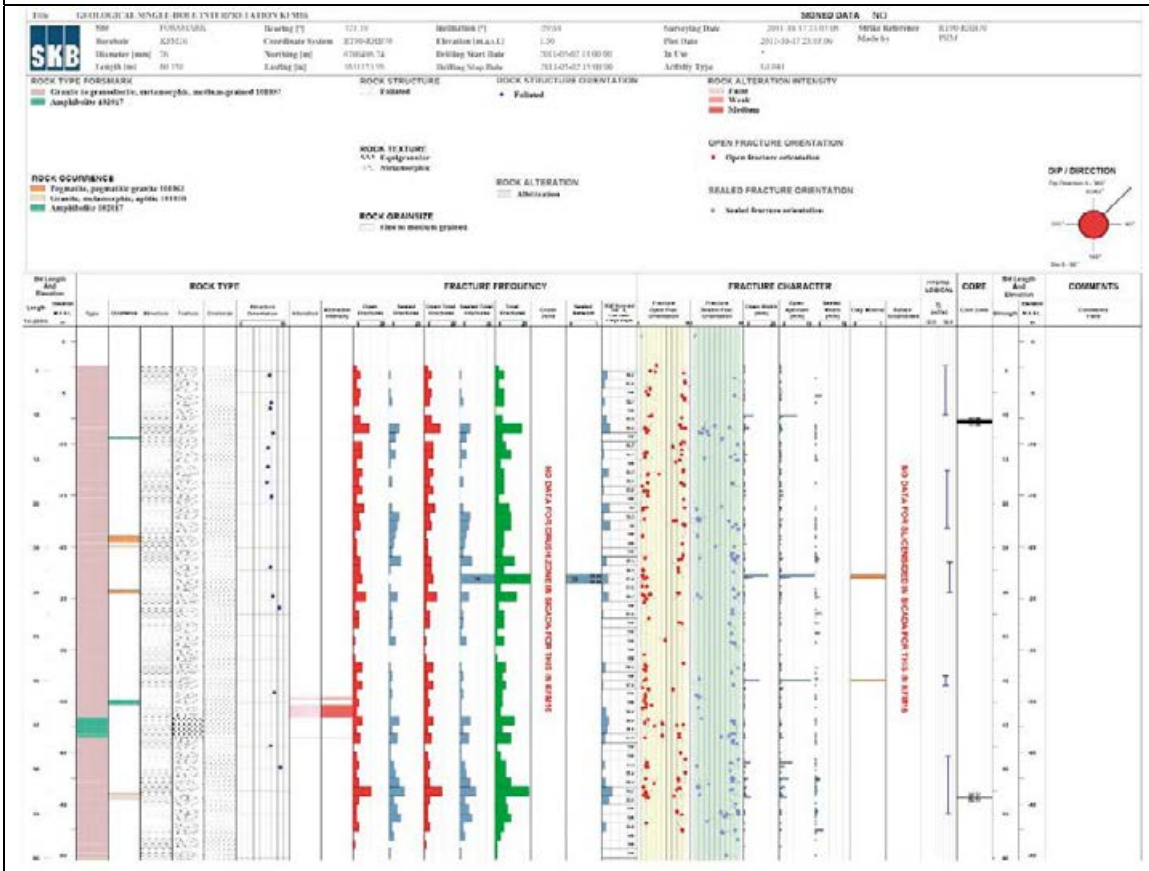

Page 1

KFM17 – 1/1

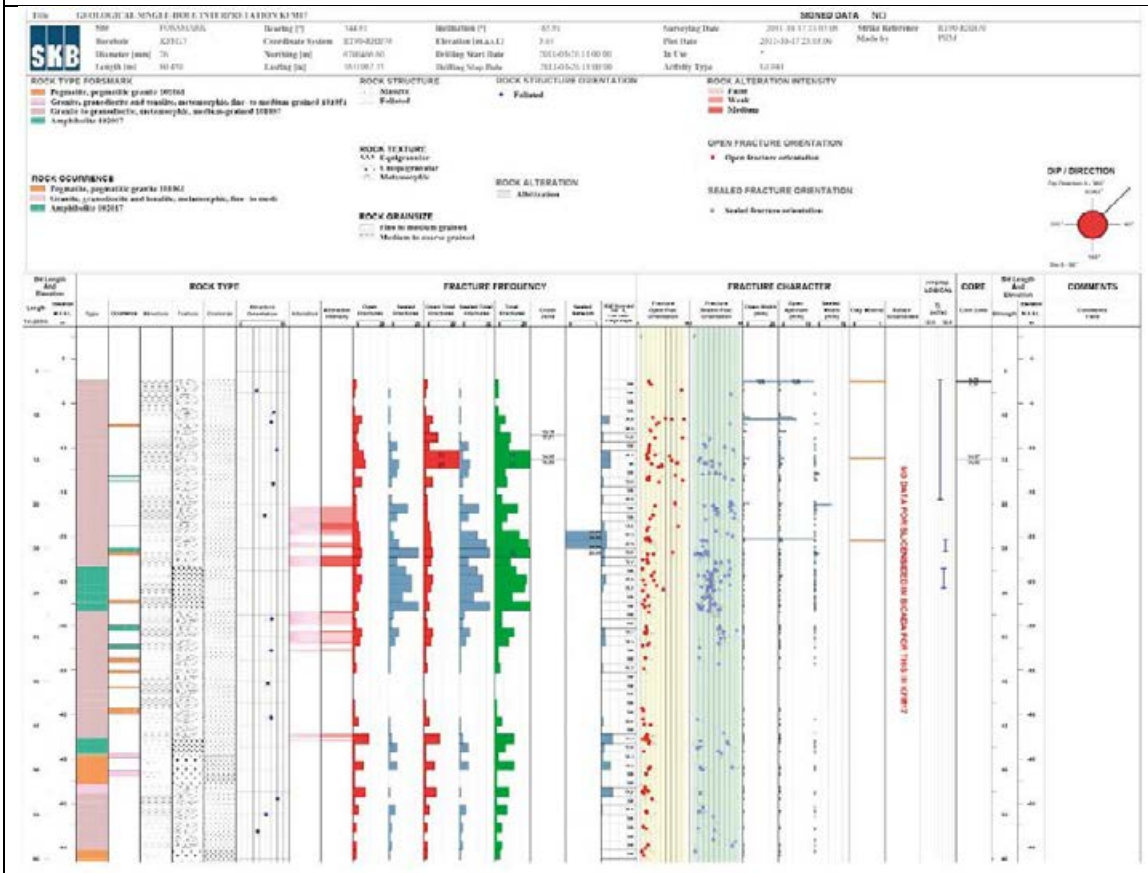
SKB
SIGNED DATA
ROCK TYPE FORSMARK
ROCK STRUCTURE
ROCK STRUCTURE ORIENTATION
ROCK ALTERATION INTENSITY
OPEN FRACTURE ORIENTATION
SEALED FRACTURE ORIENTATION
ROCK OCCURRENCE
ROCK TEXTURE
ROCK ALTERATION
ROCK GRAINSIZE
DIP / DIRECTION
ROCK TYPE
FRACTURE FREQUENCY
FRACTURE CHARACTER
CORE
COMMENTS
NO DATA FOR BLOCKBEEDS IN BOREHOLE FOR THIS INTERVAL

KFM18 – 1/1

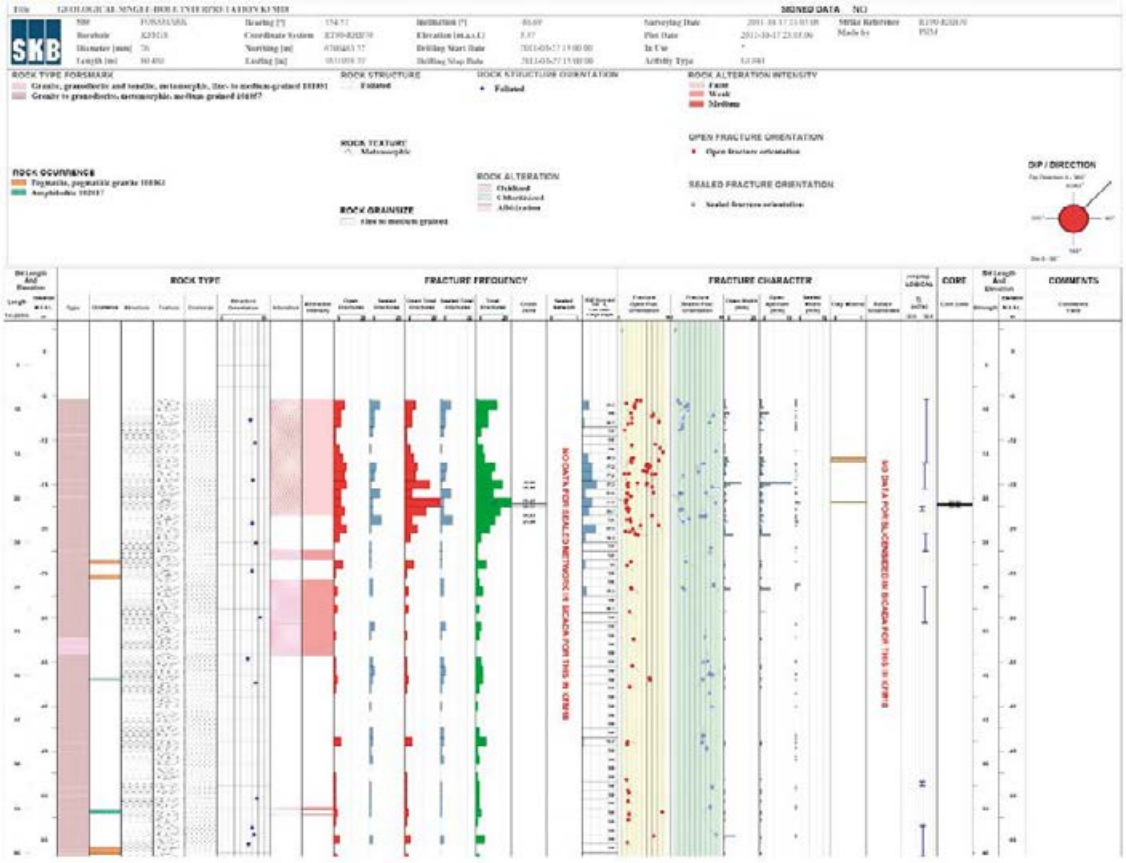

Page 1

KFM19 – 1/1

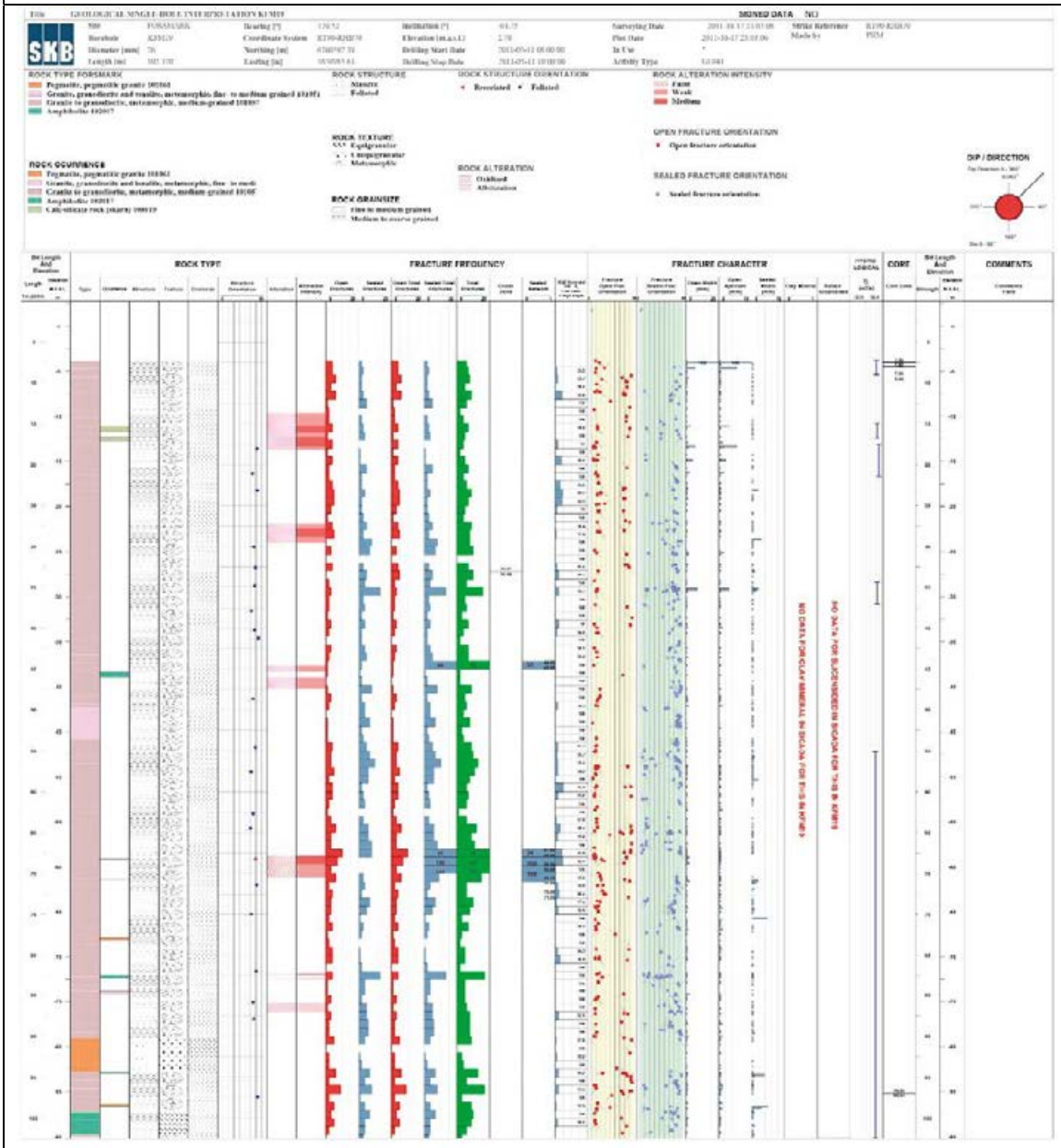

Page 1

KFM20 – 1/1

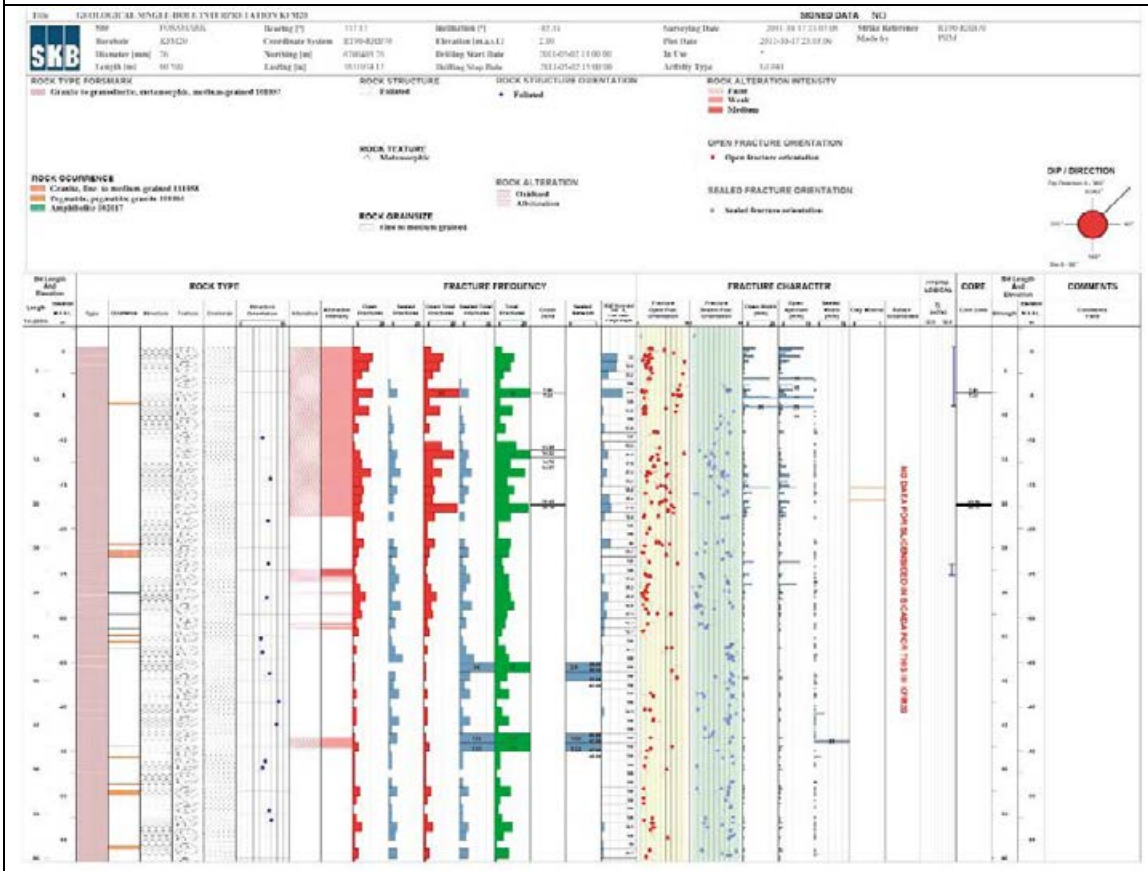
SKB
ROCK TYPE FORSMARK
ROCK OCCURRENCE
ROCK STRUCTURE
ROCK TEXTURE
ROCK GRANULITE
ROCK ALTERATION
ROCK ALTERATION INTENSITY
OPEN FRACTURE ORIENTATION
SEALED FRACTURE ORIENTATION
DIP / DIRECTION
ROCK TYPE
FRACTURE FREQUENCY
FRACTURE CHARACTER
CORE
COMMENTS

KFM21 – 1/1

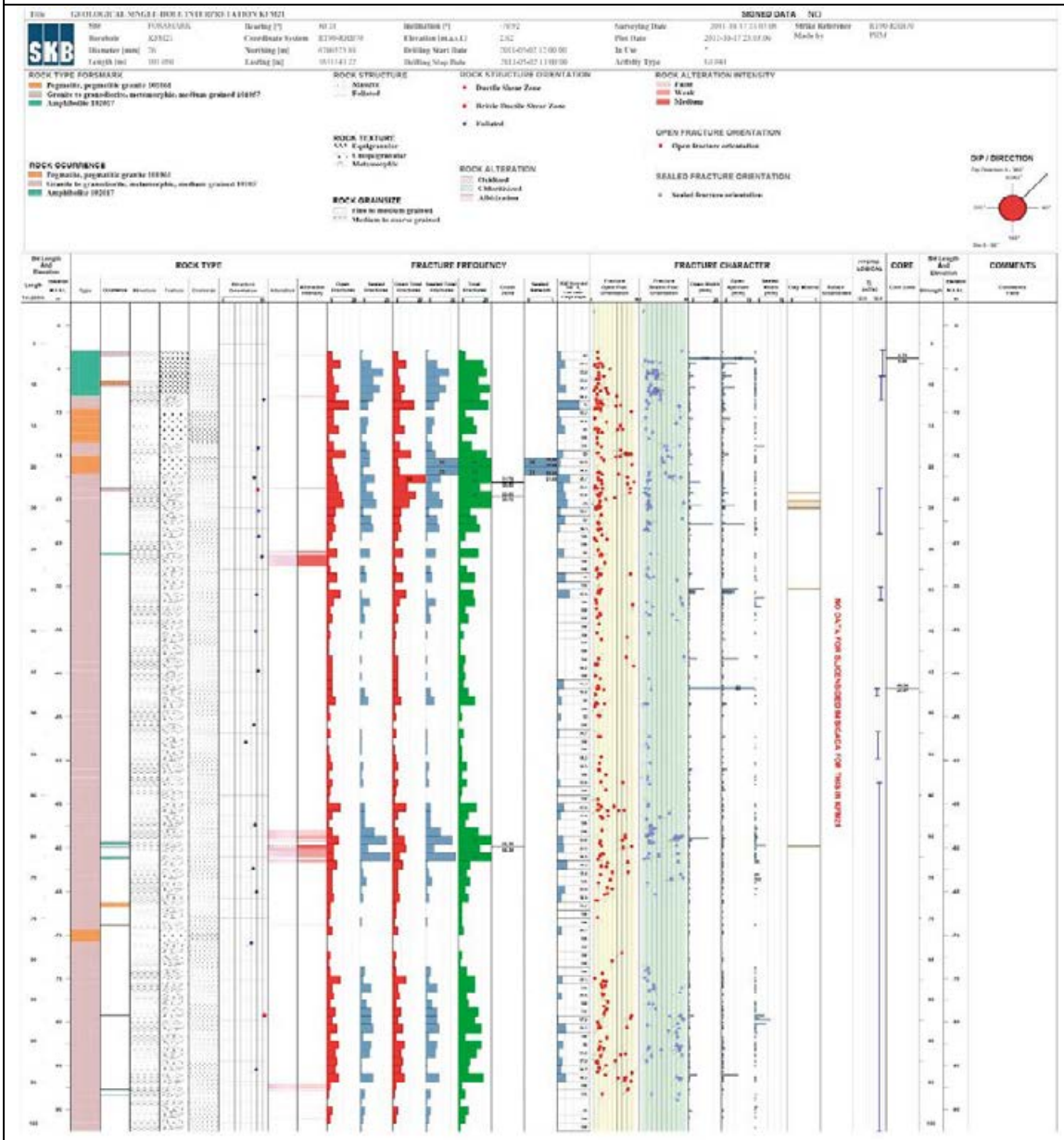
SKB
GEOLOGICAL SINGLE-HOLE INTERPRETATION KFM21
MSNED DATA NO
ROCK TYPE FORSMARK
ROCK STRUCTURE
ROCK STRUCTURE ORIENTATION
ROCK ALTERATION INTENSITY
ROCK TEXTURE
ROCK OCCURRENCE
ROCK ALTERATION
OPEN FRACTURE ORIENTATION
SEALED FRACTURE ORIENTATION
ROCK GRAINSIZE
DIP / DIRECTION
ROCK TYPE
FRACTURE FREQUENCY
FRACTURE CHARACTER
CORE
COMMENTS

KFM22 – 1/1

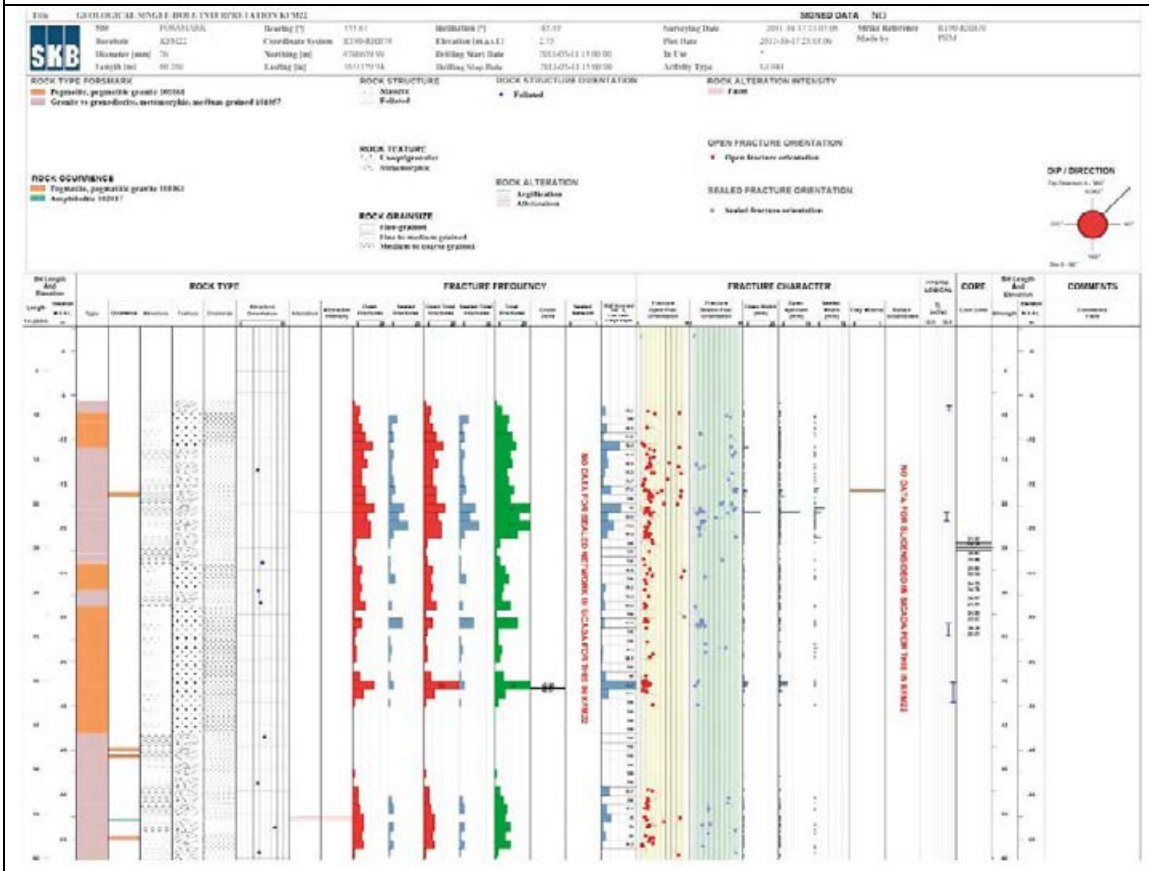
SKB
SIGNED DATA NO
ROCK TYPE FORSMARK
ROCK STRUCTURE
ROCK STRUCTURE ORIENTATION
ROCK ALTERATION INTENSITY
ROCK TEXTURE
ROCK ALTERATION
OPEN FRACTURE ORIENTATION
SEALED FRACTURE ORIENTATION
DIP / DIRECTION
ROCK OCCURRENCE
ROCK GRAINSIZE
ROCK TYPE
FRACTURE FREQUENCY
FRACTURE CHARACTER
CORE
COMMENTS
NO DATA FOR SEALED NETWORK IN SICADA FOR THIS BH KFM22
NO DATA FOR SLICKENSIDES IN SICADA FOR THIS BH KFM22

KFM23 – 1/1

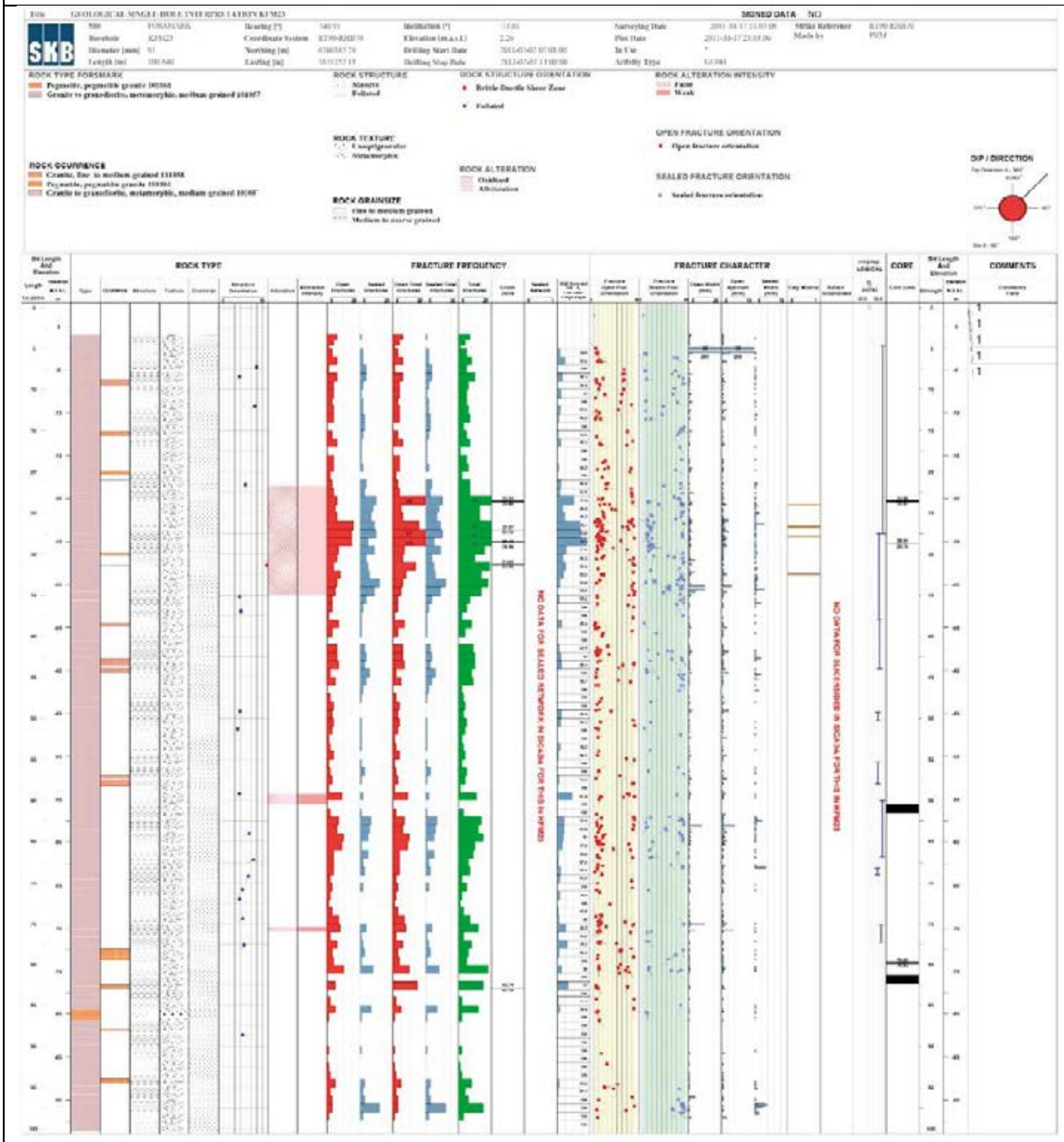
SKB
ROCK TYPE
FRACTURE FREQUENCY
FRACTURE CHARACTER
CORE
COMMENTS
DIP / DIRECTION

KFM24 – 1/4

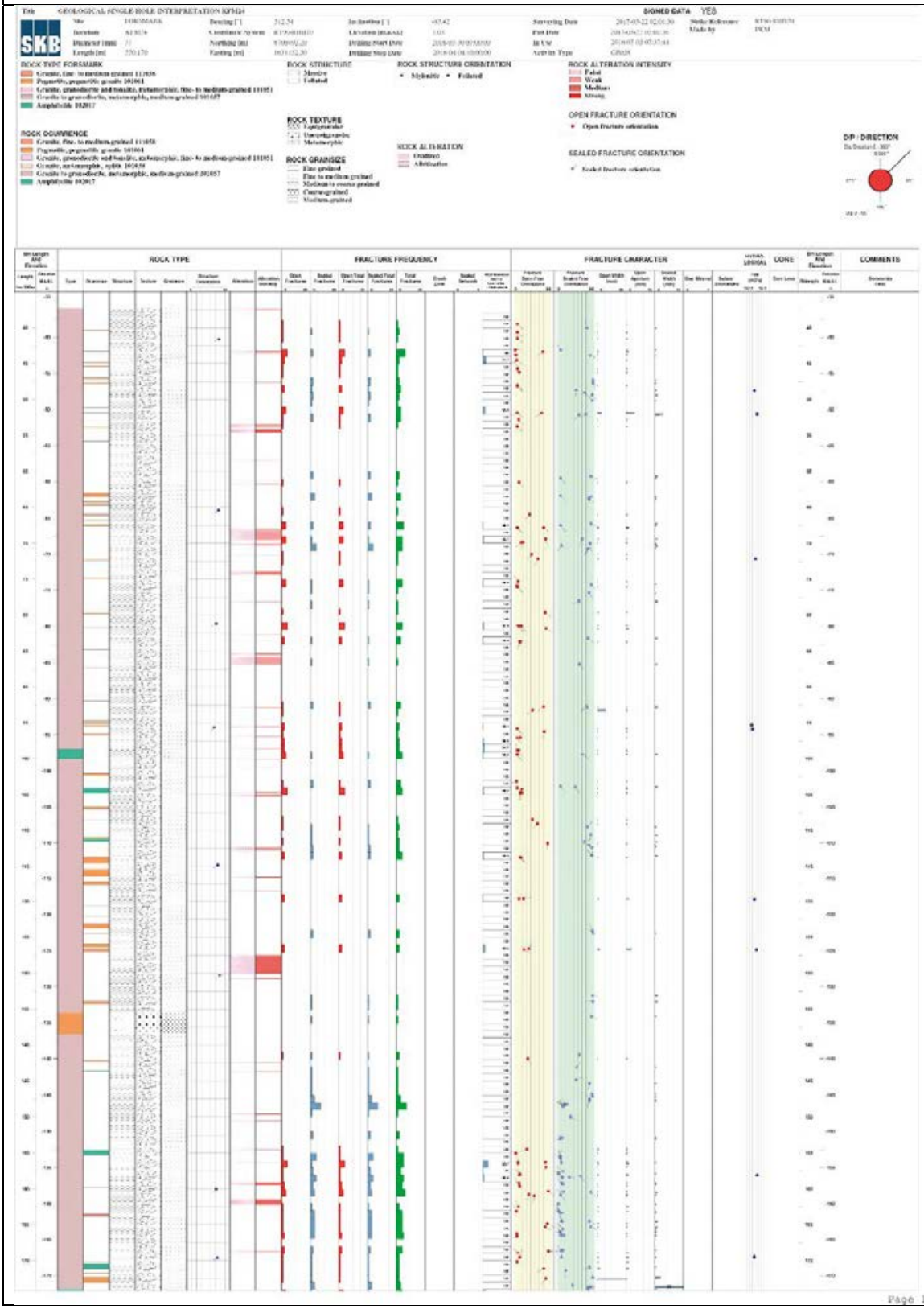
GEOLOGICAL SINGLE HOLE INTERPRETATION KFM24
SIGNED DATA YES
ROCK TYPE FORSMARK
ROCK STRUCTURE
ROCK STRUCTURE ORIENTATION
ROCK ALTERATION INTENSITY
ROCK TEXTURE
ROCK OCCURRENCE
ROCK GRAINSIZE
OPEN FRACTURE ORIENTATION
SEALED FRACTURE ORIENTATION
DIP / DIRECTION
ROCK TYPE
FRACTURE FREQUENCY
FRACTURE CHARACTER
CORE
COMMENTS

KFM24 – 2/4

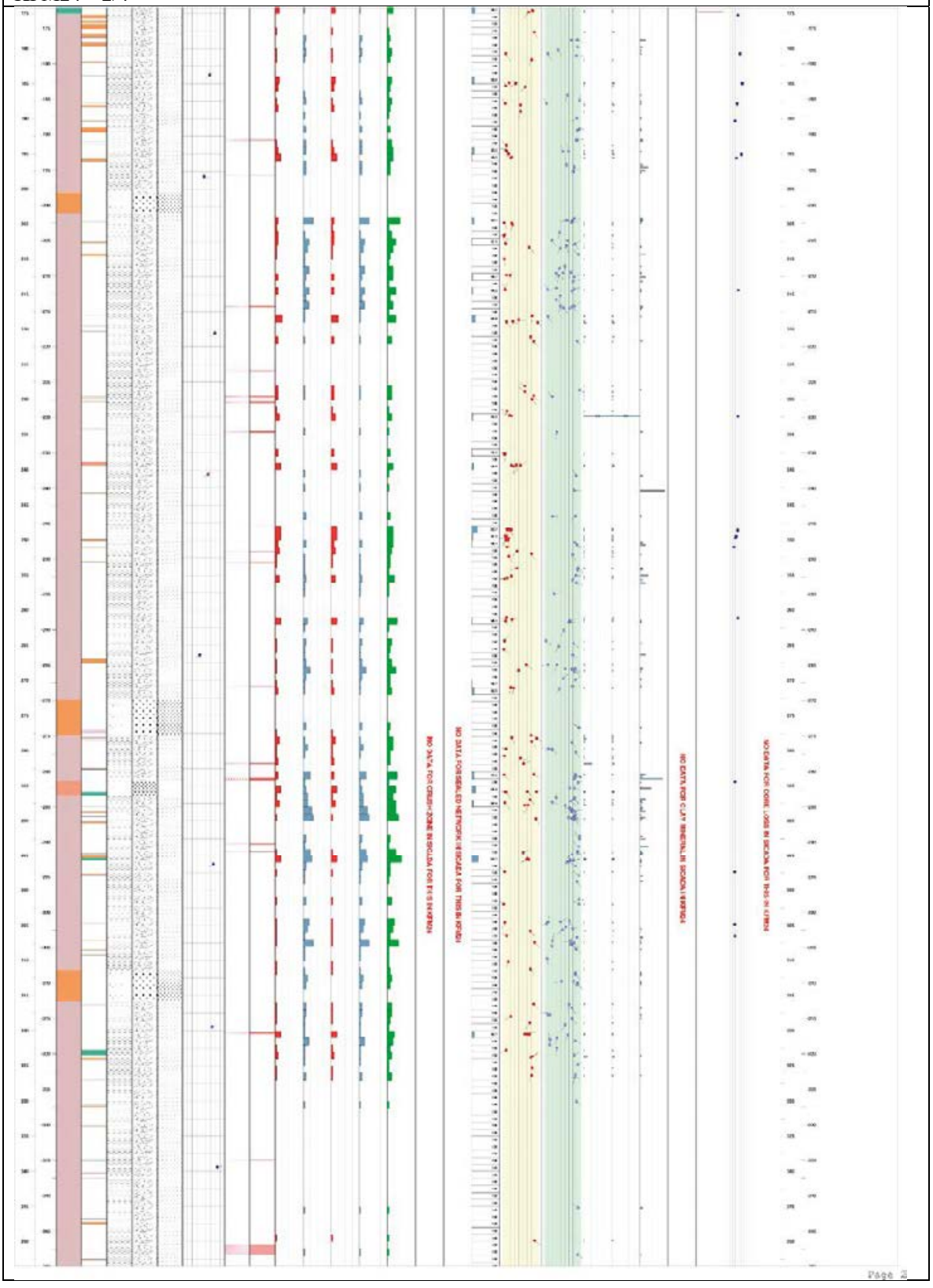

KFM24 – 3/4

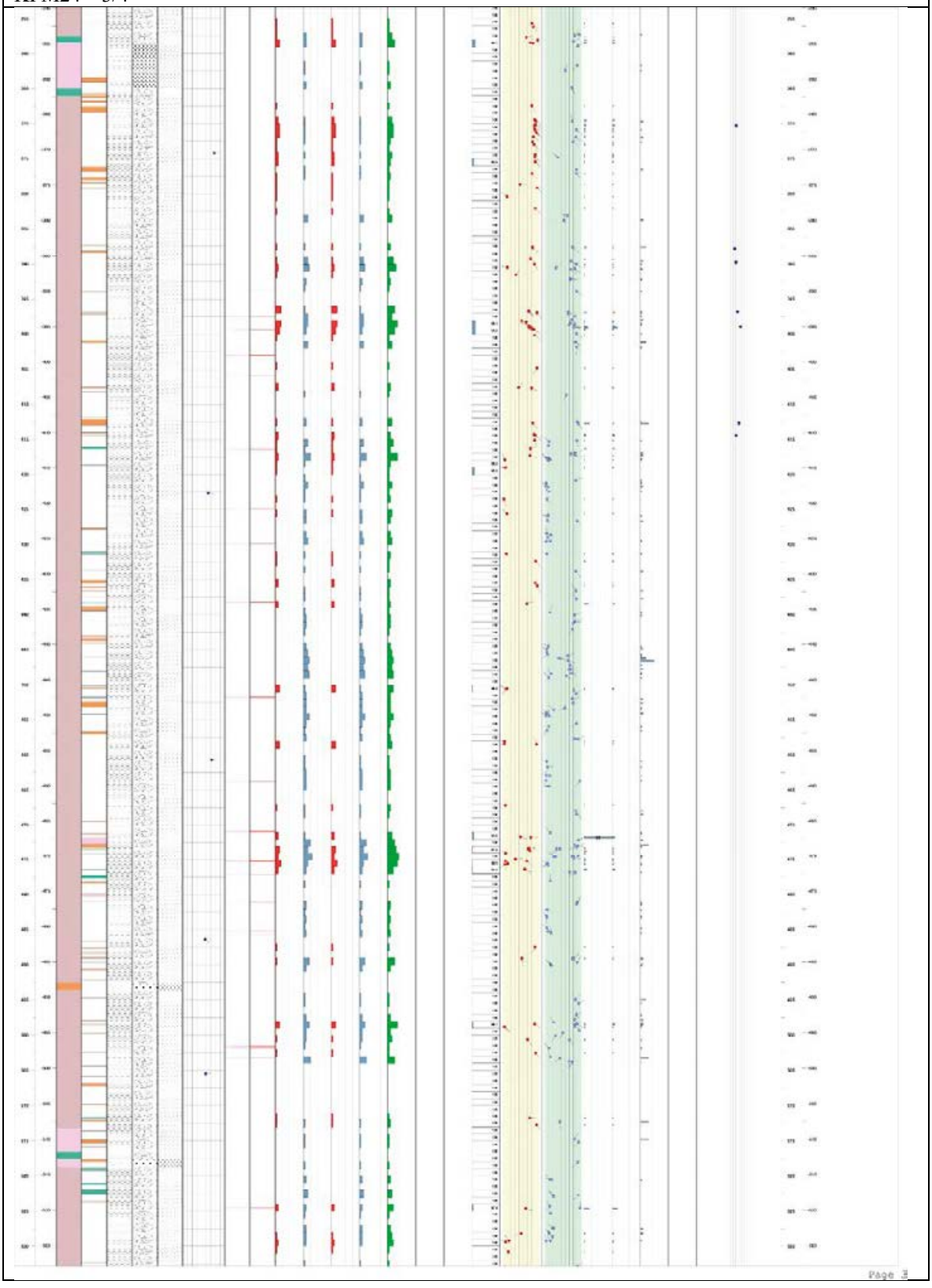

KFM24 – 4/4

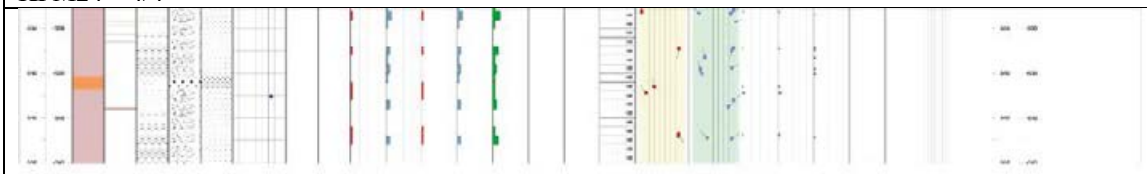

Page 4

HFM39 – 1/2

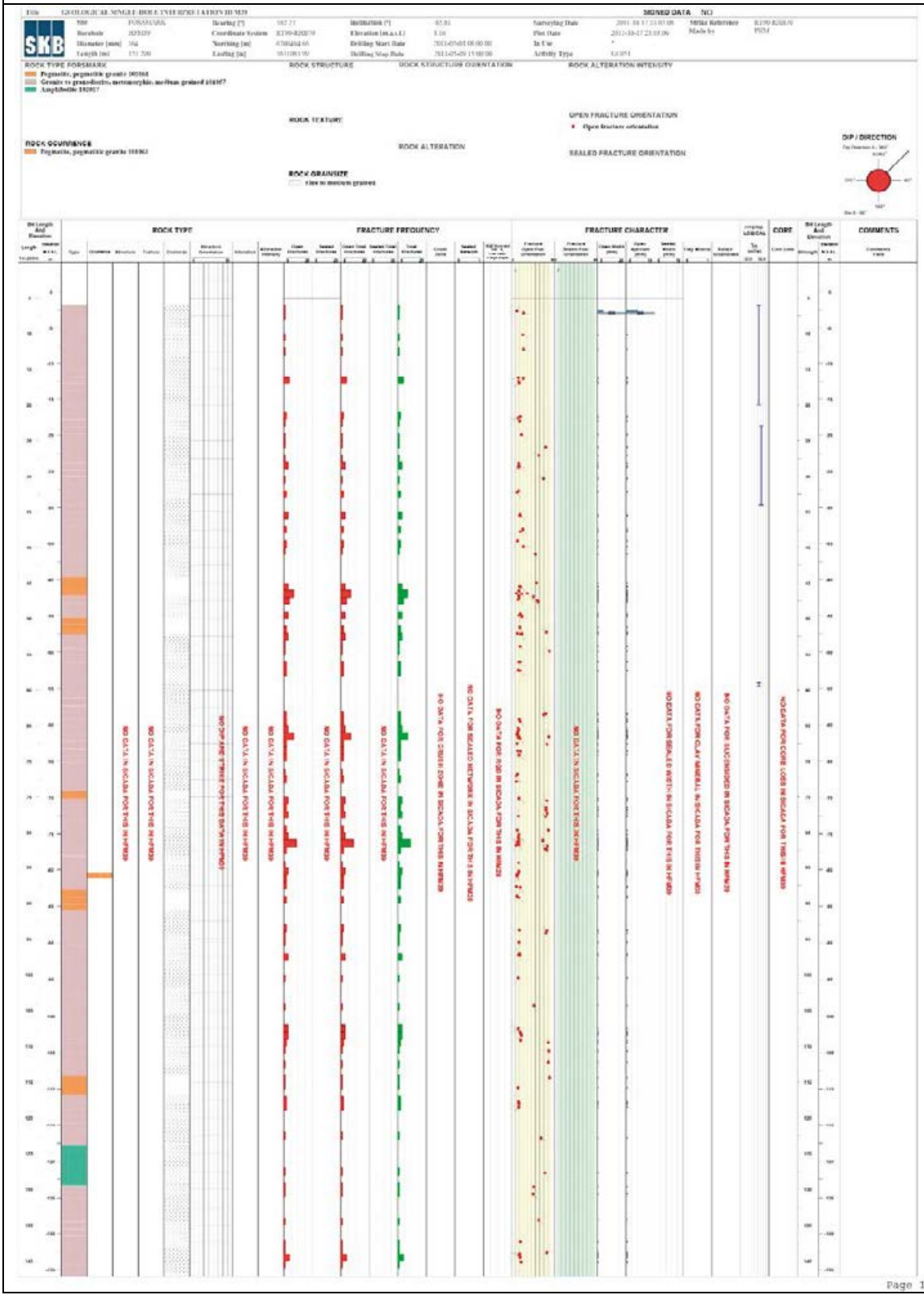
SKB
SIGNED DATA NO
ROCK TYPE FORSMARK
ROCK STRUCTURE
ROCK STRUCTURE ORIENTATION
ROCK ALTERATION INTENSITY
ROCK TEXTURE
OPEN FRACTURE ORIENTATION
ROCK ALTERATION
SEALED FRACTURE ORIENTATION
DIP / DIRECTION
ROCK GRAININESS
ROCK ROCCURRENCE
ROCK TYPE
FRACTURE FREQUENCY
FRACTURE CHARACTER
CORE
COMMENTS
Page 1

HFM39 – 2/2

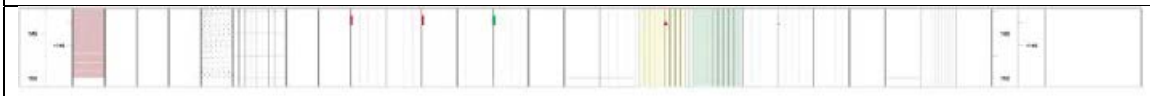

HFM40 – 1/1

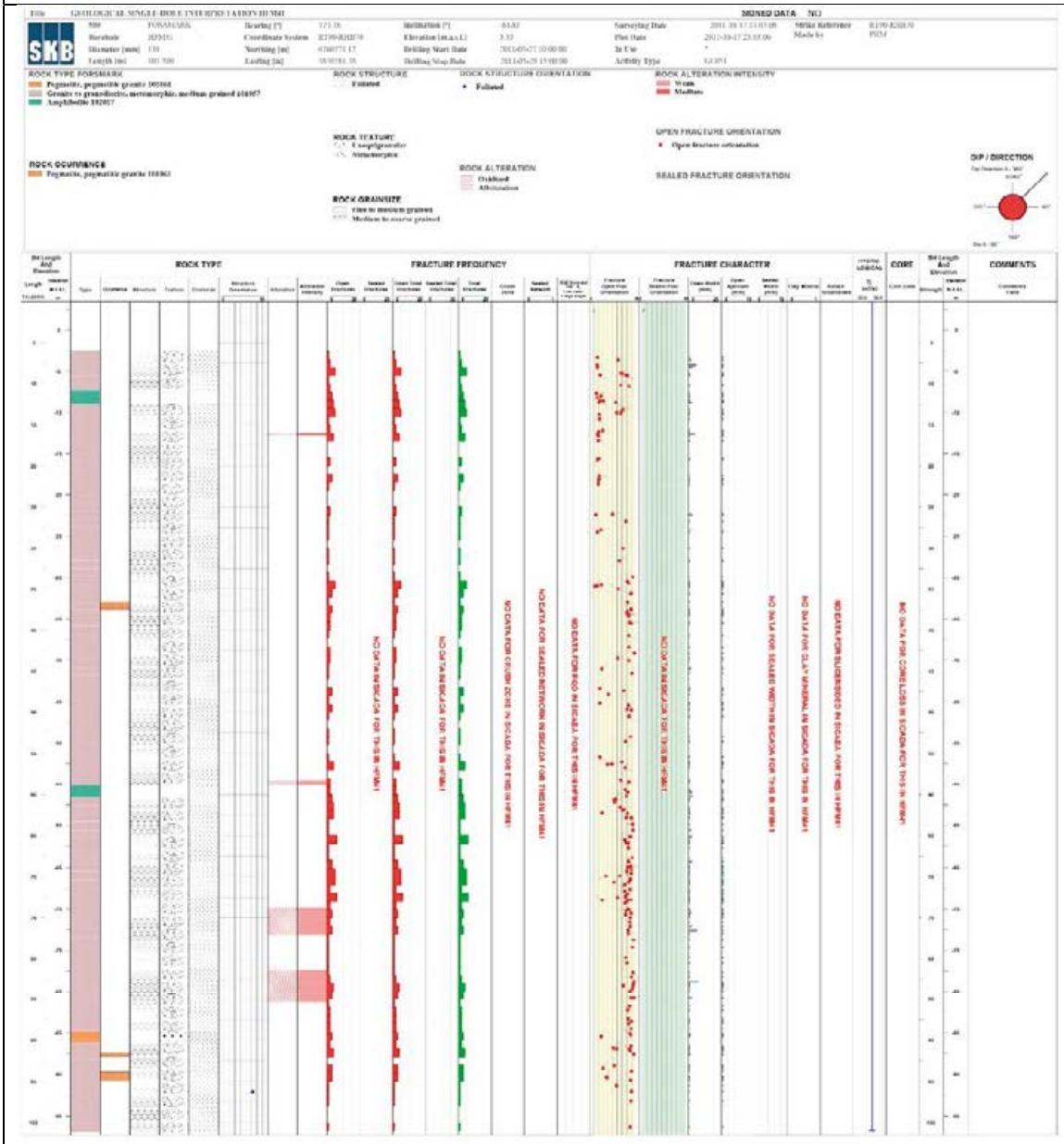
SKB
SIGNED DATA NO
ROCK TYPE FORSMARK
ROCK STRUCTURE
ROCK STRUCTURE ORIENTATION
ROCK ALTERATION INTENSITY
OPEN FRACTURE ORIENTATION
SEALED FRACTURE ORIENTATION
ROCK OCCURRENCE
ROCK ALTERATION
ROCK GRAINSIZE
DIP / DIRECTION
ROCK TYPE
FRACTURE FREQUENCY
FRACTURE CHARACTER
CORE
COMMENTS

HFM41 – 1/1

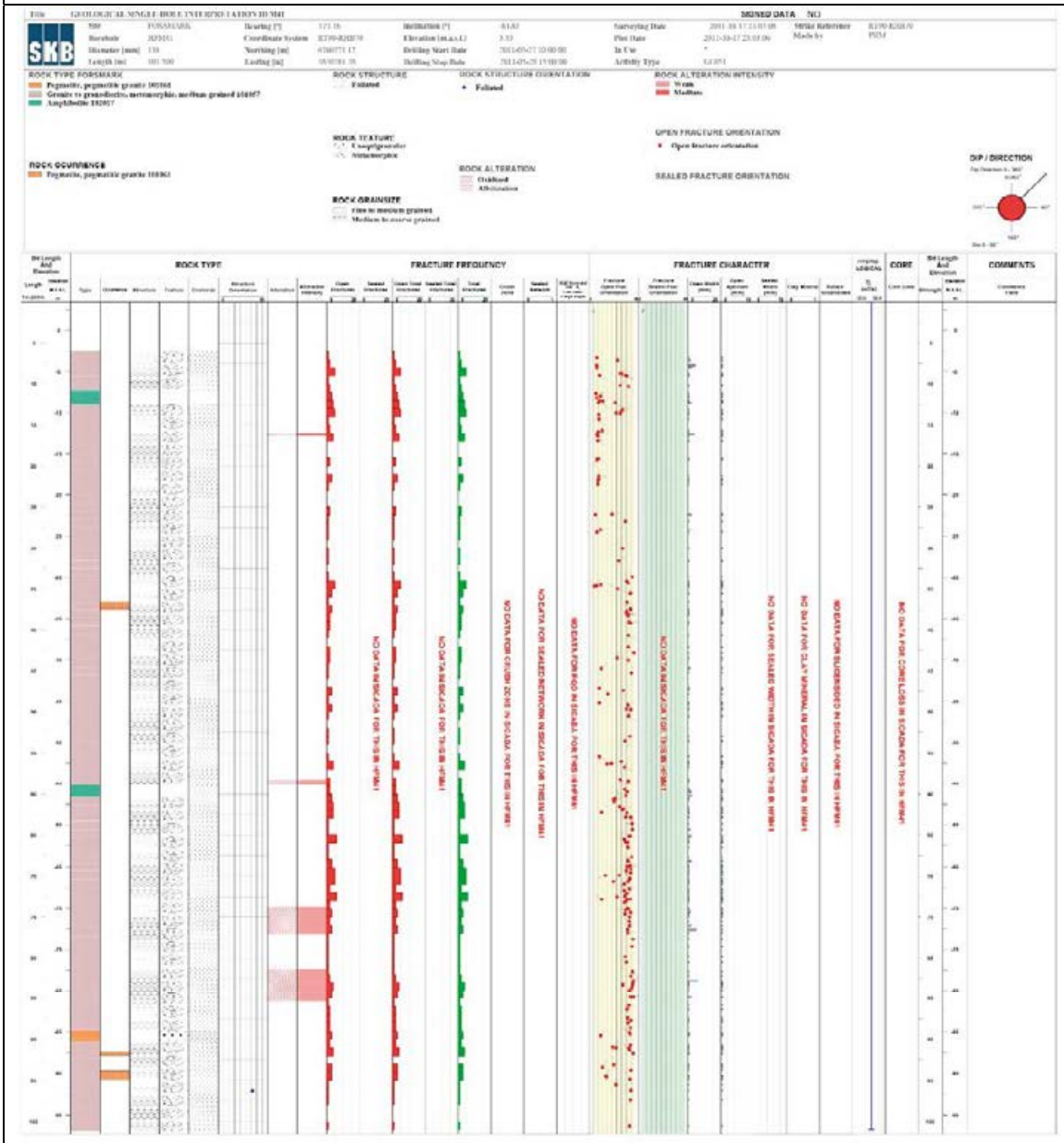

Page 1

Arkitektkopia AB, Bromma, 2019

SKB is responsible for managing spent nuclear fuel and radioactive waste produced by the Swedish nuclear power plants such that man and the environment are protected in the near and distant future.

skb.se